CONFIDENTIAL

FOUNDATION FOR MATERIALS RESEARCH IN THE SEA

STICHTING MATERIAALONDERZOEK IN DE ZEE

Rotterdamseweg 137
2628 AL DELFT - The Netherlands

ECSC CONVENTION 7210-KG/602(F7.5/84)

DRAFT FINAL REPORT

Fatigue behaviour of welded joints in offshore steel structures

Part III: fracture mechanics

by: O.D. Dijkstra
H.H. Snijder
L. Overbeeke
H. Wildschut
H.G. Scholte

ecember 1988

eel and Coal

TU Delft — DELFT UNIVERSITY OF TECHNOLOGY

tue Eindhoven — EINDHOVEN UNIVERSITY OF TECHNOLOGY

TNO — METALS RESEARCH INSTITUTE, APELDOORN
INSTITUTE FOR BUILDING MATERIALS AND STRUCTURES, RIJSWIJK

DISTRIBUTION

Directorate-General XII Science, Research and Development
(10 copies)

Executive Committee 13 - Constructional Steels and Marine Technology:

Mr. H. Arup
J. de Back
M. Bellot
M. Bonomo
A. Bragard
P. Bufalini
J. Defourny
J.J. Dufrane
F.J. Flossdorf
J. Gerald
E. Grethen
U. Girardi
D. Hanewinckel
Th. M. Hoogendoorn
H.P. Lieurade
E. Llamazares
S.J. Maddox
J. Mendia
J.L. Ramirez
E.F. Walker

Representatives of the contractors:

Mr. C. Baudry
A. Bignonnet
M. Bramante
A. Bruls
D.N. Crowther
G. Demofonti
J.A. le Duff
K. Freier
K. Forch
M. Grubisic
D. Grimme
W. Haumann
H. Hougardy
B. Jacob
M.H. Kolstein
H.P. Lehrke
W.M. Morrison
D.E. Nunn
J.L. Overbeeke
M. Poyet
L. Sanpaolesi
H.G. Scholte
U. Schriever
A.S. Schulz
C.M. Sonsino
A. Stammet

FATIGUE BEHAVIOUR OF WELDED JOINTS IN OFFSHORE STEEL STRUCTURES

Part I :	Thick Plates	- C. Noordhoek	(1)
		J. de Back	(1)
		A. Verheul	(1)
		H. Wildschut	(5)
Part II :	Tubular Connections	- H.G. Scholte	(2)
		B.C. Buisman	(2)
Part III :	Fracture Mechanics	- O.D. Dijkstra	(4)
		H.H. Snijder	(4)
		J.L. Overbeeke	(3)
		H. Wildschut	(5)
		H.G. Scholte	(2)

Final Report

Project coordinator: ir. H.G. Scholte

Delft, December 1988

ECSC Convention : 7210/KG/602 (F7.5/84)
Project number : P 1653
Beneficiary : Foundation for Materials Research in the Sea
Rotterdamseweg 137 - 2628 AL Delft - The Netherlands
Period : 01/01/1985 - 30/06/1988
Participants :
1. Delft University of Technology - Department of Civil Engineering
2. Delft University of Technology - Ship Structures Laboratory
3. Eindhoven University of Technology - Department of Mechanical Engineering
4. TNO Institute for Building Materials and Building Structures - Rijswijk
5. TNO Metal Research Institute - Apeldoorn

SUMMARY (Part I, Part II and Part III)

In this research programme three different aspects of the fatigue behaviour of welded joints are investigated. So the final report includes three parts.

PART I : Fatigue behaviour of thick plates with and without attachments.

Earlier fatigue research up to a plate thickness of 76 mm showed that an increase of the plate thickness has a decreasing effect on the fatigue performance. Since the plate thickness applied in offshore structures tends to increase with the dimensions of those structures, fatigue research is carried out on thick plates.

Plate specimens in the as-welded condition with a thickness of 70 and 160 mm are tested in air with constant amplitude loading (R=0.1) under four point bending. Three types of specimens are investigated (butt welds, transverse attachments and longitudinal attachments).

The experiments showed that the tickness effect was not limited at 70 mm but that up to a thickness of 160 mm of the main plate both the thickness of the main plate as well as the thickness of the attachments have a significant influence on the fatigue strength. The influences of both the main plate and the attachments are of the same order.

Analysis of the results of this programme and previous programmes on the fatigue behaviour of as-welded specimens by multiple regression analysis resulted in the following relation between stress range S_r, fatigue life N, thickness T of main plate and tickness t of attachment:

$$\log (S_r) = C - 0.33 \log (N) - 0.15 \log (T) - 0.15 \log (t).$$

From this analysis the influence of the tickness of the main plate is apparently equal to the influence of the tickness of the attachment. However, the number of analysed data is too small to arrive to firm conclusions.

PART II : Fatigue behaviour of butt welded tubular connections with root defects.

In the construction of offshore platforms one side welding is often unavoidable and so are root defects. To gain better knowledge of the influence of root defects on the fatigue behaviour tests have been carried out on butt welded tubular joints under axial loading with a constant amplitude.

The connections of tubes with different wall ticknesses (16 and 25 mm), with or without a high/low defect showed the lowest fatigue strength, reducing the fatigue life at least with a factor 4. Also a considerable reduction of the fatigue life (>2) was found for joints with a lack of root fusion or with a mechanical notch in the root. The effect of cold cracks in the root of the weld was very small and almost negligible. For all types of weldment it appeared that both the crack initiation and the crack growth rate depend greatly upon the very local geometry of the weldment, expecially the differences in wall thickness, misalignment and the dimensions of the defects.

PART III: Fatigue life estimation on a fracture mechanics approach.

Especially the generation of fatigue data for the longer fatigue lifes of large scale components is troublesome, time consuming and expensive. Application of a fracture mechanics approach may at least partly bypass the difficulties and restrictions.

For a further development of the fracture mechanics approach a step-by-step procedure is performed for specimens with an increasing degree of geometrical complexity. Experimental and analytical work has been carried out with regard to the fatigue behaviour of two dimensional geometries with an edge crack and of three dimensional geometries with a semi-elliptical surface crack. Some of the geometries were provided with a weldshape exactly alike a T-shape specimen with a full penetration weld. However, all specimens were manufactured out of one thick plate by machining. So no weld irregularities were present in the specimens. All experiments were carried out in four point bending.

The Paris-Erdogan relation was used as a crack growth model. Stress-intensity factors were taken from literature and determinded by finite element calculations. An evaluation was carried out by comparing the experimental and analytical results. For the specimens with a simple geometry a relatively good agreement was found between calculation and experiment. However, due to the fact that at low ΔK values the data point are below the $da/dn - \Delta K$ curve, the analytical life time underestimates the experimental lifetime. With regards to the growth of surface cracks in plates with a weld geometry the agreement between calculation and experiment was rather poor. The lifetime calculations gave conservative to very conservative results. Further investigation of the available information will be necessary in the future to solve the remaining questions.

RESUME.

Dans ce programme de recherche trois aspects, touchant les propriétés de résistance à la fatigue des assemblages soudés sont examinés.
C'est pour cela que le rapport final se compose de trois parties.

PART 1. Le compartement à la fatigue des plaques épaisses avec et sans des attaches soudées.

Recherche à la fatigue précédente, des plaques d'une épaisseur jusqu'à 76 mm a montré qu'un accroissement de l'épaisseur de la plaque réduit la résistance à la fatigue. Parce-que l'épaisseur des plaques utilisées dans les constructions off-shore a la tendance de s'agrandir avec les dimensions de ces constructions, des recherches à la fatigue sont exécutées avec des plaques plus épaisses.

Des essais avec des plaques d'une épaisseur de 70 et 160 mm sont réalisés dans l'air dans la condition 'as-welded', sous de pliage quatre points et avec une amplitude constante (R = 0,1).

Trois types d'essais sont examinés (des éprouvettes avec joint bout à bout et une attache transversale et éprouvettes avec une attache longitudinale)

Les essais des recherches précédentes avaient une épaisseur maximale de 76 mm. Les résultats des essais avec des éprouvettes d'une épaisseur de 160 mm montrent qu'aussi jusqu'à cette épaisseur il y a encore une réduction considerable de résistance à la fatigue.

Les experimentations montrent que l'épaisseur de l'attache soudée est autant importante pour la réduction de la résistance à la fatigue que l'épaisseur de la plaque primaire.

Une analyse "multiple regression" des résultats de ce programme-ci et des programmes précedentes par rapport au compartement à la fatigue des essais "as-welded" resultait dans la rélation suivante:

$\log S_r = C - 0{,}33 \log N - 0{,}15 \log T - 0{,}15 \log t.$

C = Constante

S_r = l'amplitude de la tension

N = la durée de la vie en fatigue

T = l'epaisseur de la plaque primaire

t = l'epaisseur de la plaque attachée

Aussi cette analyse montre que l'épaisseur de la plaque primaire et de la plaque attachée ont à peu près le même effet sur la réduction de la résistance à la fatigue.
Cependant le nombre des résultat est insuffisant pour tirer des conclusions sûres.

PART 2. Résistance à la fatigue des tubes avec des assemblages soudés bout à bout et avec des défauts de soudure dans la base.

Dans les constructions off-shore c'est impossible d'éviter toujours les assemblages de soudure unilatérals. Fréquemment le résultat sera un assemblage soudé avec des défauts de soudure dans la base. Pour déterminer l'influence des défauts differents sur la résistance de fatigue, deux tubes avec plus des assemblages ont été éprouvés en une charge dynamique axiale et avec une amplitude constante.

Les assemblages des tubes avec une épaisseur differente (16 et 25mm), avec et sans des défauts d'alignement montraient d'avoir la résistance à la fatigue la plus inférieure avec une réduction au moins de quatre fois la durée de la vie en fatigue. Aussi les assemblages soudés avec un manque de fusion ou une entaille mécanique avaient une résistance de fatigue inférieure (> 2). Cependent l'influence de la fissuration à froid était presque négligeable. Pour tous les assemblages il resulte que l'initiation et aussi la propagation des fissures de fatigue étaient déterminées plus fort par la configuration locale, spécialement par les differences dans l'épaisseur, par les défauts d'alignement et par les dimensions des défauts.

PART 3. Estimation de la durée de la vie selon la méthode de la méchanique de la rupture.

Spécialement la génération des données de la fatigue pour le plus longue durée de vie des gros composants est problématique, prends du temps et est chère. Application de la méthode de la méchanique de la rupture peut au moins partiellement prévenir les difficultés et les restrictions.

Pour un développement continué de la méchanique de la rupture un pied à pied procédure est executé pour les éprouvettes avec le degré croissant de la complexité géométrique. Le travail expérimentèle et analytique a été executé par rapport à le compartement fatigué du géométrie deux-dimensional avec la fissure au bord et du géométrie trois-dimensional avec une fissure de la surface semi-elliptique. Quelques géométries étaient pourvenus avec une forme de soudure. Les éprouvettes étaient fabriqués méchaniquement d'une seule plaque épaisse. Donc aucun irrégularité de soudure était présents dans les éprouvettes. Tous les expériments étaient executés à flexion à quatre points.

Le rélation Paris-Erdogan était utilisé comme une modèle de la propagation de la fissure. Facteurs d'intensités des contraintes étaient empruntés aux calculs des eléments finis. Une évaluation était executée au comparaison des résultats expérimentals et analytiques. Pour les éprouvettes avec un géométrie simple un relativement bon confirmité était trouvé entre le calcul et l'expériment. Mais, pendant que le fait que pour les bas ΔK-valeurs les points données sont sous le courbe da/dn- ΔK, la durée de la vie analytique sous-estime la durée de la vie expérimentale. Par rapport à la propagation de la fissure en plaques avec un géométrie de soudure le confirmité entre le calcul et l'expériment était considerablement mauvais. Les calculs de la durée de la vie donnaient les résultats conservateurs jusqu' à les résultats très conservateurs. En future l'investigation continuant de l'information disponible serait nécessaire pour solver les questions restées.

ZUSAMMENFASSUNG.

In dieser Forschungsarbeit sind drei verschiedene Aspekte der Dauerfestigkeit von geschweissten Verbindungen untersucht worden. Deshalb enthält dieser Schlussbericht drei Teilen:

TEIL 1. Ermüdungseigenschaften von Stahlplatten mit grossen Wandstärken, mit und ohne angeschweisste Platten.

Bereits ausgeführte Proben auf Stahlplatten bis eine Wandstärke von 76 mm. zeigten ein Abfall der Schwingfestigkeit bei zunehmender Wandstärke.
Weil in offshore Konstruktionen die Abmessungen der Wandstärke immer grösser werden, sind in dieser Forschungsarbeit Versuche durchgeführt auf Platten mit sehr grossen Wandstärken (70 bis 160 mm).
Diese Platten sind untersucht worden in Luft bei konstanter Amplitudebelastung (R =0.1) unter Biegung. Drei verscheidene Probeformen sind untersucht worden:
-Platten mit Stumpfschweissnaht, Querversteifung und Langsversteifung.

Die bisher ausgeführten Proben hatten eine Maximalwandstärke von 76 mm. Die Resultaten von Proben mit einer Wandstärke von 160 mm zeigen, dass auch bei dieser Stärke noch ein beträchlicher Abfall der Schwingfestigkeit nachgewiesen werden kann.

Bei Probestücken mit Querversteifungen beeinflüsst sowohl die Stärke der Versteifung wie auch die Stärke der Hauptplatte das Schwingfestigkeitverhalten, beide in etwa gleichem Masse.

Auswertung der Resultaten dieser und anderen Untersuchungen mit Hilfe einer "multiple regression analysis" führte zur Formel:

$$\log S_r = C - 0{,}33 \log N - 0{,}15 \log T - 0{,}15 \log t.$$

S_r = Doppelamplitude der Spannung.
N = Lebensdauer.
T = Stärke der Hauptplatte.
t = Stärke der angeschweissten Platte.

Diese Auswertung zeigt, dass die Hauptplattestärke (T) und die Versteifungsstärke (t) in etwa gleichem Masse am Abfall der

Schwingfestigkeit beitragen. Aber die Anzahl der Proberesultaten ist zu klein um zu einer zuverlässigen Aussage zu kommen.

TEIL 2. Ermüdungsverhalten von Stumpfschweissnähte in Rohrverbindungen.

In offshore Konstruktionen sind die einseitigen Schweissnahtverbindungen nicht immer zu verhüten. Manchmal sind Wurzelfehler die Folge. Zum Gewinn von besserem Wissen und mehr Einsicht im Einfluss von dieser Wurzelfehler auf die Lebensdauer ist eine Ermüdungsuntersuchung durchgeführt worden an Rohrverbindungen mit Stumpfschweissnähte, worin Fehler von verschiedener Art. Die Verbindungen sind geprüft worden unter axialer Belastung mit konstanter Amplitüde.

Die Verbindungen von Röhren mit sich ändernden Wandstärken (16 und 25mm), mit oder ohne Kantenversatz zeigten die geringste Schwingfestigkeit mit zumindest einer Vierfachen Reduktion der Lebensdauer.
Ebenso wurde eine bedeutende Abnahme der Lebensdauer (>2) festgestellt für Schweissnähte mit Wurzelbindefehler oder mit mechanischen Kerben in der Wurzel. Der Einfluss von Kaltrissbildung dahingegen war unbedeutend und konnte nahezu vernachlässigt werden. Im allgemeinen war es für alle geprüften Schweissnähte deutlich, dass Rissbeginn und Rissausbreitung stark beeinflusst wurden von der lokalen Geometrie, besonders von Variationen in Wandstärke, Kantenversatz und Abmessungen des Fehlers.

TEIL 3. Abschätzung der Ermüdungslebensdauer mit einem Bruchmechanikverfahren.

Besonders die Generierung der Ermüdungsdaten für die lange Lebensdauer der grosszügigen Komponenten ist zwierig, zeitraubend und teuer. Es könnte sein, dass durch die Anwendung des Bruchmechanik-verfahrens die Zwierigkeiten und Beschränkungen mindestens teilweise zu verhüten sind.

Für eine weitere Entwicklung des Bruchmechanikverfahrens ist ein Schritt für Schritt Verfahren gefolgt für Probekörper mit einem steigernden Grad des geometrischen Komplexitäts. Experimentelle und

analytische Arbeit ist ausgefürt worden mit Bezug auf das Ermüdungsverhalten zweidimensionaler Geometrien mit einem Randriss und dreidimensionaler Geometrien mit einem halbelliptischen Oberflachriss. Einige der Geometrien sind ausgestattet mit einer Schweissform. Die Probekörper sind aus einer dicken Platte durch Maschinenbearbeitung hergestellt. Auf diese Weise sind keine Schweissunregelmässigkeiten in den Probekörper anwesend. Alle Versuche sind ausgeführt in Vierpunktbiegung.

Die Paris-Erdogan Relation ist benützt worden als Rissfortschrittmodel. Spannungsintensitätsfaktoren sind die Literatur entnommen worden und sind durch Finite-Elemente Berechnungen festgestellt worden. Durch vergleichen der experimentelen und der analytischen Ergebnisse ist eine Evaluation durchgeführt worden. Für die Probekörper mit einer einfachen Geometrie ist eine relativ gute Uebereinstimmung zwischen Berechnung und Experiment gefunden worden. Aber, weil für niedrige ΔK Werte die Datenpunkte unter der da/dN-ΔK liegen, gibt die analytische Lebensdauer eine Unterschätzung der experimentelen Lebensdauer. Was mit Bezug auf dem Fortschritt des Oberflachrisses in den Platten mit einer Schweissgeometrie kann festgestellt werden dass, die Uebereinstimmung zwischen Berechnung und Experiment ziemlich schlecht ist. Die Lebensdauerberechnungen zeigten konservative bis sehr konservative Ergebnisse. Weitere Untersuchungen der vorhandenen Information sind in der Zukunft notwendig zur Lösung der unbeantworteten Fragen.

ACKNOWLEDGEMENTS

The authors wish to express their appreciation towards their colleagues of the European Working Groups for the valuable discussions during the meetings and towards their colleagues at the participating laboratories for the fruitful cooperation.

The SMOZ organization wishes to acknowledge the following companies and organizations for their financial aid:

- The European Community of Steel and Coal
- The five participating laboratories
- Heerema Engineering Service B.V., Leiden
- Hollandse Constructie Groep B.V., Leiden
- P. van Leeuwen Jr's Buizenhandel B.V., Zwijndrecht
- Shell Internationale Petroleum Maatschappij B.V., 's-Gravenhage.

CONTENTS

LIST OF SYMBOLS

A_f	finite width correction for membrane stresses
a	crack depth, half crack length
a_f	final defect size
a_i	initial defect size
B	plate width
B_f	finite width correction for bending stresses
C	(empirical) constant
c	half crack width
da/dN	crack growth per load cycle
$\Delta a/\Delta N$	average crack growth rate over the crack length considered
$\Delta \ell$	crack extension of semi-elliptical crack
ΔK	cyclic stress intensity factor range = $K_{max} - K_{min}$
$\bar{\Delta K}$	average ΔK over crack length considered
ΔK_{eff}	effective cyclic stress intensity range
ΔK_{th}	threshold stress intensity range at R = 0
ΔP	change in potential energy
ΔS	change in stiffness matrix S due to the virtual crack extension
$\Delta \sigma$	stress range
δ	element length
E	Young's modulus
F_{max}	maximum load in a load cycle
F_{min}	minimum load in a load cycle
ϕ	angle for location on the crack front
G	strain energy release rate
K	stress intensity factor of a crack
K	constant, determining the height of the S-N curve
K_c	fracture toughness
K_{Ic}	plane strain fracture toughness
K_{max}	maximum value of K during load cycle
K_{min}	minimum value of K during load cycle
K_t	elastic stress concentration factor
L	weld width

M	correction factor for a geometry without a weld shape
M_k	stress intensity concentration factor
m	exponent, determining the slope of the S-N curve
m	exponent, determining the slope of the da/dN curve
n	number of load cycles
N	number of load cycles to failure
N_c	corrected number of cycles in the test (the low stress cycles at the crack markings are corrected)
N_t	total number of cycles in the test (including the number of cycles used for crack marking)
ν	Poisson's ratio
R	load ratio (F_{min}/F_{max})
ρ	weld toe radius
S	stress
S_i	inner support length
S_o	outer support length
s	coordinate along crack front
σ	applied stress
σ_ℓ	local stress
σ_r	residual stress
σ_Y	yield strength
T	plate thickness
Θ	flank angle (weld toe angle)
U	effective stress intensity range ratio = $\frac{\Delta K_{eff}}{\Delta K}$
u	displacement field
Y	stress intensity correction factor for the finite geometry

Indices

b	bending
m	membrane
a	depth direction
c	width direction

1. INTRODUCTION

The traditional approach to determine the fatigue endurance of welded joints is based on experiments. The results of these experiments are often presented in S-N graphs. These graphs give the relation between the stress range (ΔS or $\Delta\sigma$) and the number of cycles to failure (N). A linear relation was used between log S and log N (see figure 1-1). Equation (1.1) gives this relation between S and N.

$$S^m N = K \qquad (1.1)$$

where:
m = exponent, determining the slope of the S-N line
K = constant, determining the height of the S-N line

The governing load parameter is in general the nominal stress range on a specific detail. For every structural detail the S-N curve has to be determined by experiments. In design codes one can find a number of S-N curves together with an atlas of details (see figures 1-2 and 1-3). Most of the results of the first and second phase [1, 2] were presented in S-N diagrams (fig. 1-1).

A more sophisticated method of determining the fatigue life is a fracture mechanics approach. This approach is based on a fatigue crack growth relation, which gives the fatigue crack growth rate (da/dN) as a function of the range of the stress intensity factor (ΔK).

$$da/dN = f(\Delta K) \qquad (1.2)$$

where:
da/dN = crack growth per load cycle
ΔK = stress intensity factor range

The stress intensity factor (K, SIF) is a measure for the magnitude of the stresses near a crack tip. In general the SIF depends on the cracked geometry considered (including the crack dimensions) and on the applied remote stress (σ).

$$K = Y \sigma \sqrt{(\pi a)} \tag{1.3}$$

where:
K = stress intensity factor
Y = correction factor for the finite geometry
σ = remote applied stress

The relation between da/dN and ΔK can be determined from small scale test specimens. Figure 1-4 gives the general relation between da/dN and ΔK. The linear part of the curve (region II) is the most interesting part of the curve for fatigue crack growth.

In this region the Paris-Erdogan equation (1.4) is valid:

$$da/dN = C(\Delta K)^m \tag{1.4}$$

where:
C and m are material constants

For complicated geometries the da/dN-ΔK curve can be determined from tests on small scale specimens and the stress intensity factor can be calculated with a finite element programme. Doing so the fatigue crack growth life can be determined by integrating the crack growth relation. Integrating equation (1.4) gives:

$$N = \frac{1}{C\ (\Delta\sigma\sqrt{\pi})^m} \int_{a_i}^{a_f} \frac{da}{Y\ (\sqrt{a})^m} \tag{1.5}$$

where:
a_i = initial defect size
a_f = final defect size

So time consuming and costly experimental work could partly be replaced by a fracture mechanics analysis. A further advantage of fracture mechanics is that the determination of the remaining life of a cracked structure is possible (fitness-for-purpose analysis).

The aim of the fracture mechanics part of the SMOZ-ECSC programme is to investigate the applicability of fracture mechanics to welded geometries. Especially the fatigue crack growth of a semi-elliptical crack at a weld toe was subject of the investigation.

The geometries of the test specimens and the theoretical models are given in section 2 of this report.

Section 3 gives the results of the experimental part of the programme. Four types of specimens, varying from small 2D specimens to larger 3D specimens with semi-elliptical crack growth at a simulated weld toe geometry are tested in four point bending. The specimens are fabricated out of a thick plate. So no real welds with residual welding stresses, weld irregularities or weld material are investigated.

Stress intensity factors are calculated with the finite element program DIANA. The analysis is based on an energy method. The calculation procedure and the results are given in section 4.

In section 5 fatigue crack growth models are described. The Paris-Erdogan relation was chosen as the most appropriate crack growth relation.

Section 6 gives an evaluation of the fracture mechanics approach by comparing the experimental results with the fracture mechanics analyses.

Applications of the fracture mechanics approach to welded joints are given in section 7.

The conclusions of this part of the programme are given in section 8.

2. SPECIMENS

2.1 Geometries

The geometries described here are used for the specimens in the experimental part of the programme (section 3) as well as for the finite element models in the analytical part of the programme (section 4). Four types of geometries A, B, C and D are investigated (see figures 2-1, 2-2, 2-3 and 2-4).

The geometries can be split up into two-dimensional (2D) geometries (A- and C-type) and three-dimensional (3D) geometries (B- and D-type). The 2D geometries show crack growth only in one direction. The relevant dimension of the crack is the crack depth 'a'. These cracks can be schematized into a 2D configuration neglecting the width dimension B.

The 3D geometries have a surface notch, with crack growth in depth and in width direction. In general the surface notch is schematized into a semi-elliptical shape with the crack depth 'a' and half the crack width 'c' as the characteristic dimensions (see figure 2-5). The three dimensions of these geometries are important for the analysis of the behaviour.

A further distinction can be made into geometries with and without a stub. The 2D geometries without a stub (A-type) are chosen for the determination of the crack growth data of the material used in the experimental part of the programme. Also some experimental measurement techniques were tried out on these specimens. In the analytical part of the programme stress intensity factors were calculated for the A-type specimens and compared with solutions from the literature. This comparison gives an idea of the accuracy of the calculation method used.

The 3D geometries without a stub (B-type) were chosen to investigate the crack growth of a semi-elliptical crack without the influence of a stress concentration.

The 2D geometries with a stub (C-type) were chosen to investigate the influence of the stress concentration due to a weld geometry in a 2D situation. The dimensions of the stub simulate the geometry of a full penetration T-joint (see figure 2-6).
In a pilot investigation [5] the influence of the stub height on the stresses at the weld toe was determined by finite element calculations. Figure 2-7 shows the finite element mesh used. The elements were 8 nodes plane strain quadratic isoparametric elements. The stresses at the weld toe (at the nearest integration point) as a function of the stub height are given in figure 2-8. From this figure it can be concluded that a stub height of 40% of the plate thickness is sufficient to have the complete influence of a larger transverse attachment. So the stub height was chosen to be 30 mm for the 70 mm thickness and 17 mm for the 40 mm thickness.
The flank angle (θ) was generally chosen to be 70°. For one geometry θ is 45°. These values are comparable with earlier experimental work on welded joints [1, 2].
The weld toe radius (ρ) was chosen to be 0.5 or 5 mm for the test specimens, simulating respectively an as-welded joint and a joint dressed by grinding.
For comparison a geometry with a sharp toe transition ($\rho = 0$) was also investigated in the theoretical part of the programme.

The 3D geometries with a stub (D-type) were chosen to investigate the influence of the stress concentration due to a weld geometry in a 3D situation with a semi-elliptical crack. The stub dimensions are equal to the stub dimensions of the C-type geometries.

The thickness of the specimens was 70 or 40 mm. So the thickness effect could be investigated. Also a comparison could be made with earlier experimental work [1, 2] on plates with the same thicknesses.

So the four types of geometries can be characterized as follows (see also table 2-1):

A-type geometries

These are single edge notched geometries with a small width, a constant nominal cross-section, and an edge notch at mid length.
The dimensions of the A-type geometries are shown in figure 2-1.

B-type geometries

These are geometries with a large width, a constant nominal cross-section, and a (semi-elliptical) surface notch at the centre of the mid length section.
The dimensions of the B-type geometries are shown in figure 2-2.

C-type geometries

These are geometries with a small width, a stub, and an edge notch at the toe of one of the flanks of the stub.
The dimensions of the C-type geometries are shown in figure 2-3.

D-type geometries

These are geometries with a large width, a stub, and a (semi-elliptical) surface notch at the toe of one of the flanks of the stub.
The dimensions of the D-type geometries are shown in figure 2-4.

2.2 Material

The material for the experimental part of the programme was a hot-rolled carbon manganese steel, grade Fe E355-KT according to Euronorm 113-72. A plate with dimensions 4000 x 1500 x 105 mm was provided by Hoogovens Groep BV, IJmuiden.
The chemical composition and the mechanical properties are listed below.

Chemical composition (%)

C	Mn	P	S	Si	Al	Cu	Cr	Ni	Mo	Nb	V	Ceq
0.16	1.44	0.016	0.008	0.45	0.05	0.02	0.03	0.035	0.003	0.033	-	0.409

Mechanical properties

Yield point [N/mm²]	Tensile strength [N/mm²]	Elongation [%]	Charpy-V at 0°C [J]
375	538	33.6	95
358	534	32.0	104

2.3 Manufacturing

All specimens, including the T-shape specimens, were manufactured from base material by machining.
In this way a much more uniform and well-defined geometry could be obtained than when manufacturing the specimens by welding. Moreover problems with respect to microstructural inhomogeneity and high residual stresses due to welding were thus avoided.

All specimens were manufactured by machining from one plate with a thickness of 105 mm. The length of the specimens was oriented in the rolling direction of the plate. To avoid an influence on the test results due to any differences in material properties over the plate thickness the upper surfaces of the specimens, containing the initial cracks, had the same position in thickness direction of the plate, as shown in figure 2-9. In order to keep residual stresses due to the machining as low as possible, the feed motion was decreased gradually to very low values at the removal of the last layers of material. After machining initial notches were made by means of spark erosion.

Finally all specimens were stress relieved at 550°C with a hold time of 90 minutes in order to reduce residual stresses resulting from manufacturing. A check on the residual stress level of spare specimens, using the bore-hole technique as well as a saw-cutting method, revealed that the residual stresses at the surface of the specimens after heat treatment were almost negligible ($\sigma_r < 10$ N/mm^2).

3. EXPERIMENTS

3.1 General

The experimental part of the programme was carried out at the TNO-Metals Research Institute (TNO-MI) and the Laboratory for Structural Fatigue, Dept. of M.E., of the Eindhoven University of Technology (TUE). The test procedure, equipment used and the results are extensively reported by the two laboratories [3, 4]. In this report the most important test procedures and the basic test results are given.

All tests were carried out in four point bending. Figure 3-1 shows an example of one of the test rigs used. The inner and outer support length (S_i and S_o) are given in figures 2-1, 2-2, 2-3 and 2-4.
The load was applied by a load controlled servo-hydraulic actuator. Constant amplitude loading was used with a load ratio $R = F_{min}/F_{max} = 0.1$. The wave form was sinusoidal. The frequency of loading was between 2 and 50 Hz, depending on the specimen type and size and on the testing machine used.
All tests were performed in air at ambient temperature.
Crack growth was monitored using a travelling microscope or a magnifying glass. A set of parallel lines with a spacing of 1 mm and a direction perpendicular to the anticipated crack path was applied to facilitate crack length measurements.
Crack front markings were made at regular intervals in order to monitor the shape of the crack front, and particularly to generate information about the crack depth in the specimens with a surface crack. The marking technique involved reduction of the applied stress range to about half its nominal value during a number of load cycles. The maximum value of the nominal stress was maintained at its original value throughout the test.
The specimens with a constant nominal cross section and an edge crack (A-specimens) were subjected to a load shedding procedure prior to the fatigue crack growth tests. In this way data could be obtained about the fatigue behaviour in the region of low growth rates. Application of load shedding during the other tests was considered inappropriate. This would inevitably preclude a correct determination of the fatigue crack growth rate during the initial stage of a test which corresponds with the major part of the fatigue endurance.

Each test was continued until a large fatigue crack had developed which covered about half the cross section area.

3.2 A-type specimens

The dimensions of the 6 A-type specimens are given in figure 2-1.

All specimens were subjected to a load shedding procedure before the actual crack growth test was started.

Specimen A-4 showed a very asymmetric fatigue crack development during the load shedding procedure. This specimen was considered unacceptable for further testing. So this test was rejected.

Specimen A-3, A-5 and A-6 were reduced in height by 20 mm after an approximate 22 mm crack growth during the load shedding procedure. So the actual fatigue crack growth tests were carried out with a specimen height of 60 mm for A-3 and of 40 mm for A-5 and A-6.

The test results of the remaining five A-type specimens are given in tables 3-1 to 3-5:

N_t = number of cycles during the test, including the number of cycles used for crack marking

a = measured crack depth

ΔK = stress intensity factor range

$$\Delta K = M_b \, \Delta\sigma_b \, \sqrt{(\pi a)} \qquad (3.1)$$

where:

M_b = correction factor for a single edge notched strip loaded in bending as given in paragraph 4.2.1

$\Delta\sigma_b$ = nominal bending stress range

$\bar{\Delta K}$ = average ΔK over crack length considered

$$\bar{\Delta K} = (\Delta K_i + \Delta K_{i+1})/2 \qquad (3.2)$$

$\Delta a/\Delta N_t$ = crack growth rate over crack length considered

$$\Delta a/\Delta N_t = (a_{i+1} - a_i)/(N_{t,i+1} - N_{t,i}) \qquad (3.3)$$

Figures 3-2 to 3-6 give a da/dN-ΔK curve for all the test specimens. In each figure the m and C value of the Paris relation (eqn. 3.4) is given.

$$da/dN = C\ (\Delta K)^m \qquad (3.4)$$

Table 3-6 gives a survey of C and m values. The C and m values for the test results of all the specimens are (see also figure 3-7):

$$C = 0.1105\ 10^{-12} \qquad (N,mm)$$
$$m = 3.081 \qquad (3.5)$$

Figure 3-8 and figure 3-9 give the da/dN-ΔK curve for additional crack growth tests in the transverse direction (comparable with the crack growth in c (width) direction in 3D specimens).

Figure 3-10 gives the curves for all specimens tested. It can be seen that the crack growth rate in the transverse direction is the same as in the depth direction.

In the evaluation the C and m values based on the test results of the five A type specimens are used (equation 3-5).

3.3 B-type specimens

The dimensions of the 4 B-type specimens are given in figure 2-2.

No load shedding procedure was applied.

The following test results are given in tables 3-7 to 3-10:

N_c = number of test cycles, corrected for the crack marking cycles, see Appendix A

a = crack depth

c = half crack width

Figures 3-11 to 3-14 give the relation between the crack dimensions and the number of cycles.
Figure 3-15 shows the fracture surface of specimen B-1-1, with the semi-elliptical crack marks.

3.4 C-type specimens

The dimensions of the 8 C-type specimens are given in figure 2-3.

No load shedding procedure was applied.

In specimen C-1-3 a very asymmetric crack developed. Therefore this test was rejected.

The test results are given in tables 3-11 to 3-17. The (for crack marking) corrected number of cycles N_c and the crack depth (a) is given.

The crack growth curves are given in figures 3-16 to 3-19.

Figure 3-20 shows the crack path of specimen C-1-2.

3.5 D-type specimens

The dimensions of the 4 D-type specimens are given in figure 2-4.

No load shedding procedure was applied.

Specimen D-1-1 failed because a fatigue crack developed at the toe of the stub opposite the initial notch. This was discovered in a late stage of the test. So no reliable crack growth data can be deduced from this test.

The test results are presented in the same way as the results of the B-type specimens in tables 3-18 to 3-20 and figures 3-21 to 3-23.

4. CALCULATION OF STRESS INTENSITY FACTORS

4.1 General

The stress intensity factor (SIF) calculations have been carried out at the TNO-Institute for Building Materials and Structures (TNO-IBBC).
The techniques used, calculation procedure and results are extensively reported [6]. In the present report the most important calculation procedures and the basic results are given.

The SIF is a measure for the magnitude of the stresses near the crack tip. The most simple geometry is a biaxially loaded infinite plate containing a slit crack (see figure 4-1), with SIF (K):

$$K = \sigma \sqrt{(\pi a)} \qquad (4.1)$$

where:
σ = applied stress
a = half crack length

For more complicated geometries with finite dimensions the SIF depends not only on the crack dimension (a) and the stress (σ) but also on a geometry depending parameter (Y).

$$K = Y \sigma \sqrt{(\pi a)} \qquad (4.2)$$

Depending on the geometry and loading condition Y has to be split up in several factors.
In 4.2 and 4.3 this has been done for the calculated geometries and load cases.

The SIFs are calculated with the general purpose finite element program DIANA [7]. The SIFs were determined by calculating the strain energy release rate (G) due to a virtual crack extension. The relation between G and K is:

$$G = \frac{K^2}{E^*} \qquad (4.3)$$

where:

$E^* = E$ for plane stress

$E^* = E(1 - \nu^2)$ for plane strain

E = Young's modulus

ν = Poisson's ratio

For <u>two dimensional</u> geometries (type A and C) G can be calculated with eqn. 4.4

$$G = \frac{-\Delta P}{\Delta a} = \tfrac{1}{2} \frac{u^T \Delta S\, u}{\Delta a} \qquad (4.4)$$

where:

ΔP = change in potential energy due to virtual crack extension

u = displacement field

Δa = virtual crack extension

ΔS = change in stiffness matrix S due to virtual crack extension

Based on a sensitivity analysis carried out in [6], the following conclusions are justified for 2D geometries:

- A fineness of the element mesh used, corresponding to $\delta/a = \tfrac{1}{2}$, is sufficient to obtain accurate results.
- Using a relative virtual crack extension $\Delta a/a$ lower than or equal to 10^{-3} leads to accurate results.
- Translation of the crack tip node leads to better results than translation of the crack tip elements (see figure 4.2).
- Accuracy of the results is improved significantly by modelling the crack tip singularity using nodes at quarter point positions.
- Use of a 3 x 3-point integration rule leads to significantly better stress intensity factor results than use of a 2 x 2-point integration rule.

All 2D SIF calculations meet the above mentioned requirements.

For the 3D calculations the following relation between the change in potential energy (ΔP) and the strain energy release rate (G) is assumed.

$$-\Delta P = \tfrac{1}{2}\, u^T \Delta S\, u = \int_{\text{crack front}} G(s) \cdot \Delta\ell(s) \cdot ds \qquad (4.5)$$

where:
$G(s)$ = strain energy release rate along the crack front
$\Delta\ell(s)$ = crack extension perpendicular to the crack front
s = coordinate along crack front
for other symbols see eqn. (4.4)

It was found that a triangular crack extension (see figure 4-3) over two quadratic isoparametric elements gives the most accurate results. With n elements along the crack front and assuming a linear distribution of $G(s)$ along one element (see figure 4-4) a set of $n + 1$ equations (4.5) can be derived. The solution of these equations gives the values of $G(s)$ in the vertex nodes of the elements.
Assuming a quadratic distribution of $G(s)$ along one element, assuming $dG(s)/ds$ has the same value at both sides of the vertex nodes (see figure 4-4) and taking into account that $dG(s)/ds = 0$ at the deepest point of the crack a set of $2n + 1$ equations can be derived to solve the $G(s)$ distribution along the crack front.
For semi-elliptical crack fronts an alternative method can be applied, using eqn. (4.6).

$$G(\phi) = g(\phi).\sqrt{\{\sin^2\phi + (a/c)^2.\cos^2\phi\}} \qquad (4.6)$$

where:
a = crack depth or half crack thickness
c = half crack width
ϕ = angle for location on the crack front (see figure 4-3)

Substituting $G(\phi)$ in eqn. (4.5) and taking ϕ as the independent variable gives eqn. (4.7) for ΔP.

$$-\Delta P = \int_{\text{crack front}} g(\phi)\ \Delta\ell(\phi)\ c\{\sin^2\phi + (a/c)^2\ \cos^2\phi\}d\phi \qquad (4.7)$$

The function of $g(\phi)$ is (analogous to G(s)) assumed to be linear or quadratic along one element.
Based on a sensitivity analysis on 3D beams, embedded cracks in infinite solids and semi-elliptical surface cracks in plates [6] the following conclusions are justified:

- The assumption of a quadratic variation of G along the edge of an element is to be preferred compared with a linear variation of G.
- The G(s) methods can be used for all crack front shapes while the $G(\phi)$ methods are valid for elliptical crack fronts only.
- The calculation of the strain energy release rate G near the free surface is influenced by the boundary layer effect.

All the 3D SIF calculations reported here are carried out with the $G(\phi)$ quadratic method.

4.2 Two dimensional geometries

4.2.1 A-type geometry

SIFs are calculated for 8 crack depths in an A-type geometry (thickness 80 mm). Figure 4-5 gives the finite element mesh. Two load cases (bending and tension (membrane)) are considered. Therefore eqn. (4.2) is extended to eqn. (4.8)

$$K = (M_b \sigma_b + M_m \sigma_m)\sqrt{(\pi a)} \qquad (4.8)$$

where:
M = stress intensity correction factor
σ = remotely applied stress
m and b are indices for membrane stress and for bending stress respectively

The results of the calculations are given in table 4-1.

A curve fitting procedure was carried out on the calculated M values. The result of this procedure is given below.

Pure bending load:

$a/T \leq 0.5$: $$M_b = 1.12 - 1.47(\frac{a}{T}) + 7.71(\frac{a}{T})^2 - 13.6(\frac{a}{T})^3 + 13.9(\frac{a}{T})^4 \quad (4.9)$$

$a/T \geq 0.5$: $$M_b = -14.11 + 86.07(\frac{a}{T}) - 163.17(\frac{a}{T})^2 + 106.78(\frac{a}{T})^3 \quad (4.10)$$

Membrane load:

$a/T \leq 0.5$: $$M_m = 1.12 - 0.21(\frac{a}{T}) + 9.2(\frac{a}{T})^2 - 15.7(\frac{a}{T})^3 + 23.4(\frac{a}{T})^4 \quad (4.11)$$

$a/T \geq 0.5$: $$M_m = -44.69 + 260.87(\frac{a}{T}) - 491.25(\frac{a}{T})^2 + 319.05(\frac{a}{T})^3 \quad (4.12)$$

Figures 4-6 and 4-7 give the relation between M and a/T for $a/T \leq 0.5$. In the same figure the result of a formula published by Brown and Srawley [8] is presented. The literature results and the DIANA results agree very well. Figures 4-8 and 4-9 give the DIANA results over the whole a/T range.

4.2.2 C-type geometries

SIFs are calculated for 6 C-type geometries (see figure 2-2).
The most important parameters are given in table 4-2. For each geometry 8 calculations have been carried out within the relative crack depth range $0 \leq a/T \leq 0.5$. Two loadcases have been considered (membrane and bending). The SIF formula is extended from eqn. 4.8 to eqn. 4.13.

$$K = [M_{k,m}\, M_m\, \sigma_m + M_{k,b}\, M_b\, \sigma_b]\sqrt{(\pi a)} \quad (4.13)$$

where:

M_k = stress intensity concentration factor for the influence of the weld geometry

M = stress intensity correction factor for the strip without the weld geometry (see paragraph 4.2.1)

Figure 4-10 gives the finite element mesh of geometry C-1-1. Figure 4-11 shows the mesh pattern near the weld toe. The crack path is assumed to be straight and perpendicular to the specimen (line A-A). The meshes of the other geometries are similar.

The assumption of a straight crack path does not agree with the experiments (see figure 3-20). In a separate study [44] it was shown that the difference between a straight and a curved crack path is negligible.

The result for geometry C-1-1 is given in table 4-3.

From the calculated strain energy release rates (G) the values for K are determined using eqn. (4.3). With eqn. (4.2) the geometry factor Y is determined.

The influence of the weld geometry can be expressed separately by the stress intensity concentration factor M_k:

$$M_k = Y/M \tag{4.14}$$

where:
M = stress intensity correction factor for the strip (see section 4.2.1, eqns. (4.9) to (4.12)

Eqn. (4.14) in eqn. (4.2) or (4.13) leads to:

$$K = M_k \, M \, \sigma \, \sqrt{(\pi a)} \tag{4.15}$$

For very small crack depths K is only dependent on the local stress field and can be determined with:

$$K = M \, \sigma_\ell \, \sqrt{(\pi a)} \tag{4.16}$$

where:
M = geometry factor for small surface cracks ($M_{a\to 0} = 1.12$)
σ_ℓ = local stress

In this case the local stress at the crack location is:

$$\sigma_\ell = K_t \sigma \qquad (4.17)$$

where:
K_t = elastic stress concentration factor

Combination of the eqns. (4.16) and (4.17) results in:

$$K = K_t M \sigma \sqrt{\pi a} \qquad (4.18)$$

Comparing eqn. 4.18 with eqn. 4.15 it is obvious that for small cracks $M_k \rightarrow K_t$. Therefore K_t is presented in table 4-3 for the uncracked situation. K_t is determined from the stress calculation of the uncracked geometry.

The M_k - a/T relation for geometry C-1-1 is plotted in figure 4-12. The curves show a rapidly decreasing influence of the weld toe (M_k) with increasing relative crack depth (a/T) until $M_k \approx 1$ at a/T = 0.4. For the bending load case the influence of the stub is greater than for the membrane load case.

In table 4-4 the stress intensity concentration factors (M_k) of all C-type specimens are summarized. From this table it can be concluded that for the 70° weld angle geometries the M_k values decrease with increasing ρ/T values. Comparing the geometries C-2-3 (θ = 45°) and C-1-1 (θ = 70°) we see lower M_k-values for the 45° weld angle geometry when a/T is small. At larger crack depths the M_k-value for the 45° weld angle is higher. This can be explained by two counteracting effects. The lower weld angle will have a decreasing effect on the M_k, but the larger stub width at the plate surface will have an increasing effect. For smaller crack depths the weld angle influence dominates while for larger crack depths the larger stub width dominates.

4.2.3 Analytical expressions for 2D M_k values

Stress intensity concentration factors as presented in table 4-4 can be used to derive expressions for M_k through curve fitting for each geometry. Assuming a function of the form of eqn. (4.19), the coefficients A, B and C can be determined:

$$M_k = A + \frac{B}{(a/T) - C} \qquad (4.19)$$

In order to keep the accuracy within acceptable limits three regions are distinguished, namely:

- region I: $0 \leq a/T < 0.025$
- region II: $0.025 \leq a/T < 0.1$
- region III: $0.1 \leq a/T < 0.4$

For a/T greater than 0.4 the weld toe has no influence, so $M_k = 1$.

In table 4-5 the curve fitting coefficients A, B and C of all the geometries are summarized.

The influence of the relative weld toe radius (ρ/T) can be determined by comparing the results of the C-type configuration with $\theta = 70°$ and various ρ/T values. The decreasing trend of the M_k values with increasing ρ/T values can be expressed by a correction factor (f_ρ) according to eqn. (4.20).

$$f_\rho = \frac{M_{k,\rho/T}}{M_{k,\rho/T=0}} \qquad (4.20)$$

where:

$M_{k,\rho/T}$ = M_k for the various ρ/T values
$M_{k,\rho/T=0}$ = M_k for geometry C-0-1 with $\rho = 0$

Values for f_ρ are tabulated in tables 4-6 and 4-7. Figures 4-13 and 4-14 give the f_ρ values in graphical form.

The analytical expression of f_ρ obtained by curve fitting is as follows:

$$f_\rho = 1 - A_\rho \, e^{-B_\rho . a/T} \qquad \text{for } a/T \leq 0.1 \qquad (4.21)$$

where:

$$A_\rho = A_{\rho 1} + \frac{A_{\rho 2}}{(\rho/T - A_{\rho 3})} \qquad (4.22)$$

$$B_\rho = B_{\rho 1} + B_{\rho 2} \, (\rho/T)^2 \qquad (4.23)$$

See table 4-8 for the coefficients $A_{\rho 1}$ to $B_{\rho 2}$.

$$f_\rho = 1 \qquad \text{for } a/T > 0.1 \qquad (4.24)$$

So the M_k value for a T-joint with $\theta = 70$ and a relative weld toe radius $0.00714 \leq (\rho/T) \leq 0.125$ can be determined as follows:

$$M_k = \{A + B/(a/T-C)\} . f_\rho \qquad (4.25)$$

where:

A, B and C = the values for C-0-1 given in table 4-5.

f_ρ = the function of eqn. (4.21 to 4.24)

4.3 Three-dimensional geometries

4.3.1 B-type geometries

For the B-type geometries itself a stress intensity factor solution from the literature was taken. A literature survey [9, 10, 11] showed that the solution proposed by Newman and Raju [12, 13] is the most complete solution and that this solution is supported by the agreement with other solutions.

So no finite element calculations were carried out for the actual B-type geometries (see figure 2-3). However SIFs were calculated in flat plates for four experimental crack shapes of the D-2-2 specimen. The results of these calculations are reported in 4.3.2.

The crack growth of the semi-elliptical crack in a plate can generally be described by the crack growth along the two axes (a for the depth direction and c for the width direction; see figure 4-15).
The stress intensity factors along these axes can be expressed as follows.

$$K_a = [A_f M_{m,a} \sigma_m + B_f M_{b,a} \sigma_b] \frac{\sqrt{(\pi a)}}{E_k} \qquad (4.26a)$$

$$K_c = [A_f M_{m,c} \sigma_m + B_f M_{b,c} \sigma_b] \frac{\sqrt{(\pi a)}}{E_k} \qquad (4.26b)$$

where:
a and c as index means crack depth and crack width direction respectively.
E_k = the complete elliptical integral of the second kind. This integral is:

$$E_k = \int_o^{\pi/2} [1 - (\frac{c^2 - a^2}{c^2}) \sin^2\varphi]^{1/2} \, d\varphi \qquad (4.27a)$$

The following approximation may be used:

$$E_k = [1 + 1.464 (\frac{a}{c})^{1.65}]^{0.5} \qquad \text{for } a \leq c \qquad (4.27b)$$

$$E_k = [1 + 1.464 (\frac{c}{a})^{1.65}]^{0.5} \qquad \text{for } a > c \qquad (4.27c)$$

c = half crack width
a = crack depth
M_m = geometry factor for membrane stress
M_b = geometry factor for bending stress
A_f = finite width correction factor for membrane stress in flat plates
B_f = finite width correction factor for bending stress in flat plates

The Newman-Raju solution is given below in the form of the original equations. These equations include finite width correction and they give a solution which is valid along the total semi-elliptical crack front and not only in depth and width direction:

$$K = (\sigma_m + H\,\sigma_b)\,\sqrt{\pi\,\frac{a}{Q}}\,F \tag{4.28}$$

$$Q = 1 + 1.464\,\left(\frac{a}{c}\right)^{1.65} \qquad \left(\frac{a}{c} \leq 1\right) \tag{4.29}$$

$$F = \left[M_1 + M_2\,\left(\frac{a}{T}\right)^2 + M_3\,\left(\frac{a}{T}\right)^4\right]\,f_\varphi\,g\,f_w \tag{4.30}$$

$$M_1 = 1.13 - 0.09\,\left(\frac{a}{c}\right) \tag{4.31}$$

$$M_2 = -0.54 + \frac{0.89}{0.2 + \left(\frac{a}{c}\right)} \tag{4.32}$$

$$M_3 = 0.5 - \frac{1.0}{0.65 + \left(\frac{a}{c}\right)} + 14\,\left(1.0 - \frac{a}{c}\right)^{24} \tag{4.33}$$

$$g = 1 + \left[0.1 + 0.35\,\left(\frac{a}{T}\right)^2\right]\,(1 - \sin\varphi)^2 \tag{4.34}$$

$$f_\varphi = \left[\left(\frac{a}{c}\right)^2\,\cos^2\varphi + \sin^2\varphi\right]^{1/4} \tag{4.35}$$

$$f_w = \left[\sec\left(\frac{\pi c}{w}\,\sqrt{\frac{a}{T}}\right)\right]^{1/2} \tag{4.36}$$

$$H = H_1 + (H_2 - H_1)\,\sin^p\varphi \tag{4.37}$$

$$p = 0.2 + \frac{a}{c} + 0.6\,\frac{a}{T} \tag{4.38}$$

$$H_1 = 1 - 0.34\,\frac{a}{T} - 0.11\,\frac{a}{c}\,\left(\frac{a}{T}\right) \tag{4.39}$$

$$H_2 = 1 + G_1\,\left(\frac{a}{T}\right) + G_2\,\left(\frac{a}{T}\right)^2 \tag{4.40}$$

$$G_1 = -1.22 - 0.12\,\frac{a}{c} \tag{4.41}$$

$$G_2 = 0.55 - 1.05\,\left(\frac{a}{c}\right)^{0.75} + 0.47\,\left(\frac{a}{c}\right)^{1.5} \tag{4.42}$$

These solutions can be presented in the format of the eqns. (4.26) by substituting $\varphi = \pi/2$ at the deepest point of the crack and $\varphi = 0$ at the free surface. For an infinite width plate this results in the following equations.

The correction factors for membrane stress are:

$$M_{m,a} = [M_1 + M_2 \left(\frac{a}{T}\right)^2 + M_3 \left(\frac{a}{T}\right)^4] \tag{4.43}$$

$$M_1 = - 1.13 - 0.09 \left(\frac{a}{c}\right) \tag{4.44}$$

$$M_2 = - 0.54 + \frac{0.89}{0.2 + \left(\frac{a}{c}\right)} \tag{4.45}$$

$$M_3 = - 0.5 - \frac{1.0}{0.65 + \left(\frac{a}{c}\right)} + 14 \left(1.0 - \frac{a}{c}\right)^{24} \tag{4.46}$$

$$M_{m,c} = M_{m,a}\, g\, f_\varphi \tag{4.47}$$

$$g = 1 + [0.1 + 0.35 \left(\frac{a}{T}\right)^2] \tag{4.48}$$

$$f_\varphi = \left(\frac{a}{c}\right)^{1/2} \tag{4.49}$$

The correction factors for bending stress are:

$$M_{b,a} = H_2\, M_{m,a} \tag{4.50}$$

$$H_2 = 1 + G_1 \left(\frac{a}{T}\right) + G_2 \left(\frac{a}{T}\right)^2 \tag{4.51}$$

$$G_1 = - 1.22 - 0.12 \frac{a}{c} \tag{4.52}$$

$$G_2 = 0.55 - 1.05 \left(\frac{a}{c}\right)^{0.75} + 0.47 \left(\frac{a}{c}\right)^{1.5} \tag{4.53}$$

$$M_{b,c} = H_1 \, M_{m,c} \tag{4.54}$$

$$H_1 = 1 - 0.34 \frac{a}{T} - 0.11 \frac{a}{c} \frac{a}{T} \tag{4.55}$$

The equations of [12, 13] hold if the following requirements are met:

. $0 \leq \frac{a}{2c} \leq 0.5$

. $\frac{2c}{w} < 0.5$

. $0 \leq \varphi \leq \pi$

. $\frac{a}{T} < 0.625 \, (\frac{a}{c} + 0.6)$ for $0 \leq \frac{a}{2c} \leq 0.1$

. $\frac{a}{T} < 0.5$ for $0.1 \leq \frac{a}{2c} \leq 0.5$

The finite width of plates is taken into account by the finite width correction factors A_f and B_f (for membrane stresses and bending stresses respectively) in the eqns. (4.26). In [12, 13] the finite width correction factors are incorporated in the stress intensity factor solution. This finite width correction factor can be explicitly expressed as A_f and B_f:

$$A_f = B_f = f_w = [\sec (\frac{\pi c}{w} \sqrt{\frac{a}{T}})]^{1/2} \tag{4.56}$$

4.3.2. D-type geometries

For D-type geometries (see figure 2-4) calculations have been carried out for geometry D-2-2 only. The dimensions of geometry D-2-2 are given in figure 4-16.

The influence of the weld shape is incorporated in the SIF equations with the stress intensity concentration factor (M_k). So the SIF formula is extended from eqn. (4.26) to (4.57).

$$K_a = [A_f M_{k,m,a} M_{m,a} \sigma_m + B_f M_{k,b,a} M_{b,a} \sigma_b] \frac{\sqrt{(\pi a)}}{E_k} \qquad (4.57a)$$

$$K_c = [A_f M_{k,m,c} M_{m,c} \sigma_m + B_f M_{k,b,c} M_{b,c} \sigma_b] \frac{\sqrt{(\pi a)}}{E_k} \qquad (4.57b)$$

where:

$M_{k,m,a}$ = the stress intensity concentration factor for membrane stress and crack growth in crack depth direction

$M_{k,m,c}$ = the stress intensity concentration factor for membrane stress and crack growth in crack width direction

$M_{k,b,a}$ = the stress intensity concentration factor for bending stress and crack growth in crack depth direction

$M_{k,b,c}$ = the stress intensity concentration factor for bending stress and crack growth in crack width direction

All other symbols have been defined before.

For four semi-elliptical cracks, measured in the experimental part of the programme, finite element calculations have been carried out (see figure 4-17):

- crack I, a = 6.49 mm, c = 10.14 mm;
- crack II, a = 8.95 mm, c = 15.80 mm;
- crack III, a = 11.85 mm, c = 25.90 mm;
- crack IV, a = 16.00 mm, c = 40.70 mm.

To calculate the stress intensity concentration factor M_k, for a cracked geometry, two finite element calculations have to be carried out: one for the plate with stub and one for the corresponding plate without stub. Then, M_k-values can be calculated using eqn. (4.58).

$$M_k = \frac{K_{\text{plate with stub}}}{K_{\text{plate}}} \qquad (4.58)$$

Figure 4-18 gives the finite element mesh of one of the calculations of the plate with stub. The mesh of the plate without stub is given in figure 4-19. The meshes of the geometries with other crack depths have a similar pattern.

Two load cases have been considered: a four point bending load case as in the test (also called the bending load case) and a membrane load case. Loads have been applied in such a way that they result in a nominal bending stress at the surface or a nominal tensile stress of $\sigma_{nom} = 1\ N/mm^2$. The results of crack I are given in tables 4-9 and 4-10.

The results of all the crack shapes are summarized in tables 4-11, 4-12 and 4-13.

The stress intensity factors (K) are given in a graphical form in figure 4-20 to 4-27. The Newman-Raju solution for the flat plate is given in these figures for comparison. In general the DIANA values and the Newman-Raju values agree very well.
The stress intensity concentration factors (M_k) are given in figures 4-28 and 4-29. The M_k factor in the depth (a) direction is smaller than unity. In the width (c) direction is M_k larger than unity. So the weld geometry reduces the SIF in the depth direction and increases the SIF in the width direction.

For larger cracks the M_k factor along the crack front decreases, but for the largest crack the calculated M_k factors increase again. This is probably caused by the influence of the finite width of the plate.

In table 4-14 the results for the depth and width direction are summarized. The three dimensional M_k values are compared with the M_k values determined for a similar two dimensional geometry (specimen C-0-2).
This comparison shows that the 2D M_k values are larger than the 3D M_k values. The ratio (ω) of $M_{k,3D}$ and $M_{k,2D}$ is also given in table 4-14. This ratio can be considered as a reduction factor for the application of 2D M_k values in a 3D geometry. Due to the limited amount of data no general expression of this reduction factor can be given.

$$\omega = \frac{M_{k,3D}}{M_{k,2D}} \qquad (4.59)$$

5. CRACK GROWTH MODELS AND PARAMETERS

5.1 General

The fatigue behaviour of welded joints depends on a large number of parameters and influencing factors [14]. These parameters can be grouped into:

- Material parameters
- Loading parameters
- Geometrical parameters
- Environmental parameters

The total fatigue life of a welded joint can be subdivided in some periods, viz. [15]:

- initiation
- micro crack growth
- macro crack growth
- final failure

In this investigation we are dealing with macro crack growth, where lineair elastic fracture mechanics can be applied [16 and 17] and where the faster short crack growth does not occur [17, 20 and 23].

In fracture mechanics the fatigue crack growth rate (crack extension for load cycle da/dN) is considered to be a function of the stress intensity factor range (ΔK)

$$da/dN = f(\Delta K) \tag{5.1}$$

5.2 Stress intensity factor

The stress intensity factor (SIF) is a parameter determining the elastic stress field around the crack tip [17] (see figure 5.1)

$$\sigma_y = \frac{K_I}{\sqrt{(2\pi r)}} \tag{5.2}$$

where:

σ_y = stress perpendicular to crack surface
K_I = opening mode (mode I) stress intensity factor
r = distance from the crack tip

So when $r \to 0$ then $\sigma_y \to \infty$. In reality the stress at the crack tip is limited due to yielding. The SIF approach is only valid when the yielding at the crack tip is limited and the plastic zone size is small. the yielding at the crack tip can cause plastic deformations, resulting in crack closure effects. This is generally more likely to occur in plane stress situations (e.g. in surface region of semi-elliptical crack) [18].

5.3 Crack growth models

Several crack growth models of the eqn. 5.1 type can be found in the literature [20, 21, 22, 23, 24, 25 and 26].
The model, most commonly used, is the Paris-Erdogan relation

$$da/dN = C\,(\Delta K)^m \qquad (5.3)$$

Eqn. 5.3 represents the linear part of the da/dN-ΔK curve of figure 5.2 (region II).

Other, more complicated models, accounts for the influence of a threshold stress intensity factor range (ΔK_{th}) or for the influence of final failure (K_{max}). Sometimes an abrupt change of the slope of the linear part of the da/dN-ΔK curve is observed. It is not clear whether this is caused by a change of stress state during crack growth or not [19].

In the present investigation the use of eqn. 5.3 is considered to be adequate. A numerical integration of eqn. 5.3 gives the fatigue crack extension and for semi-elliptical cracks also the crack shape development [27, 28, 29 and 30]. On the basis of thus calculated crack size the fatigue life of the component in question can be estimated [see also appendix C].

5.4 Crack growth parameters

From the A specimens (see section 3) the following constants in the Paris relation were obtained:

$c = 1.105\ 10^{-13}$ (N, mm)

$m = 3.081$

These values agree with the recommendations given by an IIW [45] document:

$c = 1.832\ 10^{-13}$ (N, mm)

$m = 3$

Figure 5-3 gives a comparison of these two lines.
In the evaluation of the experimental results in section 6 the results of the A-specimens will be used, while in the application to welded joints (section 7) the IIW recommendations will generally be used.

6. EVALUATION

6.1 General

In this chapter the results of the experimental and analytical work are compared and evaluated. This evaluation is carried out in two ways, viz.:

- comparison of experimental and theoretical results in a crack growth rate (da/dN-ΔK) curve. A further description of the procedure is given in section 6.2.1.
- comparison of experimental and theoretical results in a crack growth (a-N) curve. This procedure is described in section 6.2.2.

Both ways of comparison are based on the validity of the Paris-Erdogan relation (eqn. 6.1). The material properties (C and m) used, are those of the A-type specimens (see section 5.4).

$$da/dN = C\ (\Delta K)^m \qquad (6.1)$$

Figure 6-1 gives the results of the A specimens with the da/dN-ΔK curve used in the analysis (figure 6-1 is figure 3-7 plotted on another format). The evaluation of the 2D specimens (C-type) is given in section 6.3 while the 3D specimens (B- and D-type) is given in 6.4.

6.2 Evaluation procedures

6.2.1 Fatigue crack growth rate curves

The applicability of the Paris-Erdogan relation can be evaluated by comparing the da/dN-ΔK curve of the geometry considered with the curve of the A-type specimens. The experimental crack growth rate (da/dN) is plotted as a function of the theoretical SIF range (ΔK).
In the ideal situation the data points of the B, C and D geometries should fall on the da/dN-ΔK curve of the A-specimens.

In Appendix B the numerical background of the curves shown in this section is presented.

6.2.2 Fatigue crack growth curves

Here the validity of the Paris-Erdogan relation is evaluated by a lifetime calculation. This is based on an integration of the Paris-Erdogan relation (eqn. 6.2), giving a crack growth curve.

$$N = \frac{1}{C} \int_{a_i}^{a_f} \frac{da}{(\Delta K)^m} \qquad (6.2)$$

where:

a_i = initial crack depth
a_f = final crack depth

The lifetime calculations have been carried out with the computer program FAFRAM [28, 29] developed at TNO-IBBC.

In appendix C the calculation procedure is summarized and some numerical results are given.

6.3 Evaluation of the 2D geometries (C-type)

The theoretical SIFs used are determined with the DIANA formulas given in section 4.2.
The specimens are loaded in bending only, so eqn. 4.13 reduces to:

$$K = M_{k,b} \cdot M_b \cdot \sigma \sqrt{(\pi a)} \qquad (6.3)$$

with:

$M_{k,b}$ determined with eqn. 4.19
M_b determined with eqn. 4.9 and 4.10

The graphical presentation of the evaluation is given in figures 6-2 up to and including 6-15.

Two calculated crack growth curves are given in the N-a graphs. One starting with a_i = 0.5 mm and N = 0 and a second one with a_i being the first measured crack after initiation and with the corresponding number of cycles for N. So in the second curve the crack growth delay due to initiation of the artificial notch is not present.

Considering figures 6-2 and 6-3 with the results of specimen C-1-1 the following observation can be made:

a. For ΔK values below 750 $N/mm^{3/2}$ the data points are below the da/dN-ΔK curve (figure 6-2). For higher values of ΔK the data points are above the curve. This is in agreement with the results of the A specimens (see figure 6-1).
b. The calculated lifetime is smaller than the experimental one. The calculated lifetime with a_i = 0.5 mm is 78% of the total experimental lifetime, while the calculated lifetime from $a_i = a_{exp}$ = 0.65 mm to a_f is 85% of the experimental period from 0.65 to a_f (figure 6-3). This reduction in lifetime is consistent with the crack growth rate figure while most of crack growth occurs with ΔK values below 750 $N/mm^{3/2}$ (up to a $\approx$ 22.5 mm).

Specimen C-1-2 (see figures 6-4 and 6-5) show a similar behaviour as the identical specimen C-1-1.
The effects described above are somewhat more pronounced; resulting in a slightly smaller ratio N_{calc}/N_{exp} (see table 6-1).

Specimen C-1-4 with a toe radius ρ = 5.0 mm (for C-1-1 and C-1-2 ρ = 0.5 mm) has also a much slower experimental crack growth at low ΔK-values, resulting in a relatively short calculated lifetime (see figures 6-6 and 6-7).

The identical specimens C-2-1 and C-2-2 (T = 40 mm) show a rather good agreement in the da/dN-ΔK curves (figures 6-8 and 6-10). However the same pattern as for C-1-1 is present. This results again in a lower calculated lifetime (see figures 6-9 and 6-11 and table 6-1).

The general trend is also visible in the results of specimen C-2-3 and C-2-4 (figures 6-12 to 6-15).

Table 6-1 gives a comparison of the experimental and calculated lifetimes of all C specimens. In general the calculations are conservative ($N_{calc}/N_{exp} \approx 80\%$).

The results of all C specimens show that the lifetime is more dependent on the lower part of the da/dN-ΔK curve.

6.4 Evaluation of the 3D geometries

6.4.1 B-type specimens

The theoretical SIFs used are determined with the formulas of Newman-Raju as given in section 4.3.1 (eqns. 4.43 to 4.56).

The graphical presentation of the evaluation is given in figures 6-16 up to and including figure 6-23.
Analogous to the C-specimen two calculations are made (one with a_i = 0.5 mm and c_i = 5.0 mm and one with a_i and c_i at the first crack marking.
The comparison of lifetimes is given in table 6-2.

Considering the results of specimen B-1-1 (figures 6-16 and 6-17) the following observations can be made:

a. The crack growth rate in depth (a) direction is in general greater than the one predicted by the da/dN-ΔK curve, while the crack growth rate in width direction is lower than the one predicted by the curve (figure 6-16). However, the crack growth rate in depth (a) direction is in good agreement with the data points of the A-type specimens at the same ΔK-values (800 - 1000 $N/mm^{3/2}$).
b. The calculated lifetime is smaller than the experimental one (figure 6-17 and table 6-2).
c. The faster calculated crack growth in depth (a) direction (figure 6-17) seems to be inconsistent with the results shown in figure 6-16.
   However the SIF in depth direction is also influenced by the crack width dimension (c).
   The faster calculated crack growth in c direction gives a lower aspect ratio (a/c), resulting in a higher ΔK value and a faster calculated crack growth in the depth direction also.

Specimen B-1-2 shows a similar behaviour as the identical B-1-1 specimen (figures 6-18 and 6-19).

The thinner B-2-1 and B-2-2 specimens (T = 40 mm) show an increase in experimental crack growth rate at approximate $\Delta K = 750$ N/mm$^{3/2}$ in the depth direction (figures 6-21 and 6-23). This in agreement with the results of the A specimens (figure 6-1), however, the increase is more pronounced with the B-2-1 and B-2-2 specimens. The lifetime calculations give again a conservative estimate of the experimental lifetime.

The difference in the crack growth rate in the depth and in the width direction shows that there is an inconsistency in the approach. This may be caused by the experiments (larger plastic zones at the surface) or by the determination of the SIF at the surface (change of plane strain into plane stress situation).

6.4.2 D-type specimens

6.4.2.1 Evaluation based on Newman-Raju and 2D M_k factors

The theoretical SIFs used are determined by combining the flat plate solution of Newman-Raju (see 4.3.1) with the 2D M_k values determined with DIANA (see 4.2). Since only bending is considered in the experiments, the general K formula (eqn. 4.57) reduces to:

$$K_a = B_f \cdot M_{k,b,a} \cdot M_{b,a} \sigma_b \frac{\sqrt{(\pi a)}}{E_K} \qquad (6.4a)$$

$$K_c = B_f \cdot M_{k,b,c} \cdot M_{b,c} \sigma_b \frac{\sqrt{(\pi a)}}{E_K} \qquad (6.4b)$$

with:

B_f, $M_{b,a}$ and $M_{b,c}$ according to Newman-Raju (eqns. 4.43 to 4.56)

$M_{k,b,a}$ and $M_{k,b,c}$ according to DIANA (eqn. 4.19) ($M_{k,b,a}$ for actual a/T value and $M_{k,b,c}$ for a/T = 0)

The results of the evaluation is given in figures 6-24 to 6-29.
The calculated and experimental lifetimes are compared in table 6-3.

The crack growth rate curves (figures 6-24, 6-26 and 6-28) show a large discrepancy between the da/dN curve of the A-type specimens and the data points of the D-type specimens. A rough estimate of the ratio of the theoretical and experimental crack growth rate is given in table 6-4. In depth direction this ratio varies from 2.5 to 5 and in width direction from 5 to 30.
Specimen D-2-1 with the smallest ρ/T value has the largest ratios. The differences in crack growth rate result also in a great differences in lifetime (figures 6-25, 6-27 and 6-29 and table 6-3).

6.4.2.2 Evaluation specimen D-2-2 with the DIANA 3D SIFs

Four cracked geometries of specimen D-2-2 were analyzed with the DIANA finite element program using 3D modelling (see section 4.3.2). Using the SIFs determined in the depth and in the width direction a crack growth rate based comparison can be made (see figure 6-30). In figure 6-31 the 3D results are compared with the results of section 6.4.2.1. The 3D results give a significant improvement. The crack growth rate in depth direction of the smallest crack (shape I) is in the scatter band of the data points of the A specimens.
Possible reasons for the disagreement are:
- change in stress state (plane strain in the depth and plane stress in the width direction)
- crack closure due to larger plastic strains at the surface notch.

6.4.2.3 Evaluation of crack growth reduction factor ω

In section 4.3.2 it was found that the 3D M_k factors are lower than the 2D M_k factor. Table 4.14 gives the reduction factors ω found.
For the bending loadcase the reduction factor was approximately 0.9 for the depth direction and 0.8 for the width direction.

The results of crack growth calculations made with these factors are given in figures 6-32, 6-33 and 6-34. In table 6-3 the influence on the lifetime is also given. Introducing these factors gives a small improvement of the results.
However the results are still very conservative.

7. APPLICATION OF FRACTURE MECHANICS TO WELDED JOINTS

7.1 General

In this chapter fracture mechanics analysis is applied to and compared with results of fatigue tests on welded joints.
In order to make fatigue crack growth calculations possible for various geometries, the M_k formulas are extended with information from the literature (section 7.2).
For a detailed comparison the crack growth data of experiments need to be known. Up to now detailed information is limited. Instead of a calculation for a specific test specimen one can investigate the influence of certain parameters on the fatigue life (such as weld toe grinding (see 7.3.3) or the thickness influence (see 7.3.4)).

In fatigue experiments of welded joints it is often observed that a fatigue crack initiates at more than one point along the weld toe. This multi-initiation phenomenon makes modification to the single initiation fatigue crack growth model necessary. This has been done in section 7.3.2.

7.2 Extension of M_k formulae

7.2.1 General

The stress intensity factor of a crack at a weld toe is among others influenced by the following parameters:
a. overall weld geometry
b. weld toe angle
c. weld toe radius

It was found by Maddox et.al. [46] that the relative weld width L/T is the most important overall weld parameter. The weld influence is taken into account by a multiplication factor M_k (see section 4.2.2). Assuming no interaction between the influence of the relative weld width (L/T), the weld angle (θ) and the relative weld toe radius (ρ/T) the following formula for M_k can be written.

$$M_k = f_L\,(a/T,\ L/T)\ .\ f_\theta\,(a/T,\ \theta)\ f_\rho\,(a/T,\ \rho/T) \qquad (7.1)$$

where:

f_L = correction factor for the influence of the relative weld width (L/T) for a specific weld type with a certain weld angle and weld toe radius
f_θ = correction factor for the influence of the weld angle (θ)
f_ρ = correction factor for the influence of the relative weld toe radius (ρ/T)

In general the influence of θ and ρ is negligible for $a/T > 0.1$; so for $a/T > 0.1$: $f_\theta = 1$ and $f_\rho = 1$.

The value of f_ρ as determined in section 4.2.3 can be used. In section 7.2.2 the function f_L is given. A function f_θ is derived in 7.2.3.

With these expressions the complete influence of L, θ and ρ on the M_k can be determined. For T-joints with a similar geometry as the C-type specimens with $\theta = 70°$ the formula in section 4.2.3 can be used (eqn. 4.25).

7.2.2 Influence of weld width (L)

Smith and Hurworth [47] and Maddox et al. [46] have determined M_k values of butt welds and T-and X-joint geometries (see figure 7-1). For butt welds and X-joints a set of formulas for M_k values was derived by Maddox et al. These formulas are valid for a weld toe angle $\theta = 45°$ and a weld toe radius $\rho = 0$. The formulas are functions of the relative crack depth (a/T) and relative weld width (L/T).

$$M_k = f_L(a/T, L/T) \qquad (7.2)$$

The functions f_L and the range of applicability are given in table 7-1.

7.2.3 Influence of weld angle (θ)

Smith and Hurworth [47] calculated SIFs for X-joints with $\rho = 0$ and $\theta = 25$; 35; 45; 55; and 65°.The weld angle influence can be determined by dividing $M_{k,\theta}$ by $M_{k,45°}$ giving the function f_θ. The difference between tension and bending was negligible. Curve fitting on the average values gives the following formulas.

$$f_\theta = (10.a/T)^{-\frac{1}{2}\log A_\theta} \qquad \text{for } 0.001 \leq a/T \leq 0.1 \qquad (7.3)$$

$$\text{where: } A_\theta = 13.096\ 10^{-3} + 28.119\ 10^{-3}\theta - 139.45\ 10^{-6}\theta^2 \qquad (7.4)$$

$$f_\theta = 1 \qquad \text{for } a/T > 0.1 \qquad (7.5)$$

The range of application of eqns. 7.3 to 7.4 is: $25° \leq \theta \leq 65°$.

7.3 Welded joints

7.3.1 Tubular T-joint

A simple crack growth model for a tubular joint (figures 7-2 and 7-3) based on fracture mechanics was developed in 1985 and published at the OTC conference in 1986 [29].

This model was based on the following schematizations and assumptions:

a. The welded connection of the brace- and chord wall is schematized to a plate with an attachment (figure 7-4).
b. At the weld toe, a semi-elliptical crack is assumed.
c. SIFs are calculated using the formulae of Scott and Thorpe [48] for the flat plate and the M_k values published by Maddox [49] in 1972 for cruciform fillet welded joints.
d. The Paris-Erdogan relation was used as a crack growth law in the depth and the width direction ($C = 1.08\ 10^{-13}$(N,mm) and $m = 3.07$).
e. An initial crack depth and half crack width of 0.25 mm was assumed.

The agreement between the crack growth calculation and the experimental results was relatively good (see figure 7-5).

It seems worthwhile to make a fatigue crack growth analysis with more recent knowledge of SIFs and crack growth data.
In table 7-2 the input parameters of all the calculations are given.
The changes from the original calculation have been made one by one, so that the influence of the changes can be seen separately (see also table 7-3). The following changes have been made:

- da/dN-ΔK curve (calculation B)
  The values for C and m used in the OTC paper [29] ($C = 1.08\ 10^{-13}$ (N,mm) and $m = 3.07$) are changed in the values recommended by IIW ($C = 1.832\ 10^{-13}$ and $m = 3$).
  This change gives a shorter calculated lifetime (see figure 7-6).

- M_k factor (calculation C)

  The M_k factor of Maddox is changed in the M_k factor of eqn. 7.1. This change gives a longer calculated lifetime (see figure 7-7).

- SIF plate (calculation D)

  The SIF solution of Scott and Thorpe is changed in the solution of Newman and Raju.
  This change gives a shorter calculated lifetime (see figure 7-8).

It can be concluded that the modifications in the model do not give a better fit between the experiment and the calculations.
However the modifications in the model are considered to be justified by the recent information. The most probable cause of the discrepancy is that the model does not take into account the specific tubular joint effects, such as: a varying stress distribution and a curved geometry.

7.4 Fatigue crack growth model for multiple initiated cracks applied to a T-plate joint

7.4.1 General

In this section, the crack growth model is extended in order to cover growth of multiple initiated cracks. First of all, the growth of two or more neighbouring cracks is discussed in section 7.4.1.1. Subsequently two approaches for taking multiple initiation and coalescence into account, are discussed in the sections 7.4.1.2 and 7.4.1.3.

7.4.1.1 Interaction

Two or more neighbouring semi-elliptical surface cracks after multiple initiation may show interaction effects. In [34] it is prescribed that two semi-elliptical surface cracks must be recharacterized as one larger crack if the distance s between two defects is smaller than $(\ell_1 + \ell_2)/2$ where ℓ_1 and ℓ_2 are the lengths of the two defects (figure 7-9a). For two equal semi-elliptical cracks this means that they have to be recharacterized as one crack (with depth $a^* = a$ and half the width $c^* = 3c$) if the distance between the initiation points $d \leq 4c$ (figure 7-9b). In [32, 35] it is argued on the basis of experiments, that this recharacterization rule is over-conservative for fatigue crack growth. It is advised to consider fatigue cracks to behave independently until they touch.

Recharacterization as one crack (with depth a and half the width $c^* = 2\ c$) is determined by $d \leq 2c$ (figure 7-9c). This approach is supported by the fact that two fatigue cracks usually do not grow in the same plane which means that interaction is less severe than for the case where they do grow in one and the same plane. Furthermore, if cracks grow in one and the same plane, interaction effects are noticeable only for $a/c < 1$ when the cracks almost touch, as can be seen in figure 7-10 taken from [36]. The recharacterization rule of figure 7-9c is adopted here.

It should be noted that in the case of fracture toughness assessments, the over-conservatism in the recharacterization rules of [34] may be less critical. For fatigue however, these rules seem to be on the very safe side and two cracks may be assumed to behave independently until they touch (figure 7-9c) and coalesce. In [31] it is argued that crack growth of multiple initiated cracks and coalescence must be taken into account in order to describe crack shape development correctly. In the next two sections, two methods of incorporating these phenomena are considered.

7.4.1.2 Independent growth, coalescence, discrete crack width increase

In this section a model describing Multiple Initiation of cracks which grow independently followed by Coalescence and Single crack growth is described: MICS.

Based upon the conclusion of section 7.4.1, the single fatigue crack growth model has been extended as indicated in [32]. Two or more cracks are assumed to grow independently after multiple initiation (figure 7-11a) until they coalesce (figure 7-11b) after which they grow further as one crack (figure 7-11c). The coalescence criterion of figure 7-9c has been incorporated into the model. All multiple initiated cracks are assumed to have the same dimensions and they are assumed to have the same intermediate distance which means that at coalescence the crack width increases discretely from half crack width c into $c^* = kc$ where k is the number of initiation points. For the situation where two cracks are present, such a model has been applied successfully in [32]. However, a disadvantage of a model like this is that the number of initiation points and the distance between initiation points have to be known as input parameters. Therefore, the model seems to be less suitable for fatigue life prediction. However, for calculation of the remaining life of a cracked joint, where the number of initiation points and the distance between them can be measured, the model may be useful.

A refinement of the model described in this section is a local finite width correction (LFW). In the stage before coalescence (figure 7-11a), some interaction effects can be taken into account by assuming that the local finite width for each crack is equal to the distance between initiation points: LFW = d. This is indicated in figure 7-11a by the dashed local finite width. In fatigue crack growth calculations this assumption turned out to be of little importance and therefore it is left out of consideration.

In finite width plates, finite width corrections are applied as if each crack was located in the middle of the plate since no information is available on eccentrically located cracks in finite width plates.

7.4.1.3 Forcing functions

A different approach to Multiple Initiation and coalescence is the use of Forcing Functions: MIFF. These forcing functions prescribe crack shape as a function of crack depth. In fact crack growth in width direction is made dependent on crack growth in depth direction by the use of forcing functions.

Forcing functions can be obtained from test results only. All experimental parameters like e.g. specimen geometry and loading conditions that influence crack shape development also affect the forcing function. If multiple initiation followed by coalescence occurs, this is included in the forcing function. If there are interaction effects before coalescence, they are included as well. This seems to be a strong point of crack growth models that use forcing functions. However, it is simultaneously a weak point since for all combinations of parameters that influence crack shape development, different forcing functions apply and should be derived. Therefore, a classification of crack growth problems should be made with a forcing function per class. A forcing function for T-plate joints in bending would be different from a forcing function for tubular T-joints under out of plane bending loading, etc. So far, only incidentally forcing functions have been presented in literature.

In [30] a forcing function for T-plate joints in bending has been derived. The number of initiation points increases with increasing stress range and plate thickness and this affects the forcing function which depends on stress range and plate thickness as well. This forcing function [30] is:

$$\frac{a}{c} = e^{-ka} \tag{7.6}$$

where:

$$k = k_{ref} \left(\frac{\Delta\sigma_b}{\Delta\sigma_{ref}}\right)^2 \left(\frac{T}{T_{ref}}\right)^{0.5} \geq 0.2 \tag{7.7}$$

The reference values provided in [30] are $k_{ref} = 0.2\ mm^{-1}$, $\Delta\sigma_{ref} = 116\ N/mm^2$ and $T_{ref} = 26$ mm. The value of k shall never be lower than 0.2 which corresponds to low stress levels where only a few crack initiation points are present with large intermediate distances. The eqns. (7.6) and (7.7) have been derived for plate-thicknesses ranging from 16 mm to 103 mm and nominal bending stresses ranging from 100 N/mm^2 to 200 N/mm^2.

Use of forcing functions for welded tubular joints to account for crack growth at low aspect ratios as observed in tests is advised in [33] where forcing functions are given qualitatively in the form of a figure. Also in [31] a similar figure is shown (figure 7-12).
Experimental results confirm these figures [50, 37]. In [37] forcing functions for tubular X-joints loaded by in plane bending moments are given. The following empirical equation appears to describe crack shape quite well:

$$a = \exp\left(3.1244 + 1.035 \times 10^{-2}\ T + 2.2656 \ln \frac{2c}{d}\right) \tag{7.8}$$

where d is the brace diameter. In the forcing functions of [37] the crack coalescence part of figure 7-12 is neglected which corresponds to a recommendation in [33]. To the knowledge of the authors, other forcing functions for welded tubular joints than those in [37] are not available in literature at present.

7.4.2 Calculation procedure

To carry out the fatigue crack growth calculations the computer program FAFRAM [28] was modified. The normal calculation procedure is given in Appendix C and will not be repeated here. Only the consequences of modelling multiple initiation and coalescence are briefly discussed.

For the MICS model described in section 7.4.1.2 the crack width is discretely increased when the criterion for crack coalescence of figure 8c is fulfilled. Until coalescence cracks grow independently.

For the MIFF model that uses forcing functions, described in section 7.4.1.3, crack width increments are not determined by a calculated SIF, but they are determined directly from the forcing functions.

7.4.3 Calculations for a T-plate joint

The models discussed in the previous sections have been applied to a T-plate joint.

The T-plate joint considered is specimen TBB2 of [38]. The geometry, consisting of a 160 mm thick plate having a 45 mm thick attachment, is shown in figure 7-13. The joint has been loaded in four point bending with a nominal bending stress range $\Delta\sigma_b = 70$ N/mm^2. The number of cycles at which the crack width is equal to the width of the specimen is $n_2 = 2250$ kcycles. The number of cycles at the end of the test is $n_3 = 2696$ kcycles, corresponding to a crack depth at which net section yielding occurs. Crack marking results are shown in figure 7-14. From this figure it can be concluded that cracks initiate over a distance of 320 mm. About at least 14 initiation points can be distinguished from the first crack mark, corresponding to a mean distance between initiation points of $d \simeq 23$ mm. A closer investigation of the cracked surface gives an estimated number of initiation points $k = 34$ at a mean intermediate distance $d \simeq 9.5$ mm.

Fatigue crack growth calculations are carried out for this T-plate joint with the following models:

1. The Straight Fronted Crack model of figure 7-15 (2D approach).
2. The Multiple Initiation model of section 7.4.1.2, consisting of Coalescence of independently growing cracks followed by growth as one Single crack (MICS). The two estimates regarding initiation discussed before are considered:
   a. k = 34, d = 9.5 mm;
   b. k = 14, d = 23 mm.
3. The Multiple Initiation model of section 7.4.1.3 with the Forcing Function of eqns. (7-6) and (7-7) (MIFF).
4. The Single Initiation model with crack growth due to calculated SIFs in both directions and considering just one single crack (SI).

For all calculations the initial crack dimensions are taken $a_i = c_i = 0.5$ mm; the constants C and m in the Paris relation are taken $C = 0.24 \times 10^{-12}$, $m = 3$ for as welded joints [39]. The crack depth at which the calculation is stopped is $a_f = 0.9$ T. Before this value is reached, the crack width in the calculations 2 to 4 has reached a value equal to the total plate width. From this moment on, until the crack depth reaches a_f, the crack is treated as a straight fronted crack (SFC).

The results of the calculations are presented in the figures 7.16 to 7.18 where also the test results are given. In figure 7.16 the crack depth a is given as a function of the number of load cycles n. In figure 7.17 half the crack width is given as a function of the number of load cycles n. In figure 7.18 the aspect ratio a/c is given as a function of the relative crack depth a/T.

7.4.4 Discussion of results

From figure 7.16 it can be concluded that decreasing the number of initiation points results in an increase of calculated fatigue life. In that case, the straight fronted crack model (SFC) should be regarded as crack growth after an infinite number of initiations have occurred along the total plate width.

The SFC model (n_3 = 1910 kcycles) gives a very conservative estimate of the fatigue life compared with the experimental result (n_3 = 2696 kcycles). The SI model (n_3 = 2866 kcycles) gives an unconservative result. The same holds for the MIFF model. It should be noted that the geometry of specimen TBB2 does not belong to the class of geometries for which the forcing functions of eqns. (7.6) and (7.7) were derived. With eqn. (7.7) k is calculated for specimen TBB2 which results in k = 0.2. According to [30] k = 0.2 corresponds to low stress levels where only a few crack initiation points are present. This is obviously not true for specimen TBB2. The results obtained by using the MIFF model are therefore not valid. This supports the conclusion that a forcing function should only be used to analyse geometries that belong to the class of geometries for which the forcing function was derived. The MICS models appear to predict fatigue life very well: n_3 = 2342 kcycles for k = 34 and d = 9.5 mm and n_3 = 2487 kcycles for k = 14 and d = 23 mm. Furthermore they give the best approximation of the experimental a - n results in figure 7.16.

The number of cycles at which the crack width equals the plate width is predicted very accurately by these models: n_2 = 2169 kcycles and n_2 = 2329 kcycles respectively, compared with the experimental result n_2 = 2250 kcycles. In figure 7.17 it appears that the MICS models predict crack growth in width direction reasonably well. The model with k = 34 and d = 9.5 mm seems to be slightly better than the one with k = 14 and d = 23 mm. In the experiment the crack width increase is more gradual than the discrete crack width increase given by the MICS models.

Crack aspect ratio a/c is predicted very well by the MICS models as is shown in figure 7.18.

If the MICS model is applied to specimen TBB1, which has the same dimensions as specimen TBB2 but which is subjected to $\Delta\sigma_b$ = 120 N/mm^2, then the predicted numbers of cycles (n_2 = 430 kcycles, n_3 = 465 kcycles) agree very well with the experimental ones (n_2 = 350 kcycles, n_3 = 453 kcycles). Again k = 34 and d = 9.5 mm has been used. However, it may be expected that the number of initiation points is greater for TBB1 than for TBB2 since the stress level in TBB1 is higher than in TBB2.

This would tend to reduce the predicted number of cycles resulting in even better agreement between model and test.

It can be concluded that the MICS model gives a good prediction of fatigue crack growth in welded T-plate joints.

7.4.5 Summary and conclusions

The fatigue crack growth model for single semi-elliptic cracks at the toe of a weld in T-plate and tubular T-joints has been extended to include multiple initiated cracks and coalescence of these cracks. Two different approaches have been discussed:

. A model that describes independent fatigue crack growth of multiple initiated cracks which coalesce.
. A model that makes use of forcing functions for crack shape development.

A disadvantage of the former approach is that the number of initiation points and the mean intermediate distance of these initiation points should be known. A disadvantage of the latter approach is that forcing functions should be experimentally determined for various classes of welded joints. The fatigue crack growth models have been applied to T-plate joints in bending. From the fatigue crack growth calculation results, the following conclusions were drawn:

- The fatigue crack growth models that include multiple initiation and coalescence predict fatigue crack growth better than the model for single semi-elliptical cracks in welded joints.
- The model that describes independent fatigue crack growth of multiple initiated cracks which coalesce, predicts fatigue crack growth in T-plate joints very well.
- The model that makes use of forcing functions is able to predict fatigue crack growth in welded joints only if these joints belong to the class of joints for which the forcing function was derived.
- A correct forcing function gives good fatigue crack growth predictions only if stress intensity factors are used that take the complex stress field in welded tubular joints into account.

7.5 The influence of grinding on T-plate joints

Fatigue crack growth calculations have been made for T-plate joints. The results are compared with experimental results of the Dutch first phase ECSC programme [1].

The crack propagation constants used in the Paris relation are from the mean crack growth line of the draft chapter for fatigue of the new IIW document [45]. So:

$$m = 3 \quad \text{and} \quad C = 1.832\ 10^{-13} \quad \text{(units N and mm)} \tag{7.9}$$

The crack growth calculations were carried out for the T-joints (loaded in bending) with a semi-elliptical crack at the weld toe.
The initial crack dimensions were assumed to be as follows:

$$a_i = 0.15 \text{ mm} \quad \text{and} \quad c_i = 0.15 \text{ mm} \tag{7.10}$$

These dimensions are comparable with a small undercut.
For M_m and M_b the formulas of Newman and Raju [13] are used. M_k is determined with eqn. (7.1).
Two calculations are made for each geometry. In the first calculations the 2D M_k value are used without any correction for the 3D geometry. In the second calculations the 2D M_k values are reduced by using a reduction factor (ω) (see section 4.3.2).
For the depth direction $\omega_{b,a} = 0.9$
For the width direction $\omega_{b,c} = 0.8$
The welded T-joints are tested in as-welded and in ground condition. For the as-welded joints a weld toe radius of 0 is used, while the ground weld toe had a radius of $\rho = 4$ mm. The weld toe angle is $\theta = 70°$. The results of the calculations and the experiments are given in figure 7.19. The theoretical lifetime of the second calculation with the reduction factors is in good agreement with experimental results.
Both calculations give a good estimation of the beneficial effect due to grinding.

7.6 The influence of thickness on T-plate joints

Another set of calculations on T-plate joints was made to investigate the influence of the thickness. These results are compared with experiments reported by Van Leeuwen et al. [43].
T-joints with thicknesses of 16, 25, 40 and 70 mm were loaded in bending. The weld toe angle is 60°. The other parameters are the same as in 7.5.

The results of the calculations and the tests are given in fig. 7.20. Again the results of the calculations with the reduction factor are in good agreement with the test results. Both calculations show the same thickness effect as the tests at 120 and 200 N/mm². The deviations from a straight line a 200 N/mm² are, according to the authors [43], caused by plasticity at the weld toe. The relation between plate thickness and stress range can be given with eqn. (7.11).

$$\Delta\sigma_1/\Delta\sigma_2 = (T_1/T_2)^{\alpha} \qquad (7.11)$$

The DOE Guidance [42] gives $\alpha = -0.25$. An evaluation of tubular joint test data by Van Delft et al. [40] shows that $\alpha = -0.45$. The α values of the present calculations are given in table 7-4. In general the α values are greater than -0.2. This is in agreement with the reduction exponents found with 2D crack growth calculations [41]. So this 3D fracture mechanics analysis showed less thickness effects than given by the DOE Guidance [42] and by Van Delft et al. [40], but the direct comparison of fracture mechanics analysis and test results of the same geometry shows a good agreement.

8. CONCLUSIONS

The fracture mechanics part of the ECSC-SMOZ programme "Fatigue behaviour of welded joints in offshore steel structures" can be summarized with the following concluding remarks:(The remarks are given in a logical order. They can be divided in programme or procedure (P) remarks, in results (R) got from the research carried out and in conclusions (C) based on the investigations):

P - Experimental and analytical work has been carried out with regard to the fatigue behaviour of two dimensional geometries with an edge crack and of three dimensional geometries with a semi-elliptical surface crack. Some of the geometries were provided with a weld shape.

P - The specimens were manufactured out of one thick plate. So no weld irregularities were present in the specimens.

P - All experiments were carried out in a four point bending.

P - The experimental results were reported numerically and graphically. The relation between cycles (N) and the crack dimensions (crack depth a and crack width c) are given.

P - The material properties (da/dN-ΔK curve) were determined from small prismatic specimens (single edge notched specimens).

P - Finite element calculations were carried out with the computer program DIANA to determine the stress intensity factors of the cracked geometries. All calculations were carried out for the bending and for the membrane loadcase.

P - The calculation procedure was based on the energy method. The strain energy release rate was calculated with a virtual crack extension method.

C - An assumed quadratic distribution of the strain energy release rate along one element at the crack front gives a more accurate stress intensity factor for a (semi-) elliptical crack than an assumed linear distribution.

R/C - Analytical expressions for the stress intensity factor of an edge crack in a two dimensional strip were developed from the DIANA results. These expressions agree very well with expressions found in the literature.

R - The influence of the weldshape on the stress intensity factor was expressed separately by a stress intensity concentration factor (M_k). Analytical expression of M_k were developed for the 2D geometries.

R - The influence of the relative weld toe radius in 2D geometries was generalized in an analytical expression.

P - The formulas of Newman and Raju are used for a surface notch in a flat plate.

C - The influence of the weld geometry on the stress intensity factor is smaller for a 3D geometry (semi-elliptical crack) than for a 2D geometry (constant depth edge crack).

P - The Paris-Erdogan relation was used as a crack growth model.

P - An evaluation was carried out by comparing the experimental and analytical results.

C - The 2D geometries with a weld shape showed a good agreement with the crack growth rate curve of the basic specimens.
Due to the fact that at low ΔK values the data points are below the da/dN-ΔK curve, the analytical lifetime underestimates the experimental lifetime.

C - The flat plates with a surface crack showed good agreement in the depth direction in the da/dN-ΔK curve evaluation.
In the width direction the experimental crack growth rate was lower than the one of the da/dN-ΔK curve of the basic specimens.
Therefore analytical lifetime underestimates the experimental lifetime.

C - The growth of surface cracks in plates with a weld geometry showed a poor correlation with the da/dN-ΔK curve of the basic specimens. The evaluation was based on the Newman-Raju plate stress intensity factor combined with a 2D M_k solution.
The use of 3D stress intensity factors determined with DIANA showed a significant improvement in the correlation.
The lifetime calculations give conservative to very conservative results.
The reason for this decreapancy is not clear. Possible causes can be:
. change in stress state (plane strain in the depth and plane stress in the width direction).
. crack closure due to larger plastic strains at the surface notch.
Further investigation of the available information will be necessary in the future to solve the remaining questions.

R - The information with regard to stress intensity factors for welded joints was extended by information available in recent literature.

C - An application to a welded tubular joint showed no improvement with regard to an earlier developed more simple model.

C - The fracture mechanics model was extended for multiple initiated cracks. The extended model predicts the fatigue crack growth in a plate joint better than the single initiation model.

C - The calculation results for predicting the influence of grinding and of the thickness effect are in good correlation with experimental results.

REFERENCES

[1] Back, J. de, Vaessen, G.H.G., 'Fatigue and corrosion fatigue behaviour of offshore steel structures'.
Final report in ECSC-convention 7210-KB/6/602 (J.7.1 f/76)
Delft/Apeldoorn, April 1981.

[2] Back. J. de, Vaessen, G.H.G., 'Effect of plate thickness, temperature and weld toe profile on the fatigue behaviour of welded offshore structures'.
Final report in ECSC-convention 7210-KG/601 (F7.4/81)
Delft/Apeldoorn, May 1984.

[3] Kuijpers, T.B.A., 'Groei van elliptische scheuren door vermoeiing vanuit een, met een hoeklas vergelijkbare, spanningsconcentratie; Meetrapport van de in het kader van het SMOZ-III breukmechanica-project uitgevoerde experimenten'.
Rapport LSF 88-L173, faculteit Werktuigbouwkunde-vakgroep WOC, Technical University Eindhoven, January 1988.

[4] Wildschut, H., 'Fatigue crack growth tests in the framework of the research programme 'Fatigue behaviour of welded joints in offshore steel structures', performed in ECSC-Convention 7210 KG/602 (F7.5/84)'.
TNO-MI report 88M/03935/WID/VLT, March 1988.

[5] Snijder, H.H., 'Finite element calculations for determining the stub height of specimens'.
SMOZ-III, fracture mechanics, BR-85-09, TNO-IBBC, April 1985.

[6] Snijder, H.H., Dijkstra, O.D., 'Stress intensity factor calculations with the finite element program DIANA for the fracture mechanics part of the 3rd phase ECSC-SMOZ project 'Fatigue behaviour of welded joints in offshore structures'.
TNO-IBBC report BI-88-138/63.5.5860, October 1988.

[7] Borst, R. de, Kusters, G.M.A., Nauta, P., Witte, F.C. de, 'DIANA - A comprehensive but flexible finite elements system'. Finite Element Systems Handbook, edited C.A. Brebbia, Springer Verlag, Berlin, 1985.

[8] Rooke, D.P., Cartwright, D.J., 'Compendium of stress intensity factors'. Her Majesty's Stationary Office, London, UK 1976.

[9] Snijder, H.H., Dijkstra, O.D., 'Stress intensity factors for semi-elliptical surface cracks - Comparison of solutions available in literature'. Report no. B-86-198/63.5.5860.310, TNO-IBBC, Rijswijk (ZH), The Netherlands, 1986.

[10] Straalen, IJ.J. van, Dijkstra, O.D., Snijder, H.H., 'Literature survey into stress intensity factor solutions of semi-elliptical surface cracks in plane plates and welded joints'. Report no. BI-88-012/63.8.0310, TNO-IBBC, Rijswijk (ZH), The Netherlands.

[11] Straalen, IJ.J. van, Dijkstra, O.D., Snijder, H.H., 'Stress intensity factors and fatigue crack growth of semi-elliptical surface cracks at weld toes'. Paper to be presented at WELDTECH 88 - International Conference on Weld Failures, London, UK, 22-25 November 1988.

[12] Raju, I.S., Newman, J.C., 'An empirical stress intensity factor equation for the surface crack'. Engineering Fracture Mechanics, Vol. 15 (1981), pp. 185-192.

[13] Newman, J.C., Raju, I.S., Stress intensity factor equations for cracks in three-dimensional finite bodies subjected to tension and bending loads'. NASA TM 85793, Langley Research Center, Virginia, April 1984.

[14] Austen, I.M., 'Factors affecting corrosion fatigue crack growth in steels'.
European Offshore Steels Research Seminar, paper 14, Cambridge, UK, 27-29 November 1978.

[15] Schijve, J., 'Four lectures on fatigue crack growth'.
Delft University of Technology; Department of Aerospace Engineering, Report LR-254, October 1977.

[16] Engesvik, K.M., 'Analysis of uncertainties in the fatigue capacity of welded joints'.
The Norwegian Institute of Technology, Trondheim; Department of Marine Technology, Report UR-82-17, December 1981.

[17] Schijve, J. et.al., 'Vermoeiing van constructies'.
Post-graduate course Delft/Eindhoven, March 1982.

[18] Ritchie, R.O., 'Influence of microstructure on near-threshold fatigue-crack propagation in ultra-high strength steel'.
Metal Science, Vol 11, nrs 8 and 9, August/September 1977, pp 368-381.

[19] Wildschut, H., 'Literatuuronderzoek met betrekking tot levensduurberekeningsmethoden gebaseerd op de breukmechanica'.
Marien Technologisch Speurwerk betreffende onderzoek op het gebied van de levensduur van offshore-constructies (MaTS 21-2); eindrapportage eerste fase, Rapport 79M/35/010645, Metaalinstituut TNO, 19 October 1979.

[20] Irving, P.E., McCartney, L.N., 'Prediction of fatigue crack growth rates; theory, mechanisms, and experimental results.'
Metal Science, Vol 11, nrs 8 and 9, August/September 1977, pp 351-361.

[21] Johnson, R., Bretherton, I., Tomkins, B., Scott, P.M., Silvester, D.R.V., 'The effect of sea water corrosion on fatigue crack propagation in structural steel'.
European Offshore Steels Research Seminar, paper 15, Cambridge, UK, 27-29 November 1978.

[22] Snijder, H.H., Dijkstra, O.D., Eikhof, J. v.d., Delft, D.R.V. van, 'Inventory of fatigue crack growth models'.
CIAD report, chapter 6 (draft).

[23] Beevers, C.J., 'Fatigue crack growth characteristics at low stress intensities of metals and alloys'.
Metal Science, Vol 11, nrs 8 and 9, August/September 1977, pp 362-367.

[24] Ewalds, H.L., Wanhill, R.J.H., 'Fracture Mechanics'.
Edward Arnold; Delftse Uitgevers Maatschappij Delft, 1984.

[25] McEvily, A.J., 'Current aspects of fatigue'.
Metal Science, Vol 11, nrs 8 and 9, August/September 1977, pp 274-284.

[26] Burck, L.H., 'Fatigue growth of surface cracks in bending'.
Engineering Fracture Mechanics, Vol 9, 1977, pp 389-395.

[27] Scott, P.M., Thorpe, T.W., 'A critical review of crack tip stress intensity factors for semi-elliptic cracks'.
Fatigue of Engineering Materials and Structures, Vol 4, nr. 4, 1981, pp 291-309.

[28] Snijder, H.H., Dijkstra, O.D., 'FAFRAM - Computer program for the evaluation of FAtigue behaviour of structures using FRActure Mechanics'.
TNO-IBBC report BI-85-102, Rijswijk, The Netherlands, 1985.

[29] Delft, D.R.V. van, Dijkstra, O.D., Snijder, H.H., 'The calculation of fatigue crack growth in welded tubular joints using fracture mechanics'.
18th Offshore Technology Conference, OTC 5352, Houston, 1986.

[30] Vosikovsky, O., Bell, R., Burns, D.J., Mohaupt, U.H., 'Fracture mechanics assessment of fatigue life of welded plate T-Joints including thickness effect, behaviour of offshore structures'.
Elsevier, Amsterdam, 1985, pp 453 - 464.

[31] Hudak, S.J., Burnside, O.H., Chan, K.S., 'Analysis of corrosion fatigue crack growth in welded tubular joints'.
16th OTC Conference, Houston, OTC 4771, 1984.

[32] Morgan, H.G., 'Interaction of multiple fatigue cracks, paper 35, Preprints of the International Conference 'Fatigue of Welded Constructions'.
Brighton, UK, 7 - 9 April 1987, The Welding Institute.

[33] Burns, D.J., Lambert, S.B., Mohaupt, U.H., 'Crack growth behaviour and fracture mechanics approach'.
Steel in Marine Structures, edited by C. Noordhoek and J. de Back, Elsevier, 1987, pp 137 - 160.

[34] British Standards Institution, PD 6493, 'Guidance on some methods for the derivation of acceptance levels for defects in fusion welded joints', 1980.

[35] Morgan, H.G., 'Fatigue crack shape Development in cracked plates and welded joints'.
Int. Conference on 'Fatigue and crack growth in offshore structures', Proceedings of the Inst. of Mech. Engineers, edited by W.D. Dover, G. Glinka, A.G. Reynolds, London, 1986, pp 59-68.

[36] Stress Intensity Factors Handbook, 2 Volumes, Editor-in-Chief Y. Murakami, Pergamon Press.

[37] Bignonnet, A., Lieurade, H.P., Siscon, Y., Lebrun, J.L., 'Experimental study on fatigue crack propagation in welded tubular connections'.
Fatigue 84, editor C.J. Beevers, EMAS, 1984.

[38] Noordhoek, C., Delft, D.R.V. van, Verheul, A., 'The influence of plate thickness on the fatigue behaviour of welded plates up to 160 mm with an attachment or butt weld'.
Steel in Marine Structures, edited by C. Noordhoek and J. de Back, Elsevier, 1987, pp 281 - 301.

[39] Maddox, S.J., 'The effect of plate thickness on the fatigue strength of fillet welded joints'.
The Welding Institute, Cambridge, 1987.

[40] Delft, D.R.V. van, Noordhoek, C. and Back, J. de, 'Evaluation of the European fatigue test data on large-size welded tubular joints for offshore structures'.
OTC 4999, 1985.

[41] Dijkstra, O.D., Snijder, H.H., Overbeeke, J.L., Wildschut, H., 'Prediction of fatigue crack growth for welded joints using stress intensity factors determined by FEM calculations'.
Steel in Marine Structures, edited by C.Noordhoek and J. de Back, Elsevier, pp 885-899, 1987.

[42] Guidance on design and construction, New fatigue design guidance for steel welded joints in offshore structures, Department of Energy, December 1983, Issue P.

[43] Leeuwen, J.L. van , Overbeeke, J.L., Scholte, H.G. and Wildschut, H., 'Effect of plate thickness, temperature and weld profile on the fatigue and corrosion fatigue behaviour of welded offshore structures', Part I'.
Small scale tests ECSC CONVENTION 7210-KG/601 (F7.4/81) coordinated by J. de Back and G.H.G. Vaessen, 1984.

[44] Straalen, IJ.J. van, 'Finite element calculations to obtain stress intensity factors of a curved crack in a finite width strip with stub - Calculations with DIANA for specimen C-1-1 of the SMOZ fracture mechanics programme".
Report no. BI-88-013/63.8.0310, TNO-IBBC, Rijswijk, The Netherlands, 1988.

[45] The application of an engineering critical assessment in design, fabrication and inspection to assess the fitness-for-purpose of weld products.
Draft Chapter on Fatigue Proposed by Commission XIII Working Group 4, IIW-XIII-1268-88.

[46] Maddox, S.J., Lechocki, J.P., Andrews, R.M., 'Fatigue analysis for the revision of PD 6493: 1980'.
The Welding Institute Report 3873/1/86, Cambridge, 1986.

[47] Smith, I.J. and Hurworth, S.J., 'The effect of geometry changes upon the predicted fatigue strength of welded joints'.
The Welding Institute Report 7819.01/84/394.3, Cambridge, 1984.

[48] Scott, P.M., Thorpe, T.W., 'A critical review of crack tip stress intensity factors for semi-elliptic cracks'.
The Int. Journal 'Fatigue and engineering materials and structures', 1981, Vol. 4, no. 4, pp. 291-309.

[49] Maddox, S.J., 'An analysis of fatigue cracks in fillet welded joints'.
Welding Institute report E/49/72.

[50] Connolly, M.P., Dover, W.D., 'On the fracture mechanics analysis of Tubular joints'.
Offshore Mechanics and Arctic Engineering - OMAE 1987, Houston, pp. 287-293.

TABLES

LIST OF TABLES

AUFSTELLUNG DER TABELLEN

LISTE DES TABLES

Table 2-1: Survey of geometry types

	2D geometry	3D geometry
	edge crack	semi-elliptical crack
without weld shape	A-type	B-type
with weld shape	C-type	D-type

Table 3-1 : Test results specimen A-1

N_t [x 10^3]	a [mm]	ΔK [$Nmm^{-3/2}$]	$\bar{\Delta K}$ [$Nmm^{-3/2}$]	$\Delta a/\Delta N_t$ [10^{-6}mm/c]
0	6.2	198.6		
492.8	7.2	212.9	205.8	2.03
881.3	8.12	225.3	219.1	2.37
1492.9	9.14	238.4		
1827.5	10.06	249.8	244.1	2.75
2156.1	11.03	261.5	255.7	2.95
2367.3	12.25	276.0	268.8	5.78
2839.1	13.06	285.4		
3061.8	14.02	296.5	291.0	4.31
3235.9	15.03	308.2	302.4	5.80
3376.9	16.03	319.8	314.0	7.09
3895.2	17.20	333.4		
4026.6	18.20	345.2	339.3	7.61
4167.3	19.33	358.7	352.0	8.03
4254.8	20.36	371.2	365.0	11.77
4415.1	21.18	381.3		
4505.4	22.22	394.4	387.9	11.52
4575.2	23.10	405.7	400.1	12.61
4664.1	24.30	421.6	413.6	13.50
4795.4	25.12	432.7		
4852.4	26.07	445.9	439.3	16.67
4931.5	27.30	463.6	454.8	15.55
4973.9	28.20	477.1	470.4	21.22
5125.9	29.18	492.3		
5151.8	30.00	505.4	498.8	31.66
5199.6	31.25	526.3	515.8	26.15
5238.6	32.25	543.8	535.1	25.64
5295.4	33.40	565.0		
5324.6	34.51	586.6	575.8	38.01
5356.4	35.75	612.2	599.4	38.99
5422.1	37.57	652.9		
5440.1	38.75	681.5	667.2	65.56
5454.1	39.70	706.0	693.8	67.86
5467.3	40.84	737.2	721.6	86.36

Table 3-2a: Test results specimen A-2

N_t [x 10^3]	a [mm]	ΔK [$Nmm^{-3/2}$]	$\bar{\Delta K}$ [$Nmm^{-3/2}$]	$\Delta a/\Delta N_t$ [10^{-6}mm/c]
22.1	6.15	394		
			403	19.10
72.1	6.73	411		
			419	11.50
122.1	7.31	427		
			438	15.10
172.1	8.06	448		
257.1	8.45	458		
			463	18.75
277.1	8.83	468		
			474	18.00
302.1	9.28	479		
			484	18.00
322.1	9.64	488		
			493	17.75
342.1	9.99	497		
412.1	10.37	506		
			514	21.83
442.1	11.03	522		
			530	21.83
472.1	11.68	537		
			542	21.25
492.1	12.08	547		
542.1	12.49	556		
			562	25.75
562.1	13.00	568		
			575	27.75
582.1	13.56	581		
			587	26.75
602.1	14.09	593		
712.1	14.55	603		
			612	36.75
732.1	15.28	620		
			629	36.50
752.1	16.01	637		
792.3	16.55	649		
			654	45.5
802.3	17.00	659		
			666	52.0
812.3	17.52	672		
			678	49.5
822.3	18.02	683		
			690	53.5
832.3	18.55	696		
			703	56.5
842.3	19.12	709		
869.1	19.40	716		
			725	69.5
879.1	20.09	733		
			743	78.5
889.1	20.88	752		
			764	95.0
899.1	21.83	775		
			779	107
902.1	22.15	783		
912.1	22.87	802		
			809	112
917.1	23.43	816		
			824	119
922.1	24.02	832		
			843	137
928.1	24.85	854		
			859	128
931.1	25.23	864		
			871	173
934.1	25.75	878		
			885	150
937.1	26.40	891		

Table 3-2b: Test results specimen A-2
(continued)

N_t [x 10^3]	a [mm]	ΔK [$Nmm^{-3/2}$]	$\bar{\Delta K}$ [$Nmm^{-3/2}$]	$\Delta a/\Delta N_t$ [10^{-6} mm/c]
947.1	26.63	904		
			914	167
951.1	27.34	924		
			934	173
955.1	28.03	944		
			956	195
959.1	28.81	968		
			981	204
963.1	29.63	994		
			1002	230
965.1	30.09	1009		
972.1	30.59	1026		
			1033	200
974.1	30.99	1040		
			1049	240
976.1	31.51	1057		
			1067	267
978.1	32.04	1076		
			1086	263
980.1	32.57	1095		
			1106	287
982.1	33.14	1116		
			1128	297
984.1	33.74	1139		
1000.1	34.20	1158		
			1168	250
1002.1	34.70	1178		
			1193	370
1004.1	35.40	1208		
			1223	335
1006.1	36.11	1238		
			1257	420
1008.1	36.95	1276		
			1296	418
1010.1	37.79	1315		
			1338	450
1012.1	38.69	1360		
			1386	495
1014.1	39.68	1412		
1020.1	40.80	1475		
			1511	590
1022.1	41.98	1546		
			1568	695
1023.1	42.68	1590		
			1612	650
1024.1	43.33	1634		
			1659	715
1025.1	44.04	1683		
			1714	835
1026.1	44.88	1744		
			1840	948
1028.6	47.25	1935		
			1993	1270
1029.6	45.82	2050		
			2126	1395
1030.7	50.05	2202		

Table 3-3a: Test results specimen A-3

N_t [x 10^3]	a [mm]	ΔK [$Nmm^{-3/2}$]	$\bar{\Delta K}$ [$Nmm^{-3/2}$]	$\Delta a/\Delta N_t$ [10^{-6} mm/c]
0	1.52	-		
54.8	1.57	242	246	1.56
121.9	1.68	250	259	2.49
222.3	1.93	267	271	3.64
256.6	2.05	275	282	3.51
319.5	2.25	288	292	6.81
332.6	2.38	296	308	4.36
427.8	2.80	319	331	5.40
511.2	3.25	342	357	6.50
611.2	3.90	372	381	7.60
661.2	4.28	389		
849.8	4.45	414	423	9.47
896.8	5.34	431	440	10.70
941.2	5.81	448	457	11.87
981.2	6.29	465	474	13.63
1021.2	6.83	483	490	15.13
1047.3	7.23	496		
1141.2	7.65	510	518	16.5
1171.2	8.15	525	535	21.3
1201.2	8.79	544	554	21.7
1231.2	9.44	563	574	25.5
1261.2	10.20	585		
1326.2	10.86	603	612	32.7
1346.2	11.52	621	631	36.5
1366.2	12.25	641	651	36.7
1386.2	12.98	661	673	43.3
1406.2	13.85	684		
1442.2	14.35	702	710	60.0
1452.2	15.13	718	727	63.5
1462.2	15.76	735	745	78.0
1472.2	16.54	755	767	87.5
1482.2	17.42	778	785	98.0
1487.2	17.91	792		
1511.2	18.71	813	822	123
1516.2	19.32	830	839	130
1521.2	19.97	847	857	134
1526.2	20.64	866	877	149
1531.2	21.39	887	900	176
1536.2	22.27	912		

Table 3-3b: Test results specimen A-3
(continued)

N_t [x 10^3]	a [mm]	ΔK [$Nmm^{-3/2}$]	$\bar{\Delta K}$ [$Nmm^{-3/2}$]	$\Delta a/\Delta N_t$ [10^{-6} mm/c]
1549.2	23.35	943		
			950	215
1551.2	23.78	956		
			962	190
1553.2	24.16	967		
			974	228
1555.2	24.62	981		
			988	232
1557.2	25.08	995		
			1003	232
1559.2	25.55	1010		
			1018	252
1561.2	26.05	1026		
1570.2	27.04	1069		
			1079	310
1572.2	28.00	1089		
			1100	320
1574.2	28.64	1111		
			1122	315
1576.2	29.27	1133		
			1147	365
1578.2	30.00	1160		
			1173	358
1580.2	30.72	1186		
			1202	423
1582.2	31.56	1218		
			1235	407
1584.2	32.38	1251		
1589.2	34.04	1320		
			1331	495
1590.2	34.54	1342		
			1353	470
1591.2	35.01	1363		
			1376	555
1592.2	35.56	1389		
			1401	495
1593.2	36.06	1413		
			1428	620
1594.2	36.68	1443		
			1459	625
1595.2	37.30	1475		
			1493	690
1596.2	37.99	1511		
			1529	665
1597.2	38.66	1547		
			1569	760
1598.2	39.42	1591		
			1609	775
1599.2	40.04	1627		
1602.7	42.55	1790		
			1829	1140
1603.7	43.62	1867		
			1890	1190
1604.2	44.21	1912		
			1936	1230
1604.7	44.83	1960		
			1990	1450
1605.2	45.55	2019		
			2053	1550
1605.7	46.33	2086		
			2123	1650
1606.2	47.15	2160		
			2205	1900
1606.7	48.10	2250		

Table 3-4: Test results specimen A-5

N_t [x 10^3]	a [mm]	ΔK [$Nmm^{-3/2}$]	$\bar{\Delta K}$ [$Nmm^{-3/2}$]	$\Delta a/\Delta N_t$ [10^{-6}mm/c]
10	2.89	358.9	378.4	4.27
230	4.83	398.0		
100	4.24	373.8	394.8	5.20
300	5.28	415.8		
510	6.16	449.6	467.8	16.17
570	7.13	486.0	509.6	21.00
630	8.39	533.1	555.4	29.25
670	9.56	577.7	600.1	38.00
700	10.70	622.5		
770	12.11	680.9	704.3	70.67
785	13.17	727.7	751.7	102.00
795	14.19	775.7	800.5	140.00
802	15.17	825.3	849.3	146.67
808	16.05	873.2	911.0	210.00
814	17.31	948.7	981.4	245.00
818	18.29	1014.1	1047.3	300.00
821	19.19	1080.4	1120.4	326.67
824	20.17	1160.4	1205.6	396.00
826.5	21.16	1250.8		

Table 3-5: Test results specimen A-6

N_t [x 10^3]	a [mm]	ΔK [$Nmm^{-3/2}$]	$\bar{\Delta K}$ [$Nmm^{-3/2}$]	$\Delta a/\Delta N_t$ [10^{-6}mm/c]
50	2.30	392.6		
150	3.39	467.1	429.8	10.50
200	4.05	510.6	488.9	14.00
250	5.25	579.1	544.9	24.00
270	5.92	615.4	597.2	33.50
310	6.16			
330	7.26	686.3		
345	8.57	755.7	721.0	87.33
355	9.82	823.5	789.6	125.00
361	10.75	875.7	849.6	155.00
377	12.17	959.9		
381	13.11	1019.3	989.6	235.00
385	14.21	1093.7	1056.5	275.00
388	15.16	1163.0	1238.3	316.67
391	16.26	1250.7	1206.9	366.67
393	17.25	1337.6	1294.2	495.00
395	18.23	1432.8	1385.2	490.00
396.5	19.23	1540.8	1486.8	666.67
398	20.45	1690.5	1615.7	813.33
399	21.66	1862.3		

Table 3-6: Survey of crack growth parameters of A specimens

Specimen	C [N, mm]	m [-]
A-1	$0.288\ 10^{-12}$	2.94
A-2	$0.219\ 10^{-13}$	3.32
A-3	$0.425\ 10^{-13}$	3.21
A-5	$0.465\ 10^{-15}$	3.92
A-6	$0.185\ 10^{-13}$	3.35
all	$0.1105\ 10^{-12}$	3.081

Table 3-7: Test results specimen B-1-1

thickness T = 70 mm
width B = 210 mm
stress range $\Delta\sigma$ = 225 N/mm²

number of cycles N_c	crack depth a [mm]	crack width c [mm]
407000.	8.1	9.0
471200.	11.1	13.7
503400.	14.5	17.15
529600.	18.0	22.05
548900.	21.0	27.7
564700.	23.7	32.7
578300.	26.1	37.85
591900.	28.2	42.7
602900.	30.3	48.2
612900.	32.0	53.25
620900.	33.7	58.1
632400.	35.4	62.8
640900.	37.1	69.7
646400.	39.5	75.55

Table 3-8: Test results specimen B-1-2

thickness T = 70 mm
width B = 210 mm
stress range $\Delta\sigma$ = 225 N/mm²

number of cycles N_c	crack depth a [mm]	crack width c [mm]
0.	0.4	5.5
407000.	3.2	6.0
557000.	9.6	11.4
605000.	13.5	16.3
638000.	17.1	21.7
675000.	21.3	28.4
696000.	24.1	33.8
712000.	26.5	38.8

Table 3-9: Test results specimen B-2-1

thickness T = 40 mm
width B = 120 mm
stress range $\Delta\sigma$ = 203.8 N/mm²

number of cycles N_c	crack depth a [mm]	crack width c [mm]
359750	2.53	5.89
535550	5.04	6.64
659850	7.62	9.51
735100	9.49	12.32
797950	11.58	15.93
843250	13.04	19.33
877300	14.32	22.61
900750	15.68	26.43
922150	16.79	29.92
938150	17.76	33.14
952230	18.74	36.40
963950	19.78	39.83
975250	20.98	43.73
982900	22.21	47.90

Table 3-10: Test results specimen B-2-2

thickness T = 40 mm
width B = 120 mm
stress range $\Delta\sigma$ = 244.5 N/mm²

number of cycles N_c	crack depth a [mm]	crack width c [mm]
0.	.50	6.00
272750.	6.08	8.28
322050.	8.40	11.25
351150.	10.02	13.71
380850.	11.94	17.00
402900.	13.44	20.24
420600.	14.86	23.54
437850.	16.46	27.59
450300.	17.97	31.71
460700.	19.50	36.34

Table 3-11: Test results specimen C-1-1

thickness $T = 70$ mm
weld toe radius $\rho = 0.5$ mm
weld toe angle $\Theta = 70$ deg
stress range $\Delta\sigma = 76$ N/mm²

number of cycles N_c	crack depth a [mm]
200000.	0.65
351000.	1.27
471000.	1.97
658000.	2.97
778000.	3.91
898000.	4.99
1016000.	6.08
1106000.	6.95
1186000.	8.00
1256000.	8.96
1316000.	9.97
1346000.	10.59
1391000.	11.37
1431000.	12.07
1471000.	12.94
1511000.	13.99
1541000.	14.86
1571000.	15.78
1601000.	16.87
1621000.	17.78
1651000.	19.05
1681000.	20.59
1696000.	21.48
1706000.	22.14
1721000.	23.16
1731000.	24.15
1741000.	25.11
1751000.	26.44
1756000.	27.10
1766000.	28.61
1772000.	29.97
1775000.	30.53
1779000.	31.49
1783000.	32.42
1787000.	33.59
1790000.	34.56
1793000.	35.63

Table 3-12: Test results specimen C-1-2

thickness $T = 70$ mm
weld toe radius $\rho = 0.5$ mm
weld toe angle $\Theta = 70$ deg
stress range $\Delta\sigma = 76$ N/mm²

number of cycles N_c	crack depth a [mm]
500000	1.08
655000	1.95
816000	3.02
966000	3.91
1116000	5.07
1194000	5.95
1304000	6.97
1384000	7.95
1464000	8.98
1524000	9.94
1592000	11.01
1657000	12.07
1702000	12.95
1747000	13.96
1792000	15.09
1822000	15.96
1852000	16.80
1892000	18.15
1912000	18.84
1932000	19.67
1957000	20.96
1977000	22.05
1992000	23.07
2002000	23.78
2012000	24.71
2022000	25.71
2032000	26.86
2038000	27.71
2044000	28.75
2050000	29.99
2054000	30.95
2058000	32.02
2062000	33.25
2064000	33.98
2067000	35.02
2069000	35.80
2071000	36.73
2073000	37.77
2075000	38.83
2076500	39.74

Table 3-13: Test results specimen C-1-4

thickness T = 70 mm
weld toe radius ρ = 5.0 mm
weld toe angle Θ = 70 deg
stress range $\Delta\sigma$ = 76 N/mm²

number of cycles N_c	crack depth a [mm]
1000000	1.54
1139000	2.01
1415000	3.04
1625000	4.04
1775000	5.07
1938000	6.10
2058000	7.10
2148000	7.98
2238000	9.04
2298000	9.83
2348000	10.53
2424000	11.68
2474000	12.52
2514000	13.29
2554000	14.11
2599000	15.08
2629000	15.80
2674000	16.97
2714000	18.03
2744000	19.01
2774000	20.06
2794000	21.00
2814000	22.04
2829000	22.88
2844000	23.88
2854000	24.76
2864000	25.67
2874000	26.74
2884000	27.98
2889000	28.79
2894000	29.78
2899000	30.81
2903000	31.84
2906000	32.71
2909000	33.64
2914000	35.57
2916000	36.46
2918000	37.32
2920000	38.43
2922000	39.59

Table 3-14: Test results specimen C-2-1

thickness $T = 40$ mm
weld toe radius $\rho = 0.5$ mm
weld toe angle $\Theta = 70$ deg
stress range $\Delta\sigma = 102$ N/mm²

number of cycles N_c	crack depth a [mm]
111000	0.56
290000	1.08
383750	1.70
443750	2.19
503750	2.79
551970	3.26
581970	3.61
611970	4.08
641970	4.53
671970	5.09
712650	5.92
732650	6.29
762650	7.03
787110	7.66
817110	8.53
837710	9.20
852510	9.73
867510	10.35
882510	11.12
897610	11.86
903530	12.30
911930	12.89
919530	13.50
927530	14.24
930410	14.55
938410	15.53
941410	16.08
944410	16.67
947510	17.32
950410	18.12
951300	18.27
954300	19.12
957300	20.13
958800	20.72
960300	21.52
961300	22.10
962870	22.87
963870	23.60

Table 3-15: Test results specimen C-2-2

thickness T = 40 mm
weld toe radius ρ = 0.5 mm
weld toe angle θ = 70 deg
stress range $\Delta\sigma$ = 102 N/mm²

number of cycles N_c	crack depth a [mm]
101800	0.56
190100	0.90
287600	1.41
356800	2.02
409360	2.51
439360	2.89
469360	3.18
499360	3.61
529360	4.05
568890	4.61
588890	4.95
608890	5.37
648890	6.07
684790	6.79
704790	7.25
724790	7.79
744790	8.29
757070	8.64
772070	9.12
787070	9.63
802070	10.24
818760	10.95
828760	11.48
838760	12.07
848800	12.67
853800	13.22
858800	13.74
863800	14.34
868800	15.14
873190	15.88
876190	16.43
879190	17.09
882190	17.85
884060	18.29
885060	18.61
888060	19.57
889060	19.99
890060	20.38
891400	21.01
892400	21.48
893400	22.01
894400	22.67
895400	23.34

Table 3-16: Test results specimen C-2-3

thickness T = 70 mm
weld toe radius ρ = 0.5 mm
weld toe angle θ = 45 deg
stress range $\Delta\sigma$ = 76 N/mm²

number of cycles N_c	crack depth a [mm]
300000	0.68
375000	1.12
731000	2.00
881000	3.00
1042000	4.10
1162000	5.05
1252000	5.91
1360000	7.08
1420000	7.83
1480000	8.70
1540000	9.61
1610000	10.83
1683000	12.01
1723000	12.82
1763000	13.79
1798000	14.71
1843000	15.98
1873000	17.00
1903000	17.97
1923000	18.76
1943000	19.60
1963000	20.57
1983000	21.74
1998000	22.75
2013000	23.93
2023000	24.86
2033000	26.08
2039000	26.89
2045000	27.84
2051000	28.88
2055000	29.70
2059000	30.61
2063000	31.56
2067000	32.64
2071000	33.87
2074000	34.88
2077000	35.99

Table 3-17: Test results specimen C-2-4

thickness $T = 70$ mm
weld toe radius $\rho = 0.5$ mm
weld toe angle $\theta = 45$ deg
stress range $\Delta\sigma = 76$ N/mm²

number of cycles N_c	crack depth a [mm]
368000	1.09
568000	1.89
732000	2.76
882000	3.74
1002000	4.67
1152000	5.87
1242000	6.70
1332000	7.78
1412000	8.86
1472000	9.79
1512000	10.53
1575000	11.63
1625000	12.65
1670000	13.65
1715000	14.85
1745000	15.66
1775000	16.56
1805000	17.54
1835000	18.66
1855000	19.50
1875000	20.42
1895000	21.51
1910000	22.48
1925000	23.62
1935000	24.53
1945000	25.50
1955000	26.68
1961000	27.50
1967000	28.36
1973000	29.40
1979000	30.52
1983000	31.41
1987000	32.37
1991000	33.46
1994000	34.43
1997000	35.48

Table 3-18: Test results specimen D-1-2

thickness	T	= 70	mm
width	B	= 210	mm
weld toe radius	ρ	= 5.0	mm
weld toe angle	θ	= 70	deg
stress range	$\Delta\sigma$	= 110	N/mm^2

number of cycles N_c	crack depth a [mm]	crack width c [mm]
520000	2.9	5.4
990000	5.6	8.5
1340000	8.4	13.2
1590000	10.6	18.1
1788000	12.7	22.3
1993000	14.4	26.45
2183000	16.2	31.0
2378000	18.0	36.05
2613000	23.3	52.15
2777000	25.8	61.1
2912000	27.8	71.65

Table 3-19: Test results specimen D-2-1

thickness	T	= 40	mm
width	B	= 120	mm
weld toe radius	ρ	= 0.5	mm
weld toe angle	θ	= 70	deg
stress range	$\Delta\sigma$	= 107	N/mm^2

number of cycles N_c	crack depth a [mm]	crack width c [mm]
1519000	6.52	17.23
1882150	7.16	20.77
2219550	8.22	25.66
2500850	9.24	27.41
2798300	10.38	31.46
3128000	11.80	37.36

Table 3-20: Test results specimen D-2-2

thickness	T	= 40	mm
width	B	= 120	mm
weld toe radius	ρ	= 5.0	mm
weld toe angle	θ	= 70	deg
stress range	$\Delta\sigma$	= 116	N/mm^2

number of cycles N_c	crack depth a [mm]	crack width c [mm]
0	.5	5.63
369200	2.51	5.63
767400	3.9	5.63
1124750	4.92	7.54
1500100	6.49	10.14
1789500	7.87	12.61
2097950	8.94	15.80
2353250	9.99	18.98
2607900	11.02	22.56
2799750	11.72	25.90
3017850	13.20	30.35
3150200	14.08	33.55
3257100	14.98	36.81
3357600	15.86	40.70
3432050	16.67	44.54
3484450	17.39	48.08
3519600	18.12	51.95
3538700	18.71	55.58

Table 4-1: Calculated stress intensity factors for A-type geometry
(T = 80 mm)
Load case: b = pure bending, m = membrane

$$G = \frac{K^2}{E}(1 - \nu^2);\ K = M_b\ \sigma\ \sqrt{\pi a}\ \text{or}\ K = M_m\ \sigma\ \sqrt{\pi a};\ \sigma = 1\ N/mm^2$$

crack depth a	a/T	load case	G/2 [10^{-4} N/mm]	K [$Nmm^{-3/2}$]	M_b or M_m
2	0.0250	b	0.159067	2.7195	.0809
		m	0.169053	2.7933	.1144
5	0.0625	b	0.379587	4.1856	1.0561
		m	0.443260	4.5231	1.1412
11	0.1375	b	0.803595	6.0901	1.0360
		m	1.13896	7.2503	1.2334
22	0.2750	b	1.79596	9.1044	1.0951
		m	3.65296	12.9845	1.5619
31	0.3875	b	3.20873	12.1694	1.2331
		m	8.70612	20.0455	2.0312
40	0.5000	b	6.01525	16.6621	1.4864
		m	21.4702	31.4791	2.8081
51.4386	0.6430	b	16.3118	27.4382	2.1586
		m	79.3192	60.5053	4.7601
68.5714	0.8571	b	230.769	103.2031	7.0315
		m	1670.16	277.6406	8.9163

Table 4-2: Parameters of the C-type geometries considered in the stress intensity factor calculations

geometry	weld angle θ [°]	weld toe radius ρ [mm]	plate thickness T [mm]	ρ/T [-]
C-0-1	70	0	70	0
C-1-1	70	0.5	70	0.0071
C-2-1	70	0.5	40	0.0125
C-1-3	70	5.0	70	0.0714
C-0-2	70	5.0	40	0.1250
C-2-3	45	0.5	70	0.0071

Table 4-3: Stress intensity factors calculated with DIANA for geometry C-1-1
Load case b = pure bending, m = membrane

$$G = \frac{K^2}{E}(1 - \nu^2);\ K = Y\,\sigma\,\sqrt{\pi a};\ \sigma = 1\ N/mm^2;\ Y = M\ .\ M_k$$

relative crack depth a/T	load case	G [10^{-4} N/mm]	K [$Nmm^{-3/2}$]	M	M **)	M_k
0 *)	b					4.2 *)
	m					3.6
0.0071	b	0.498413	3.3914	2.7060	1.1099	2.4381
	m	0.377619	2.9520	2.3554	1.1118	2.1185
0.0250	b	0.753117	4.1689	1.7780	1.0809	1.6449
	m	0.625237	3.7985	1.6200	1.1144	1.4537
0.0625	b	1.09094	5.0175	1.3534	1.0561	1.2815
	m	1.06915	4.9672	1.3398	1.1412	1.1740
0.1375	b	1.70596	6.2744	1.1410	1.0360	1.1014
	m	2.19685	7.1202	1.2948	1.2334	1.0498
0.2750	b	3.29427	8.7190	1.1212	1.0951	1.0238
	m	6.49470	12.2425	1.5743	1.5619	1.0079
0.3875	b	5.69088	11.4598	1.2414	1.2331	1.0067
	m	15.2942	18.7868	2.0351	2.0312	1.0019
0.5000	b	10.5439	15.5987	1.4876	1.4864	1.0008
	m	37.3910	29.3746	2.8013	2.8081	0.9976

*) For the uncracked situation the stress concentration factor K_t has been tabulated.

**) Taken from section 4.2.1.

Table 4-4: Stress intensity concentration factors (M_k) for the C-type geometries

geometry		C-0-1	C-1-1	C-2-1	C-1-3	C-0-2	C-2-3
θ		70°	70°	70°	70°	70°	45°
ρ [mm]		0	0.5	0.5	5.0	5.0	0.5
T [mm]		70	70	40	70	40	70
ρ/T [-]		0	0.0071	0.0125	0.0714	0.125	0.0071
a/T [-]	load case *)						
0	b	-	4.2	3.4	1.91	1.65	3.8
	m	-	3.6	3.1	1.79	1.56	3.4
0.0071	b	2.555	2.438	2.329	1.747	1.553	2.250
	m	2.164	2.119	2.068	1.621	1.481	2.036
0.0250	b	1.664	1.645	1.630	1.508	1.415	1.599
	m	1.452	1.454	1.461	1.387	1.329	1.451
0.0625	b	1.289	1.282	1.275	1.265	1.242	1.299
	m	1.173	1.174	1.183	1.175	1.167	1.200
0.1375	b	1.104	1.101	1.101	1.102	1.099	1.113
	m	1.049	1.050	1.050	1.052	1.053	1.055
0.2750	b	1.025	1.024	1.024	1.024	1.024	1.026
	m	1.008	1.008	1.008	1.008	1.008	1.009
0.3875	b	1.007	1.007	1.007	1.007	1.007	1.007
	m	1.002	1.002	1.002	1.002	1.002	1.002
0.5000	b	1.001	1.001	1.001	1.001	1.001	1.001
	m	0.998	0.998	0.998	0.998	0.998	0.997

*) Load case b = pure bending, m = membrane/tension

Table 4-5: Curve fitting coefficients for M_k values of the C-type geometries

geometry			C-0-1	C-1-1	C-2-1	C-1-3	C-0-2	C-2-3
θ			70°	70°	70°	70°	70°	45°
ρ [mm]			0	0.5	0.5	5.0	5.0	0.5
T [mm]			70	70	40	70	40	70
ρ/T [-]			0	0.0071	0.0125	0.0714	0.125	0.0071
region	coefficient	load case						
I	B	b	1.1362	1.0844	1.0051	0.93857	1.1051	1.1549
		m	1.0291	0.98450	0.95712	0.88735	0.55917	1.0477
0 ≤ a/T < 0.025	B	b	0.015011	0.017089	0.021136	0.034400	0.017967	0.013344
		m	0.012040	0.014306	0.016470	0.027978	0.083384	0.012170
	C	b	-.0034398	-.0054849	-.0088258	-.035412	-.032972	-.0050447
		m	-.0034689	-.0054695	-.0076857	-.030996	-.083315	-.0051735
II	A	b	0.88539	0.90441	0.92508	0.88135	0.91392	0.90177
		m	0.93832	0.93563	0.90530	0.89344	0.87639	0.82271
0.025 ≤ a/T < 0.1	B	b	0.031426	0.028889	0.026057	0.037100	0.035634	0.034620
		m	0.016203	0.016549	0.020816	0.024581	0.030448	0.035415
	C	b	-.015361	-.014008	-.011964	-.034205	-.046115	-.024654
		m	-.0065430	-.0069246	-.012460	-.024804	-.042272	-.031368
III	A	b	0.95471					0.95186
		m	0.96858					0.96882
0.1 ≤ a/T < 0.4	B	b	0.019388					0.020127
		m	0.011363					0.011580
	C	b	0.0047441					0.011730
		m	0.0044927					0.0052740

Table 4-6: Weld toe radius influence f_ρ for the bending loadcase, $\Theta = 70°$, C-type specimens

ρ/T	M_k					$f_\rho = M_{k,\rho/T}/M_{k,\rho/T=0}$				
a/T	0.0000	0.0071	0.0125	0.0714	0.1250	0.0000	0.0071	0.0125	0.0714	0.1250
0	-	4.2	3.4	1.91	1.65	-	-	-	-	-
0.0071	2.555	2.438	2.329	1.747	1.553	1.0000	0.9542	0.9115	0.6838	0.6078
0.0250	1.664	1.645	1.630	1.508	1.415	1.0000	0.9886	0.9796	0.9063	0.8504
0.0625	1.289	1.282	1.275	1.265	1.242	1.0000	0.9946	0.9891	0.9814	0.9635
0.1375	1.104	1.101	1.101	1.102	1.099	1.0000	0.9973	0.9973	0.9982	0.9955
0.2750	1.025	1.024	1.024	1.024	1.024	1.0000	0.9990	0.9990	0.9990	0.9990
0.3875	1.007	1.007	1.007	1.007	1.007	1.0000	1.0000	1.0000	1.0000	1.0000
0.5000	1.001	1.001	1.001	1.001	1.001	1.0000	1.0000	1.0000	1.0000	1.0000

Table 4-7: Weld toe radius influence f_ρ for the tension loadcase, $\Theta = 70°$, C-type specimens

ρ/T	M_k					$f_\rho = M_{k,\rho/T}/M_{k,\rho/T=0}$				
a/T	0.0000	0.0071	0.0125	0.0714	0.1250	0.0000	0.0071	0.0125	0.0714	0.1250
0	-	3.6	3.1	1.79	1.56	-	-	-	-	-
0.0071	2.164	2.119	2.068	1.621	1.481	1.0000	0.9792	0.9556	0.7491	0.6844
0.0250	1.452	1.454	1.461	1.387	1.329	1.0000	1.0014	1.0062	0.9552	0.9153
0.0625	1.173	1.174	1.183	1.175	1.167	1.0000	1.0009	1.0085	1.0017	0.9949
0.1375	1.049	1.050	1.050	1.052	1.053	1.0000	1.0010	1.0010	1.0029	1.0038
0.2750	1.008	1.008	1.008	1.008	1.008	1.0000	1.0000	1.0000	1.0000	1.0000
0.3875	1.002	1.002	1.002	1.002	1.002	1.0000	1.0000	1.0000	1.0000	1.0000
0.5000	0.998	0.998	0.998	0.998	0.998	1.0000	1.0000	1.0000	1.0000	1.0000

Table 4-8: Curve fitting coefficients for f_ρ

loading	$A_{\rho 1}$	$A_{\rho 2}$	$A_{\rho 3}$	$B_{\rho 1}$	$B_{\rho 2}$
bending	.70754	-.020160	-.024502	75.323	-1541.7
tension	.71032	-.024015	-.028061	105.29	-1993.8

Table 4-9: Calculation results for specimen D-2-2 with crack I, a = 6.49 mm, c = 10.14 mm; bending

without stub					
node	ϕ [°]	$\Delta P/2$ [Nmm]	$G/2$ [Nmm^{-1}]	K [Nmm$^{-3/2}$]	
1	0.0	-0.891270E-07	0.237008E-04	3.30739	
	5.625		0.203452E-04	3.06433	
2	11.25	-0.163407E-06	0.188614E-04	2.95047	
	16.875		0.183395E-04	2.90936	
3	22.5	-0.163084E-06	0.178362E-04	2.86916	
	28.125		0.174966E-04	2.84171	
4	33.75	-0.174598E-06	0.175146E-04	2.84318	
	39.375		0.176476E-04	2.85396	
5	45.	-0.190986E-06	0.176213E-04	2.85182	
	50.625		0.175767E-04	2.84821	
6	56.25	-0.206551E-06	0.176899E-04	2.85737	
	61.875		0.178223E-04	2.86804	
7	67.5	-0.219630E-06	0.178184E-04	2.86773	
	73.125		0.177959E-04	2.86592	
8	78.75	-0.228156E-06	0.178838E-04	2.87299	
	84.375		0.179935E-04	2.88178	
9	90.	-0.116111E-06	0.180302E-04	2.88473	

with stub					
node	ϕ [°]	ΔP [Nmm]	G [Nmm^{-1}]	K [Nmm$^{-3/2}$]	M_k
1	0.0	-0.300260E-06	0.867187E-04	4.47348	1.35257
	5.625		0.651423E-04	3.87722	1.26527
2	11.25	-0.482120E-06	0.547113E-04	3.55326	1.20430
	16.875		0.501562E-04	3.40213	1.16937
3	22.5	-0.422122E-06	0.461066E-04	3.26190	1.13688
	28.125		0.428658E-04	3.14517	1.10679
4	33.75	-0.408465E-06	0.408992E-04	3.07218	1.08054
	39.375		0.395905E-04	3.02262	1.05910
5	45.	-0.415126E-06	0.382501E-04	2.97102	1.04180
	50.625		0.371204E-04	2.92681	1.02760
6	56.25	-0.426661E-06	0.365031E-04	2.90238	1.01575
	61.875		0.360903E-04	2.88592	1.00623
7	67.5	-0.438420E-06	0.355303E-04	2.86344	0.998504
	73.125		0.350703E-04	2.84484	0.992645
8	78.75	-0.446728E-06	0.349766E-04	2.84104	0.988879
	84.375		0.350501E-04	2.84403	0.986900
9	90.	-0.226074E-06	0.350745E-04	2.84501	0.986231

Table 4-10: Calculation results for specimen D-2-2 with crack I, a = 6.49 mm, c = 10.14 mm; membrane

without stub				
node	ϕ [°]	$\Delta P/2$ [Nmm]	$G/2$ [Nmm^{-1}]	K [$Nmm^{-3/2}$]
1	0.0	-0.993108E-07	0.257342E-04	3.44635
	5.625		0.230032E-04	3.25835
2	11.25	-0.190311E-06	0.220052E-04	3.18689
	16.875		0.219782E-04	3.18493
3	22.5	-0.202643E-06	0.221324E-04	3.19609
	28.125		0.225192E-04	3.22389
4	33.75	-0.231605E-06	0.232173E-04	3.27348
	39.375		0.240535E-04	3.33191
5	45.	-0.269390E-06	0.248361E-04	3.38568
	50.625		0.255868E-04	3.43647
6	56.25	-0.307416E-06	0.263435E-04	3.48691
	61.875		0.270456E-04	3.53307
7	67.5	-0.340363E-06	0.276313E-04	3.57112
	73.125		0.281109E-04	3.60198
8	78.75	-0.362912E-06	0.285002E-04	3.62684
	84.375		0.287581E-04	3.64321
9	90.	-0.185635E-06	0.288447E-04	3.64869

with stub					
node	ϕ [°]	ΔP [Nmm]	G [Nmm^{-1}]	K [$Nmm^{-3/2}$]	M_k
1	0.0	-0.290277E-06	0.817468E-04	4.34335	1.26028
	5.625		0.640090E-04	3.84335	1.17954
2	11.25	-0.488741E-06	0.556872E-04	3.58481	1.12486
	16.875		0.525513E-04	3.48242	1.09341
3	22.5	-0.461172E-06	0.503055E-04	3.40719	1.06605
	28.125		0.489715E-04	3.36171	1.04275
4	33.75	-0.486013E-06	0.486628E-04	3.35110	1.02371
	39.375		0.489616E-04	3.36137	1.00884
5	45.	-0.536337E-06	0.494101E-04	3.37673	0.997357
	50.625		0.499899E-04	3.39649	0.988366
6	56.25	-0.591980E-06	0.507003E-04	3.42054	0.980966
	61.875		0.514356E-04	3.44525	0.975143
7	67.5	-0.641964E-06	0.520834E-04	3.46688	0.970810
	73.125		0.526469E-04	3.48558	0.967684
8	78.75	-0.676959E-06	0.531328E-04	3.50163	0.965477
	84.375		0.534688E-04	3.51269	0.964174
9	90.	-0.345039E-06	0.535815E-04	3.51638	0.963738

Table 4-11: Stress intensity factors (K) of geometry D-2-2 with stub

K in [N/mm$^{3/2}$] for σ_n = 1 N/mm^2

		crack	I	II	III	IV	remark
		a [mm]	6.49	8.95	11.85	16.00	
		c [mm]	10.14	15.80	25.90	40.70	
		0.0	4.47348	5.17115	5.91947	7.91952	surface
		5.625	3.87722	4.31672	4.96683	6.29214	
		11.25	3.55326	3.87889	4.45343	5.48364	
	a	16.875	3.40213	3.71617	4.23748	5.25833	
b	n	22.5	3.26190	3.56313	4.05317	5.05004	
e	g	28.125	3.14517	3.43100	3.90461	4.86126	
n	l	33.75	3.07218	3.34278	3.81419	4.72824	
d	e	39.375	3.02262	3.28154	3.75657	4.62633	
i		45.	2.97102	3.22519	3.69420	4.51356	
n	ϕ	50.625	2.92681	3.17707	3.63444	4.40194	
g		56.25	2.90238	3.14187	3.58705	4.30628	
	(°)	61.875	2.88592	3.11390	3.54671	4.22392	
		67.5	2.86344	3.08577	3.50523	4.14760	
		73.125	2.84484	3.06299	3.47019	4.08389	
		78.75	2.84104	3.05137	3.44941	4.03840	
		84.375	2.84403	3.04713	3.43964	4.01175	
		90.	2.84501	3.04566	3.43627	4.00259	depth
		0.0	4.34335	5.16604	5.95726	8.71014	surface
		5.625	3.84335	4.40390	5.26432	7.24663	
		11.25	3.58481	4.06136	4.91564	6.61388	
		16.875	3.48242	3.98859	4.80046	6.54614	
m	a	22.5	3.40719	3.93477	4.75252	6.54409	
e	n	28.125	3.36171	3.90831	4.76710	6.59884	
m	g	33.75	3.35110	3.92465	4.84836	6.72373	
b	l	39.375	3.36137	3.96590	4.95927	6.87763	
r	e	45.	3.37673	4.01181	5.05520	7.00907	
a		50.625	3.39649	4.06003	5.14403	7.12879	
n	ϕ	56.25	3.42054	4.10882	5.23652	7.25098	
e		61.875	3.44525	4.15470	5.32155	7.36446	
	(°)	67.5	3.46688	4.19417	5.38670	7.45573	
		73.125	3.48558	4.22683	5.43682	7.52741	
		78.75	3.50163	4.25239	5.47723	7.58210	
		84.375	3.51269	4.26891	5.50400	7.61689	
		90.	3.51638	4.27442	5.51292	7.62846	depth

Table 4-12: Stress intensity factors (K) of geometry D-2-2 without stub

K in [N/mm$^{3/2}$] for σ_n = 1 N/mm^2

		crack	I	II	III	IV	remark
		a [mm]	6.49	8.95	11.85	16.00	
		c [mm]	10.14	15.80	25.90	40.70	
		0.0	3.30739	3.90260	4.60161	7.11341	surface
		5.625	3.06433	3.56498	4.12286	6.41731	
		11.25	2.95047	3.41423	3.93496	6.26841	
	a	16.875	2.90936	3.37163	3.91275	6.43338	
b	n	22.5	2.86916	3.33231	3.88050	6.59873	
e	g	28.125	2.84171	3.30309	3.85329	6.77582	
n	l	33.75	2.84318	3.29701	3.86538	7.00512	
d	e	39.375	2.85396	3.30023	3.88996	7.24296	
i		45.	2.85182	3.29751	3.89404	7.44002	
n	ϕ	50.625	2.84821	3.29340	3.88640	7.61033	
g		56.25	2.85737	3.29449	3.87965	7.77283	
	(°)	61.875	2.86804	3.29567	3.87020	7.91706	
		67.5	2.86773	3.29109	3.85325	8.03109	
		73.125	2.86592	3.28610	3.83640	8.11906	
		78.75	2.87299	3.28649	3.82770	8.18540	
		84.375	2.88178	3.28898	3.82457	8.22717	
		90.	2.88473	3.28978	3.82343	8.24107	depth
		0.0	3.44635	4.18739	5.10821	5.98295	surface
		5.625	3.25835	3.89800	4.65906	5.29701	
		11.25	3.18689	3.81258	4.56563	5.02177	
		16.875	3.18493	3.84388	4.66969	4.98567	
m	a	22.5	3.19609	3.88384	4.76539	4.94273	
e	n	28.125	3.22389	3.93905	4.87607	4.89556	
m	g	33.75	3.27348	4.02028	5.04160	4.87576	
b	l	39.375	3.33191	4.11222	5.22198	4.85889	
r	e	45.	3.38568	4.19922	5.37290	4.81305	
a		50.625	3.43647	4.28090	5.50500	4.75205	
n	ϕ	56.25	3.48691	4.35803	5.63255	4.69505	
e		61.875	3.53307	4.42691	5.74481	4.64101	
	(°)	67.5	3.57112	4.48397	5.83035	4.58640	
		73.125	3.60198	4.52969	5.89529	4.53816	
		78.75	3.62684	4.56479	5.94642	4.50280	
		84.375	3.64321	4.58712	5.97964	4.48162	
		90.	3.64869	4.59459	5.99073	4.47432	depth

Table 4-13: Stress intensity concentration factors (M_k) of geometry D-2-2

		crack	I	II	III	IV	remark
		a [mm]	6.49	8.95	11.85	16.00	
		c [mm]	10.14	15.80	25.90	40.70	
		0.0	1.35257	1.32505	1.28639	1.32368	surface
		5.625	1.26527	1.21087	1.20470	1.18787	
		11.25	1.20430	1.13610	1.13176	1.09197	
	a	16.875	1.16937	1.10219	1.08299	1.05469	
b	n	22.5	1.13688	1.06927	1.04450	1.02171	
e	g	28.125	1.10679	1.03872	1.01332	0.992994	
n	l	33.75	1.08054	1.01388	0.986757	0.969744	
d	e	39.375	1.05910	0.994337	0.965709	0.952137	
i		45.	1.04180	0.978068	0.948681	0.937775	
n	ϕ	50.625	1.02760	0.964678	0.935169	0.926324	
g		56.25	1.01575	0.953674	0.924581	0.917196	
	(°)	61.875	1.00623	0.944846	0.916415	0.910129	
		67.5	0.998504	0.937613	0.909681	0.904326	
		73.125	0.992645	0.932105	0.904543	0.899900	
		78.75	0.988879	0.928459	0.901170	0.896864	
		84.375	0.986900	0.926467	0.899353	0.895156	
		90.	0.986231	0.925794	0.898740	0.894569	depth
		0.0	1.26028	1.23371	1.16621	1.22447	surface
		5.625	1.17954	1.12978	1.12991	1.12923	
		11.25	1.12486	1.06525	1.07667	1.05511	
		16.875	1.09341	1.03765	1.02800	1.01753	
m	a	22.5	1.06605	1.01311	0.997299	0.991720	
e	n	28.125	1.04275	0.992196	0.977652	0.973881	
m	g	33.75	1.02371	0.976213	0.961671	0.959831	
b	l	39.375	1.00884	0.964418	0.949691	0.949561	
r	e	45.	0.997357	0.955370	0.940870	0.942077	
a		50.625	0.988366	0.948406	0.934429	0.936725	
n	ϕ	56.25	0.980966	0.942816	0.929689	0.932862	
e		61.875	0.975143	0.938510	0.926323	0.930201	
	(°)	67.5	0.970810	0.935370	0.923907	0.928358	
		73.125	0.967684	0.933139	0.922231	0.927128	
		78.75	0.965477	0.931563	0.921097	0.926296	
		84.375	0.964174	0.930630	0.920457	0.925821	
		90.	0.963738	0.930316	0.920242	0.925664	depth

Table 4-14: SIF and M_k for geometry D-2-2

loadcase	direction	crack depth a [mm]	crack width c [mm]	SIF [$Nmm^{-3/2}$] in plate with stub	SIF [$Nmm^{-3/2}$] in flat plate	M_k 3D	M_k 2D	ratio $M_{k,3D}/M_{k,2D}$ ω
tension	depth a	6.49	10.14	3.516	3.649	0.964	1.041	.926
		8.95	15.80	4.274	4.595	0.930	1.020	.912
		11.85	25.90	5.513	5.991	0.920	1.008	.913
		16.00	40.70	7.628	8.241	0.926	1.000	.927
tension	width c	6.49	10.14	4.343	3.446	1.260	1.498	.841
		8.95	15.80	5.166	4.187	1.234	1.498	.824
		11.85	25.90	5.957	5.108	1.166	1.498	.778
		16.00	40.70	8.710	7.113	1.225	1.498	.818
bending	depth a	6.49	10.14	2.845	2.885	0.986	1.078	.915
		8.95	15.80	3.046	3.290	0.926	1.043	.888
		11.85	25.90	3.436	3.823	0.899	1.021	.872
		16.00	40.70	4.003	4.474	0.895	1.000	.895
bending	width c	6.49	10.14	4.473	3.307	1.353	1.650	.820
		8.95	15.80	5.171	3.903	1.325	1.650	.803
		11.85	25.90	5.919	4.588	1.286	1.650	.779
		16.00	40.70	7.920	5.983	1.324	1.650	.802

Table 6-1: Comparison lifetime C-specimens

Specimen	$a_i = 0.5$			$a_i = a_{exp}$			
	N_{exp} [10^3]	N_{calc} [10^3]	N_{calc}/N_{exp} [-]	a_i [mm]	ΔN_{exp} [10^3]	ΔN_{calc} [10^3]	$\Delta N_{calc}/\Delta N_{exp}$ [-]
C-1-1	1795	1393	0.776	0.65	1595	1350	0.846
C-1-2	2078	1401	0.674	1.08	1578	1253	0.794
C-1-4	2924	1683	0.576	1.54	1924	1229	0.639
C-2-1	964	720	0.747	0.56	853	717	0.841
C-2-2	896	720	0.804	0.56	794	706	0.889
C-2-3	2079	1429	0.687	0.68	1779	1360	0.764
C-2-4	2000	1429	0.715	1.09	1632	1244	0.762

Table 6-2: Comparison lifetime B-specimens

Specimen	$a_i = 0.5$ $c_i = 5.0$			$a_i = a_{exp}$				$c_i = c_{exp}$
	N_{exp} [10^3]	N_{calc} [10^3]	N_{calc}/N_{exp} [-]	a_i [mm]	c_i [mm]	ΔN_{exp} [10^3]	ΔN_{calc} [10^3]	$\Delta N_{calc}/\Delta N_{exp}$ [-]
B-1-1	652	403	0.618	8.1	9.0	245	184	0.751
B-1-2	712	365	0.513	3.2	6.0	305	220	0.721
B-2-1	983	555	0.565	2.53	5.89	623	370	0.595
B-2-2	461	310	0.672	6.08	8.28	188	138	0.735

Table 6-3: Comparison lifetime D-specimens

Specimen	$a_i = 0.5$ $c_i = 5.0$			$a_i = a_{exp}$				$c_i = c_{exp}$
	N_{exp} [10^3]	N_{calc} [10^3]	N_{calc}/N_{exp} [-]	a_i [mm]	c_i [mm]	ΔN_{exp} [10^3]	ΔN_{calc} [10^3]	$\Delta N_{calc}/\Delta N_{exp}$ [-]
D-1-2	2990	1040	0.348	2.9	5.4	2470	763	0.309
D-1-2*		1601	0.535				1226	0.496
D-2-1	3391	762	0.225	6.52	17.23	1872	206	0.110
D-2-1*		1123	0.331				337	0.180
D-2-2	3539	1225	0.346	2.51	5.63	3170	870	0.274
D-2-2*		1878	0.531				1400	0.442

*) calculations with reduction factors $\omega_{b,a} = 0.9$ and $\omega_{b,c} = 0.8$

Table 6-4: Ratio theoretical*)-experimental crack growth rate for D-specimens

Specimen	D-1-2	D-2-1	D-2-2
T [mm]	70	40	40
ϕ [°]	70	70	70
ρ [mm]	5.0	0.5	5.0
ρ/T	0.0714	0.013	0.125
$\frac{da/dN_{calc}}{da/dN_{exp}}$	2.5	5	2.5
$\frac{dc/dN_{calc}}{dc/dN_{exp}}$	6	30	5

*) theoretical crack growth rate is based on SIF determined by Newman-Raju plate solution combined with DIANA 2D M_k factors (figures 6-24, 6-26 and 6-28)

Table 7-1: Stress intensity concentration factors (M_k) for butt welds and X-joints.

Loading	applicability		Stress intensity concentration factor*)	eqn.
	L/T	a/T	$M_k = f_L$ (a/T, L/T)	
membrane	≤ 2	$\leq 0.05\ (L/T)^{0.55}$	$M_{km} = 0.51\ (L/T)^{0.27}\ (a/T)^{-0.31}$	7-2a
	"	$> 0.05\ (L/T)^{0.55}$	$= 0.83\ (L/T)^{0.46}\ (a/T)^{-0.15}\quad (M_{km} \geq 1)$	7-2b
	> 2	≤ 0.073	$= 0.615\ (a/T)^{-0.31}$	7-2c
	"	> 0.073	$= 0.83\ (a/T)^{-0.20}\quad (M_{km} \geq 1)$	7-2d
bending	≤ 1	$\leq 0.03\ (L/T)^{0.55}$	$M_{kb} = 0.45\ (L/T)^{0.21}\ (a/T)^{-0.31}$	7-2e
	"	$> 0.03\ (L/T)^{0.55}$	$= 0.68\ (L/T)^{0.21}\ (a/T)^{-0.19}\quad (M_{kb} \geq 1)$	7-2f
	> 1	≤ 0.03	$= 0.45\ (a/T)^{-0.31}$	7-2g
	"	> 0.03	$= 0.68\ (a/T)^{-0.19}\quad (M_{kb} \geq 1)$	7-2h

*) M_k for $\theta = 45°$ ($f_\theta = 1$) and $\rho = 0$ ($f_\rho = 1$).

Table 7-2: Input parameters of the crack growth calculations of tubular joint B3

parameter		value	
plate thickness	T	32	mm
weld angle	θ	45°	
weld toe radius	ρ	4	mm *)**)
weld width	L	35	mm**)
initial crack depth	a_i	0.25	mm
initial half crack width	c_i	0.25	mm
membrane stress range	$\Delta\sigma_m$	35	N/mm²
bending stress range	$\Delta\sigma_b$	100	N/mm²

*) weld toe was ground and the Maddox M_k was justified for this

**) these parameters were not used in the original calculations

Table 7-3: Survey of crack growth model for tubular joint B3

	A	B	C	D
see figure	7-5	7-6	7-7	7-8
SIF plate	S-T	S-T	S-T	N-R
M_k	M	M	$f_L f_\theta f_\rho$	$f_L f_\theta f_\rho$
da/dN-ΔK curve: C	OTC	IIW	IWW	IWW
da/dN-ΔK curve: m				

S-T - Scott - Thorpe

N-R - Newman - Raju

M - Maddox (1972)

$f_L f_\theta f_\rho$ - eqn. 7.1

OTC - Original calculation $C = 1.08\ 10^{-13}$ (N, mm); m = 3.07

IIW - $C = 1.832\ 10^{-13}$ (N, mm); m = 3

Table 7-4: Plate thickness reduction exponents α

plate thickness [mm]	reduction factors $\omega_{b,a}$	reduction factors $\omega_{b,c}$	plate thickness [mm]: 16	25	40	70
16	1.0	1.0	-	-0.168	-0.175	-0.181
	0.9	0.8	-	-0.167	-0.172	-0.179
25	1.0	1.0	-0.168	-	-0.181	-0.187
	0.9	0.8	-0.167	-	-0.176	-0.184
40	1.0	1.0	-0.175	-0.181	-	-0.191
	0.9	0.8	-0.172	-0.176	-	-0.190
70	1.0	1.0	-0.181	-0.187	-0.191	-
	0.9	0.8	-0.179	-0.184	-0.190	-

FIGURES

LIST OF FIGURES

AUFSTELLUNG DER ABBILDUNGEN

LISTE DES FIGURES

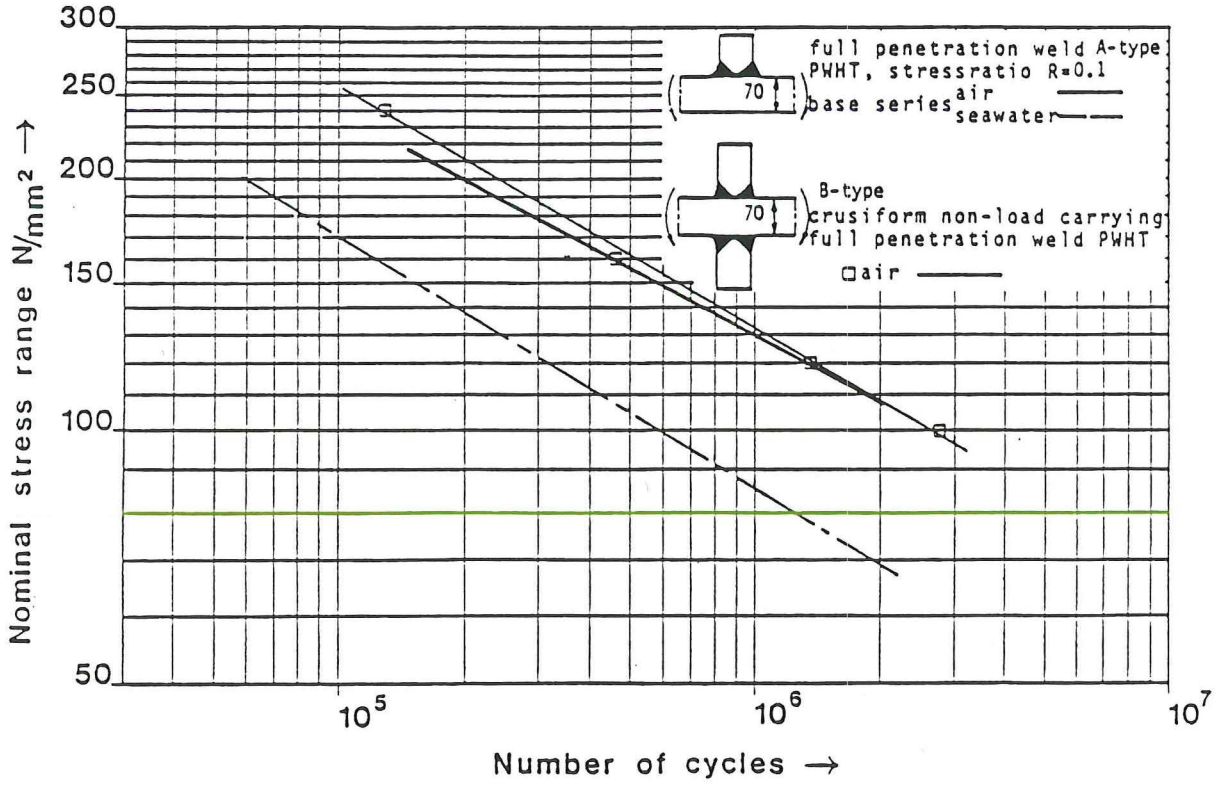

Figure 1-1: S-N diagram

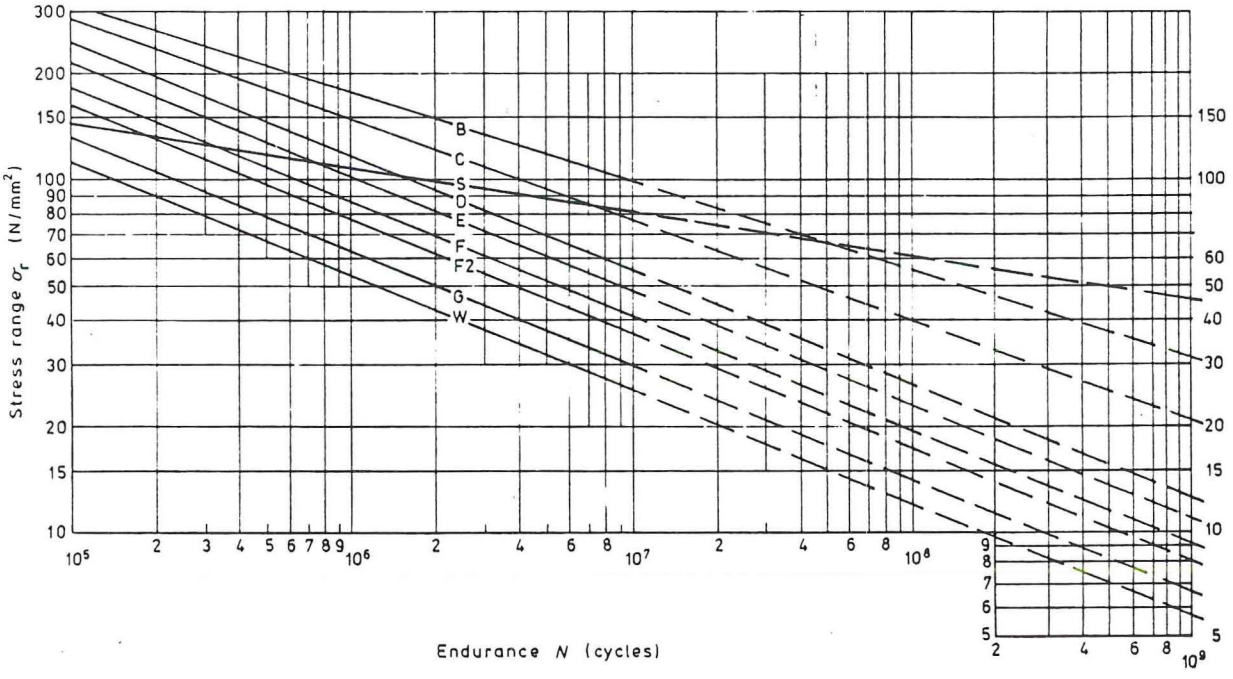

NOTE 1. The use of these curves for calculation purposes is not recommended.

NOTE 2. For endurances greater than 10^7 cycles adjustments should be made in accordance with **11.3.**

Figure 14. Summary design σ_r–N curves (mean minus two standard deviations)

Figure 1-2: S-N curves of BS 5400

(b) Welded details on surface of member

Product form	Rolled steel structural plates, sections and built-up members											Reinforcing steel in concrete
Location of potential crack initiation	At a long welded attachment (in direction of σ_r)								At a short welded attachment		At any attachment	At welded intersections in fabric or between hot rolled bars
	Away from weld end			At an intermediate gap in a longitudinal weld	At a cope hole	At a weld end						
					Narrow attachment		Wide attachment				Close to edge of member	
							On one side only	On both sides symmetrically				
Dimensional requirements	Butt weld full penetration			Fillet weld		Weld toe not less than 10 mm from member edge					Weld toe within 10 mm of member edge	
				Intermittent $\frac{m}{h} < 2.5$		Weld length (parallel to σ_r) $l > 150$ mm			$l < 150$ mm			
					Attachment width $w \leq 50$ mm		$w > 50$ mm					
Manufacturing requirements (see also Part 6)	Grind smooth any undercut on member edges										Grind any undercut	Resistance or manual plus grind smooth undercut
	Dress flush reinforcement	Automatic no stop-starts									Avoid weld returns round laps (see z)	
Special inspection requirements	Proved free of all significant defects											
Design stress area	Minimum transverse cross section of member at location of potential crack initiation											
Special design stress parameter									$r \leq 0.5\sigma$	$r > 0.5\sigma$		
Type number	2.1*	2.2*	2.3	2.4*	2.5	2.6	2.7*	2.8*	2.9	2.10*	2.11*	2.12
Class	B‡	C‡	D†	E†	F†	F2†	G†	F2†	F†	E‡	G†	D†

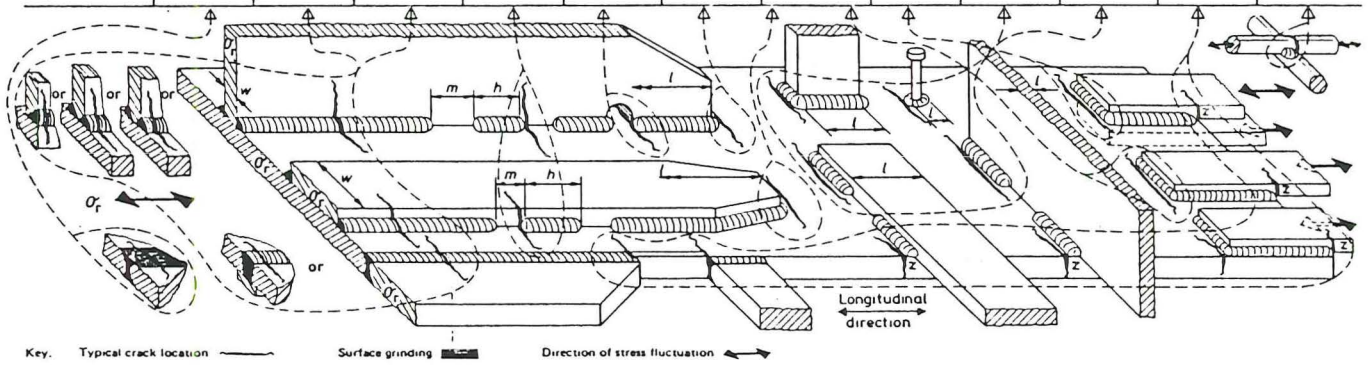

Key. Typical crack location ——— Surface grinding ▬▬ Direction of stress fluctuation ⟷

NOTE. Weld throat cracks are type 3 (see table 17(c)).

*See H.3.3.

†Important features that change significantly from one type to another.

‡Classifications that should be used with caution.

Figure 1-3: Atlas of weld details (extract of BS 5400)

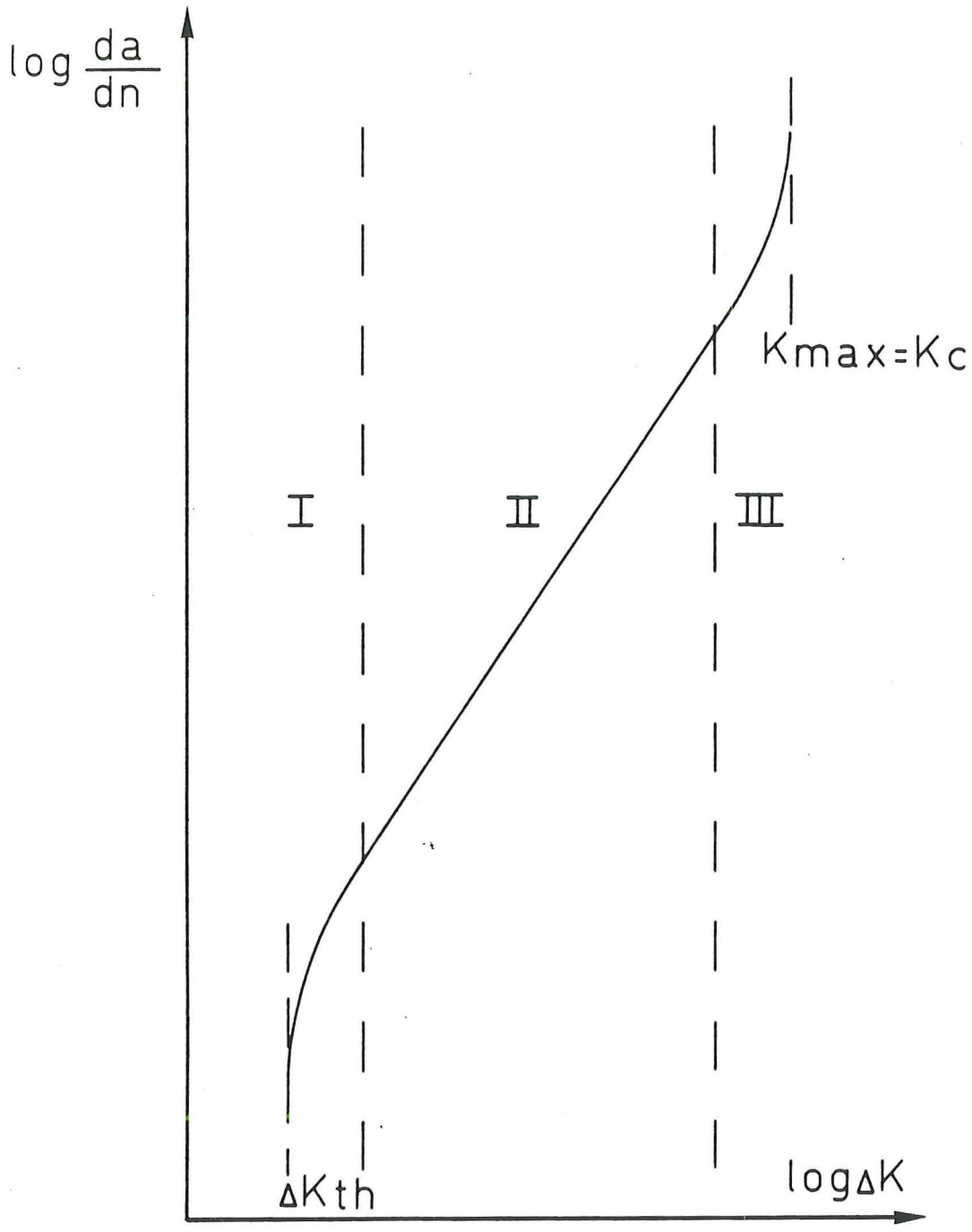

Figure 1-4: da/dN-ΔK curve

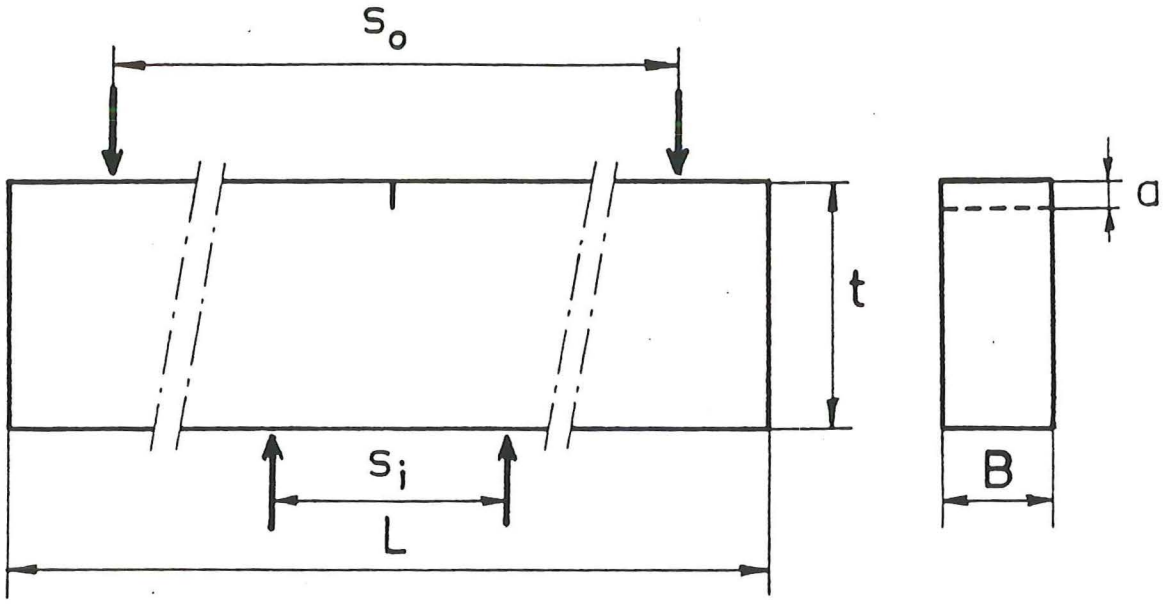

specimen	t mm	B mm	L mm	s_o mm	s_i mm
A1	80	20	600	400	200
A2	80	20	600	400	200
A3	80	35	600	500	200
A4	80	35	600	500	200
A5	40	20	400	240	120
A6	40	20	400	240	120

Figure 2-1: Geometry and dimensions of type A specimens

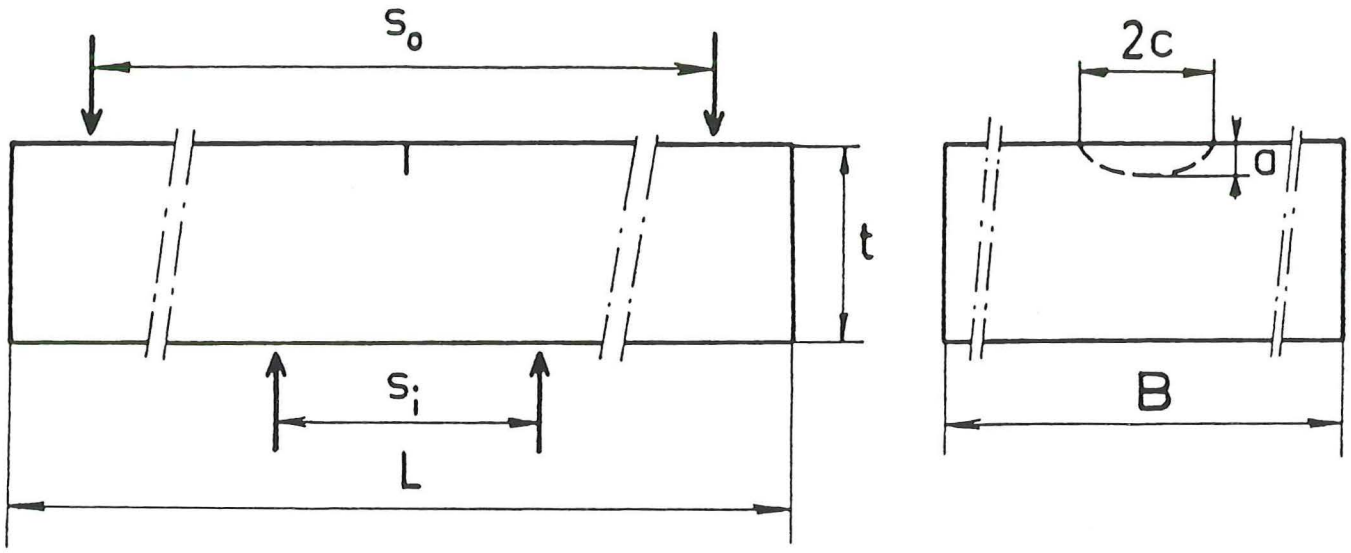

specimen	t mm	B mm	L mm	s_o mm	s_i mm
B-1-1 B-1-2	70	210	1500	1420	320
B-2-1 B-2-2	40	120	1000	920	320

Figure 2-2: Geometry and dimensions of type B specimens

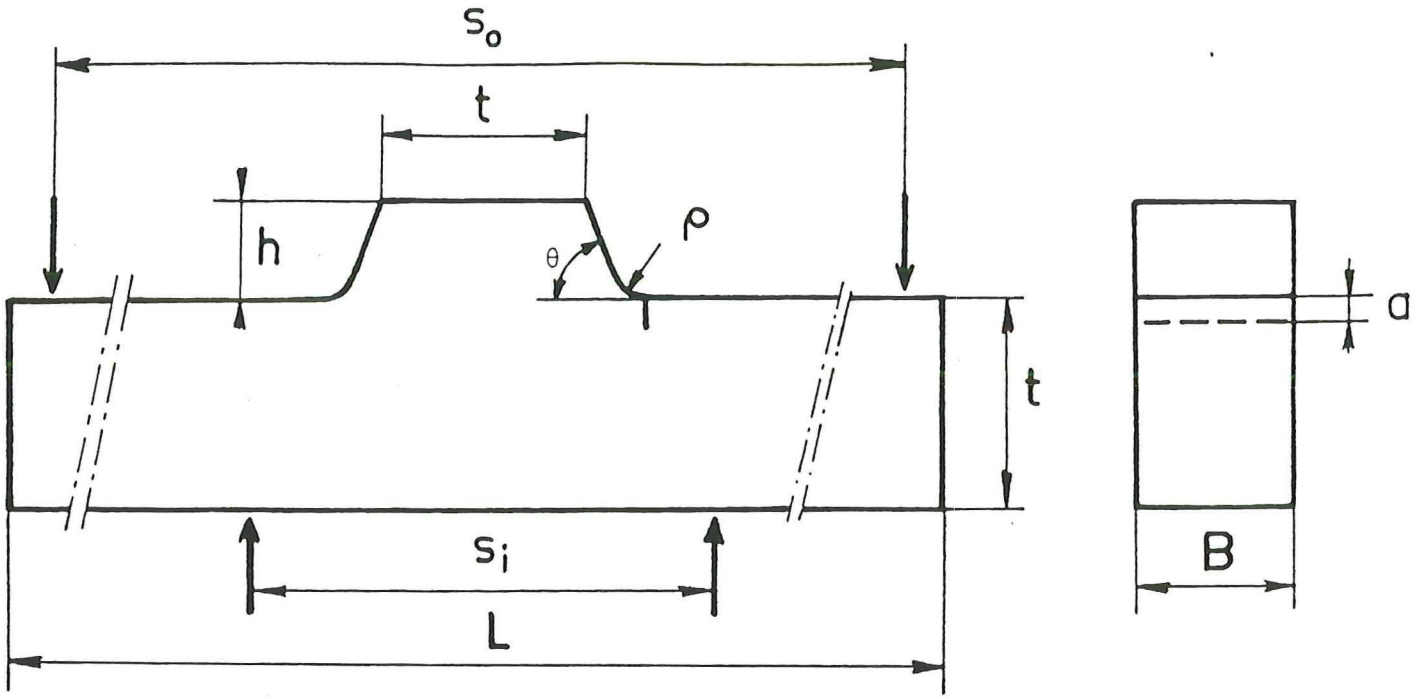

specimen	t mm	B mm	h mm	L mm	θ o	ρ mm	s_o mm	s_i mm
C-1-1	70	35	30	600	70	0.5	520	280
C-1-2							510	255
C-1-3	70	35	30	600	70	5.0	510	255
C-1-4								
C-2-1	40	20	17	400	70	0.5	310	150
C-2-2								
C-2-3	70	35	30	600	45	0.5	510	255
C-2-4								

Figure 2-3: Geometry and dimensions of type C specimens

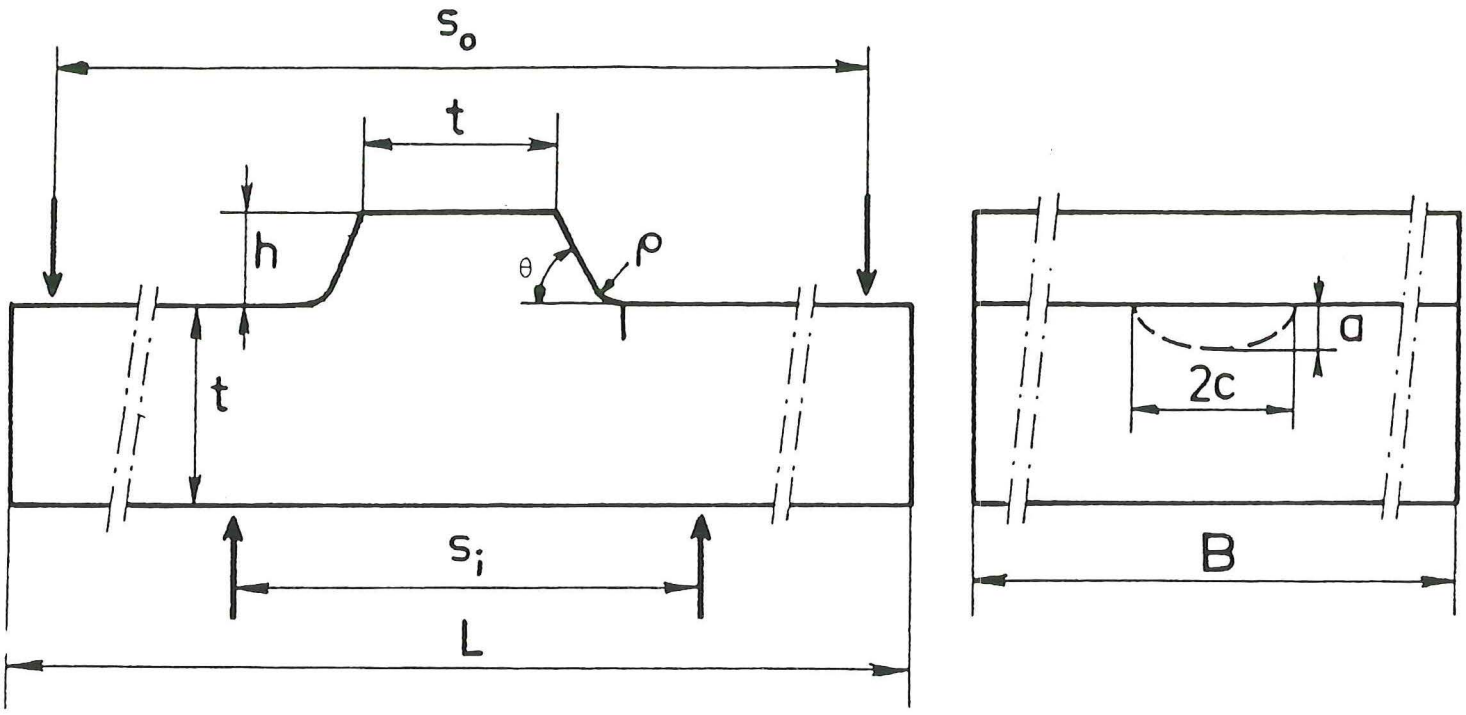

specimen	t mm	B mm	h mm	L mm	θ o	ρ mm	s_o mm	s_i mm
D-1-1	70	210	30	1500	70	0.5	1420	320
D-1-2	70	210	30	1500	70	5.0	1420	320
D-2-1	40	120	17	1000	70	0.5	920	320
D-2-2	40	120	17	1000	70	5.0	920	320

Figure 2-4: Geometry and dimensions of type D specimens

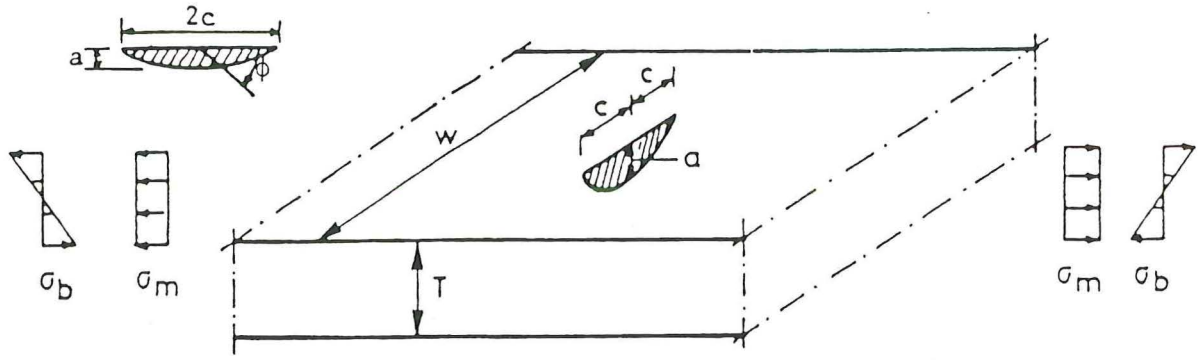

Figure 2-5: Characteristic dimensions of a semi-elliptical surface notch

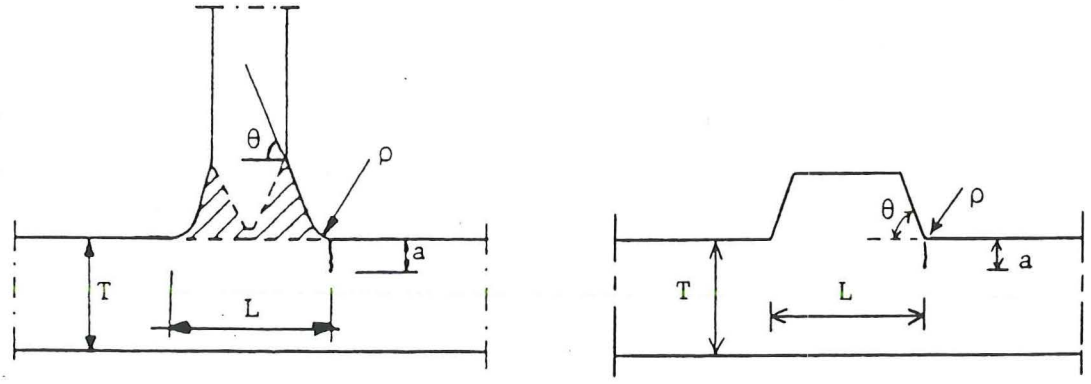

Figure 2-6: Simulation of a T-joint by a plate with stub

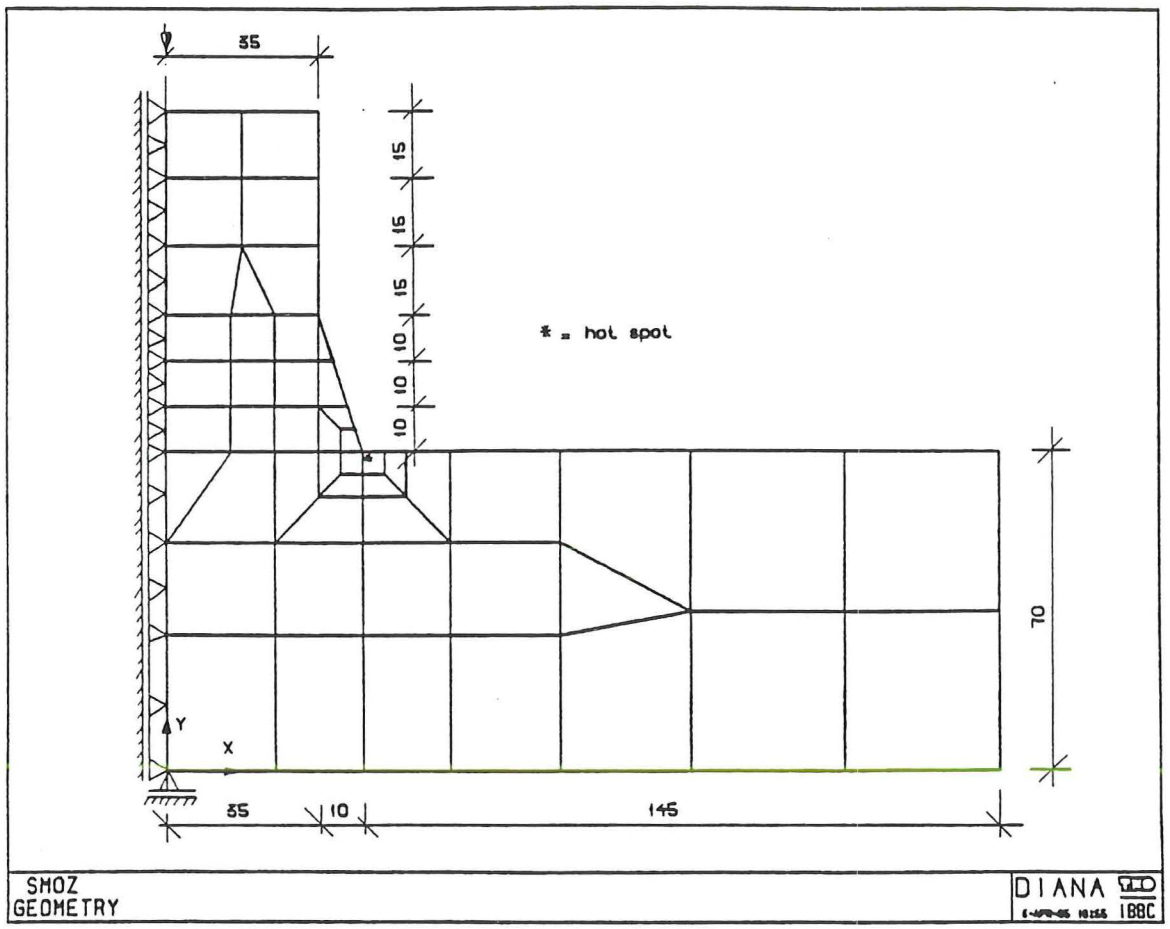

Figure 2-7: Finite element mesh of the calculations for the influence of the stub height

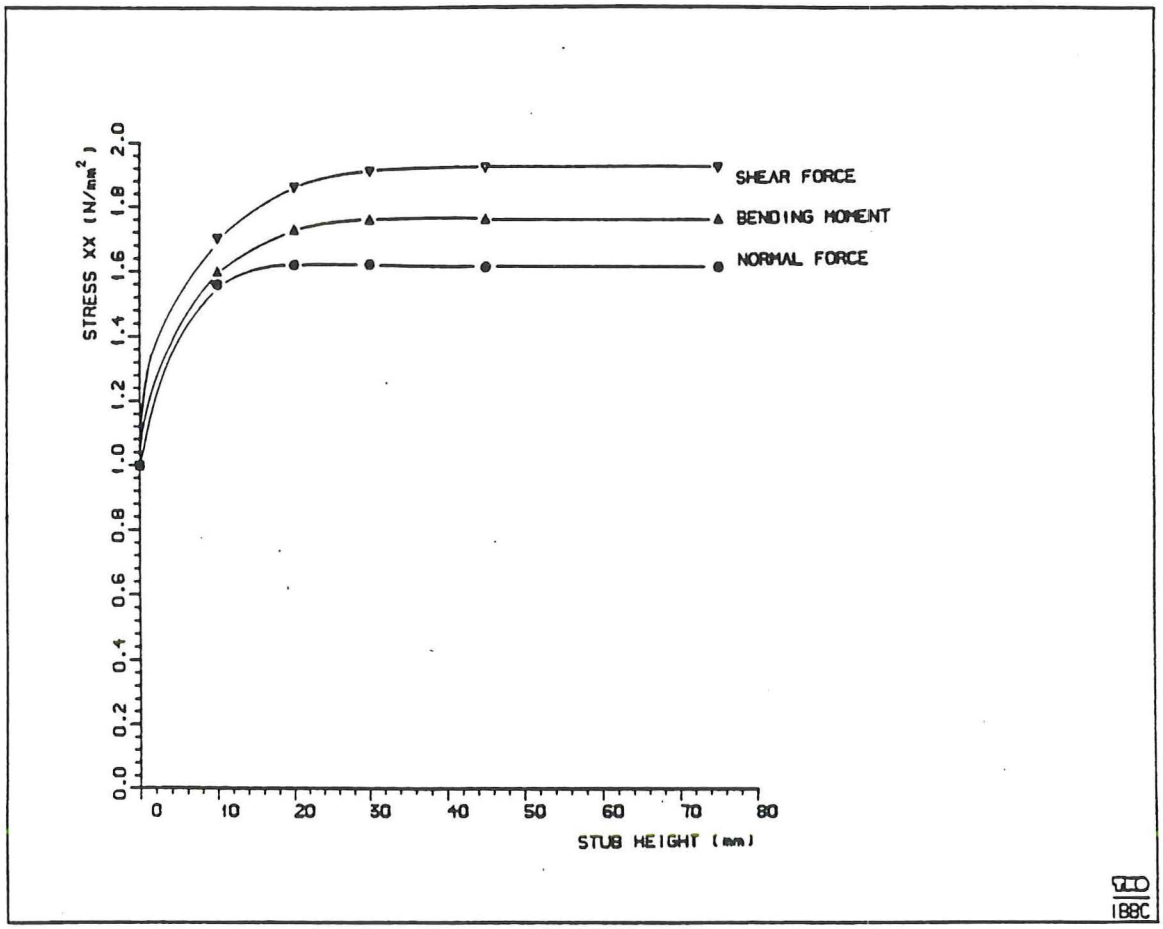

Figure 2-8: Relation stresses at the weld toe - stub height

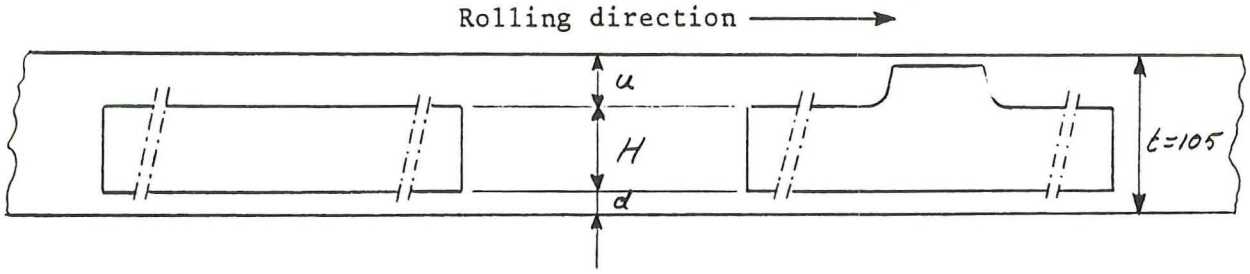

Specimen	H mm	u mm	d mm	Specimen	H mm	u mm	d mm
A 1,2	80	22	3	C 1 - 1,2,3,4	70	32	3
A 3,4	100	2	3	C 2 - 1,2	40	32	33
A 5,6	60	12	33	C 2 - 3,4	70	32	3
B 1 - 1,2	70	32	3	D 1 - 1,2	70	32	3
B 2 - 1,2	40	32	33	D 2 - 1,2	40	32	33

Figure 2-9: Location of specimens in base plate

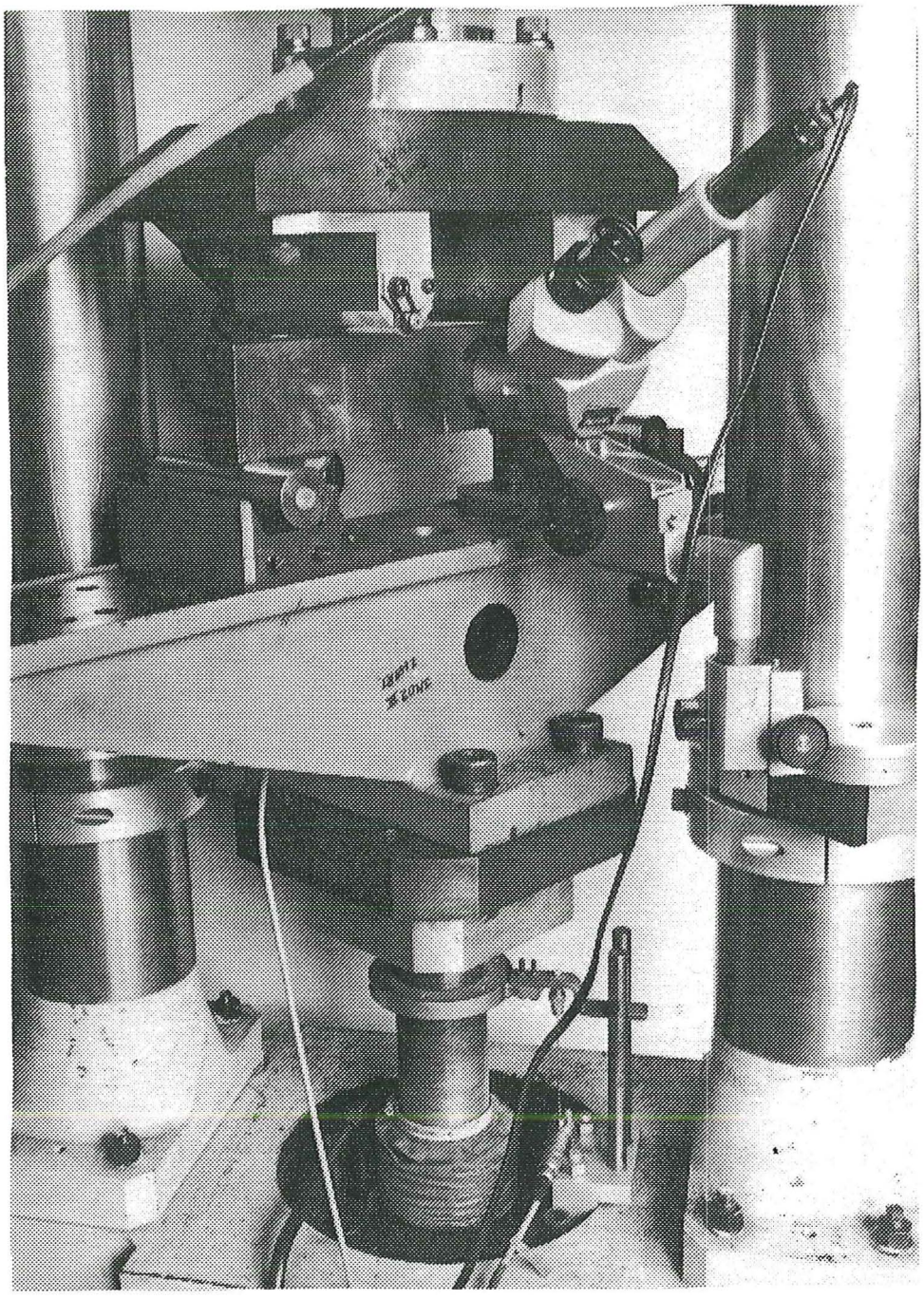

Figure 3-1: Four point bending test rig (Eindhoven University of Technology)

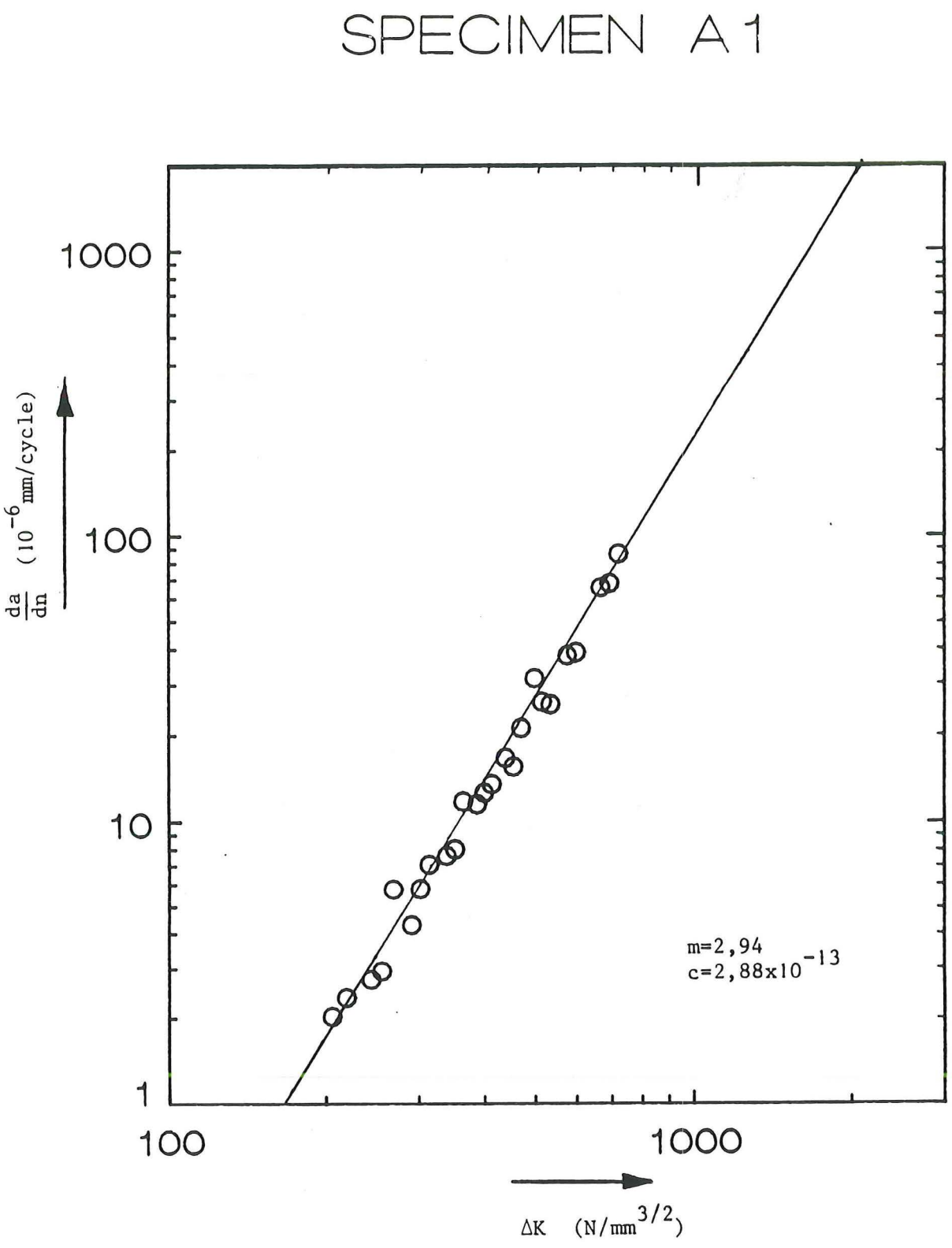

Figure 3-2: Crack growth rate data specimen A-1

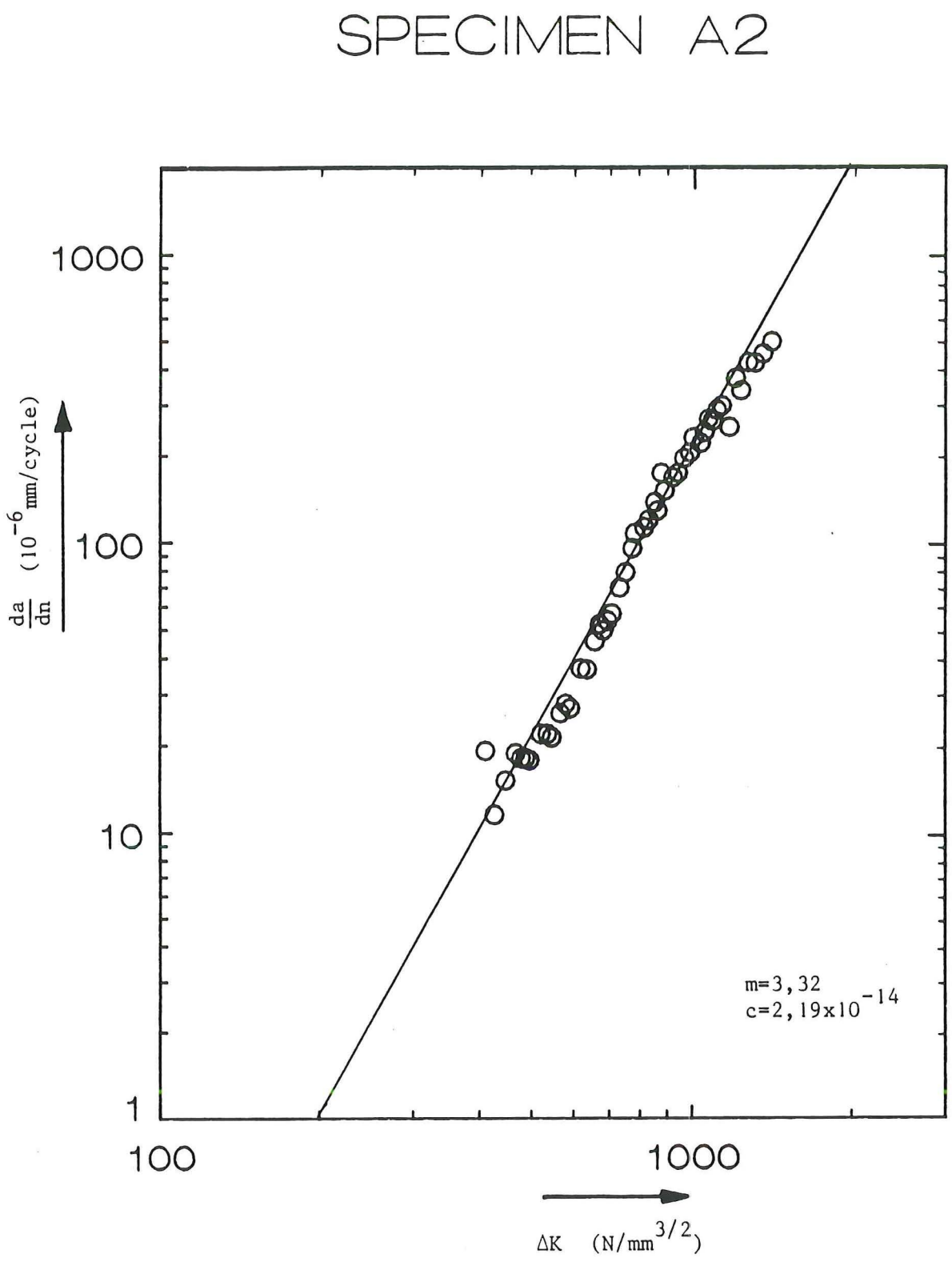

Figure 3-3: Crack growth rate data specimen A-2

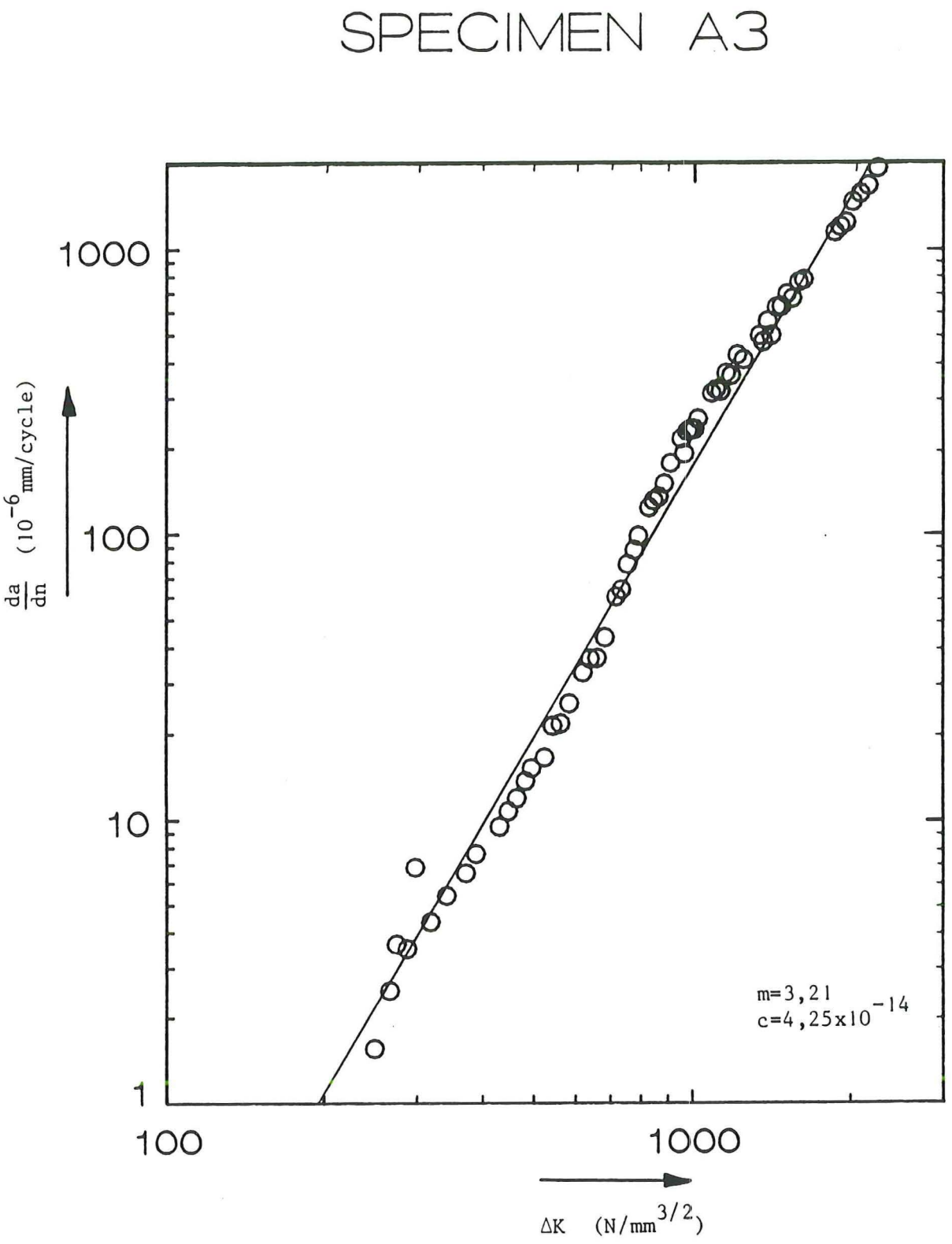

Figure 3-4: Crack growth rate data specimen A-3

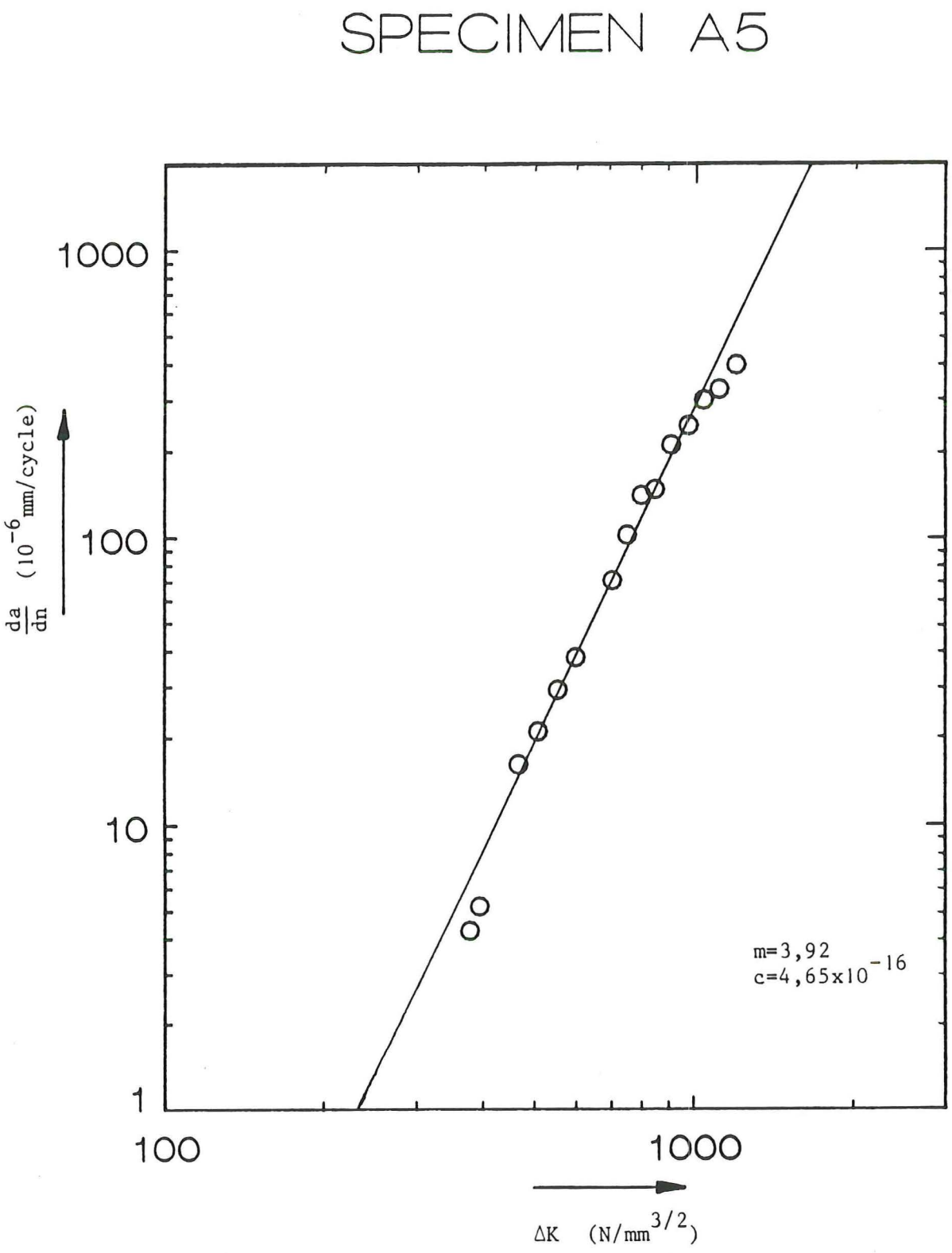

Figure 3-5: Crack growth rate data specimen A-5

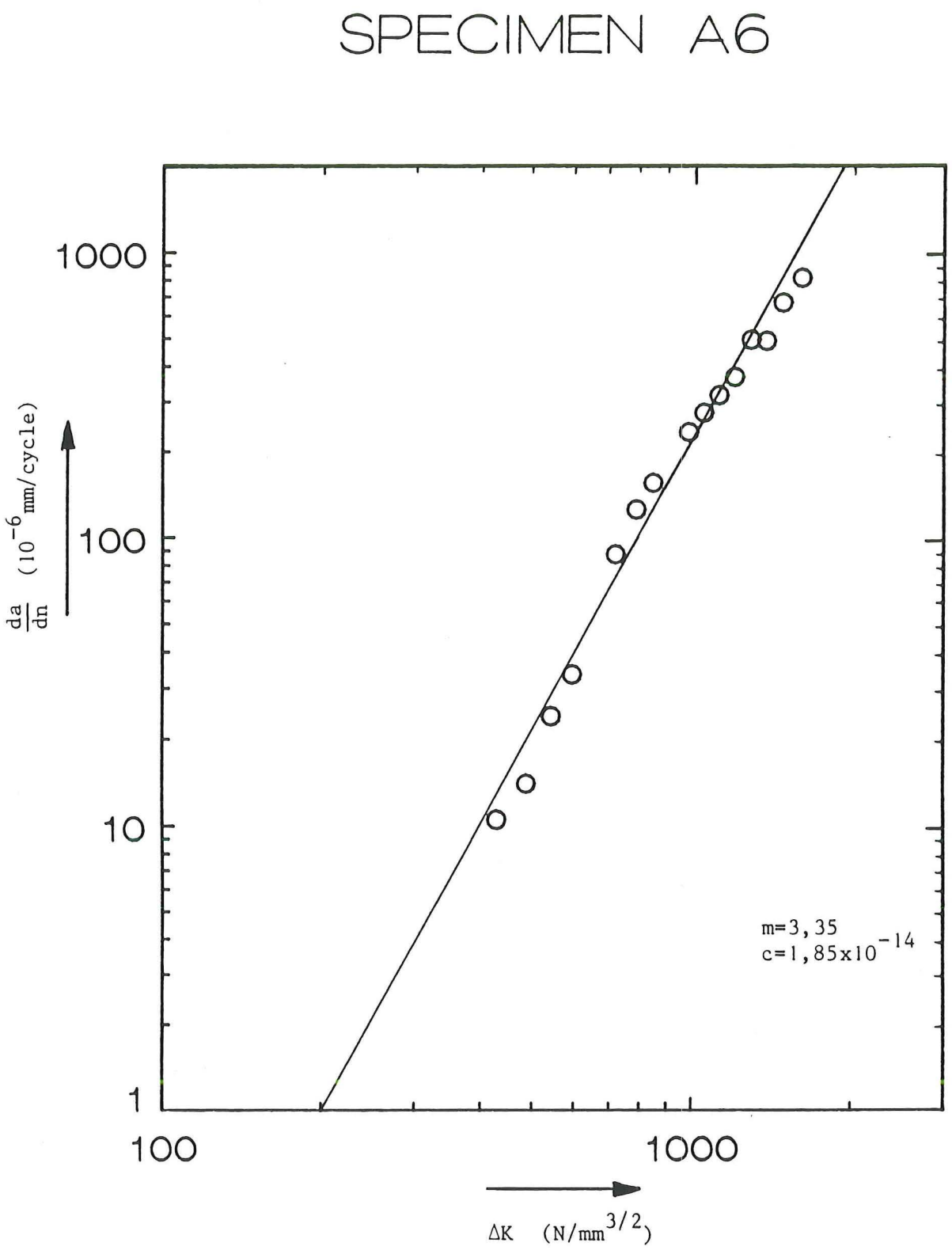

Figure 3-6: Crack growth rate data specimen A-6

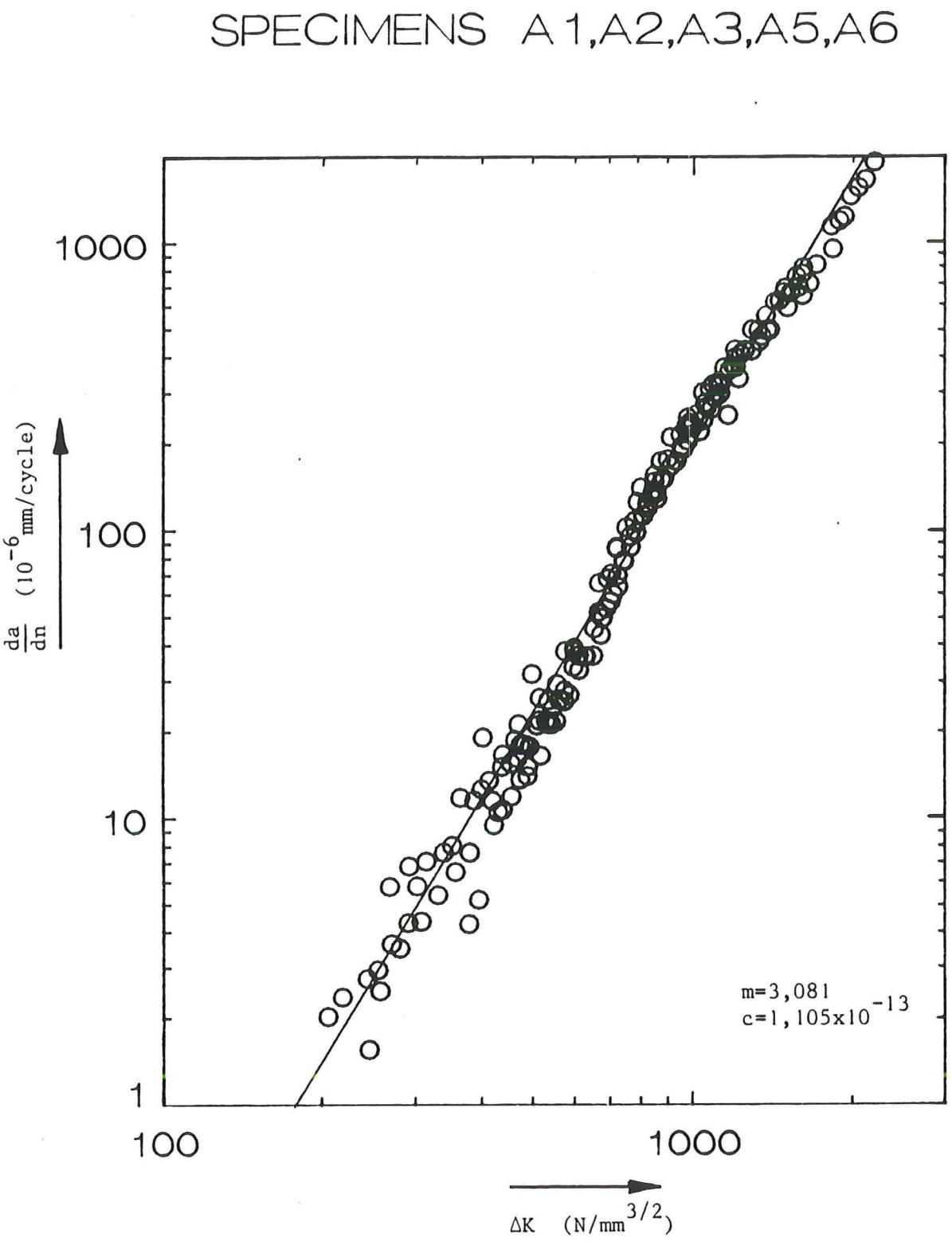

Figure 3-7: Crack growth rate data of all A specimens

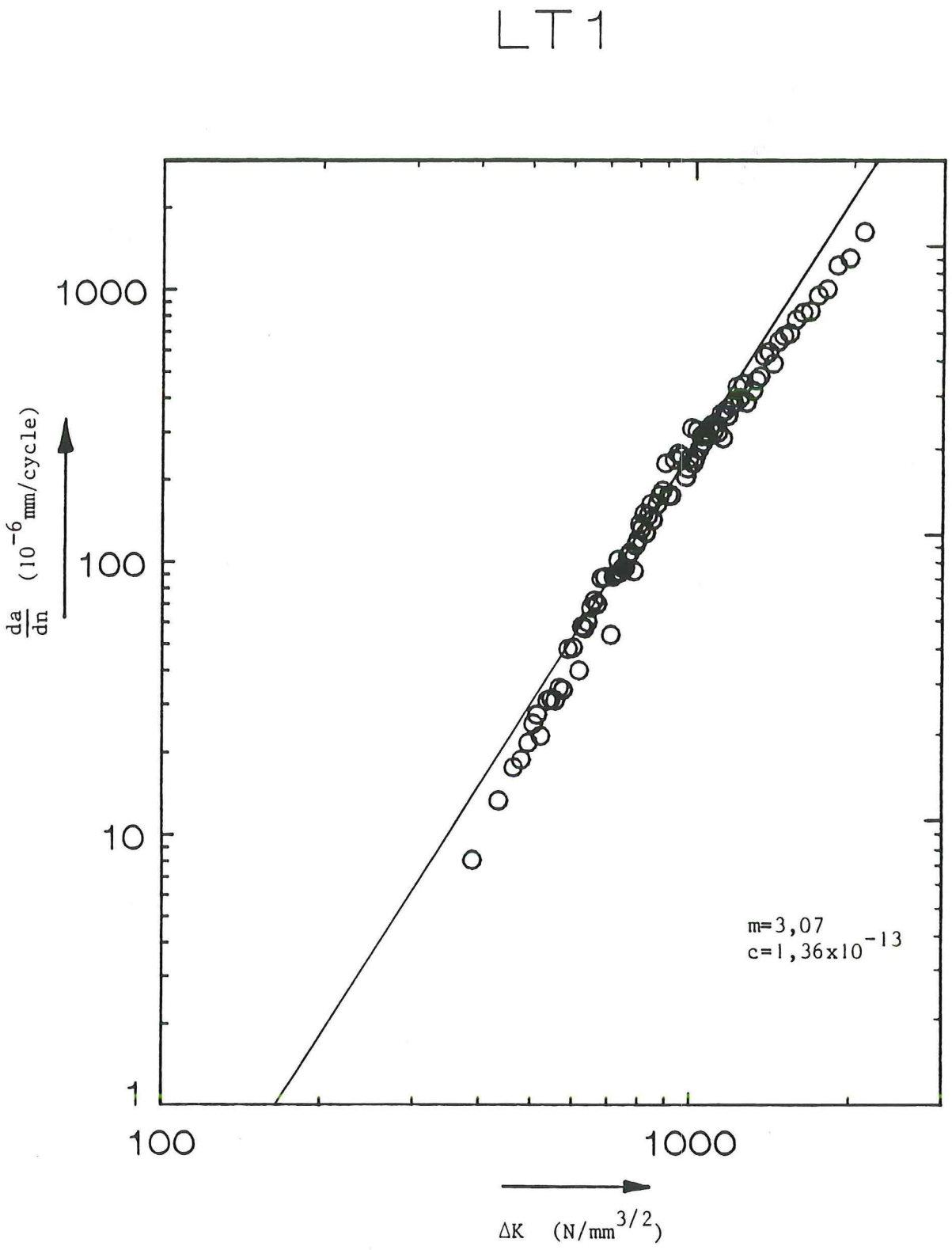

Figure 3-8: Crack growth rate data specimen LT-1 (transverse direction)

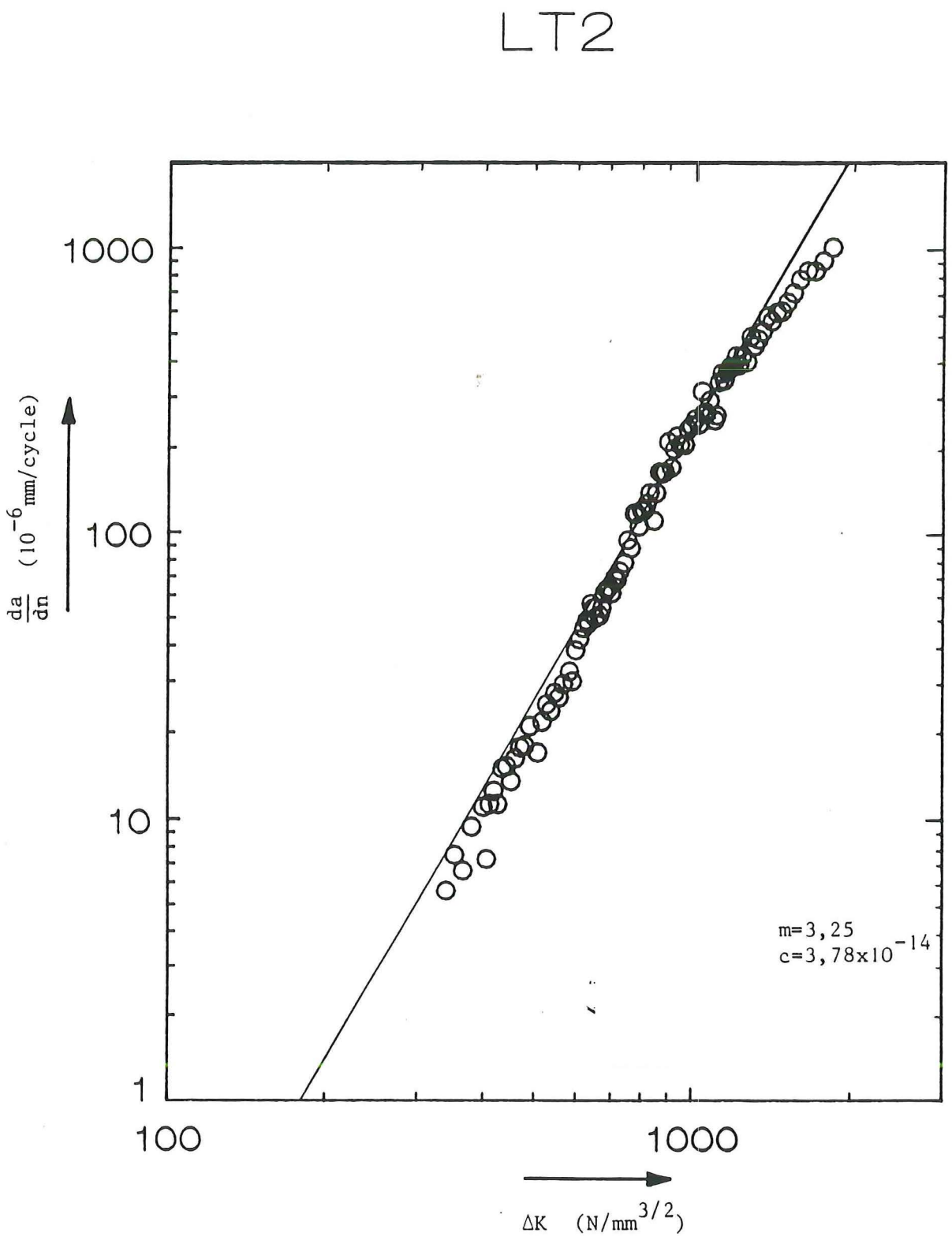

Figure 3-9: Crack growth rate data specimen LT-2 (transverse direction)

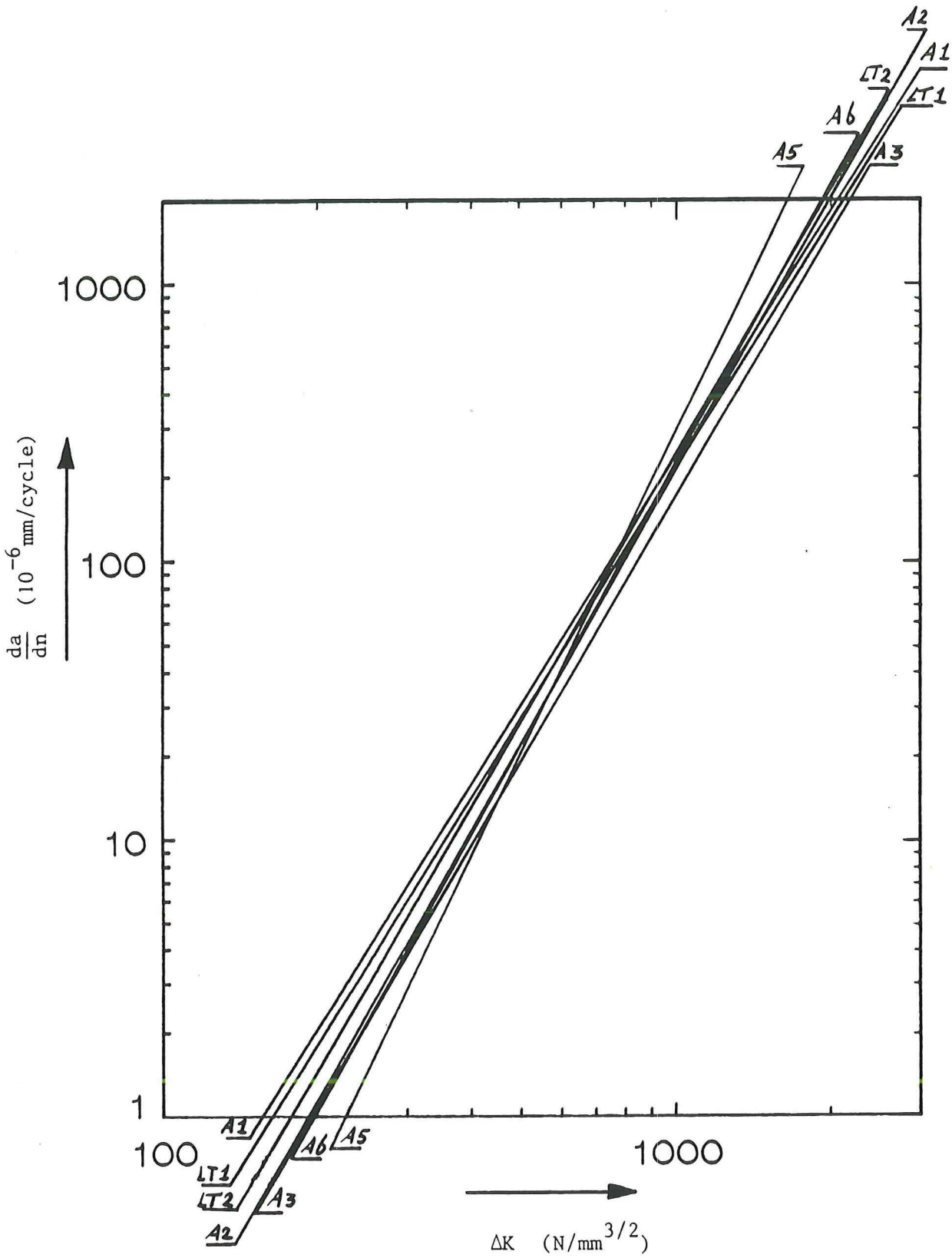

Figure 3-10: Crack growth rate curves of all A and LT specimens

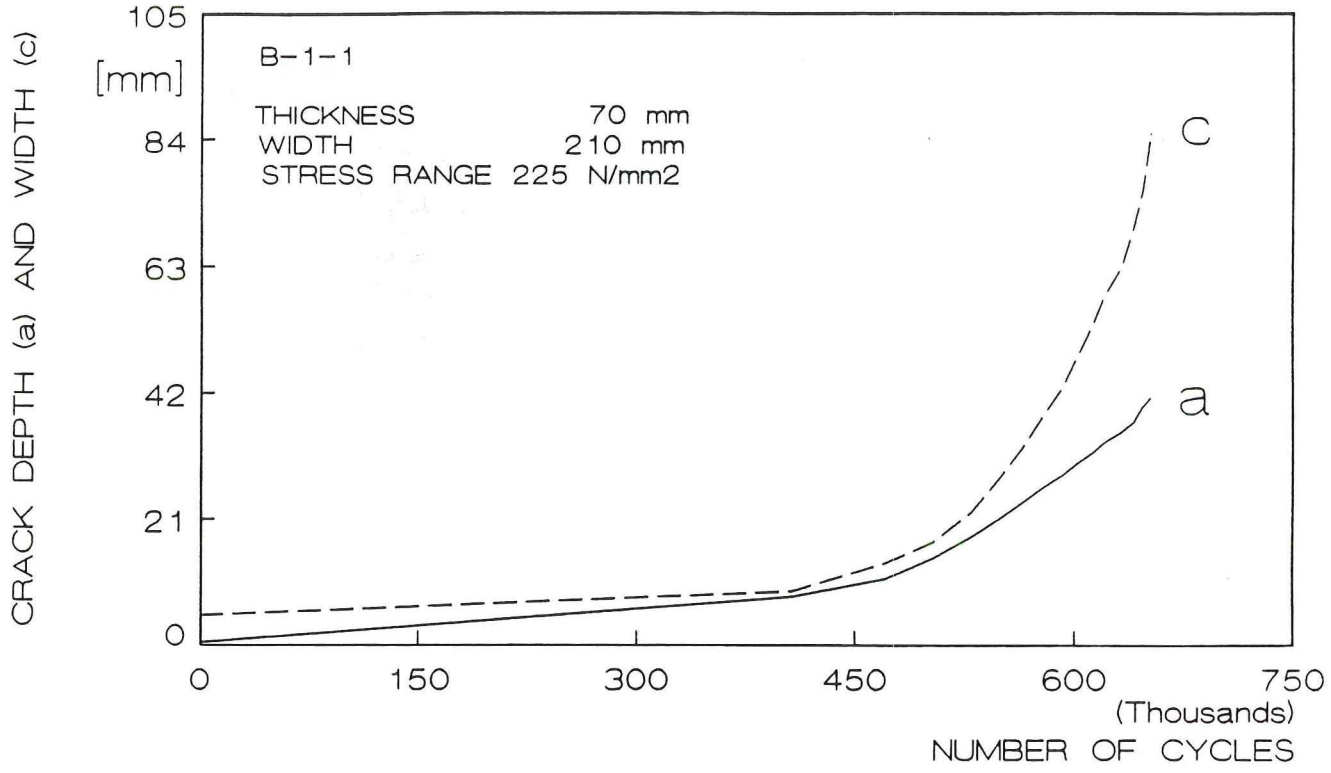

Figure 3-11: Crack growth curve specimen B-1-1

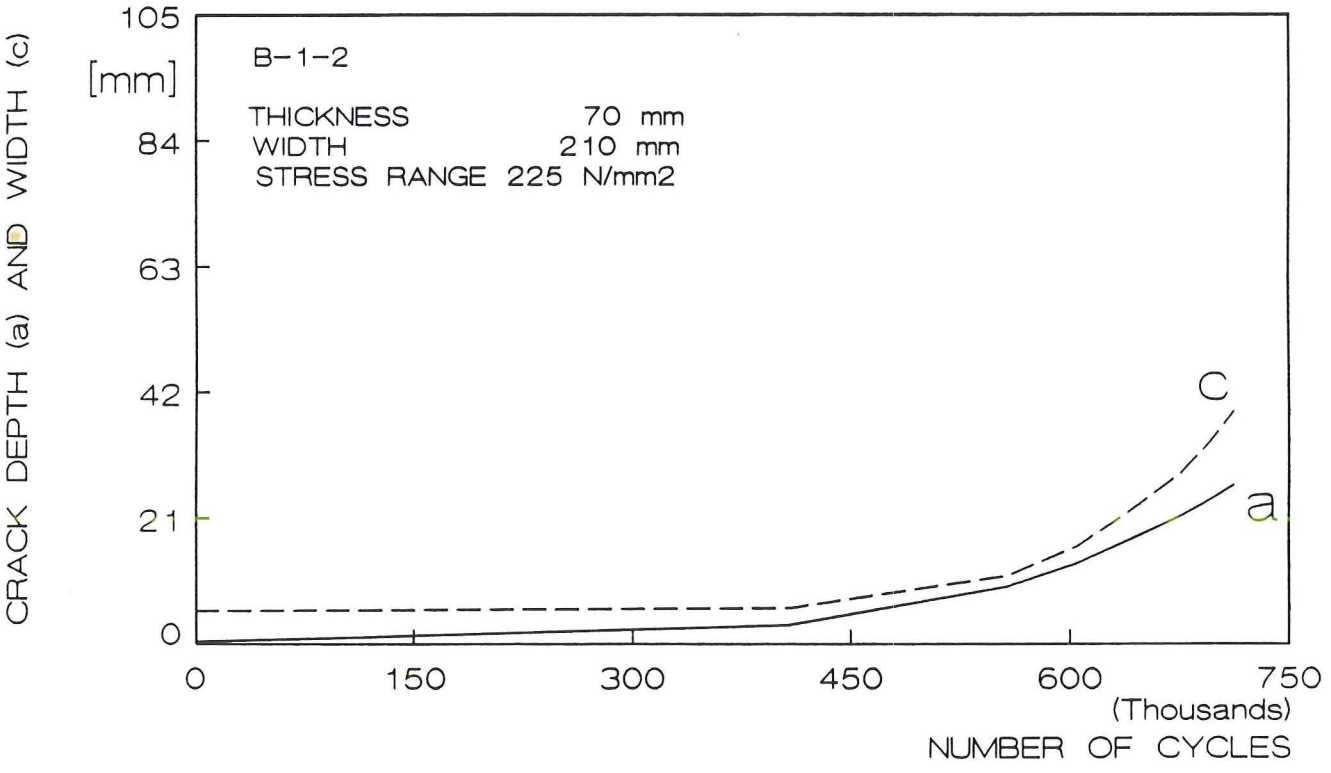

Figure 3-12: Crack growth curve specimen B-1-2

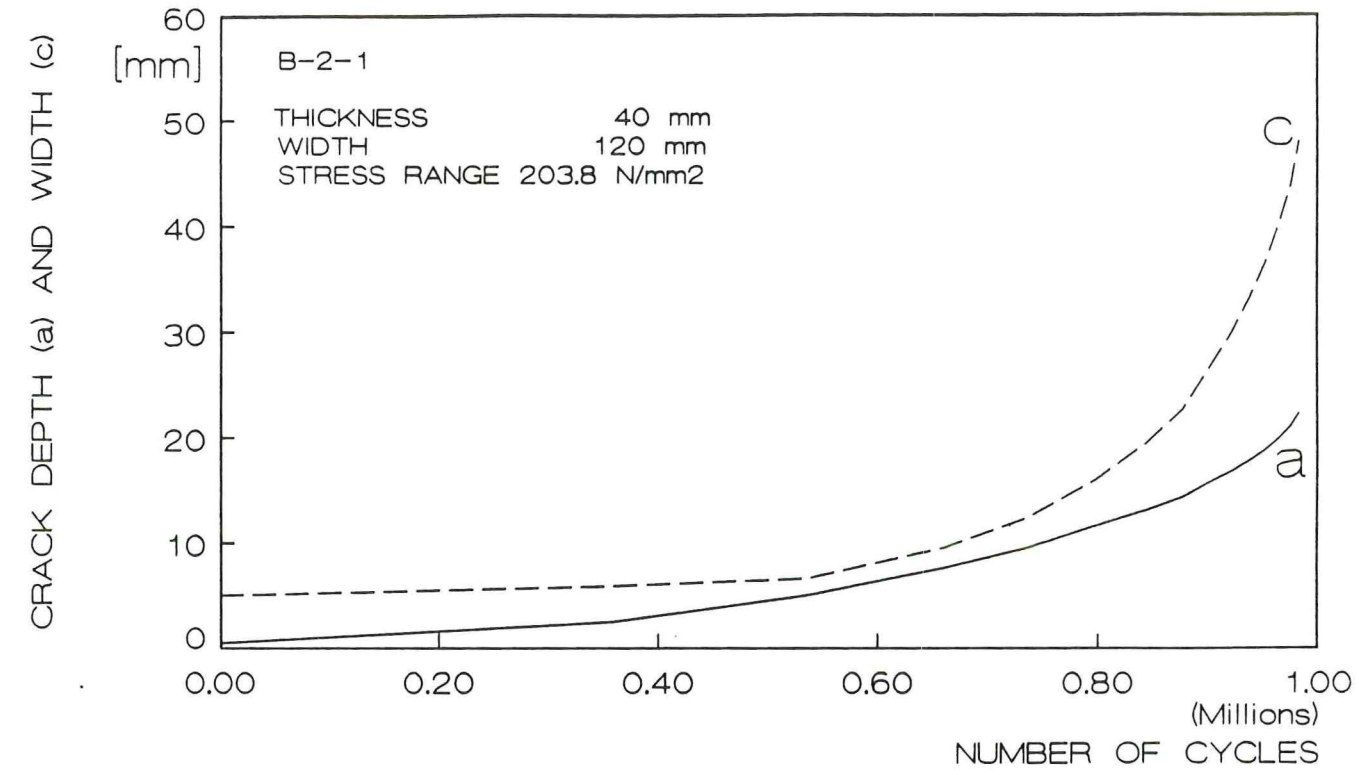

Figure 3-13: Crack growth curve specimen B-2-1

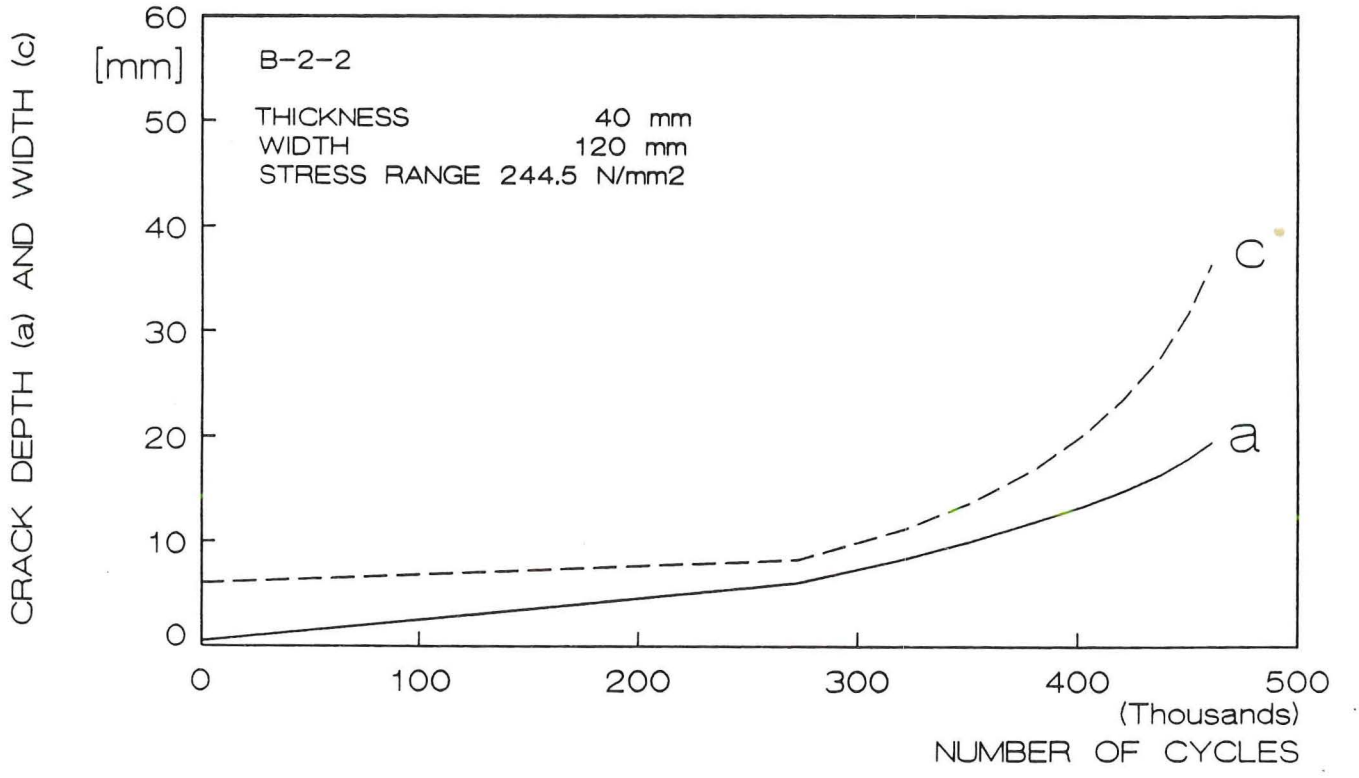

Figure 3-14: Crack growth curve specimen B-2-2

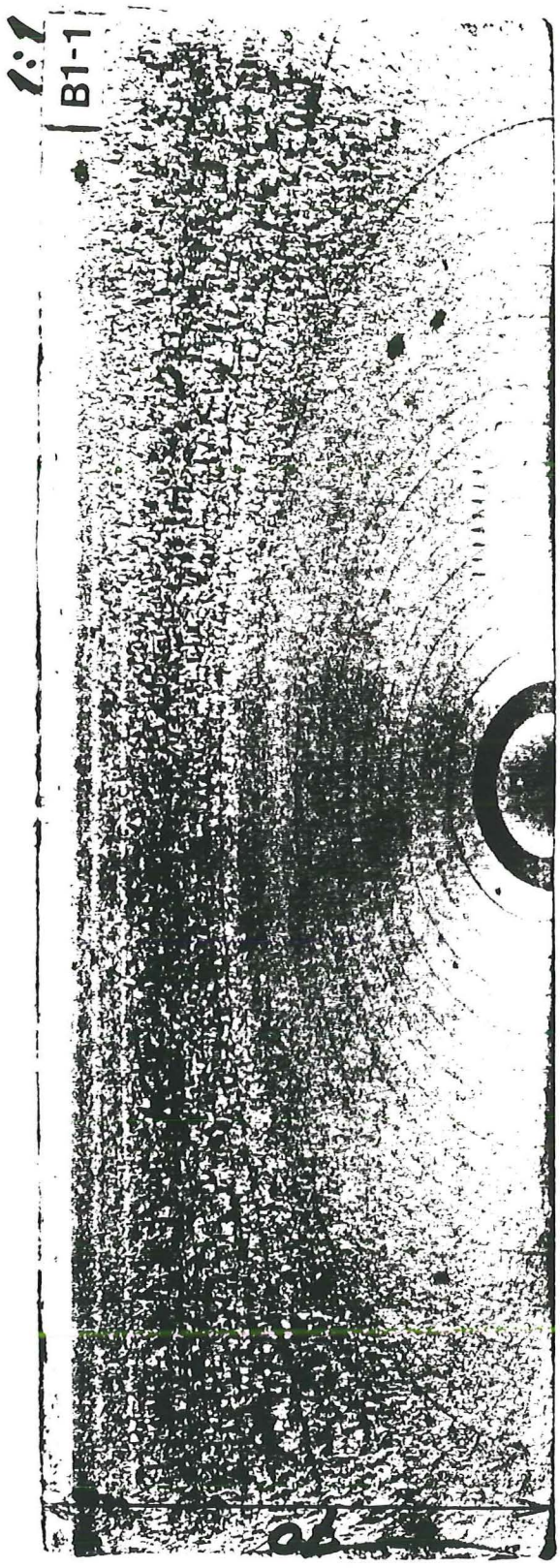

Figure 3-15: Fracture surface of specimen B-1-1 with crack markings

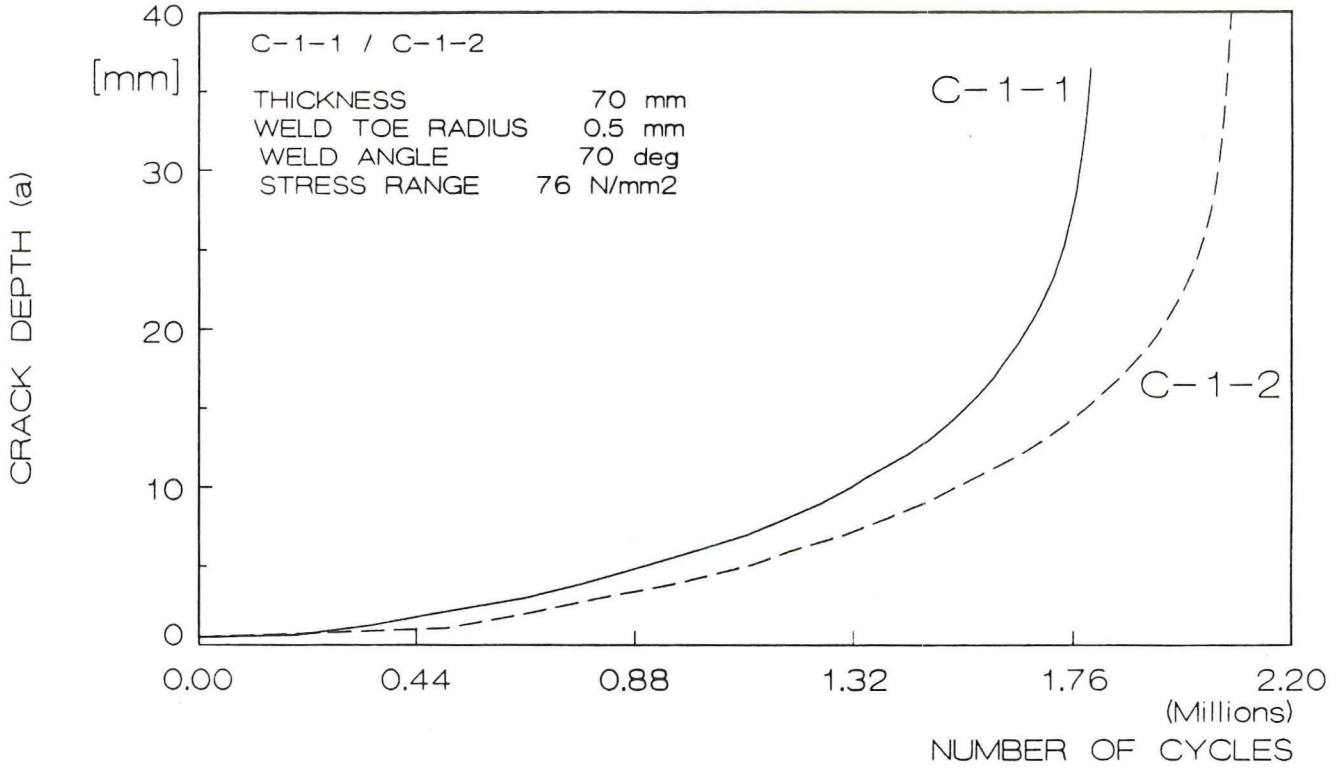

Figure 3-16: Crack growth curve specimen C-1-1 and C-1-2

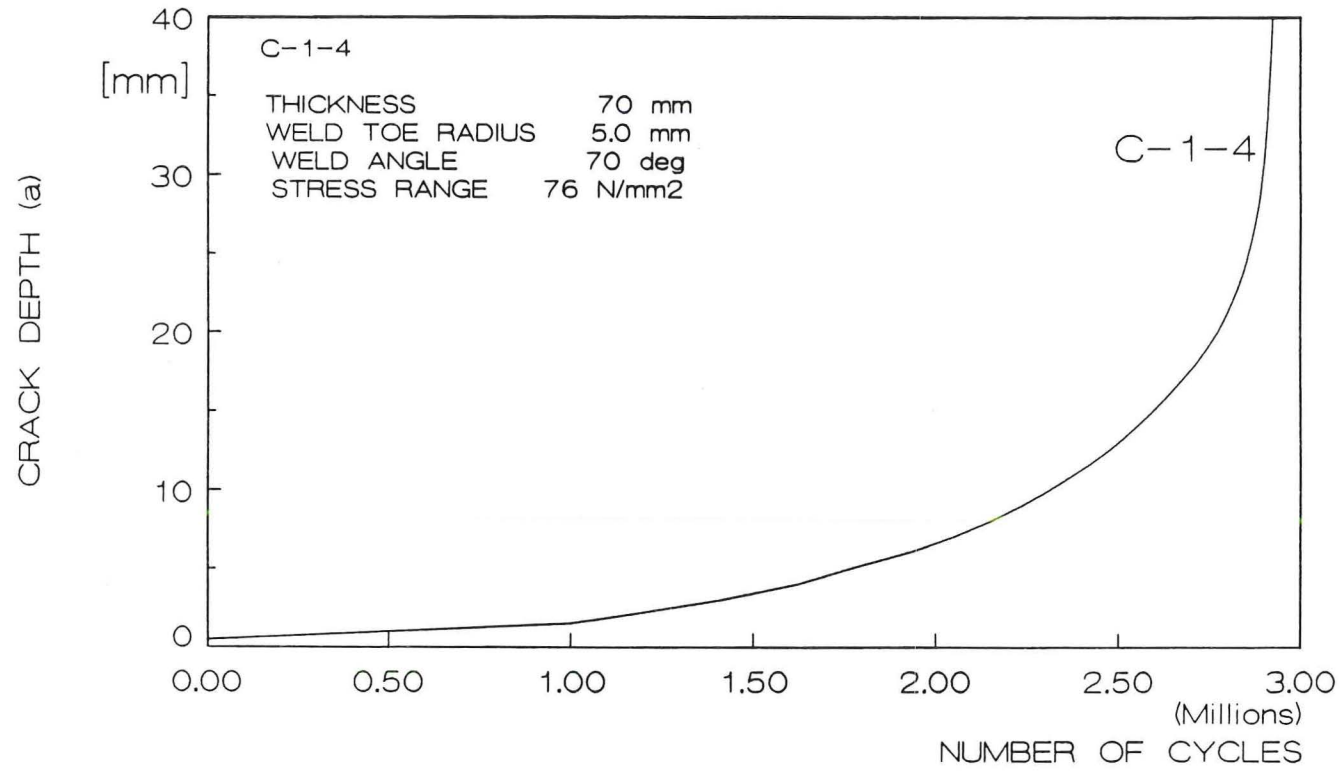

Figure 3-17: Crack growth curve specimen C-1-4

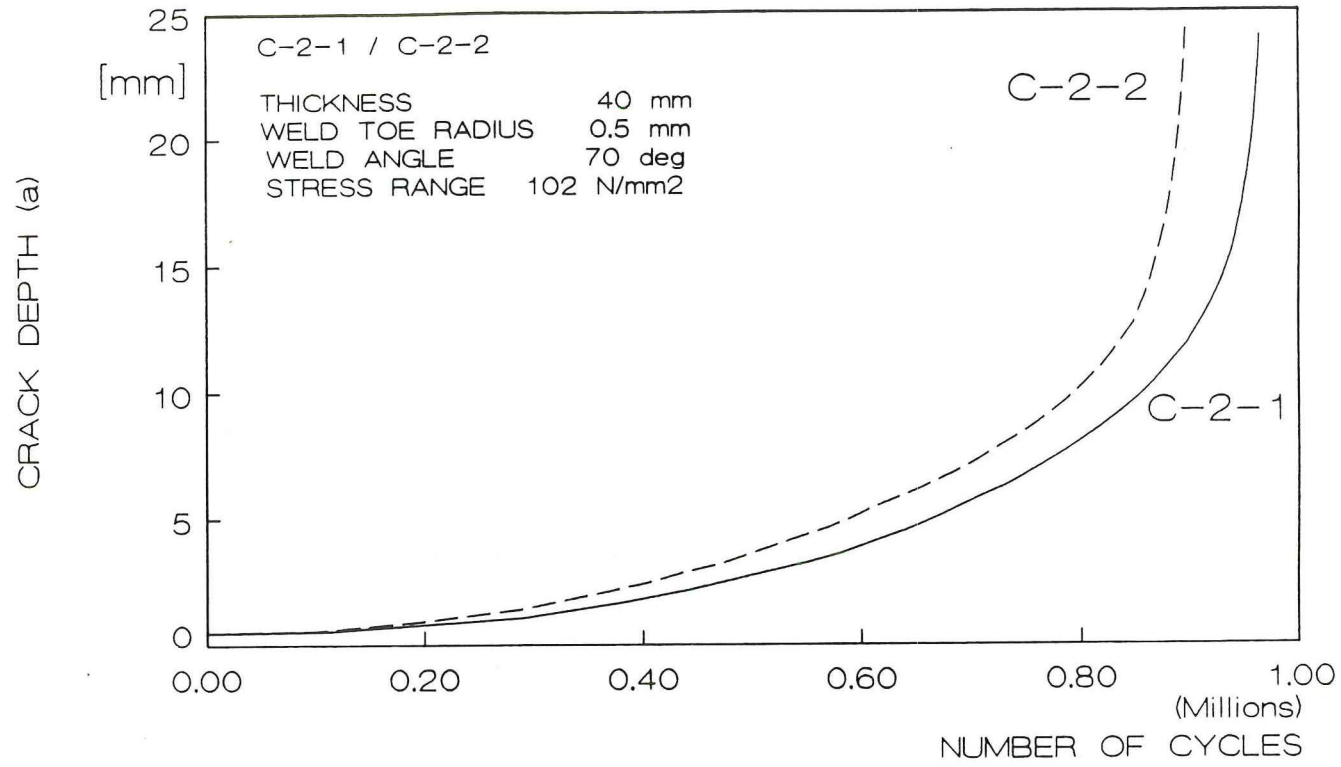

Figure 3-18: Crack growth curve specimen C-2-1 and C-2-2

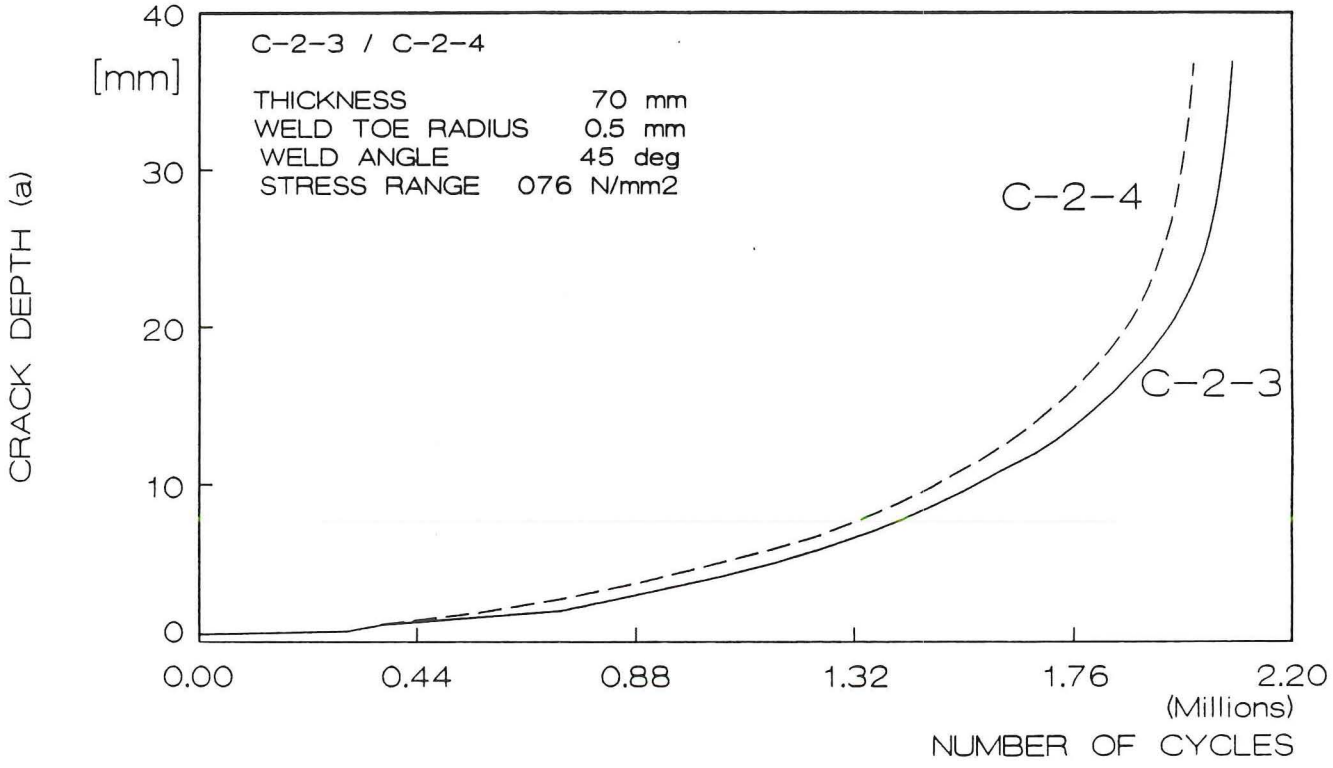

Figure 3-19: Crack growth curve specimen C-2-3 and C-2-4

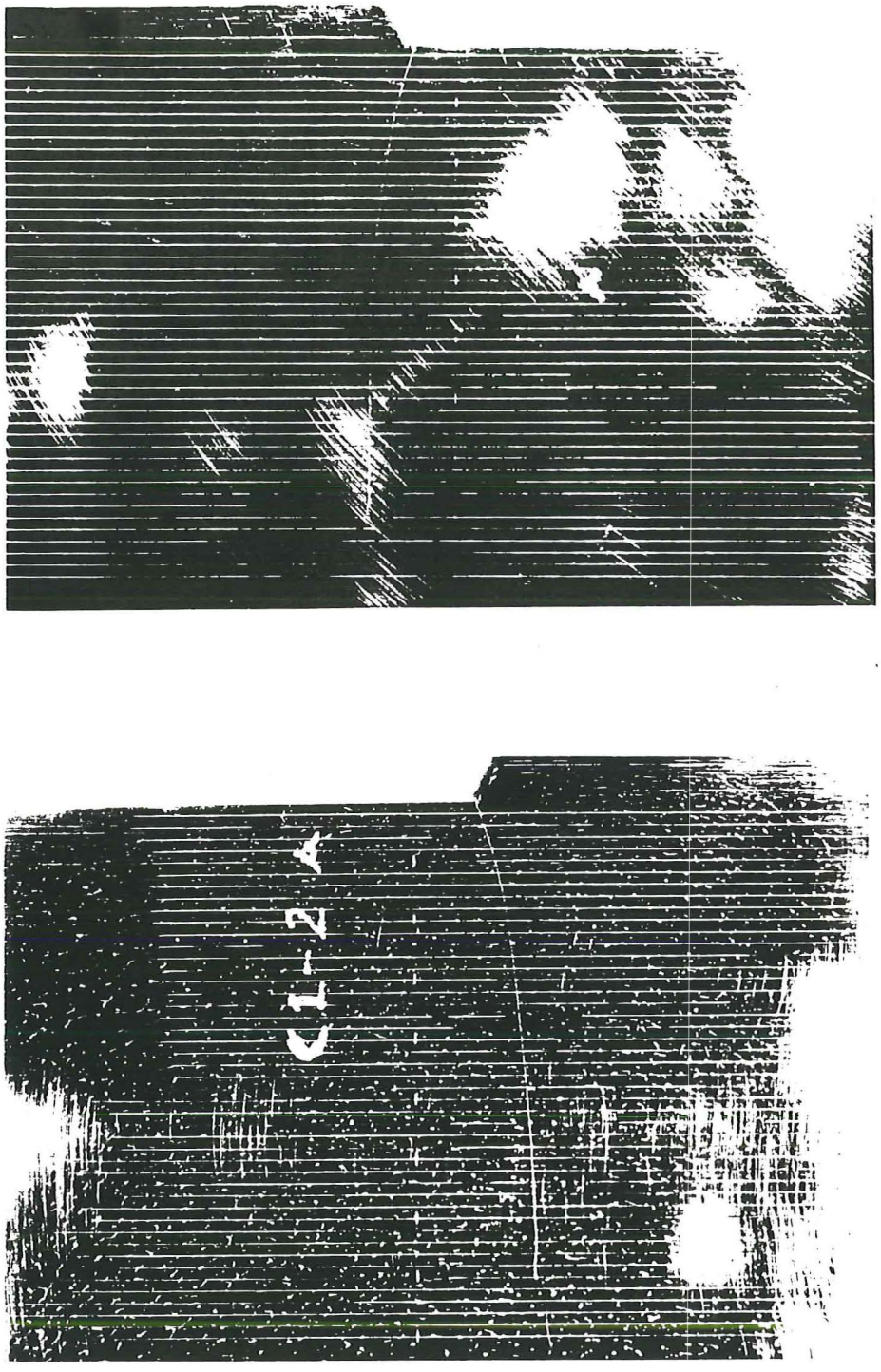

Figure 3-20: Crack growth path specimen C-1-2

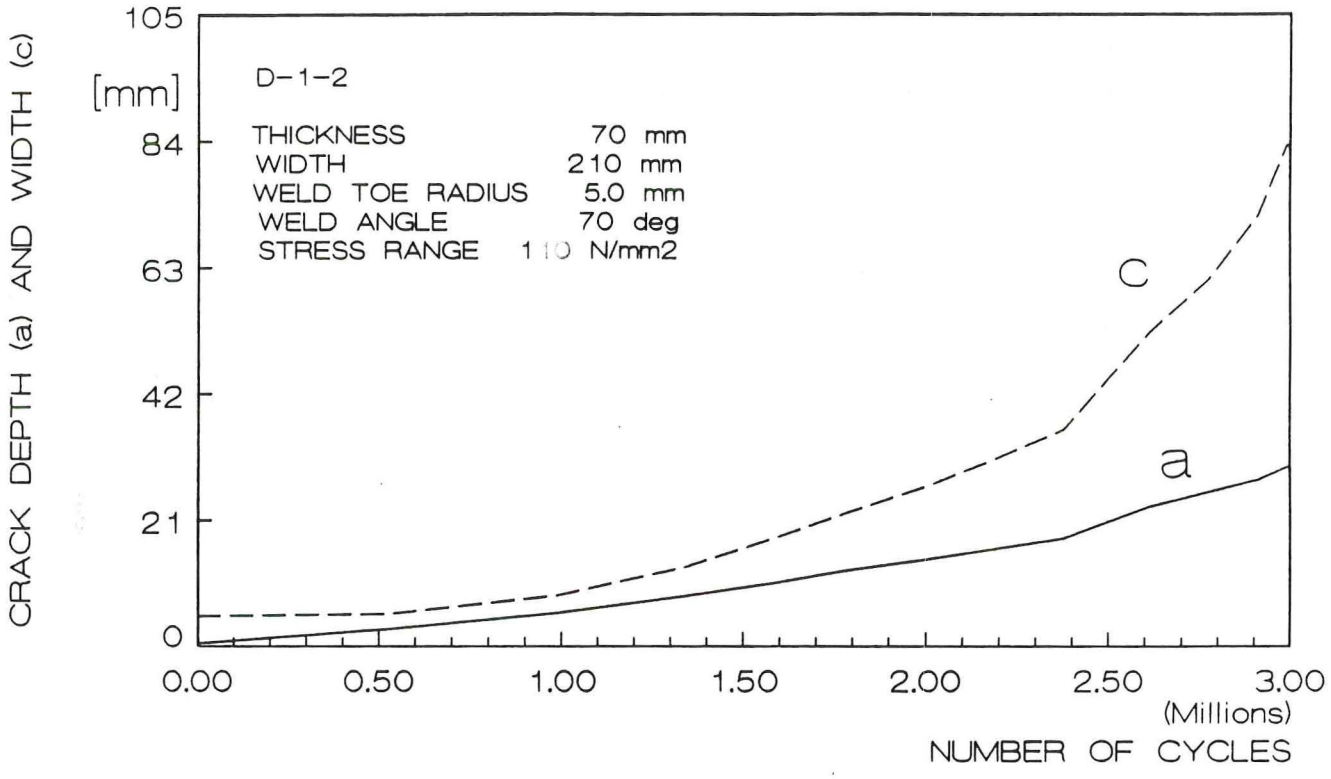

Figure 3-21: Crack growth curve specimen D-1-2

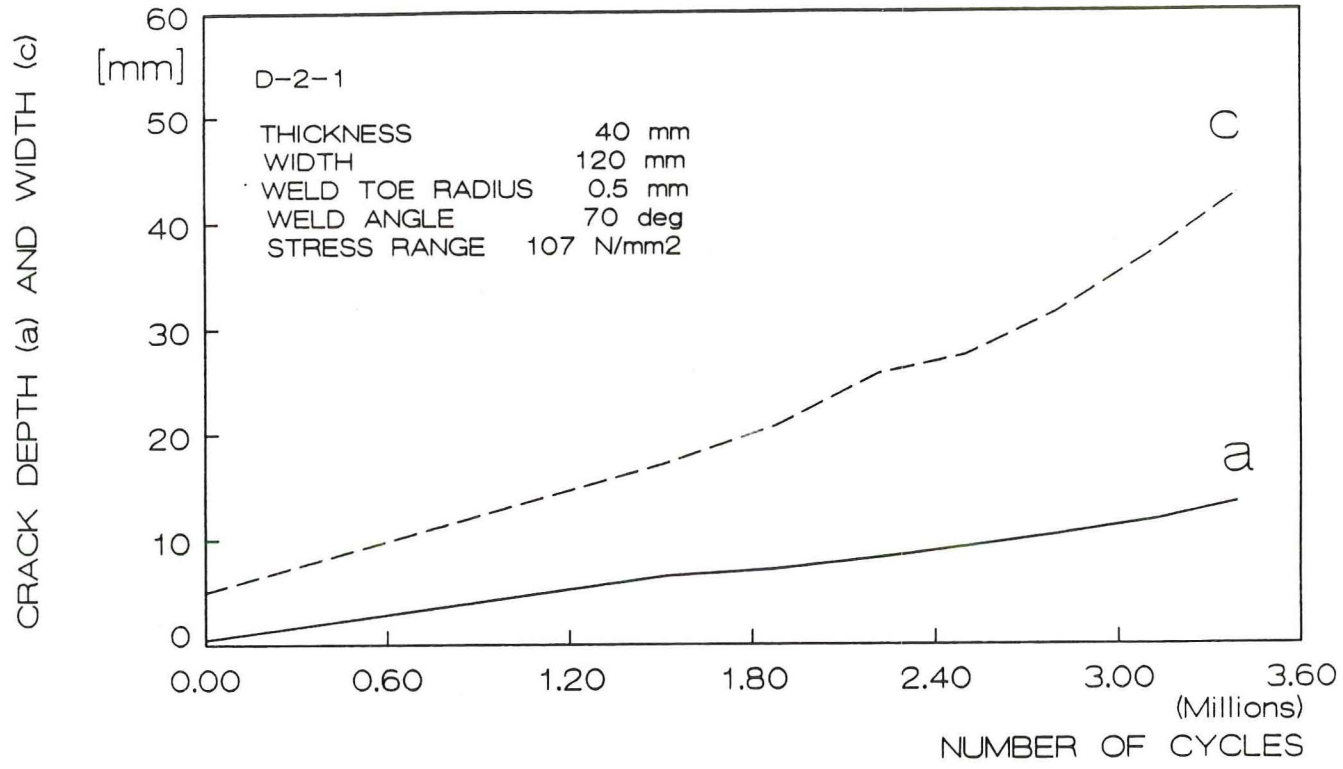

Figure 3-22: Crack growth curve specimen D-2-1

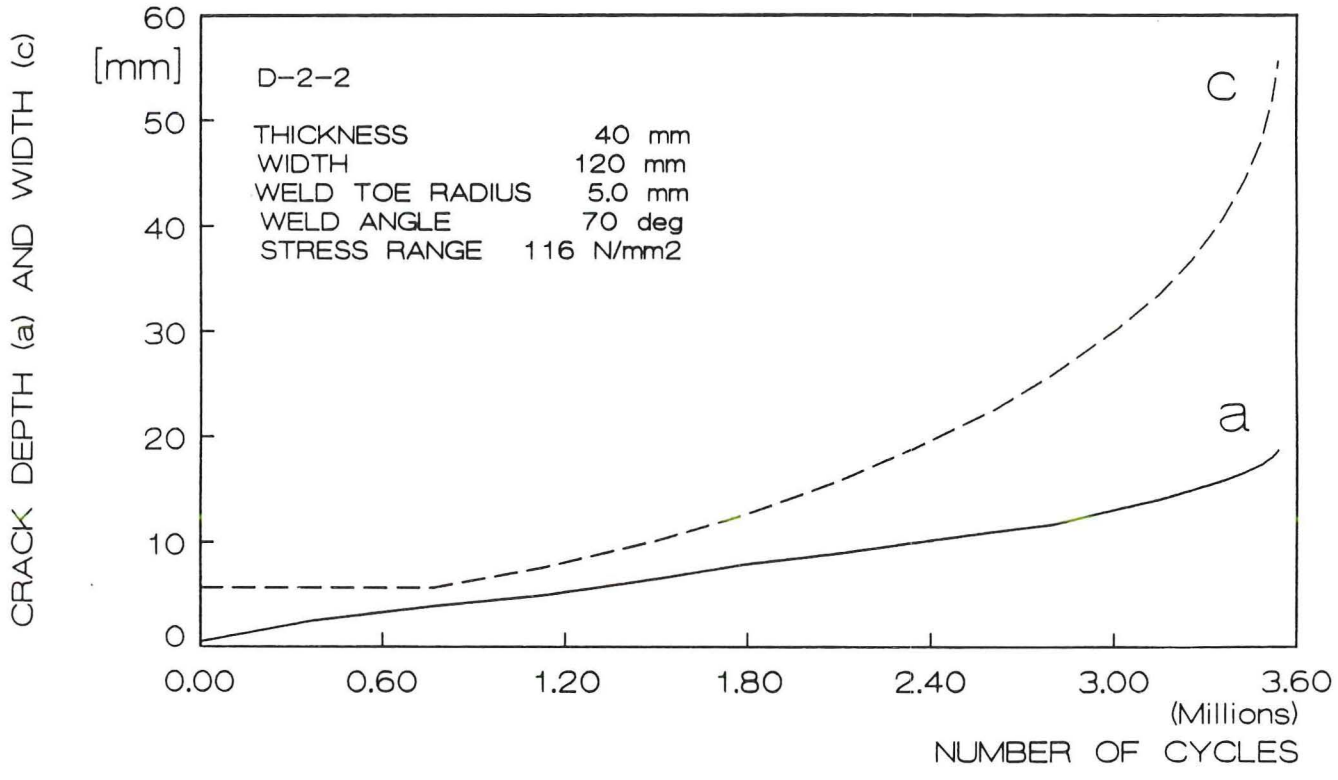

Figure 3-23: Crack growth curve specimen D-2-2

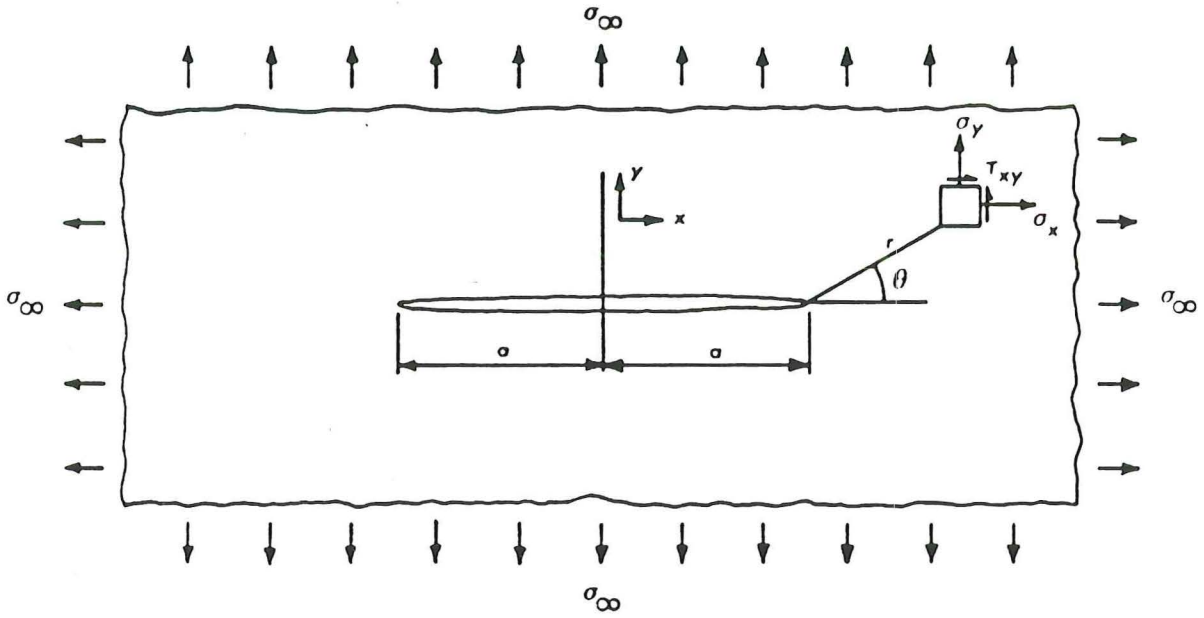

Figure 4-1: A biaxially loaded infinite plate containing a slit crack

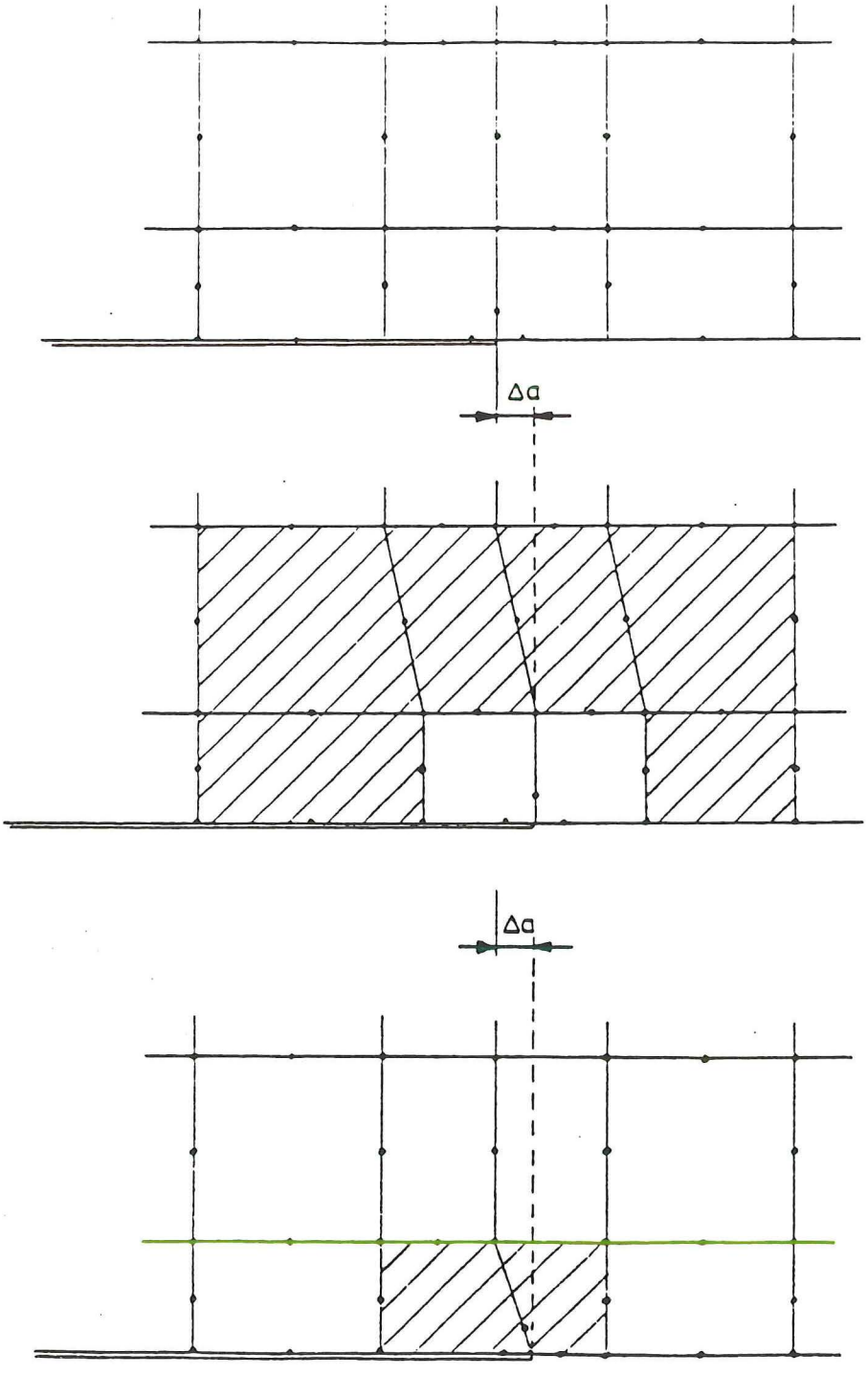

Figure 4-2: Virtual crack extension

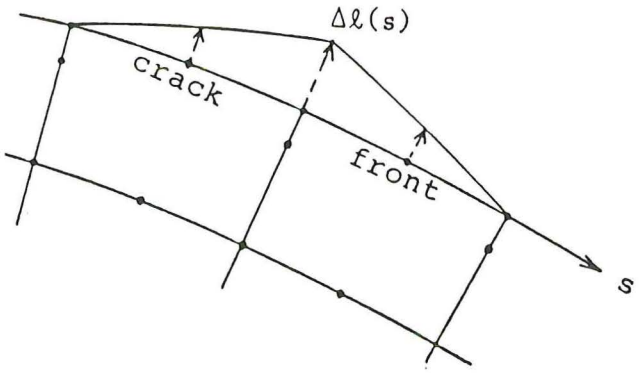

Figure 4-3: Triangular virtual crack extension

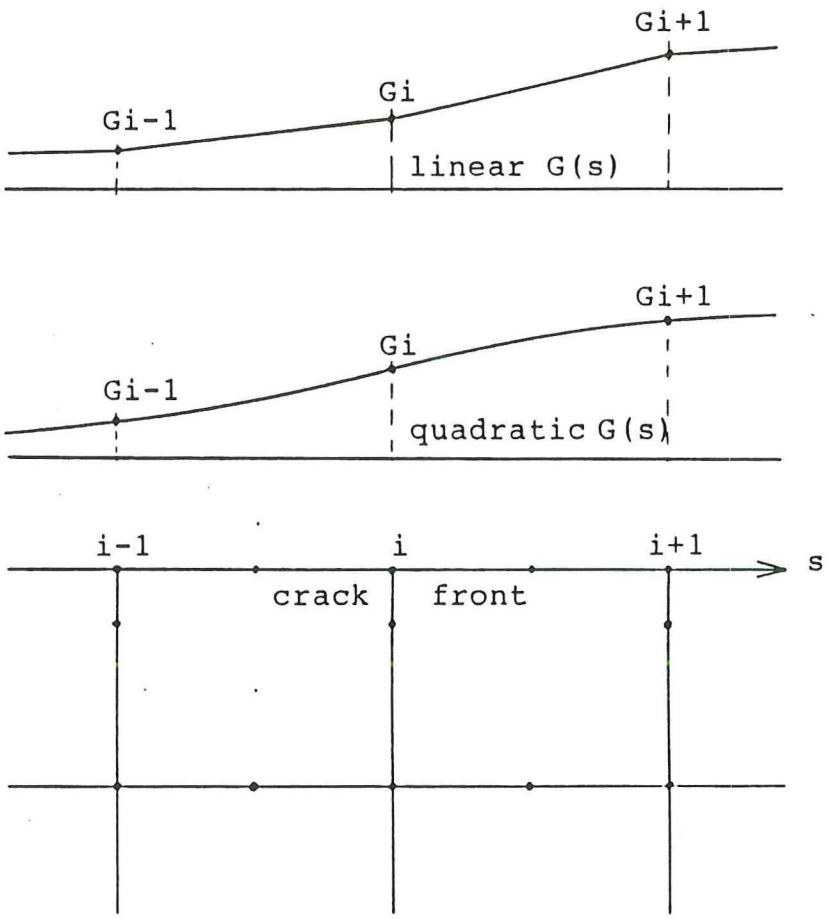

Figure 4-4: Assumed linear and quadratic distribution of (G)s along crack front

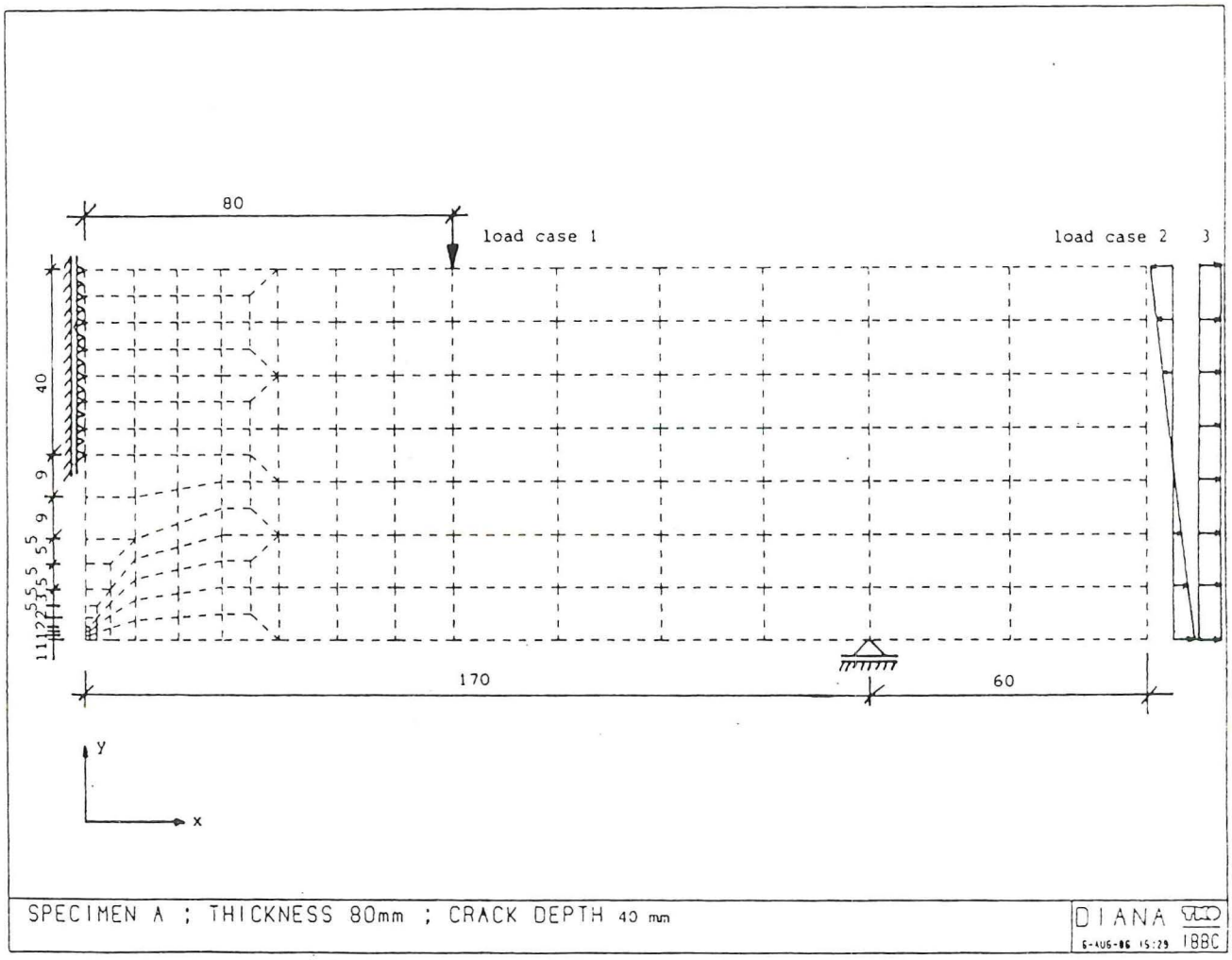

Figure 4-5: Finite element mesh of A-type specimen (T = 80 mm)

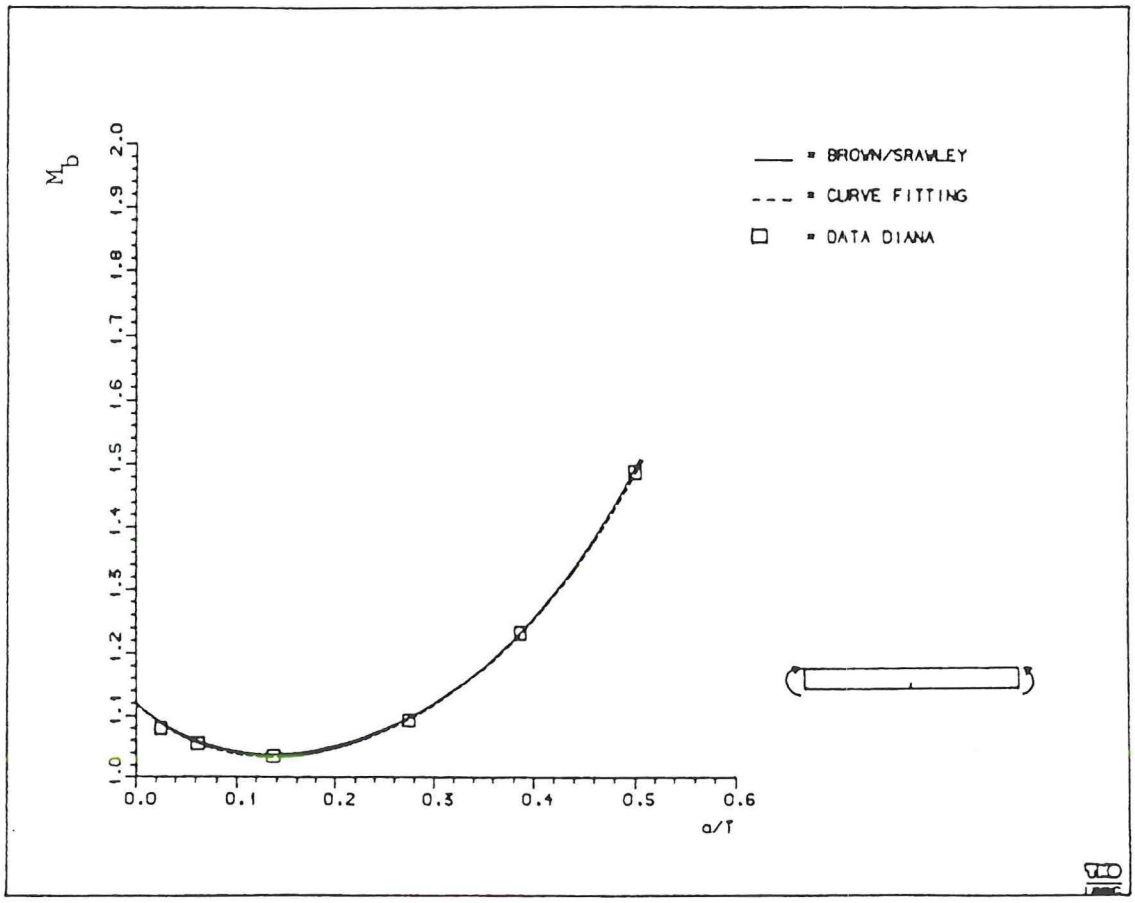

Figure 4-6: Stress intensity correction factor for an edge crack in a strip loaded in bending (M_b)

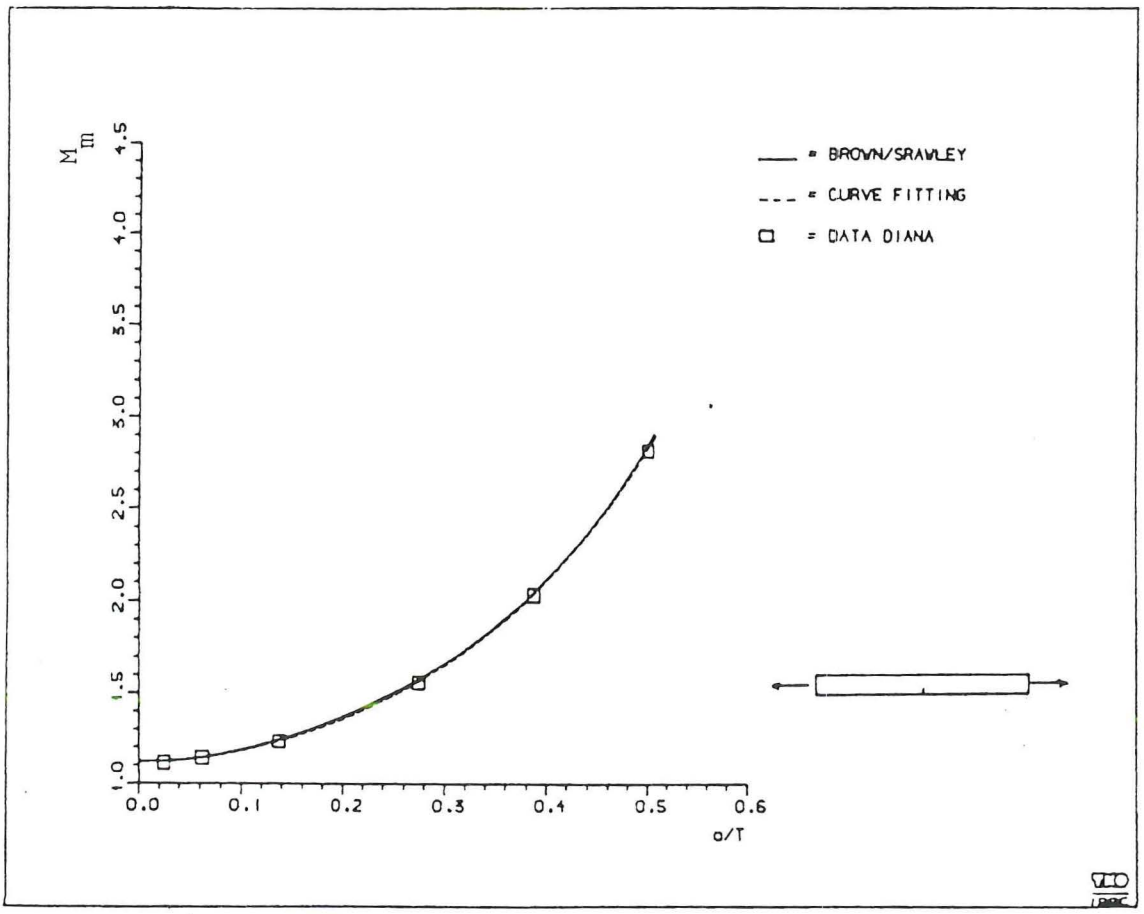

Figure 4-7: Stress intensity correction factor for an edge crack in a strip loaded in tension (M_m)

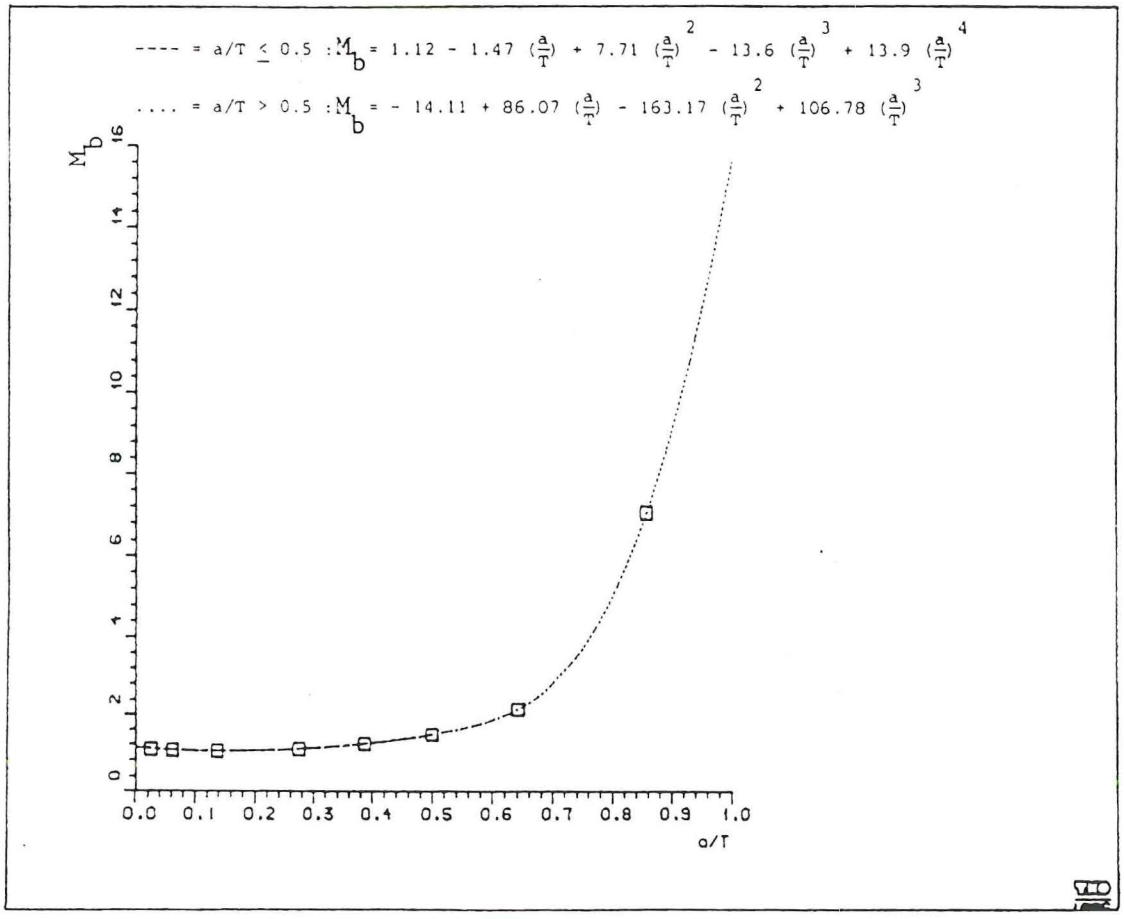

Figure 4-8: Analitical expression for M_b based on DIANA

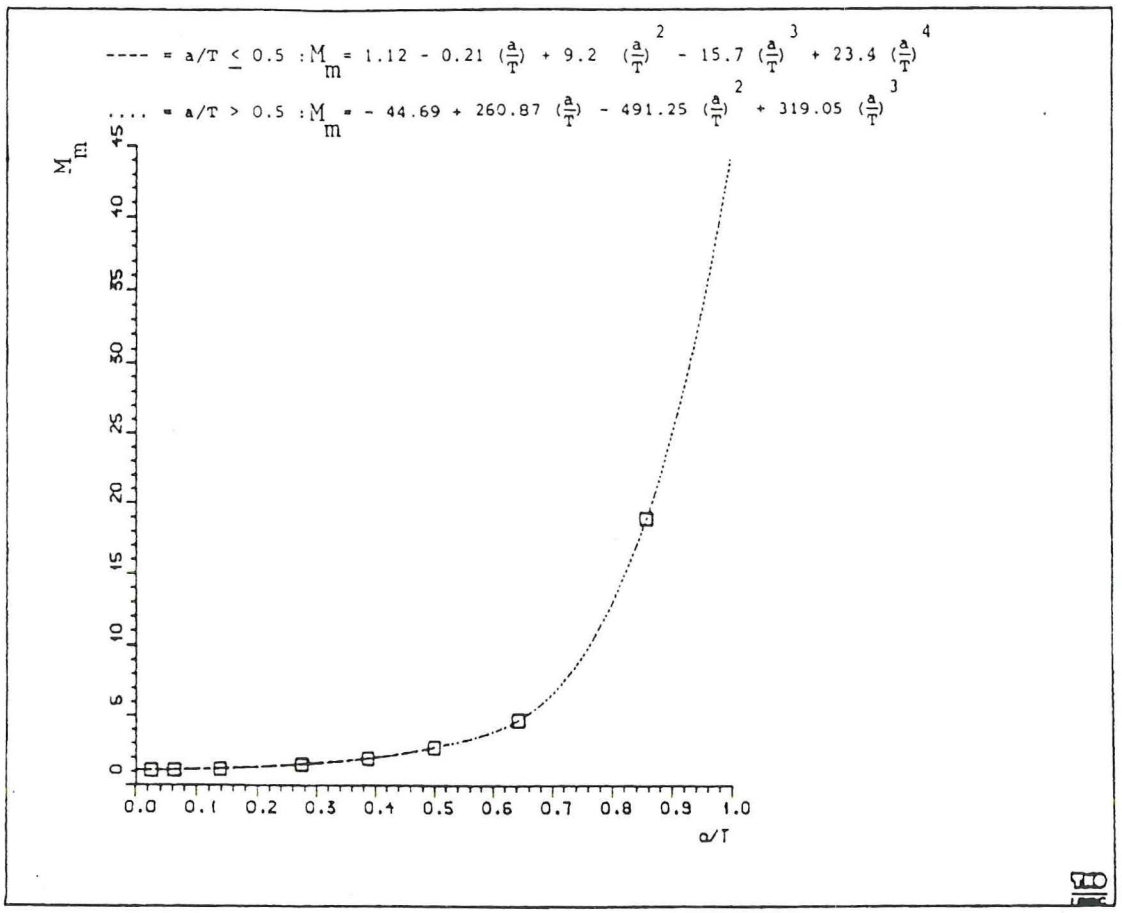

Figure 4-9: Analitical expression for M_m based on DIANA

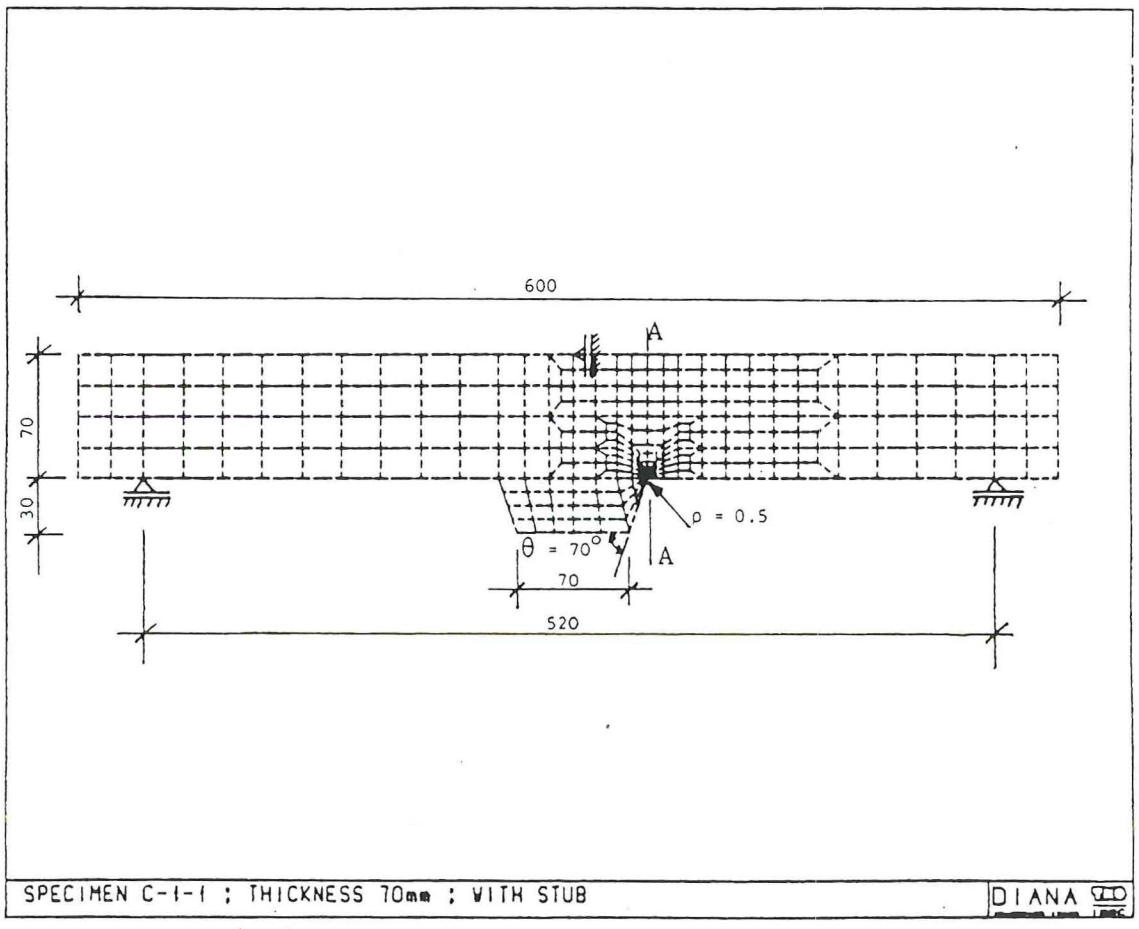

Figure 4-10: Finite element mesh geometry C-1-1

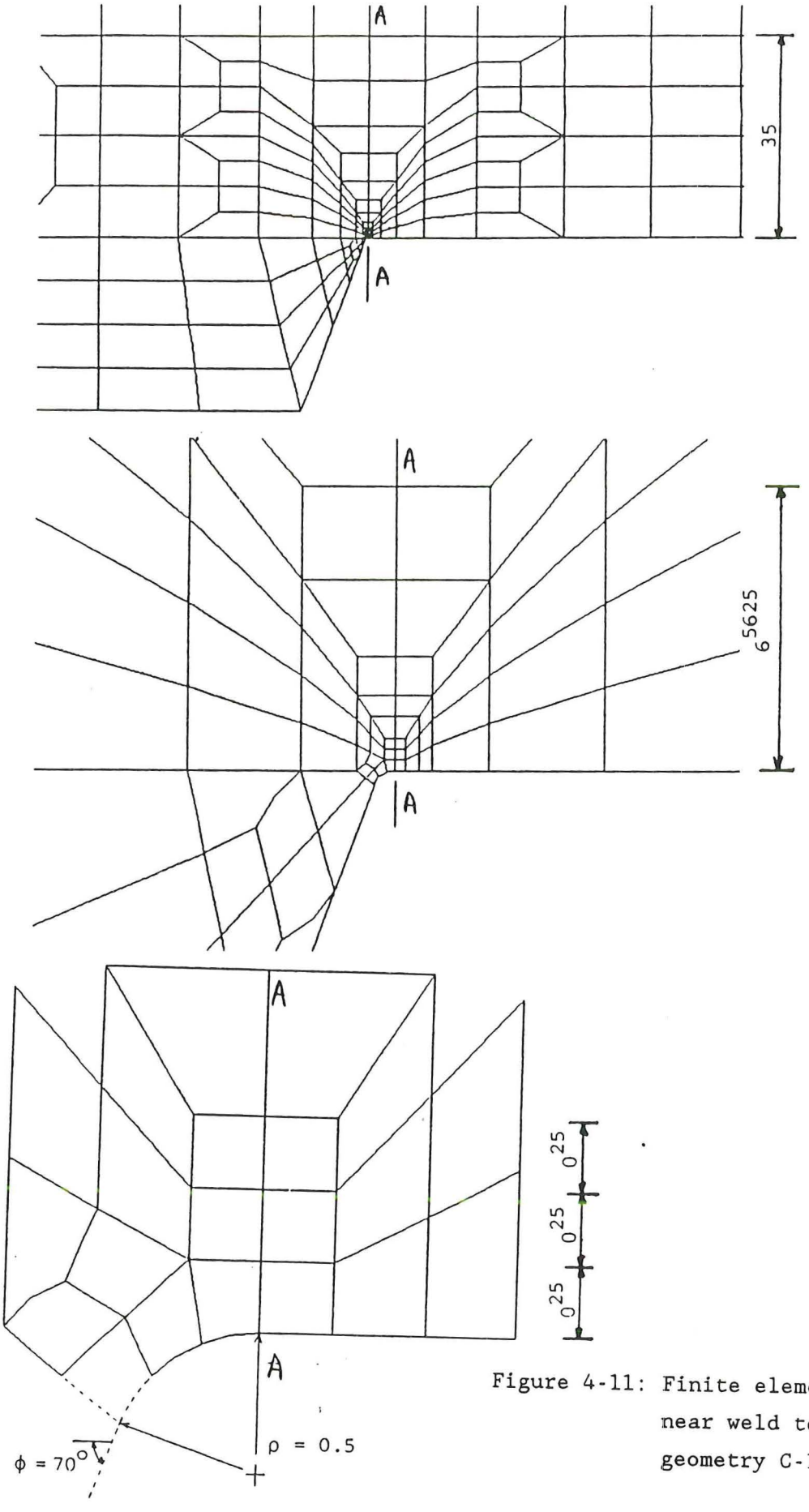

Figure 4-11: Finite element mesh near weld toe of geometry C-1-1

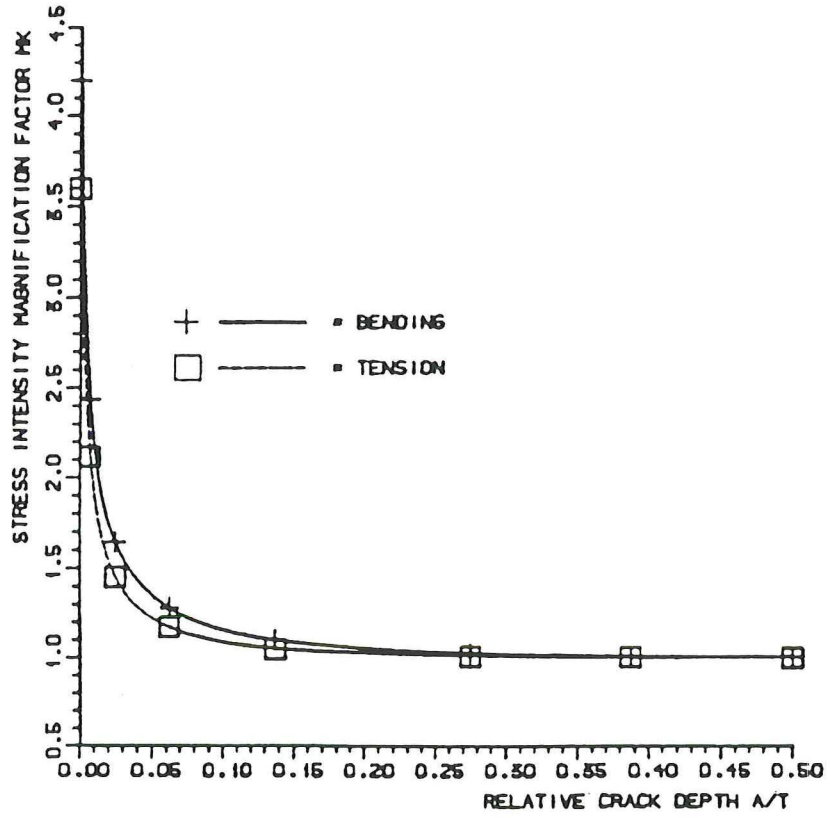

Figure 4-12: Stress intensity concentration factor M_k for C-1-1

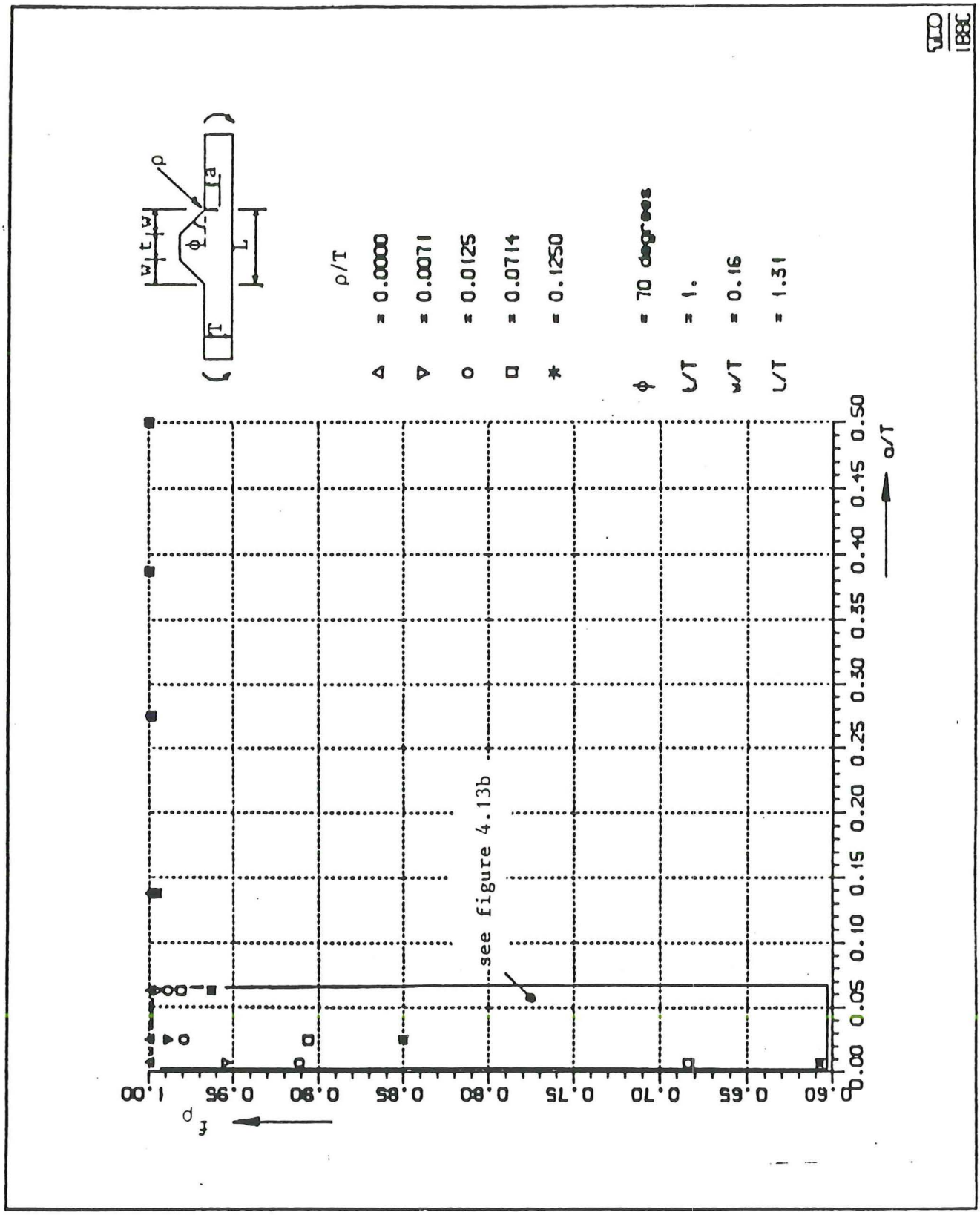

Figure 4-13a: f_ρ as a function of a/T for the bending loadcase

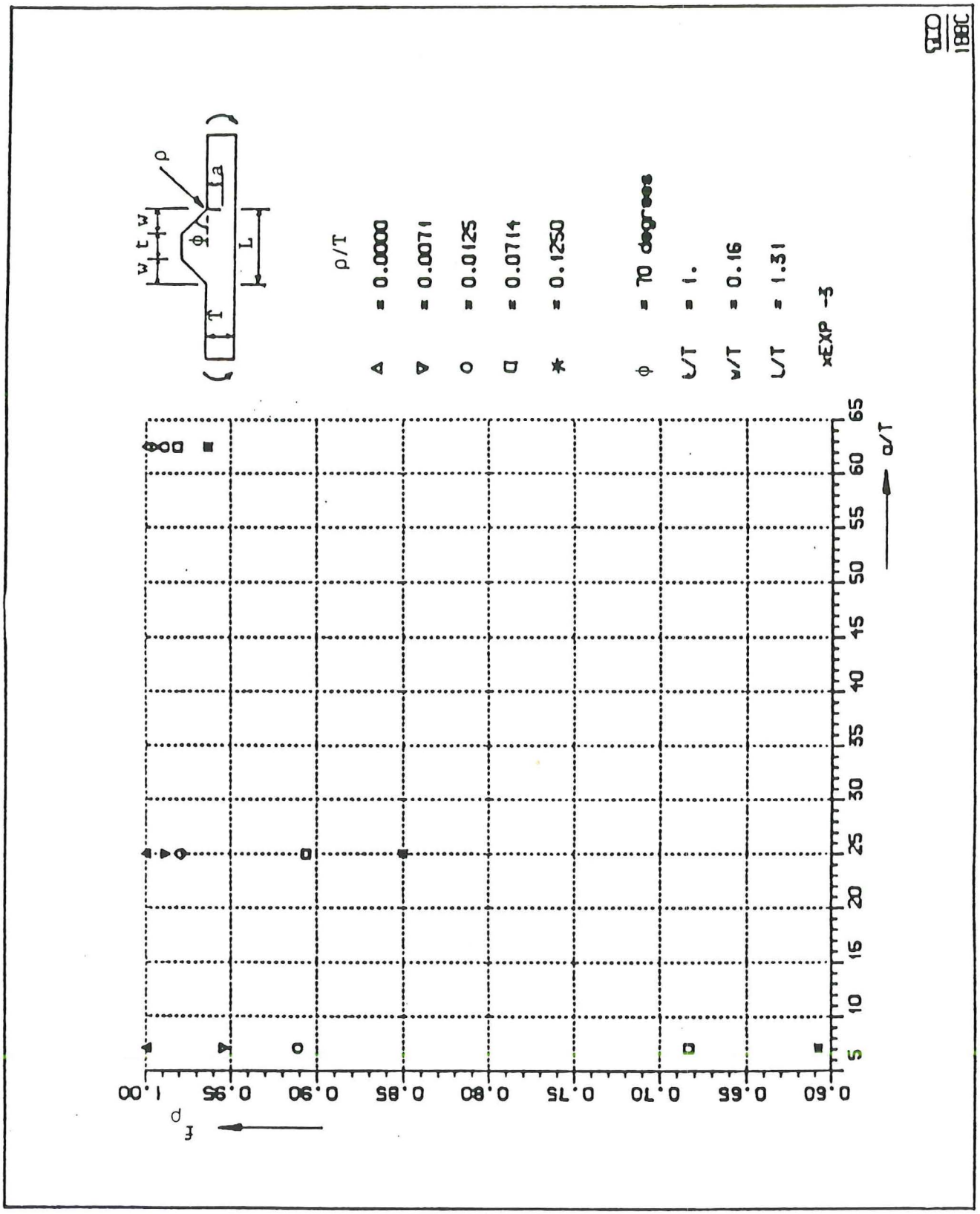

Figure 4-13b: f_ρ as a function of a/T for the bending loadcase, shallow cracks

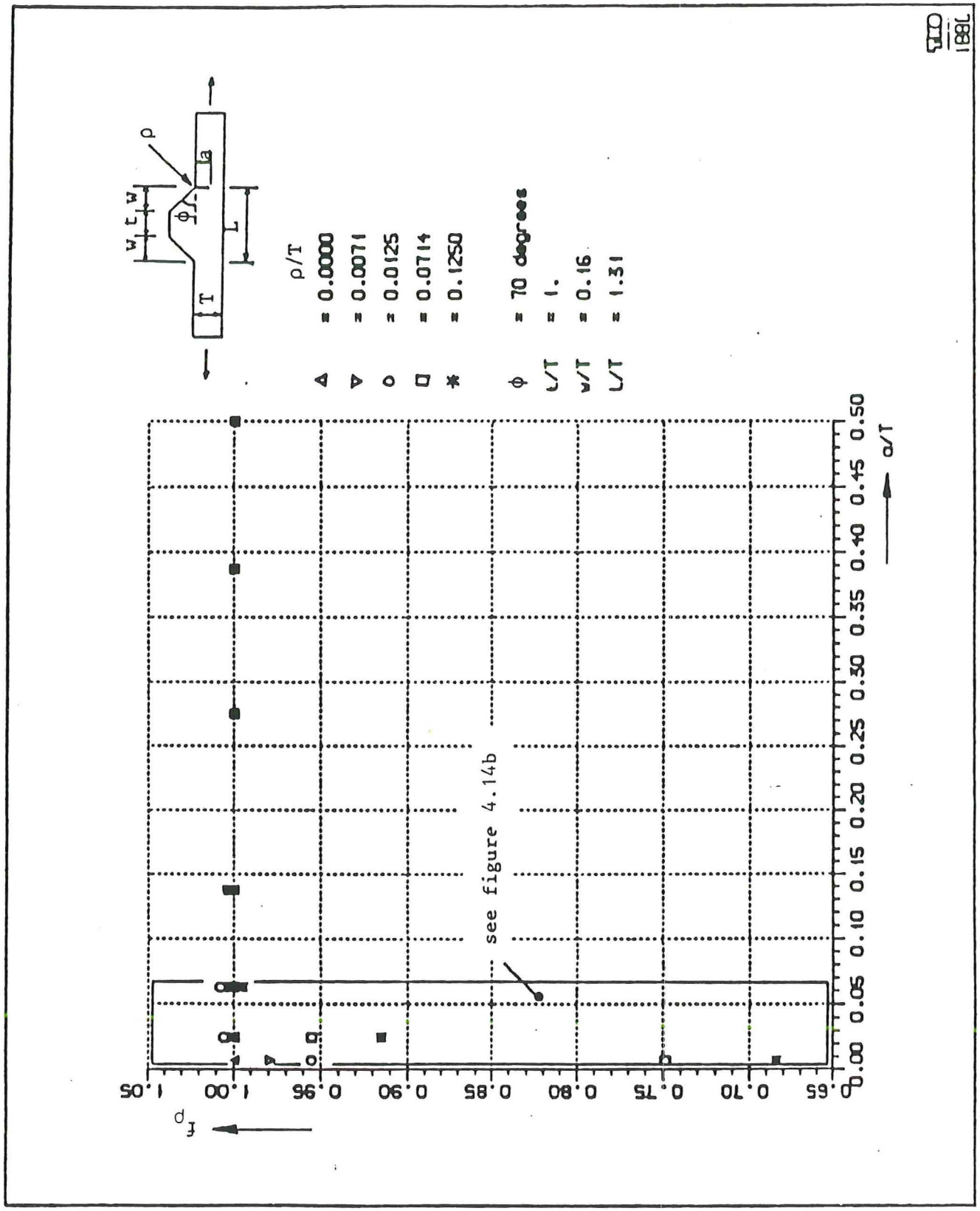

Figure 4-14a: f_ρ as a function of a/T for the tension loadcase

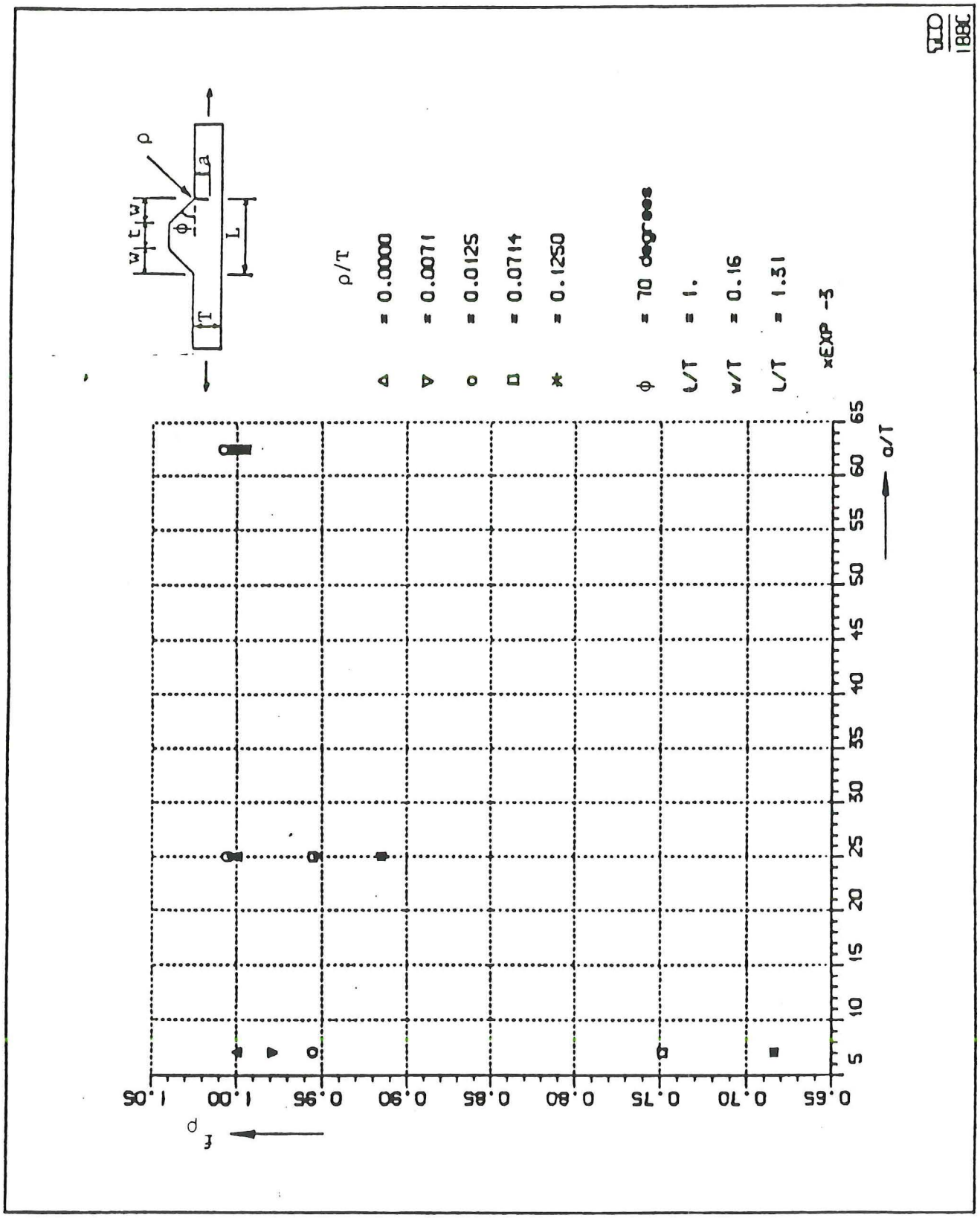

Figure 4-14b: f_ρ as a function of a/T for the tension loadcase, shallow cracks

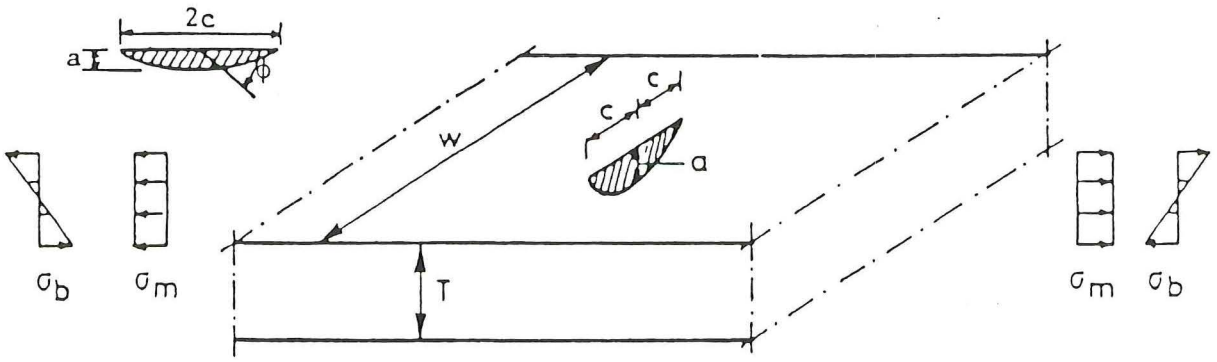

Figure 4-15: Finite width plate containing a semi-elliptical crack

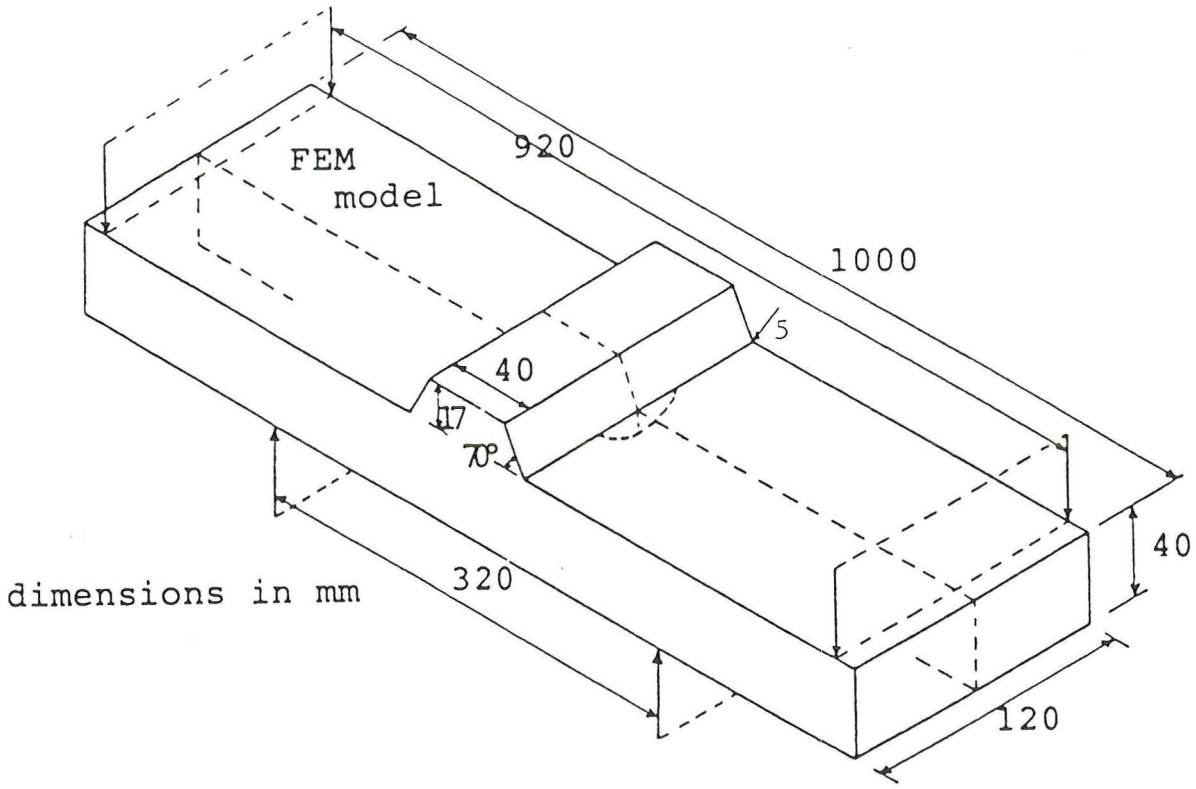

Figure 4-16: Dimensions of specimen D-2-2

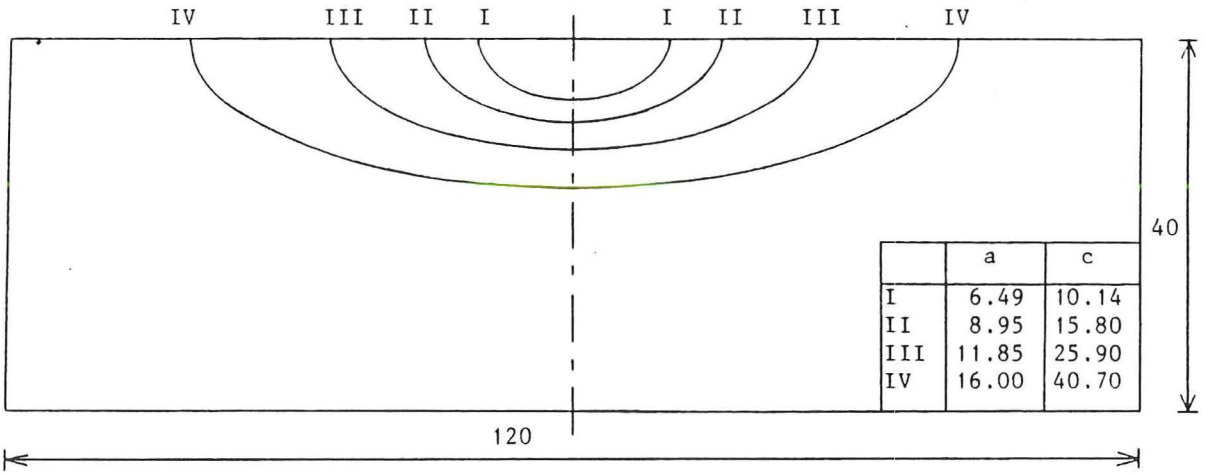

	a	c
I	6.49	10.14
II	8.95	15.80
III	11.85	25.90
IV	16.00	40.70

Figure 4-17: Calculated crack shapes of specimen D-2-2

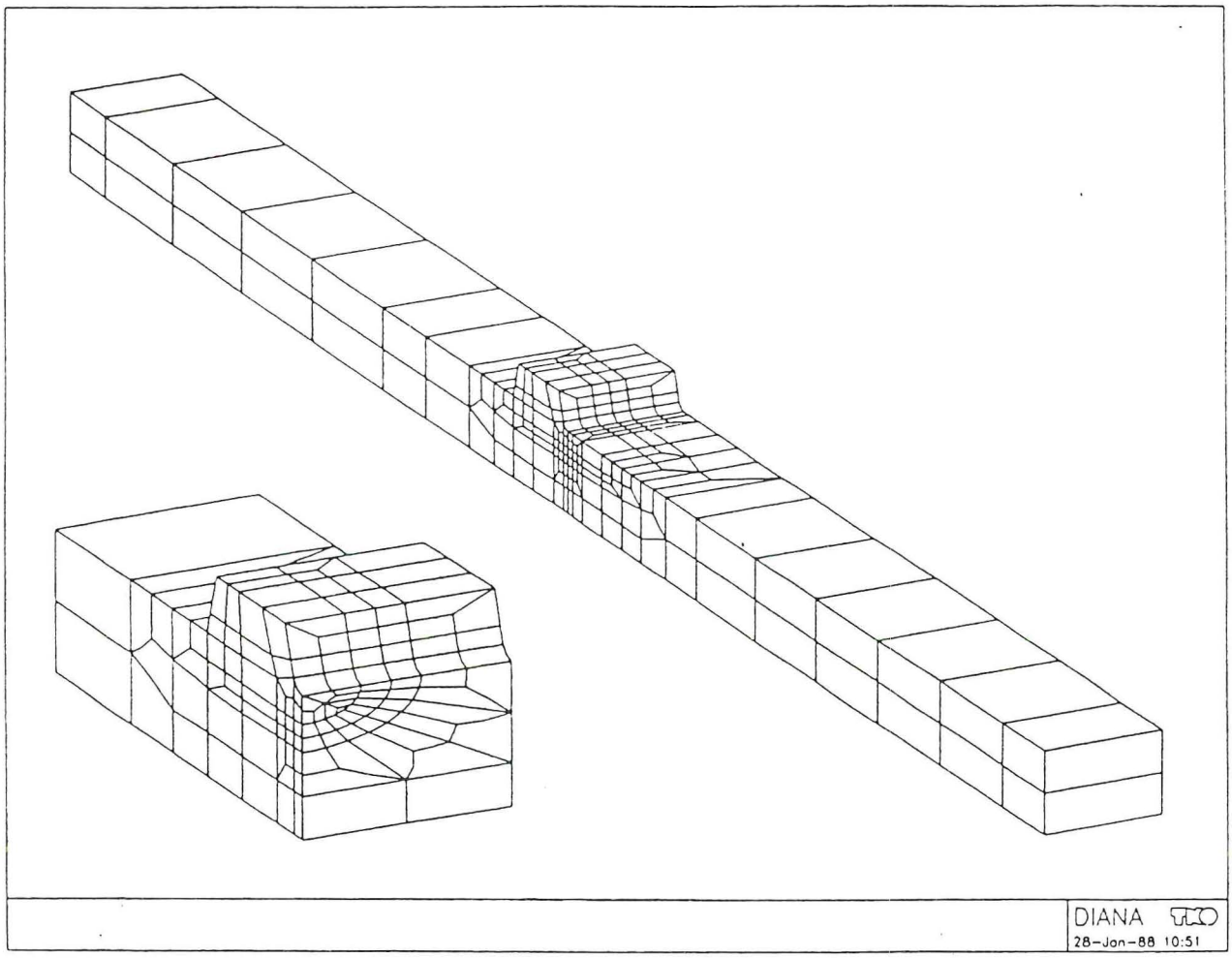

Figure 4-18: Mesh of specimen D-2-2 with stub, crack III, a = 11.85 mm, c = 25.90 mm

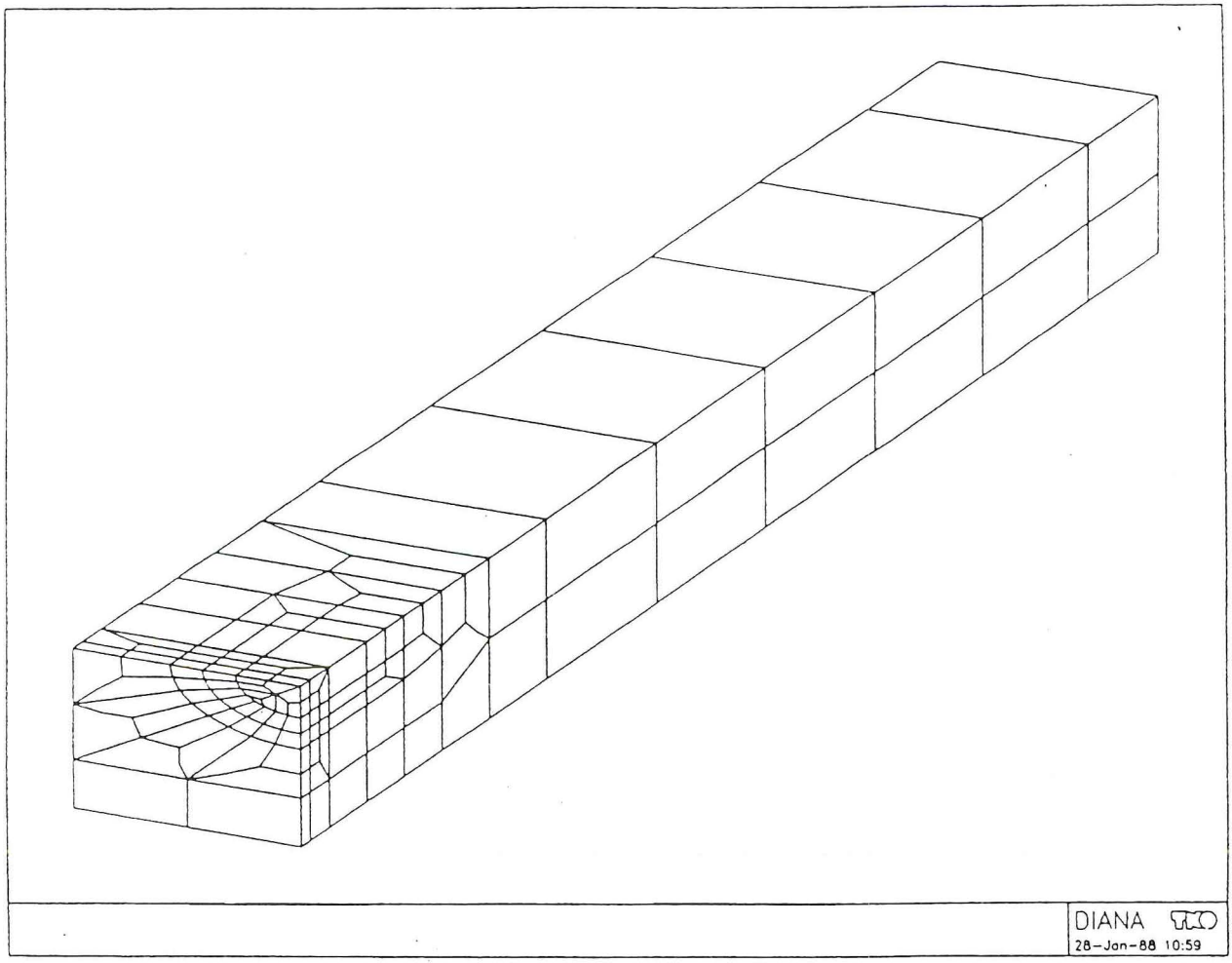

Figure 4-19: Mesh of specimen D-2-2 without stub, crack III, a = 11.85 mm, c = 25.90 mm

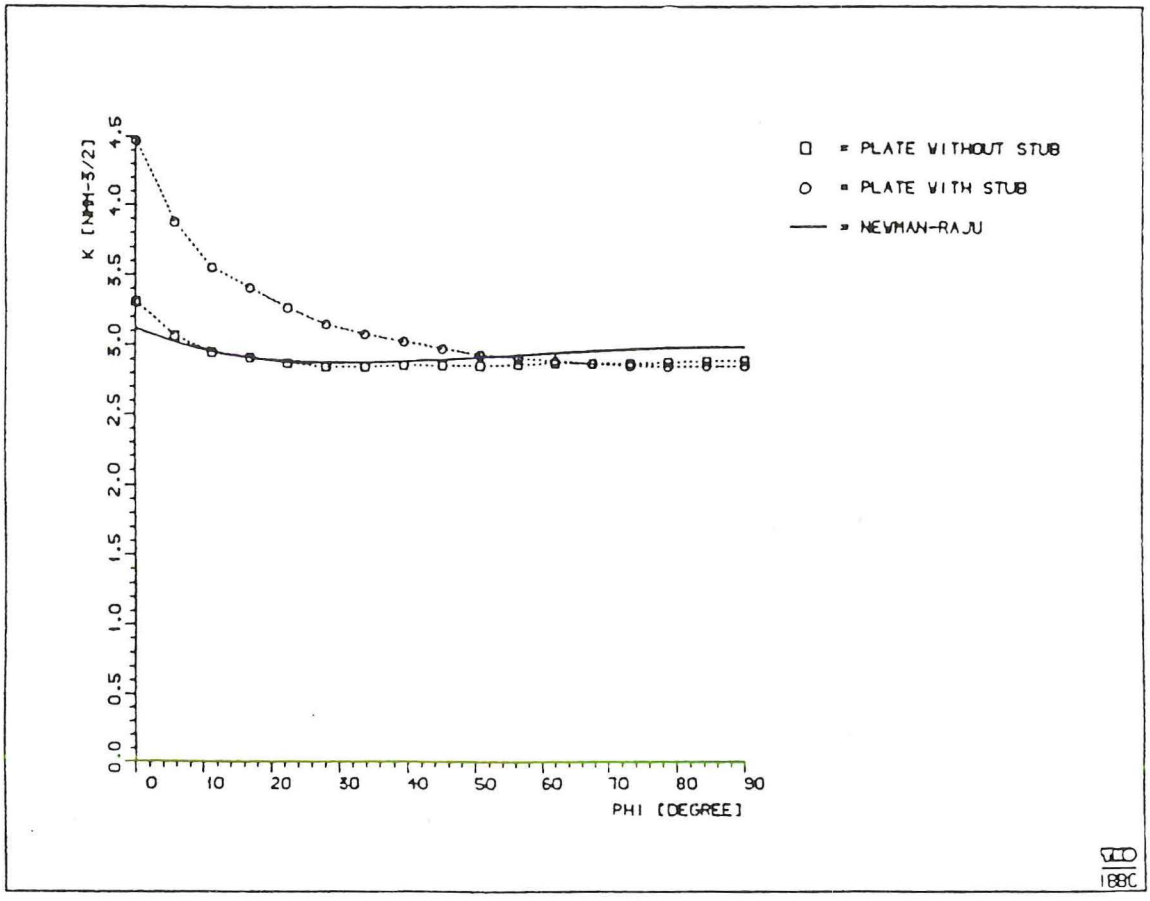

Figure 4-20: SIF for D-2-2 with crack I, bending

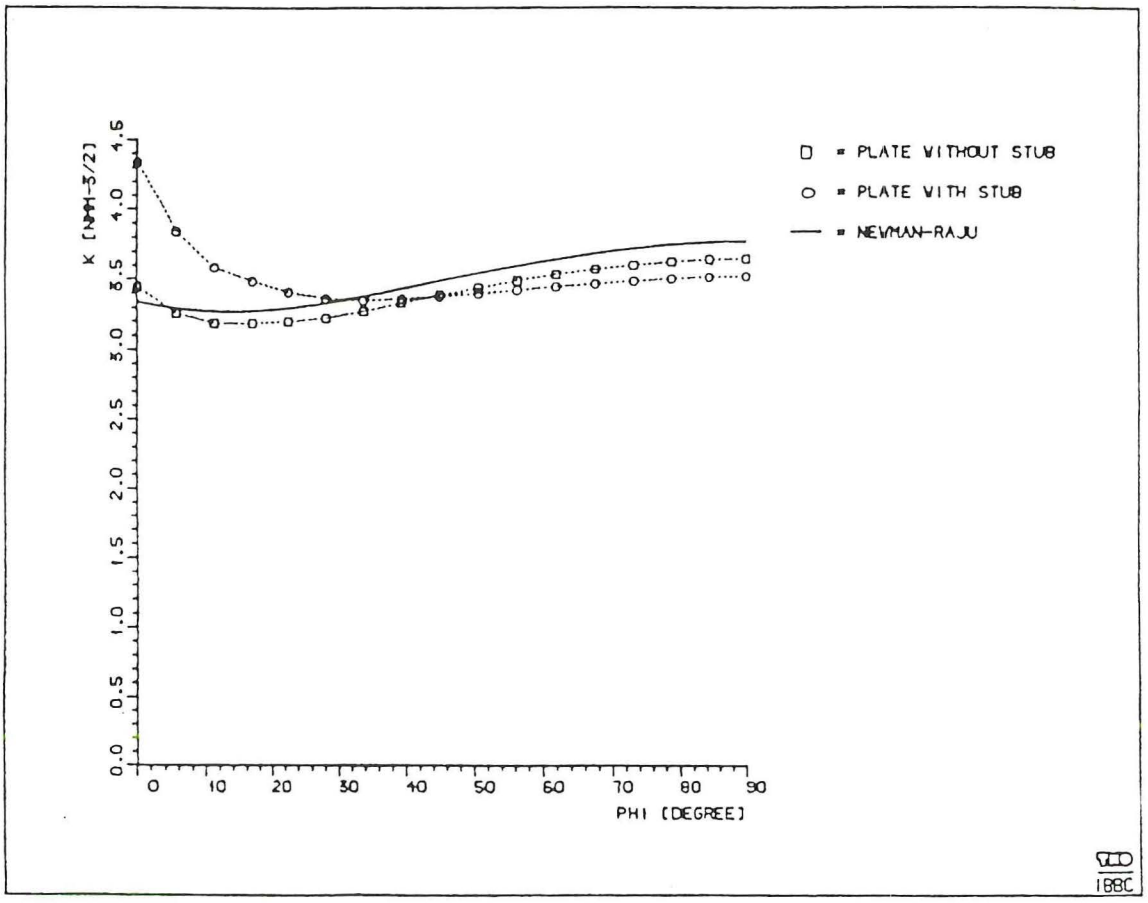

Figure 4-21: SIF for D-2-2 with crack I, membrane

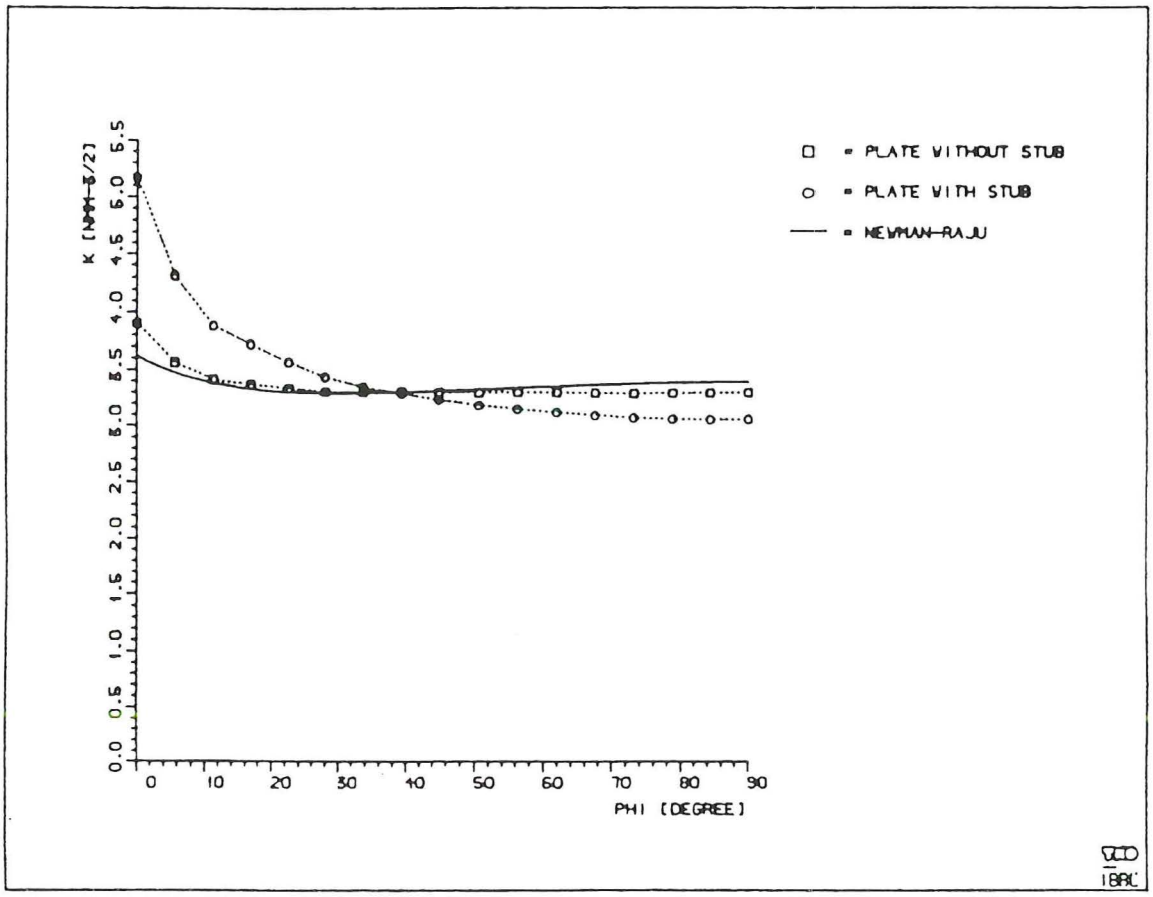

Figure 4-22: SIF for D-2-2 with crack II, bending

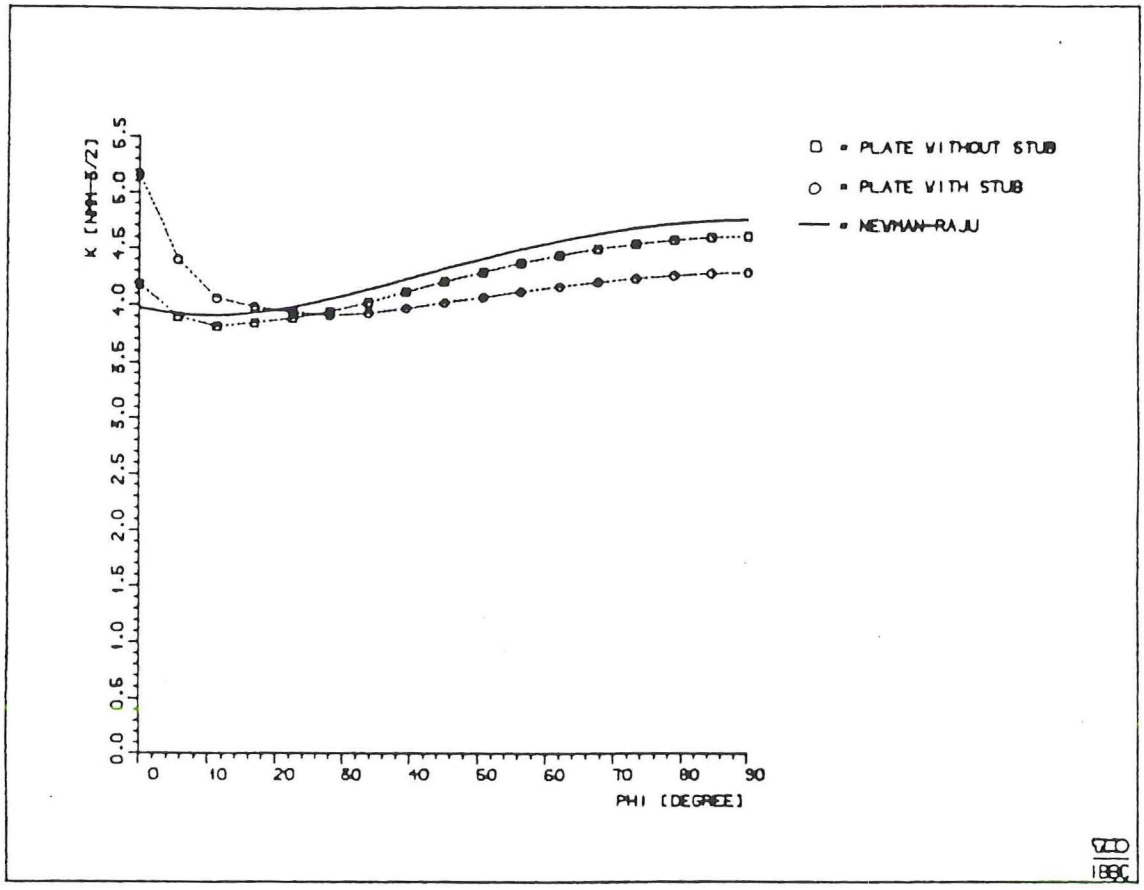

Figure 4-23: SIF for D-2-2 with crack II, membrane

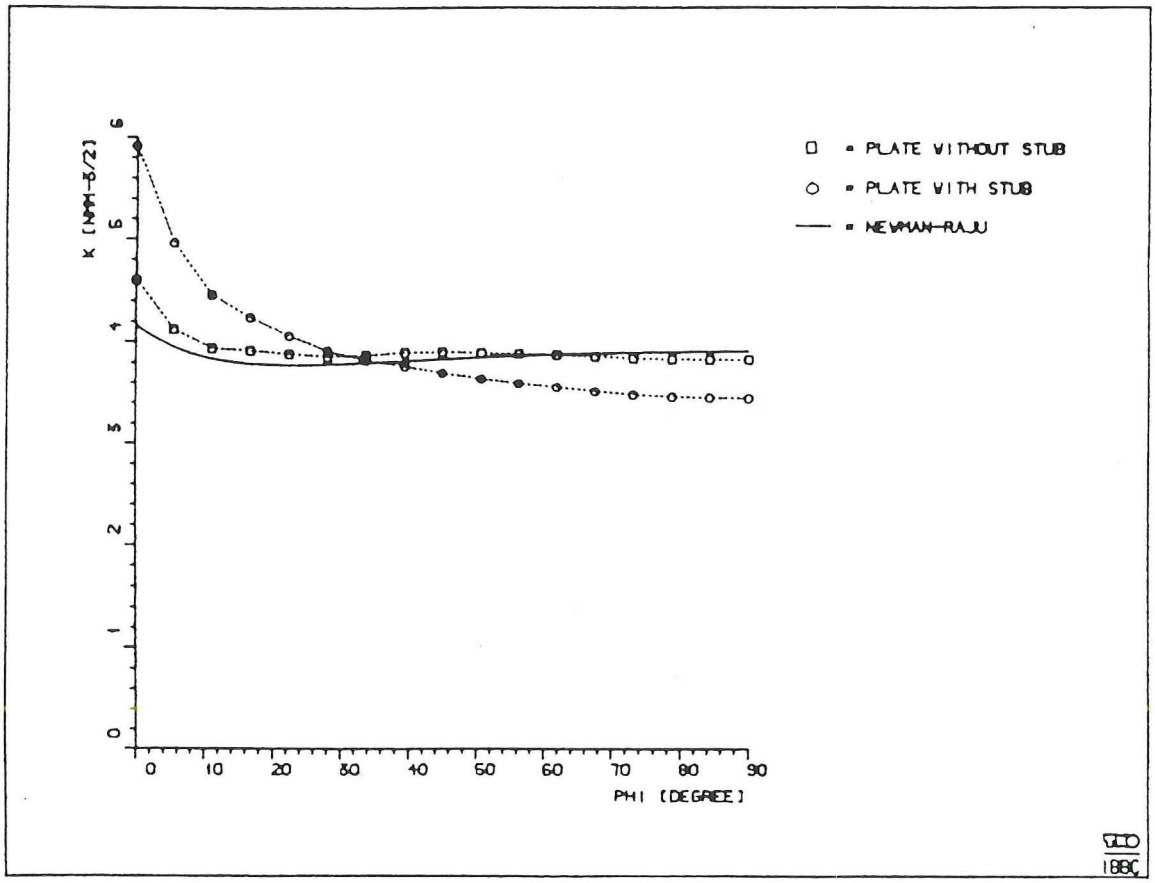

Figure 4-24: SIF for D-2-2 with crack III, bending

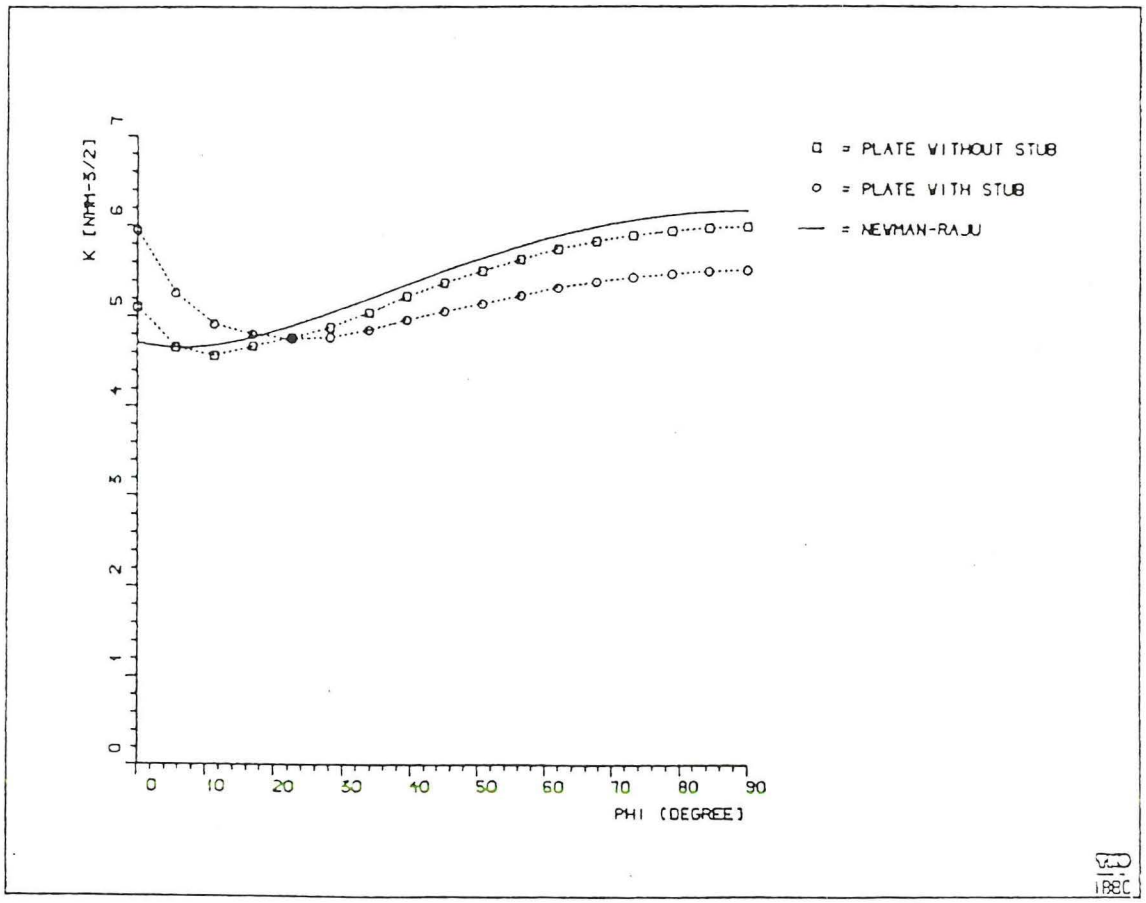

Figure 4-25: SIF for D-2-2 with crack III, membrane

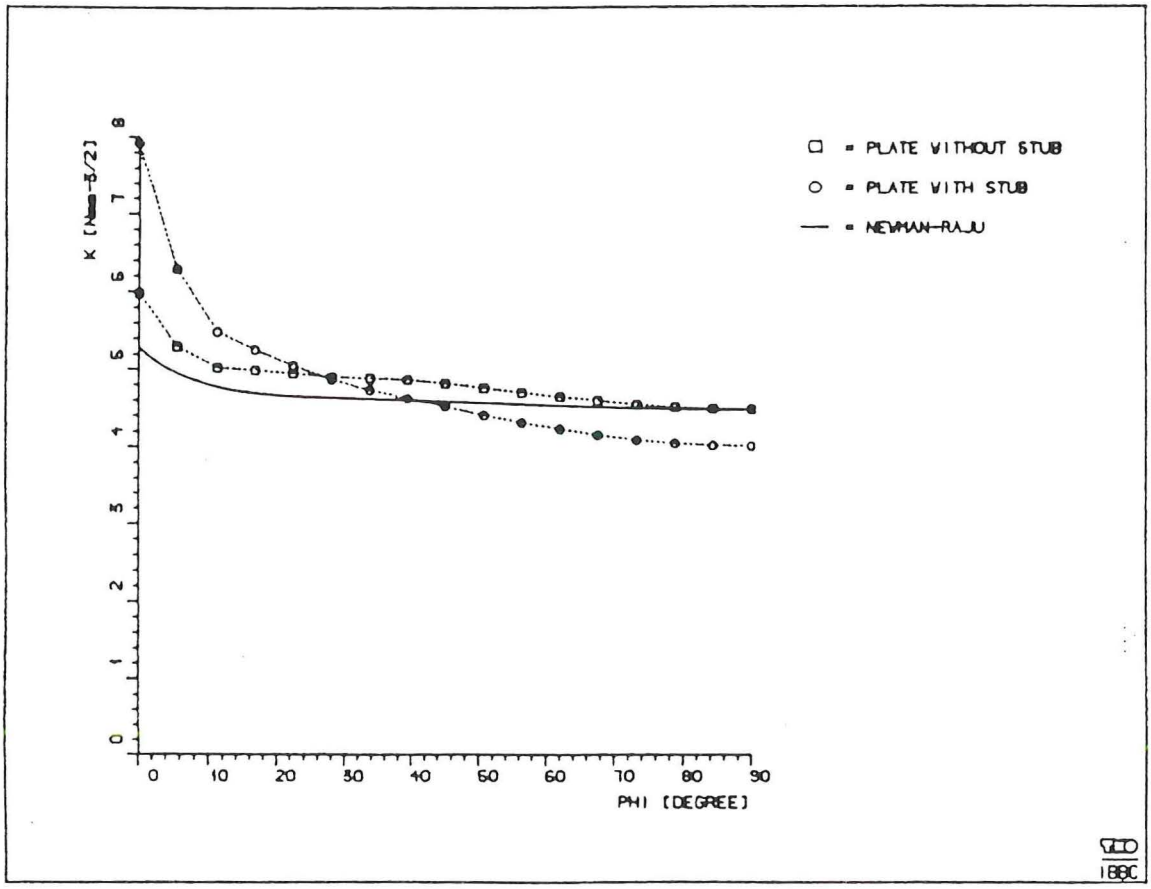

Figure 4-26: SIF for D-2-2 with crack IV, bending

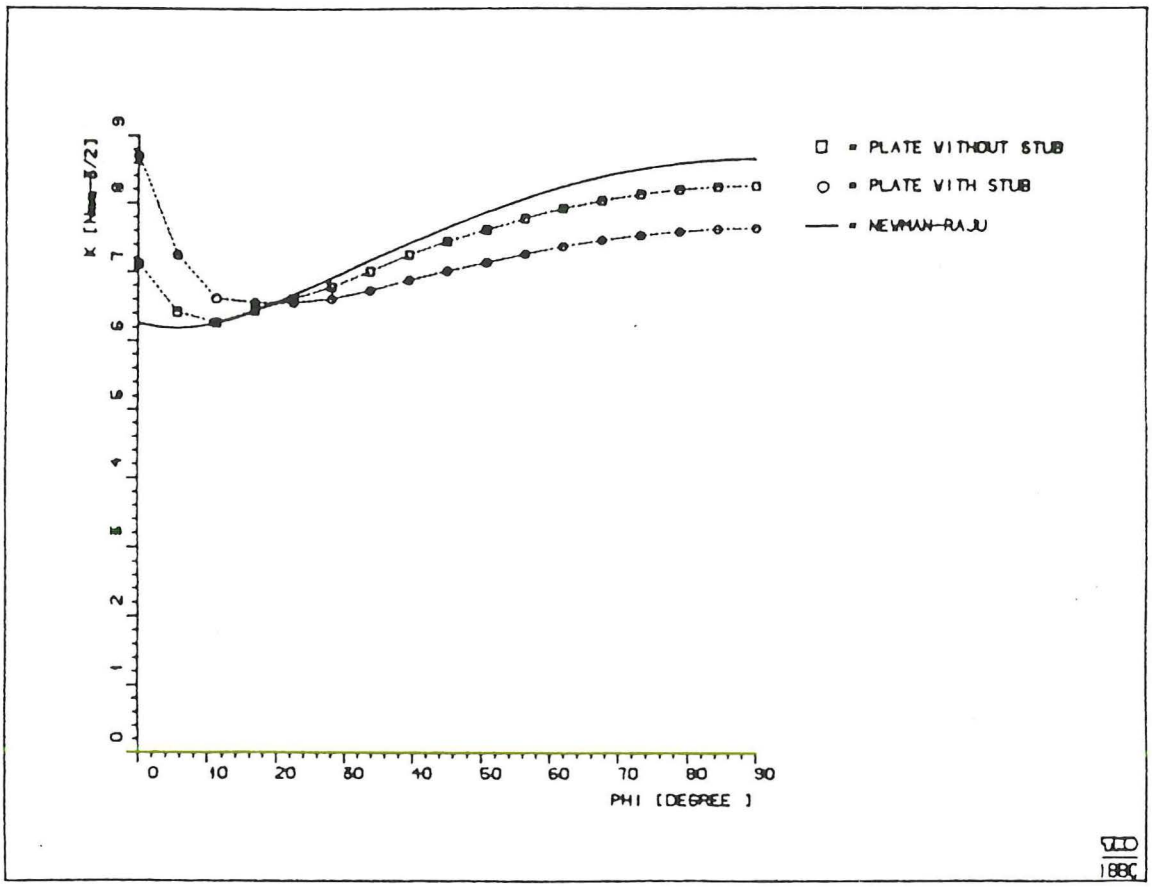

Figure 4-27: SIF for D-2-2 with crack IV, membrane

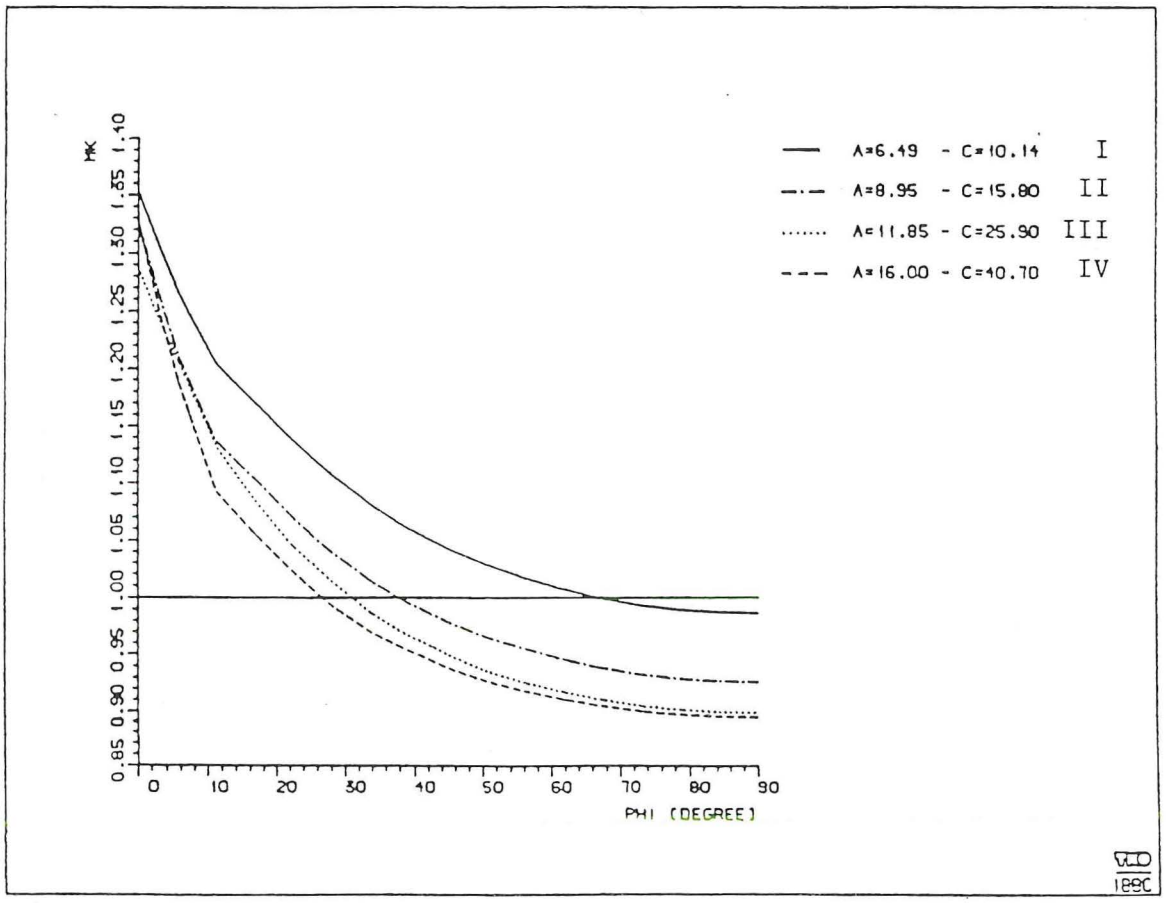

Figure 4-28: M_k factors for specimen D-2-2, bending

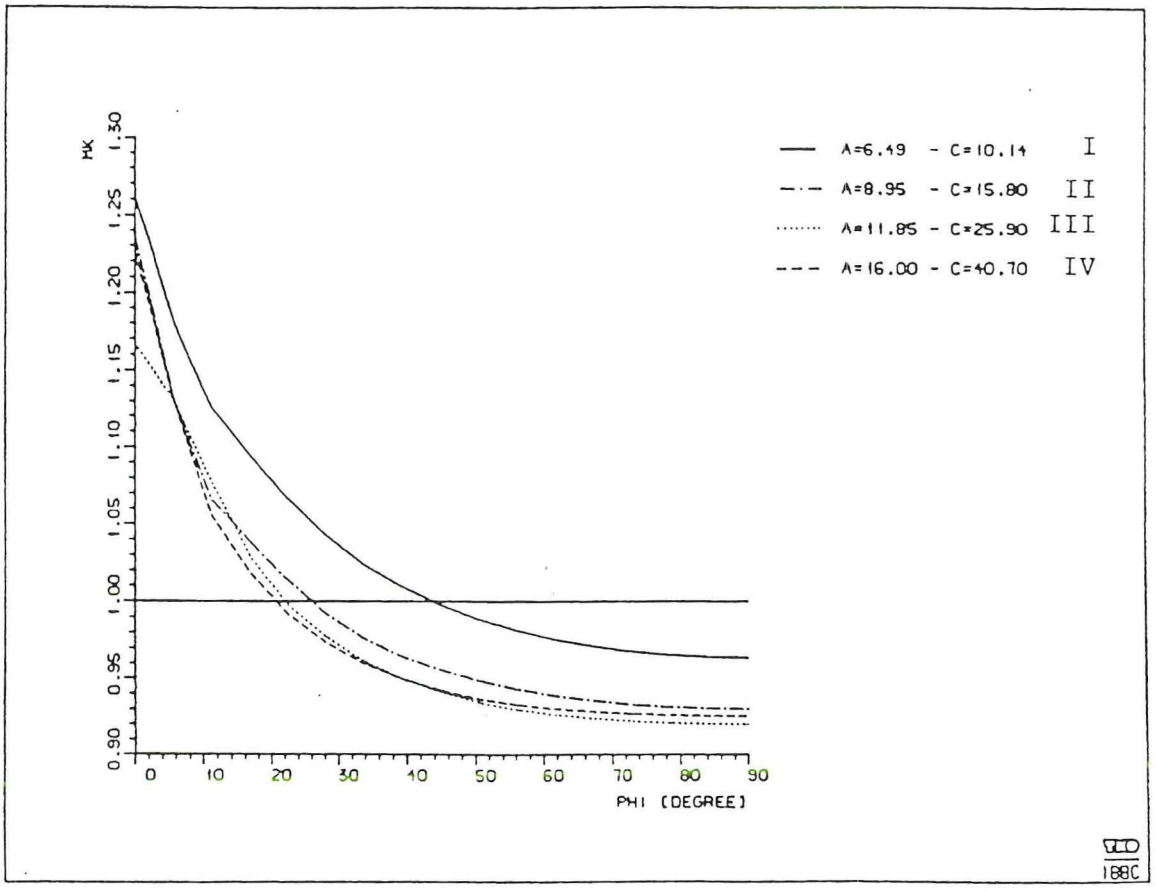

Figure 4-29: M_k factors for specimen D-2-2, membrane

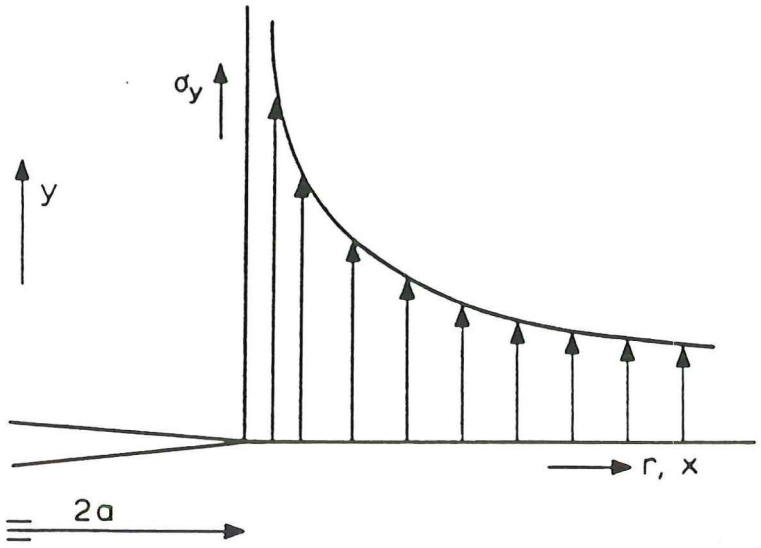

Figure 5-1: Elastic stress σ_y at the crack tip

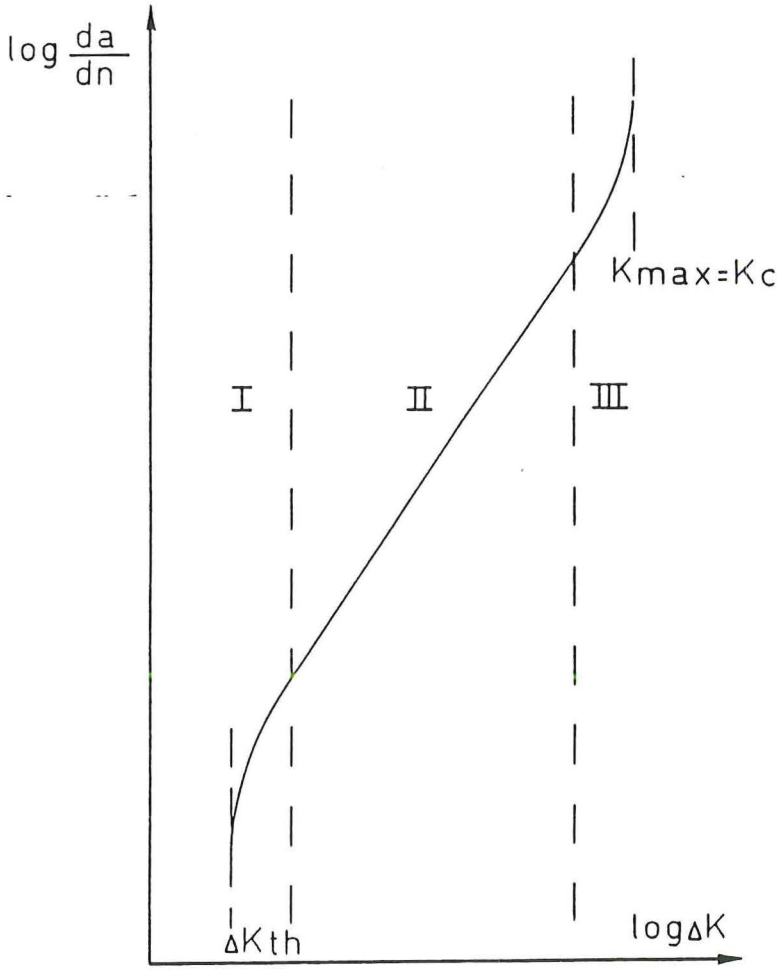

Figure 5-2: Division of da/dN - ΔK diagram in three regimes

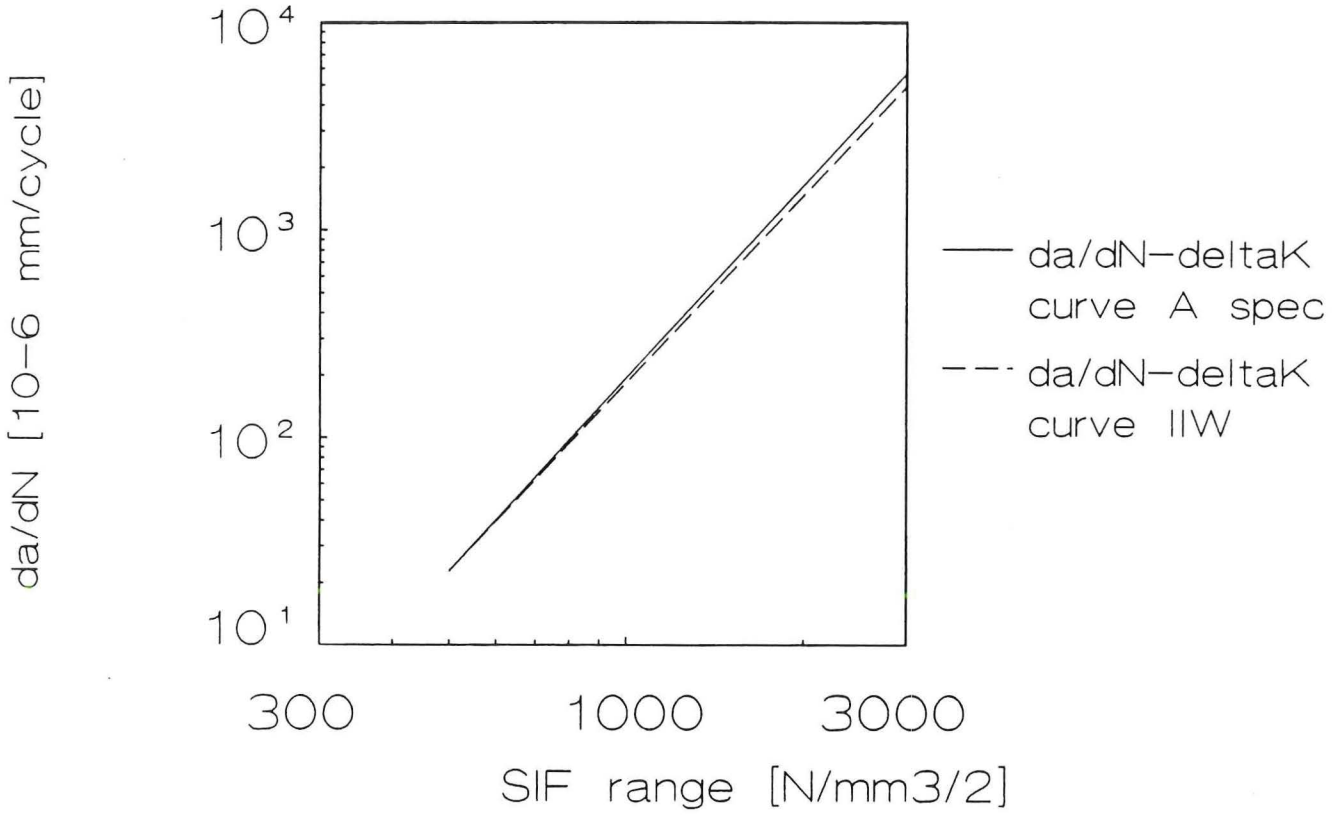

Figure 5-3: Comparison of crack growth rate curves (A specimens / IIW)

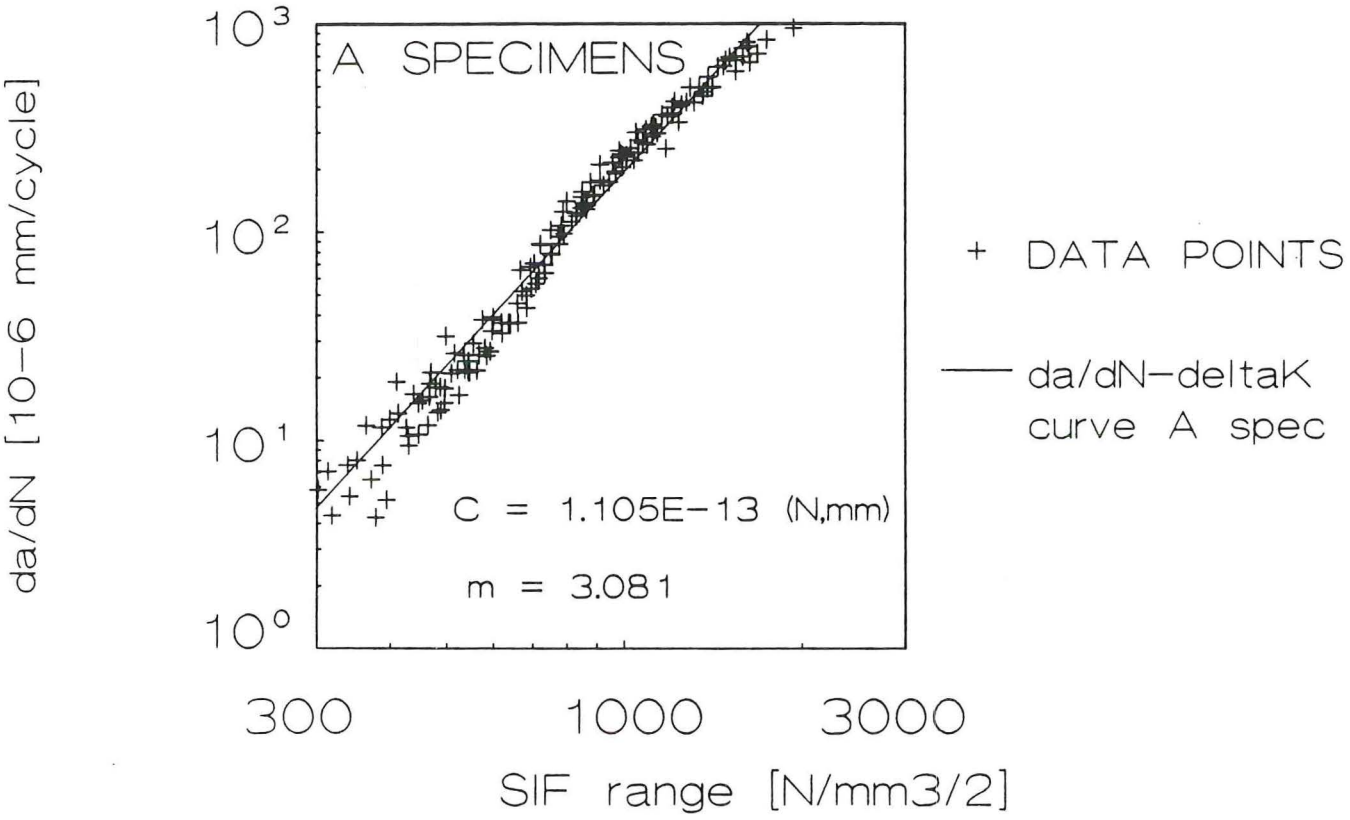

Figure 6-1: Crack growth rate data A-specimens and average da/dN-ΔK curve

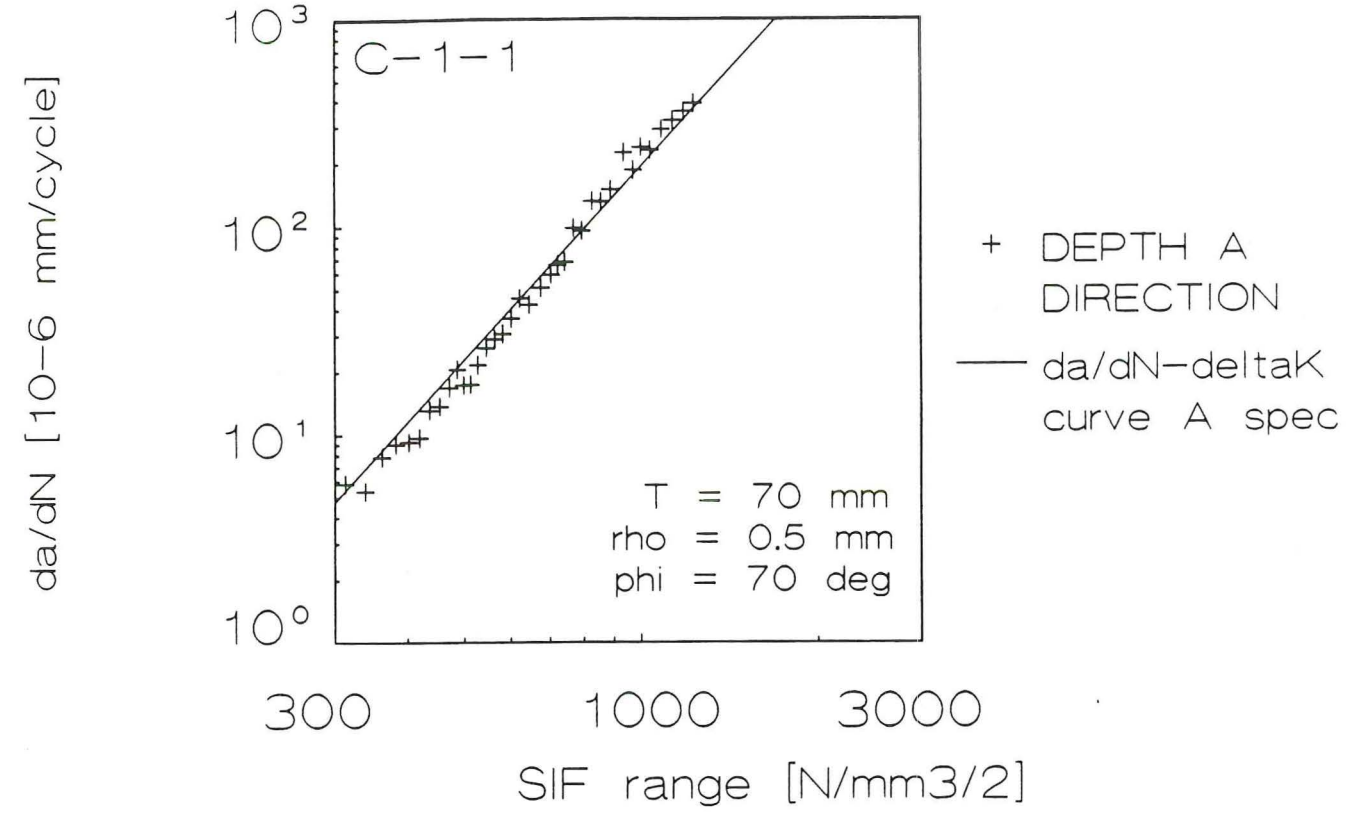

Figure 6-2: Crack growth rate data specimen C-1-1

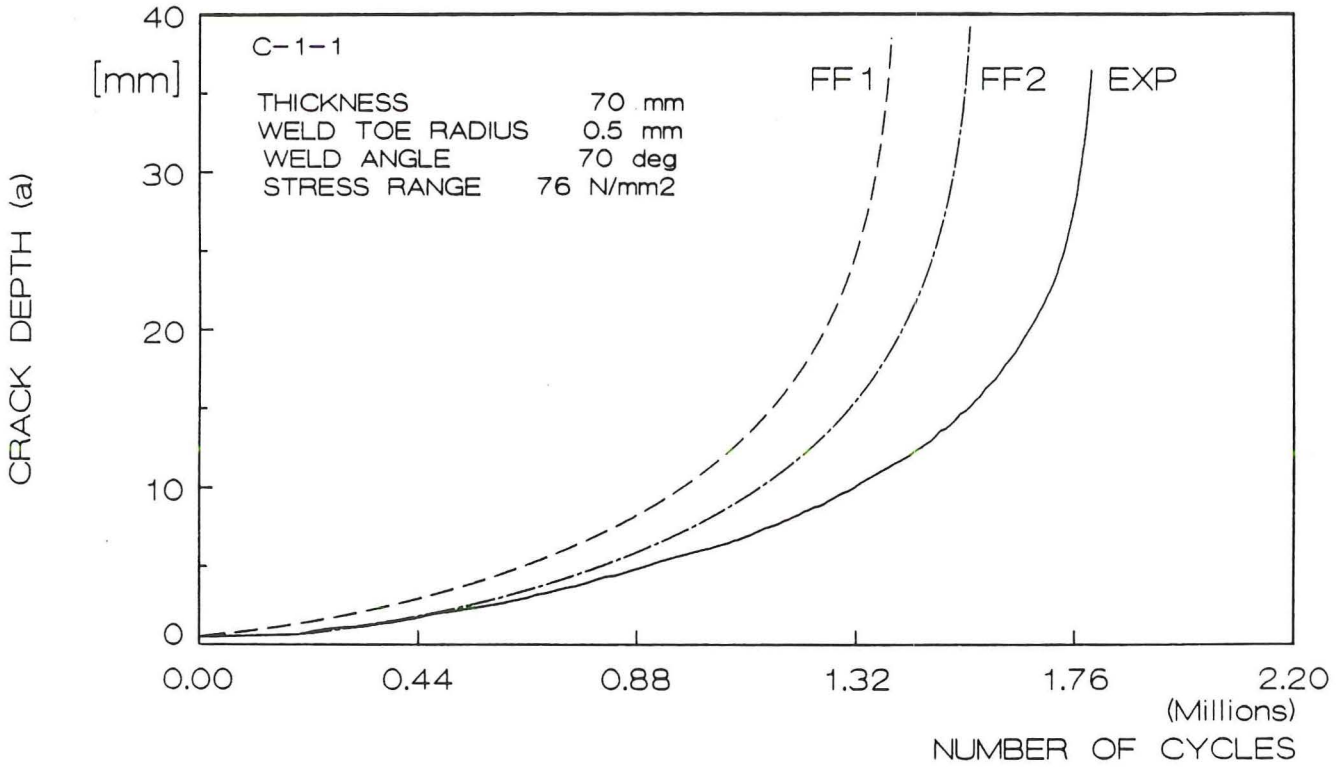

Figure 6-3: Crack growth curves specimen C-1-1

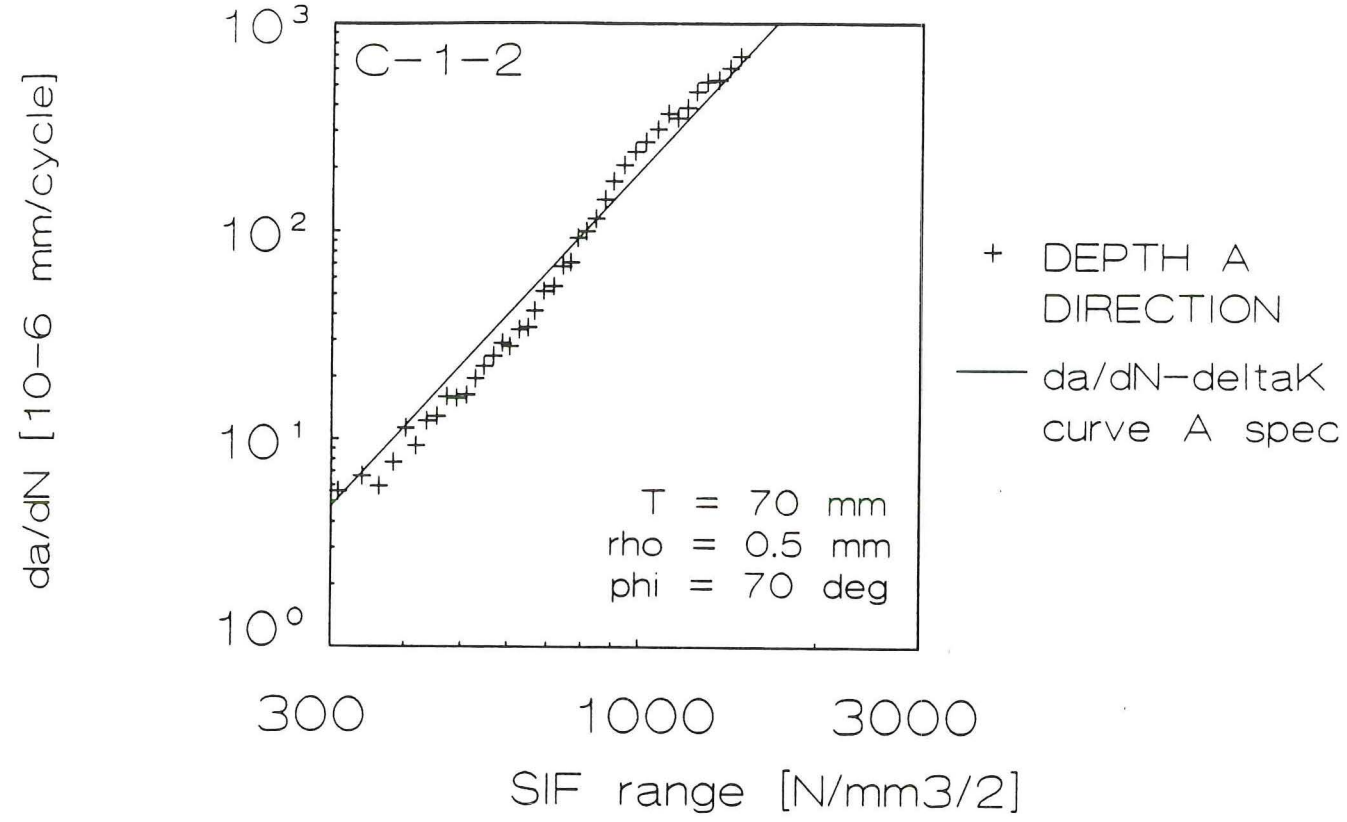

Figure 6-4: Crack growth rate data specimen C-1-2

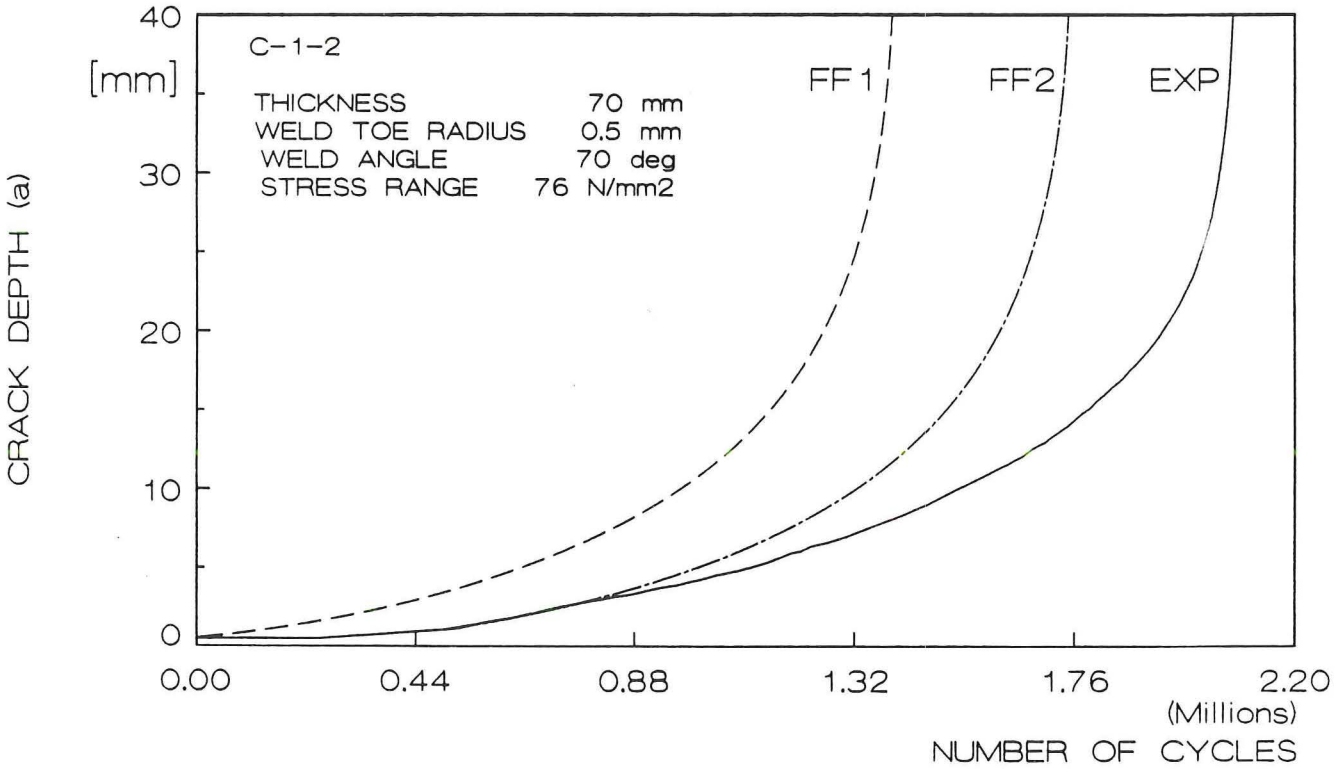

Figure 6-5: Crack growth curves specimen C-1-2

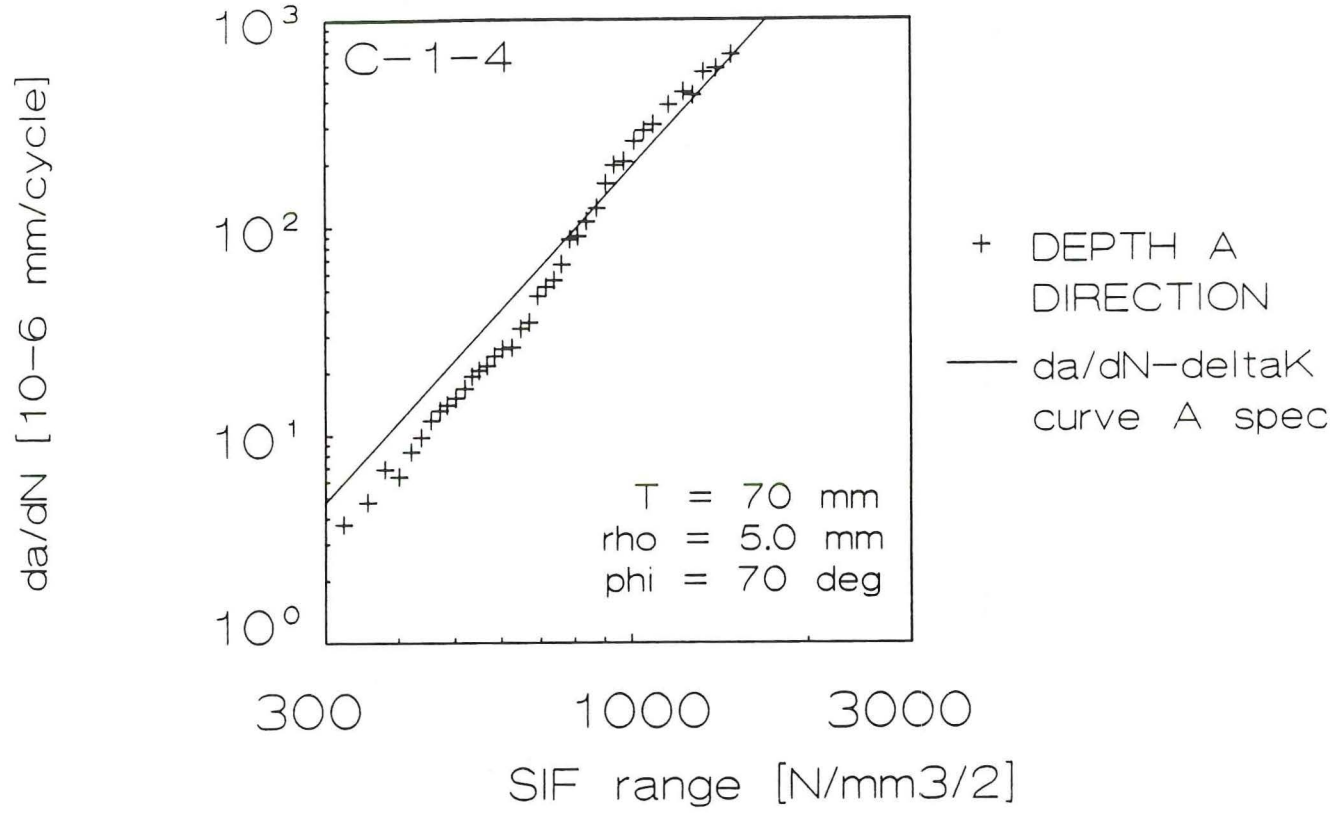

Figure 6-6: Crack growth rate data specimen C-1-4

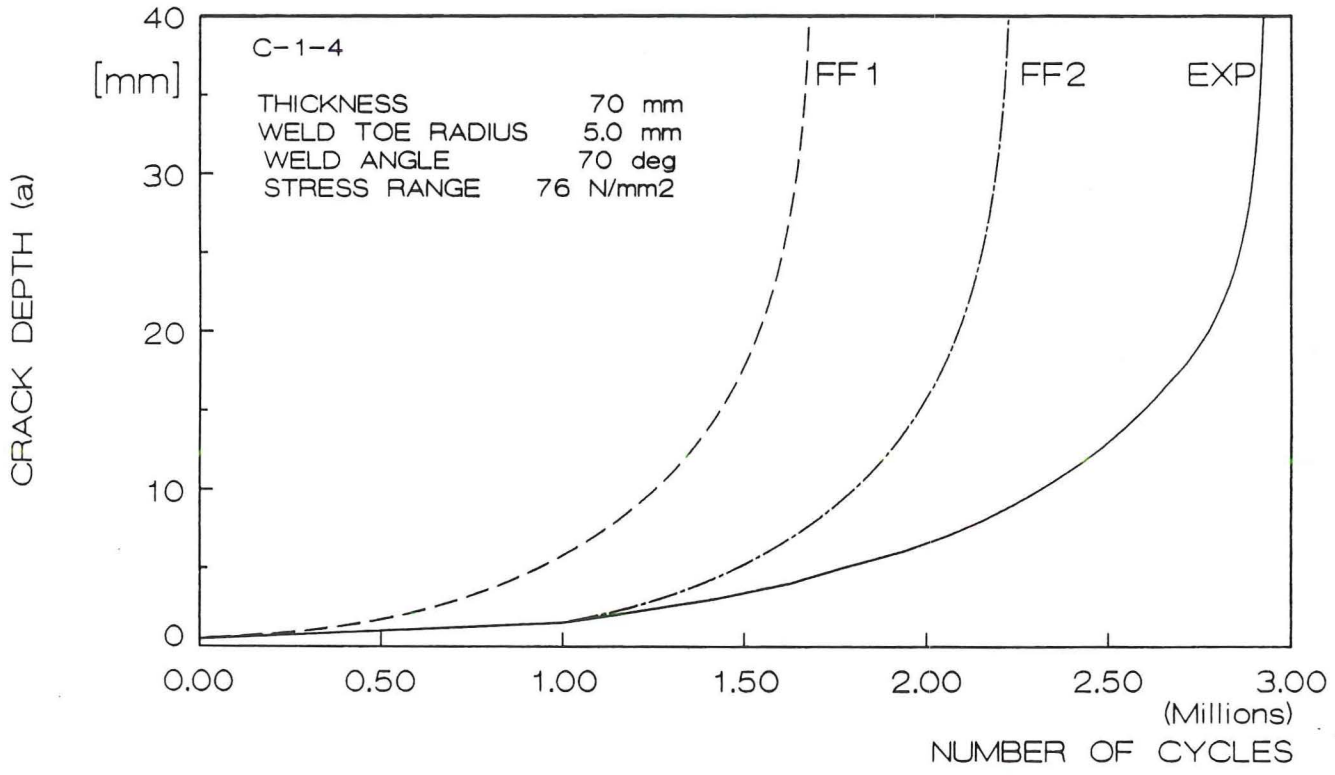

Figure 6-7: Crack growth curves specimen C-1-4

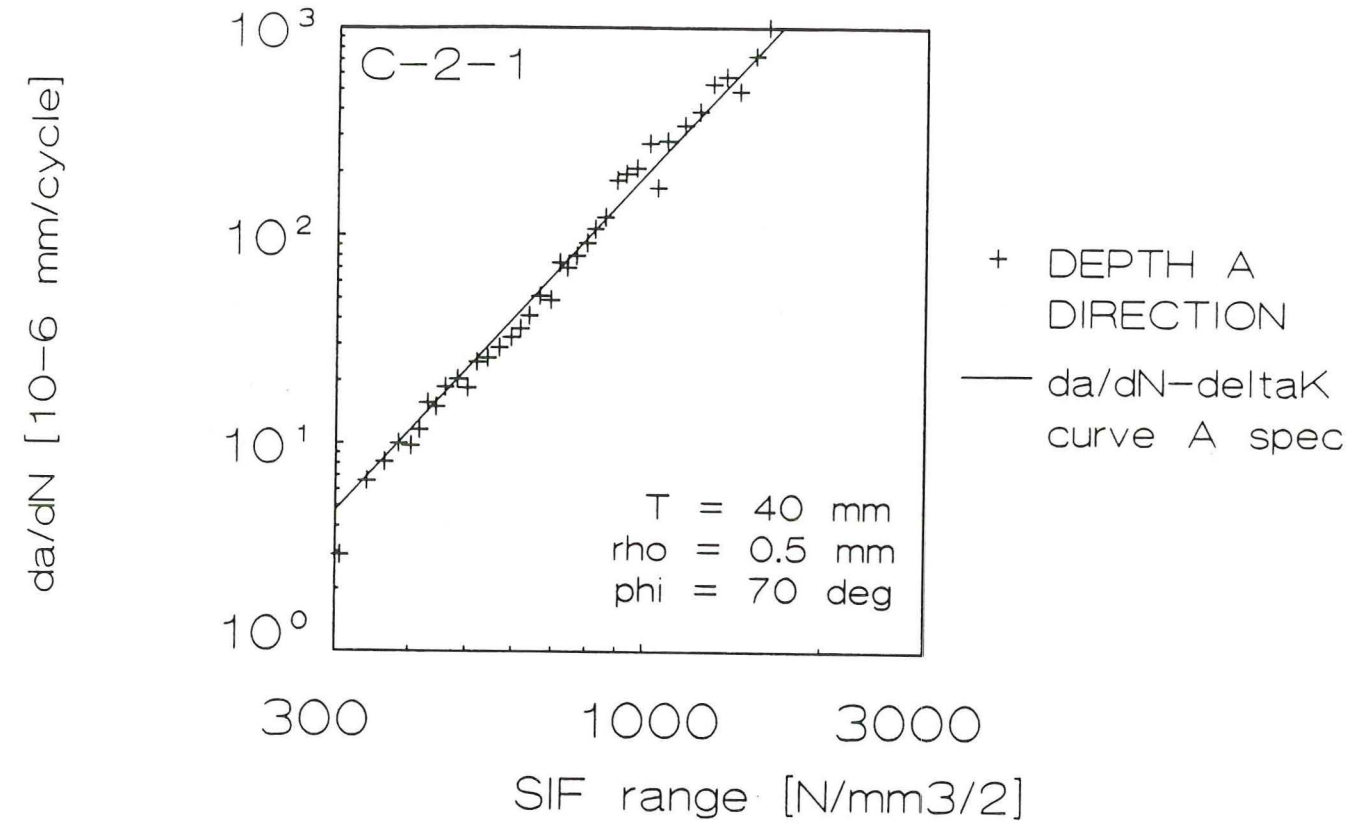

Figure 6-8: Crack growth rate data specimen C-2-1

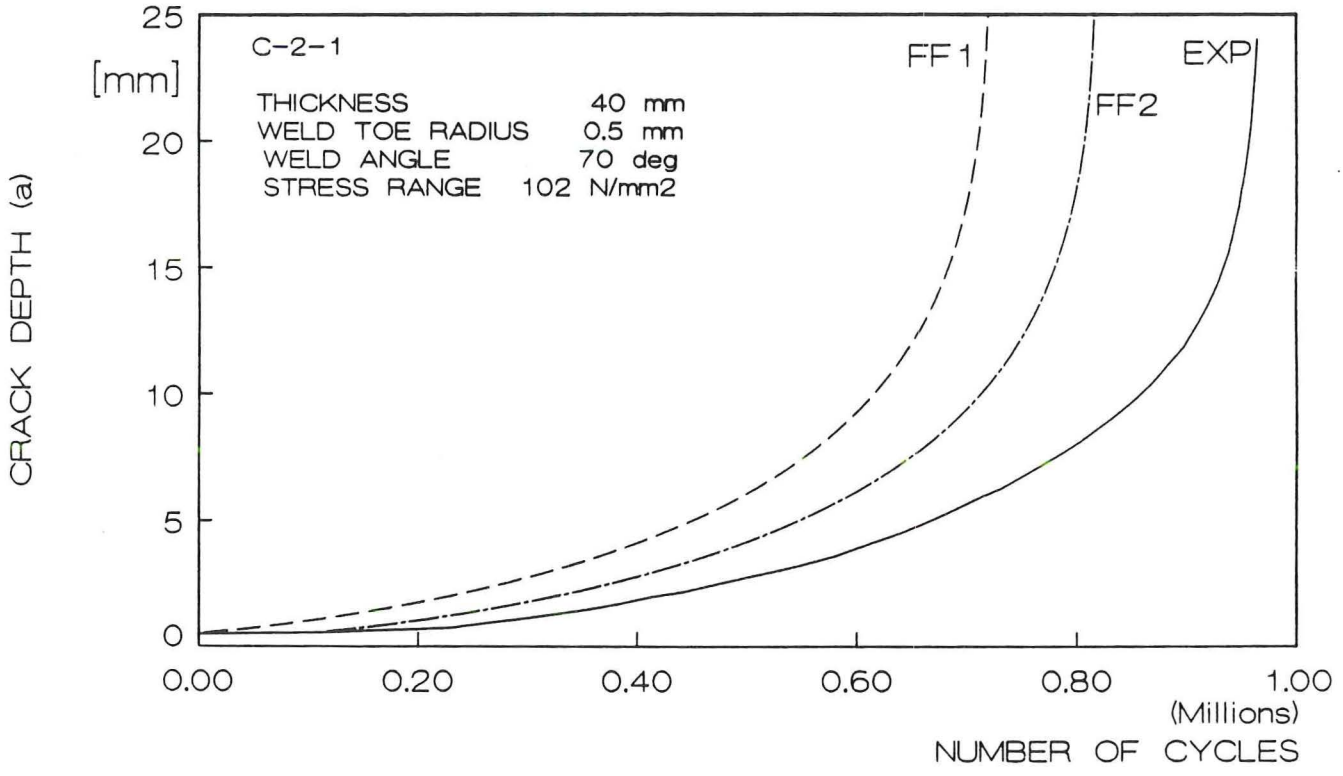

Figure 6-9: Crack growth curve specimen C-2-1

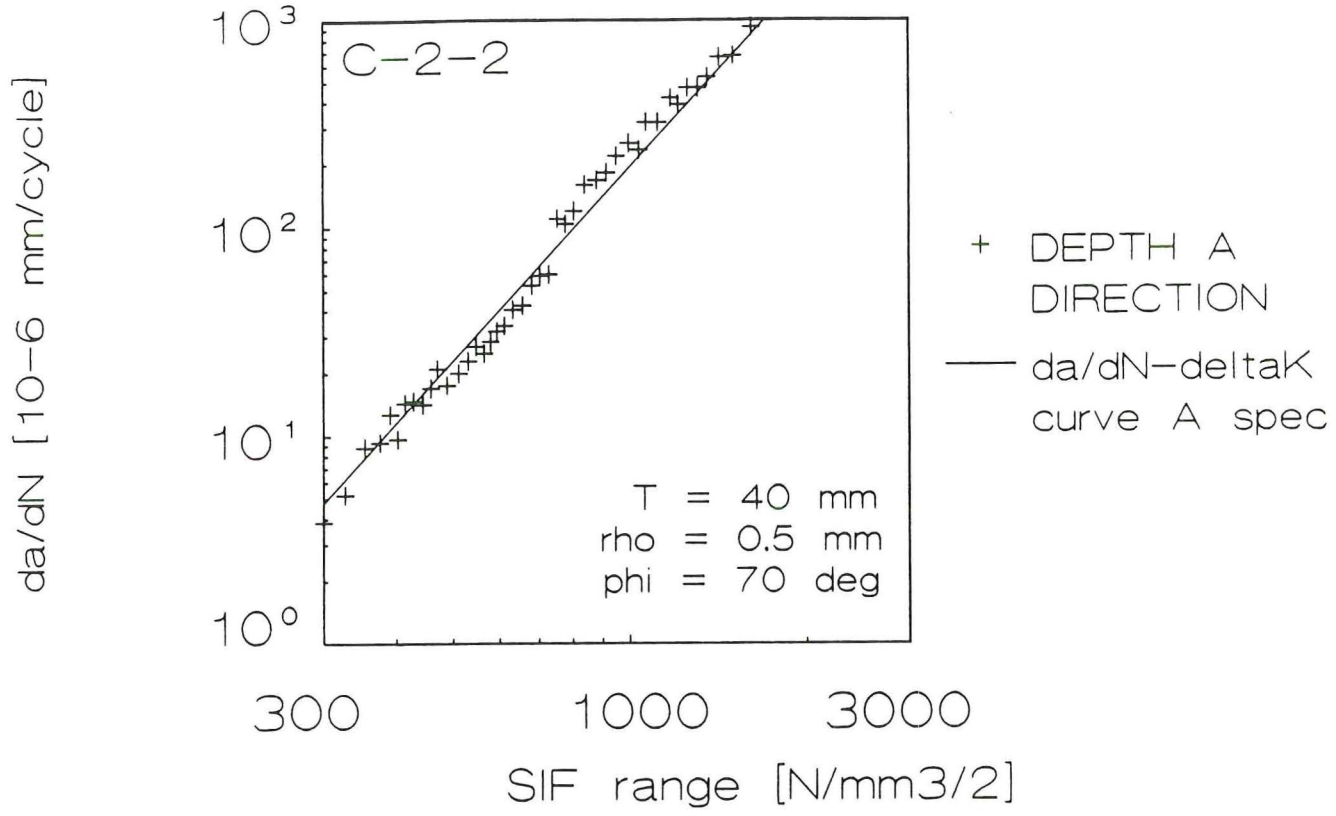

Figure 6-10: Crack growth rate data specimen C-2-2

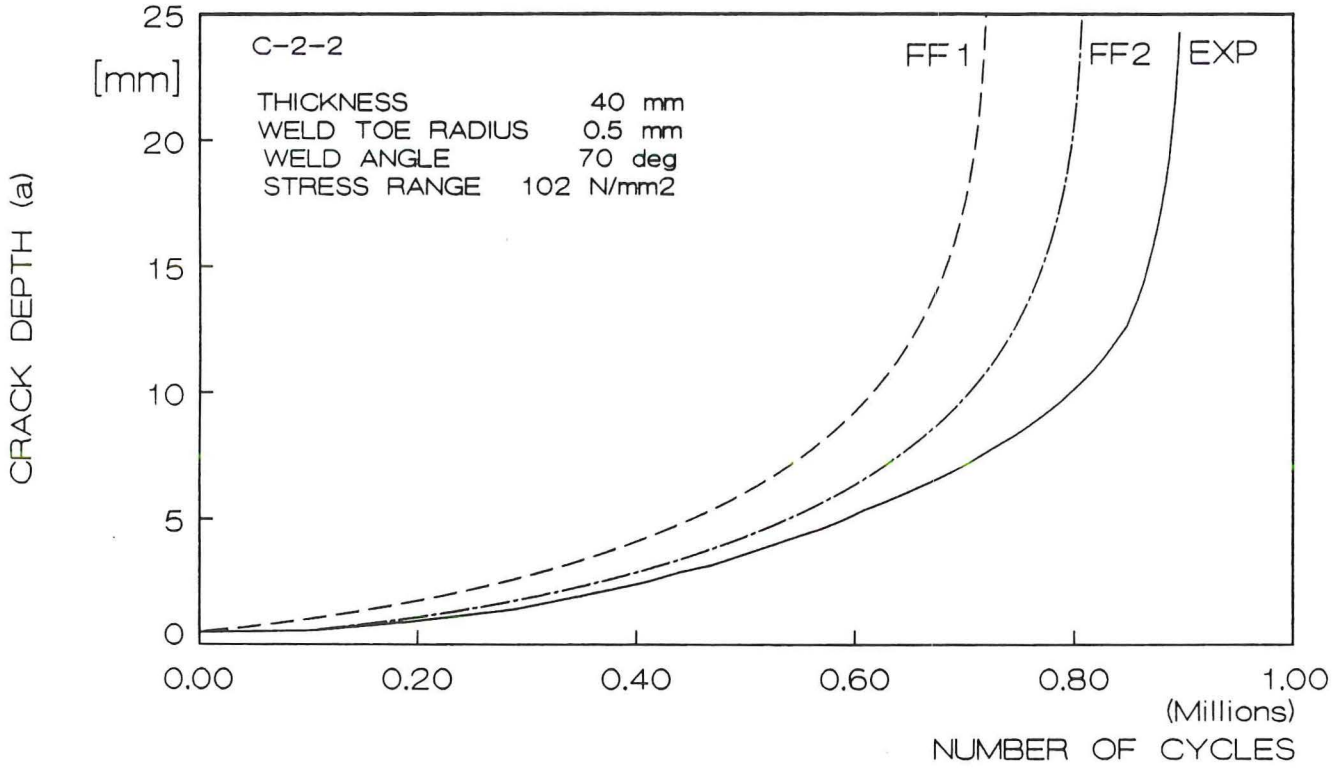

Figure 6-11: Crack growth curves specimen C-2-2

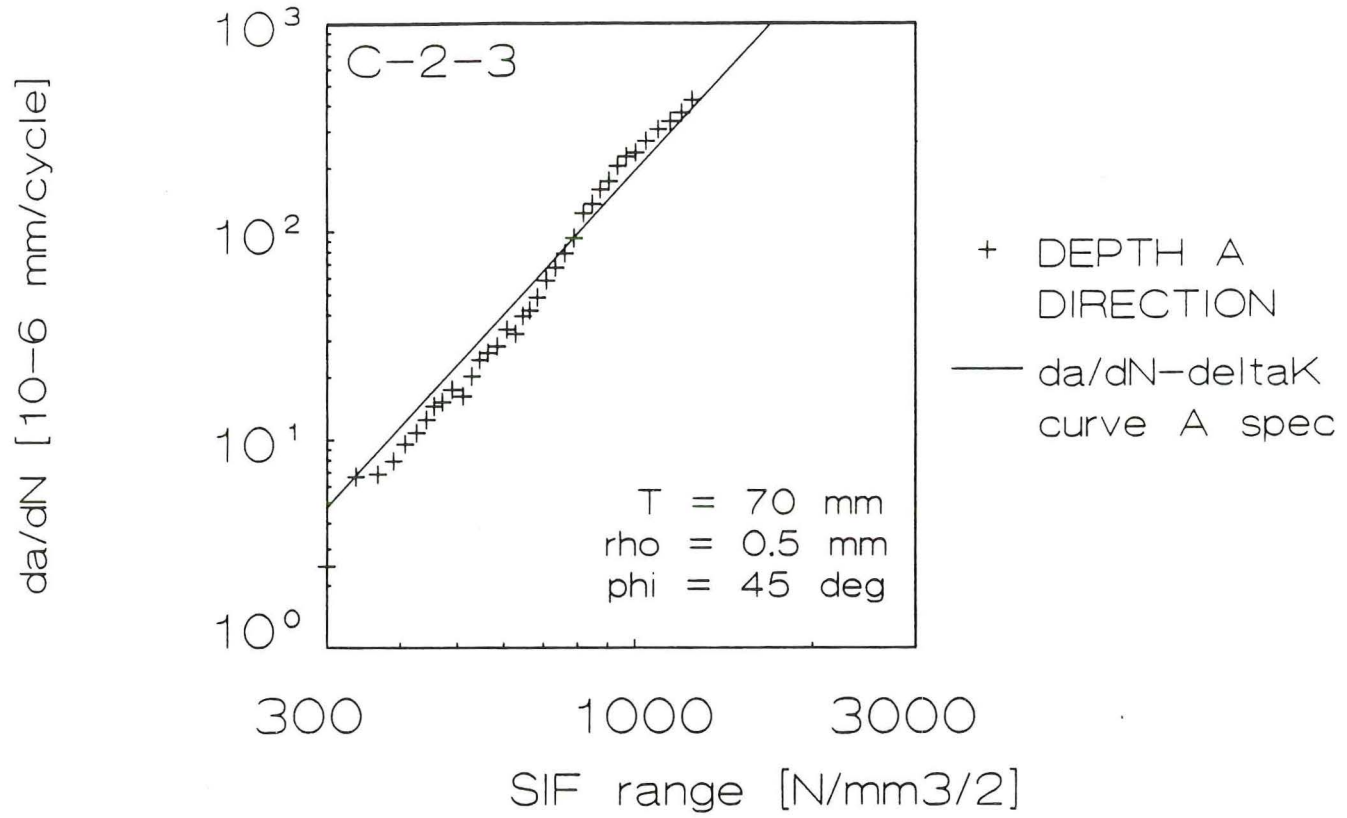

Figure 6-12: Crack growth rate data specimen C-2-3

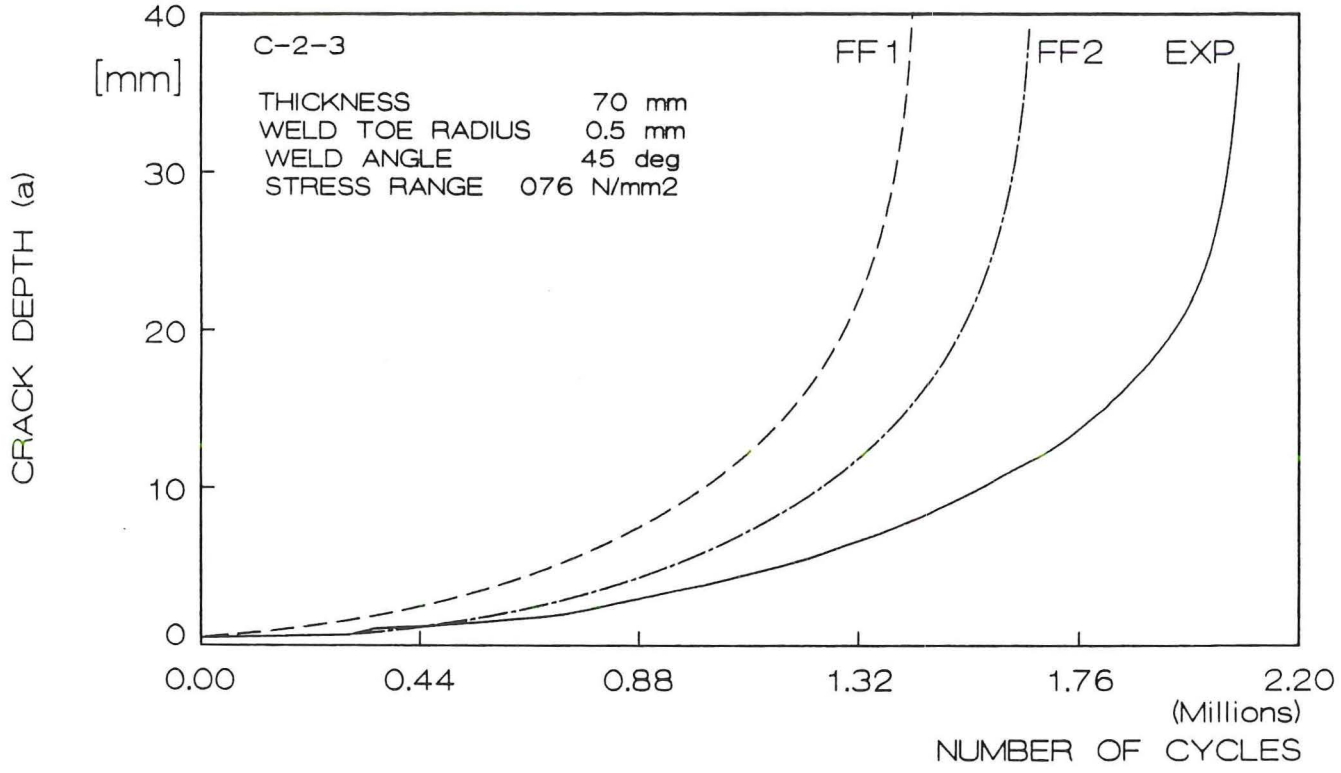

Figure 6-13: Crack growth curves specimen C-2-3

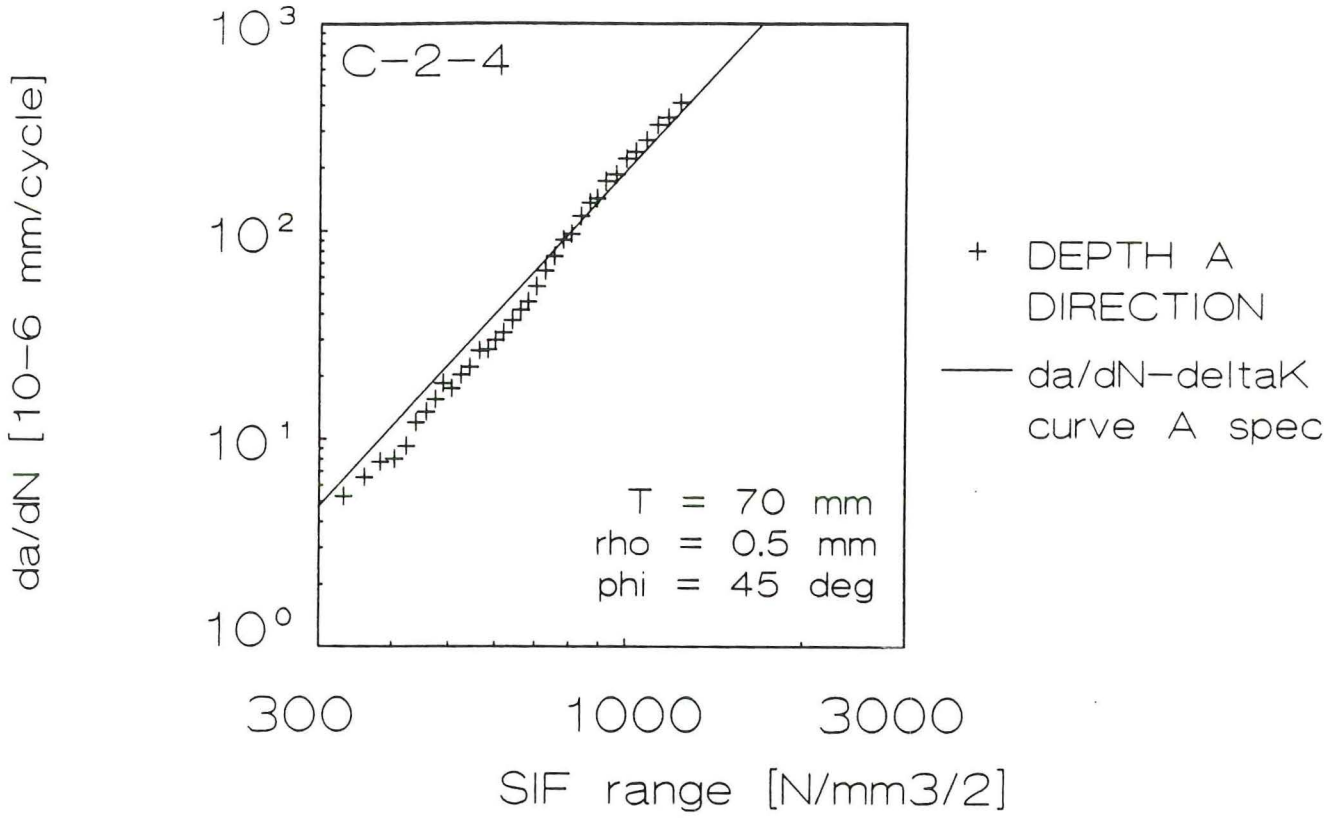

Figure 6-14: Crack growth rate data specimen C-2-4

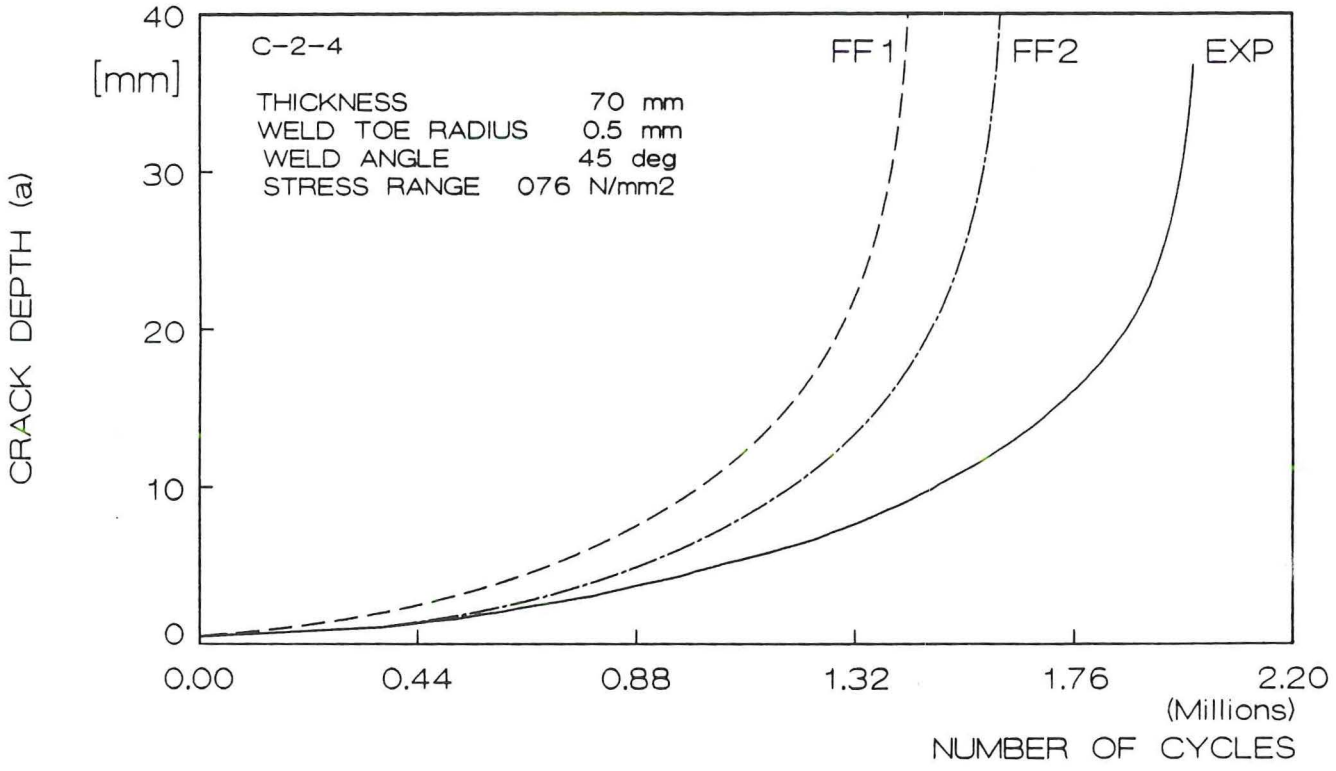

Figure 6-15: Crack growth curves specimen C-2-4

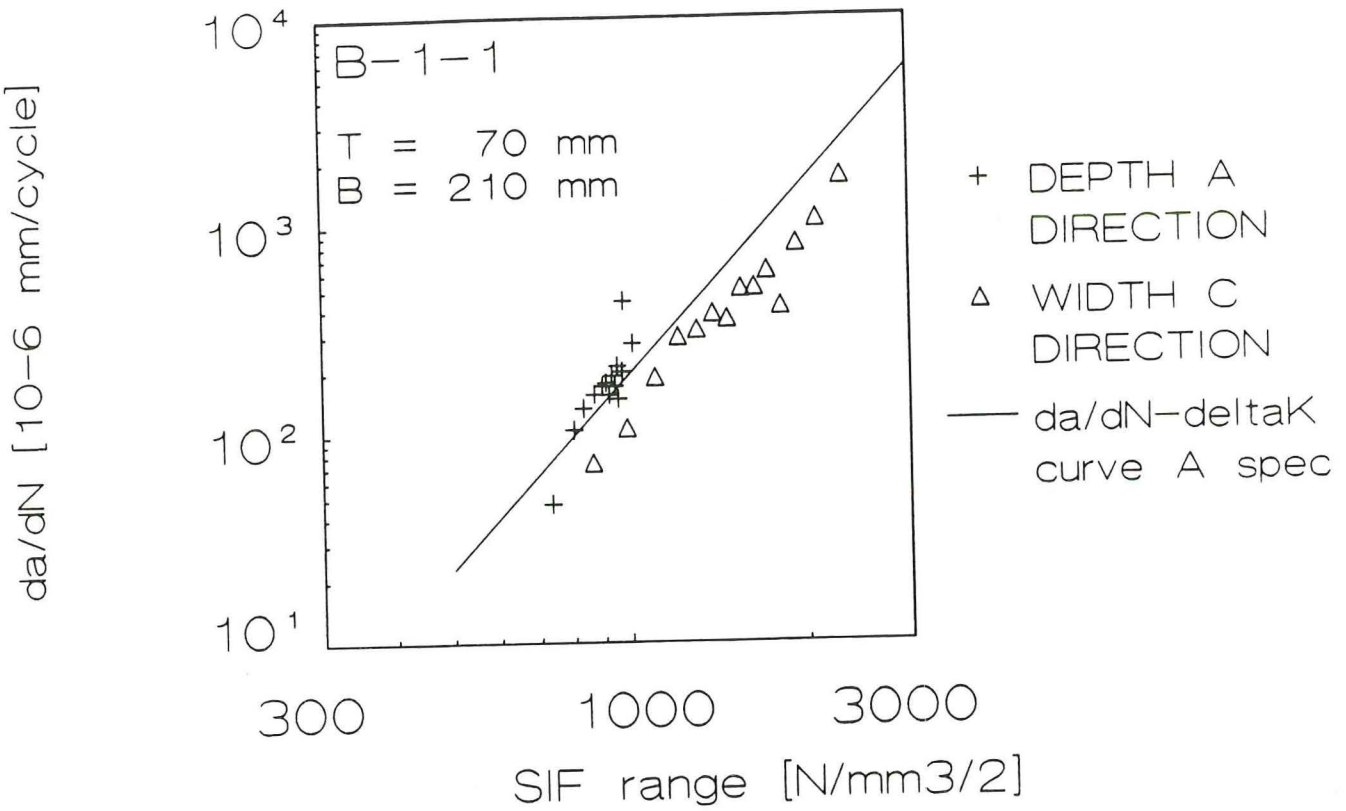

Figure 6-16: Crack growth rate data specimen B-1-1

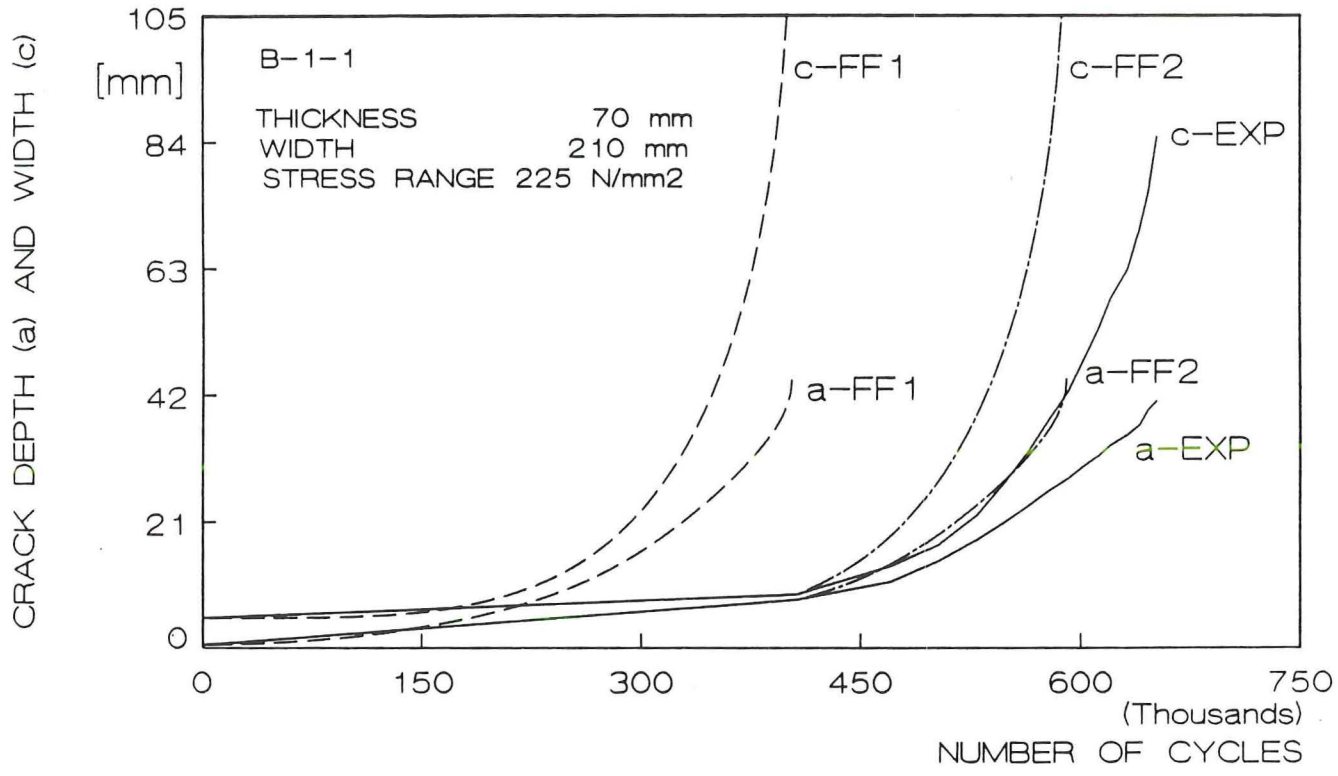

Figure 6-17: Crack growth curves specimen B-1-1

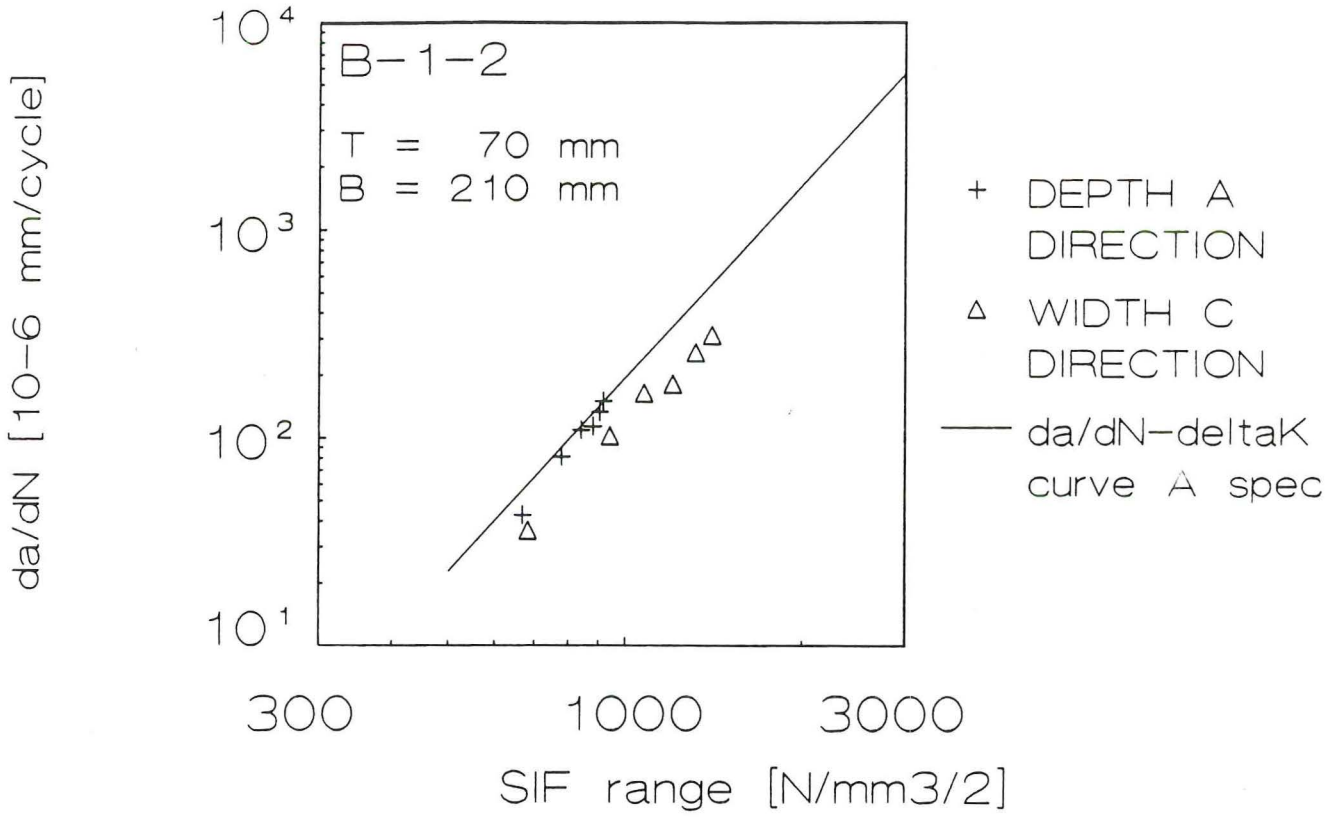

Figure 6-18: Crack growth rate data specimen B-1-2

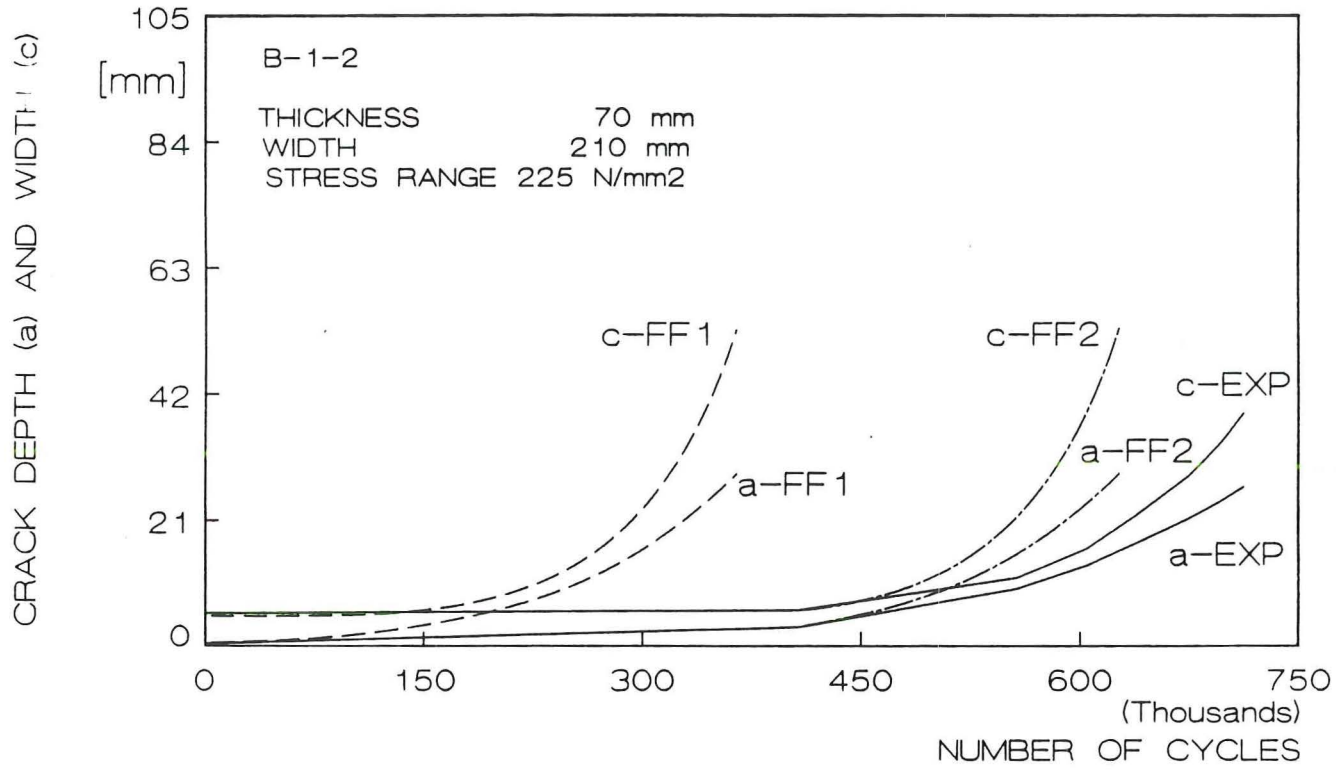

Figure 6-19: Crack growth curves specimen B-1-2

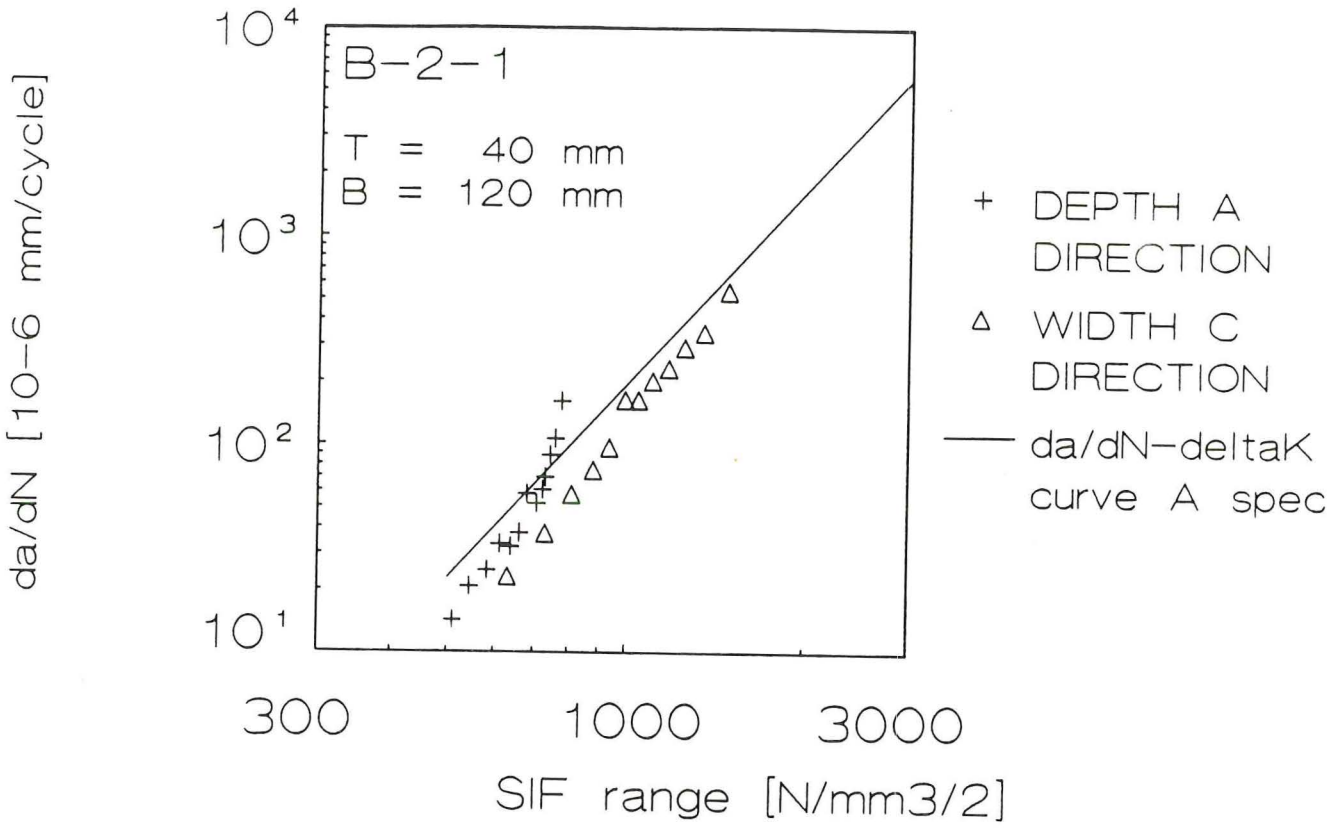

Figure 6-20: Crack growth rate data specimen B-2-1

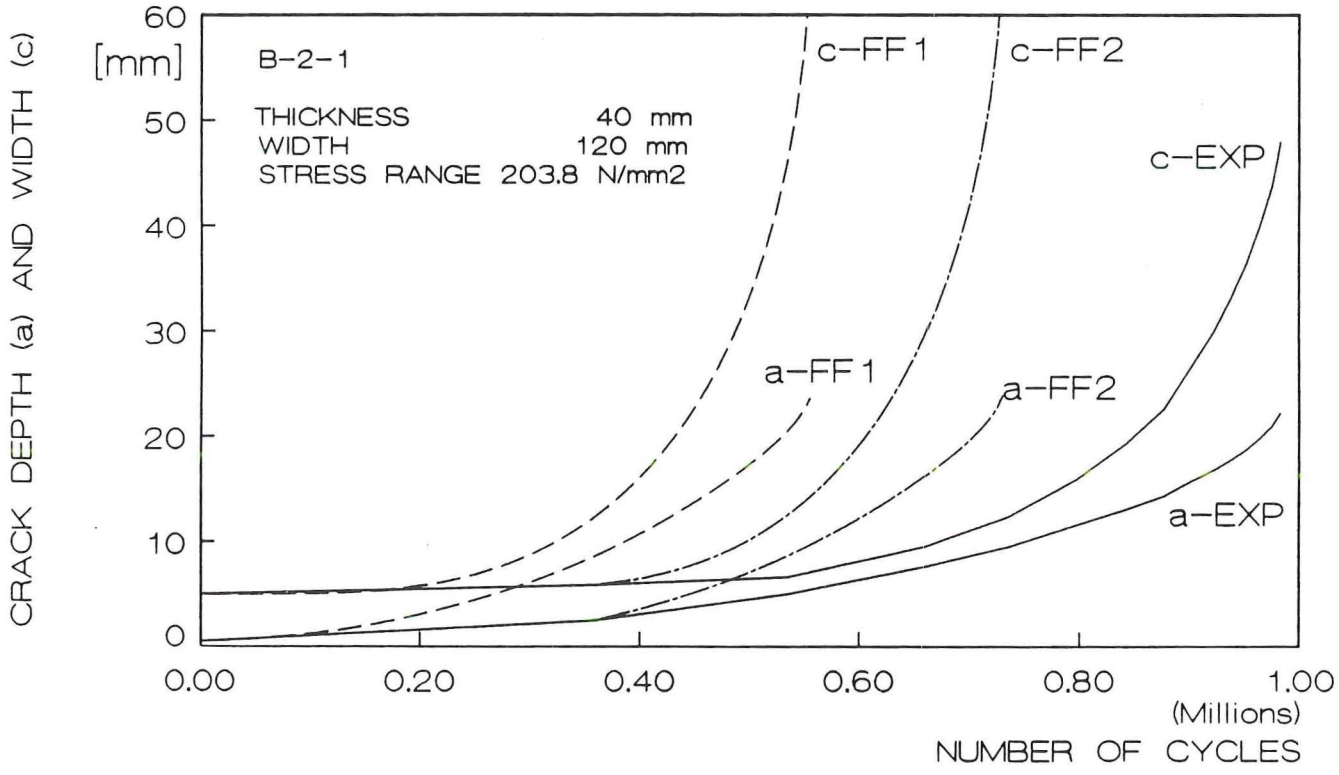

Figure 6-21: Crack growth curves specimen B-2-1

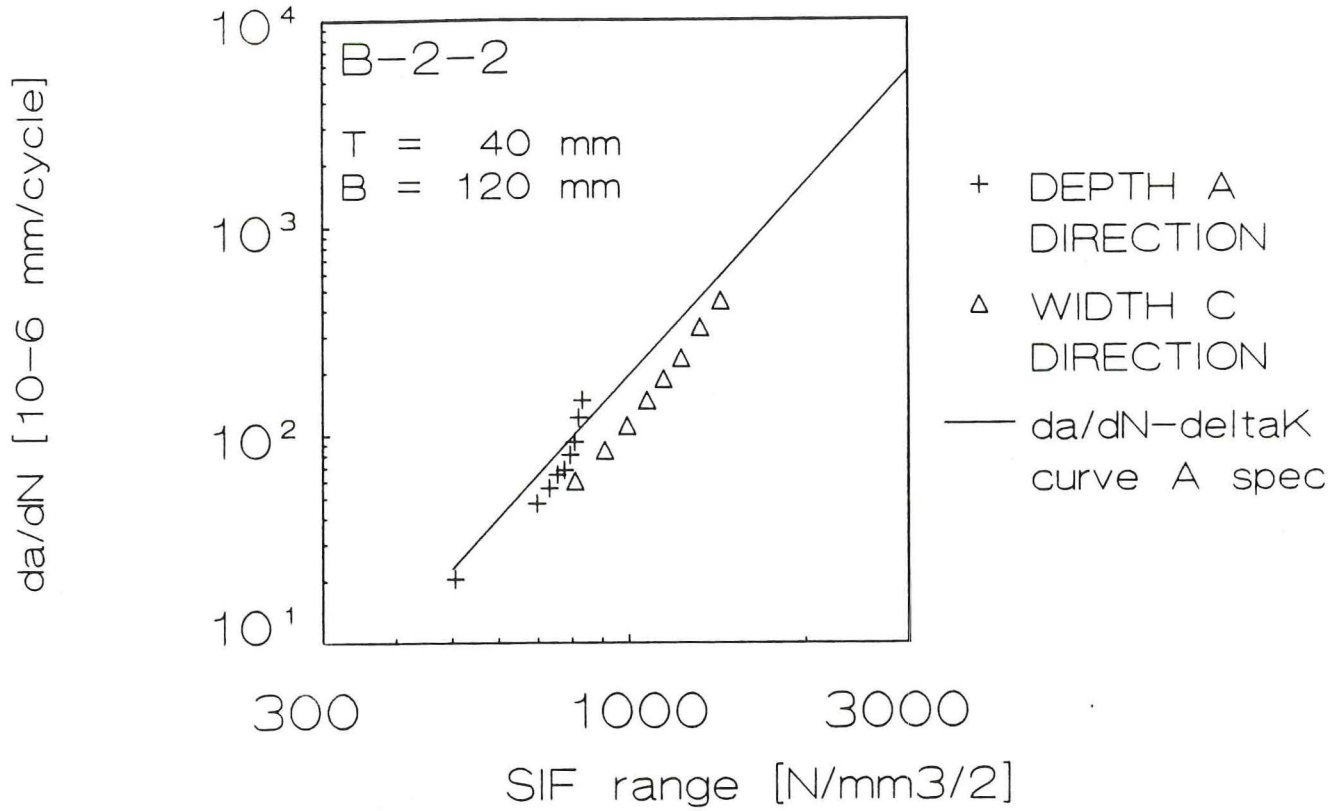

Figure 6-22: Crack growth rate data specimen B-2-2

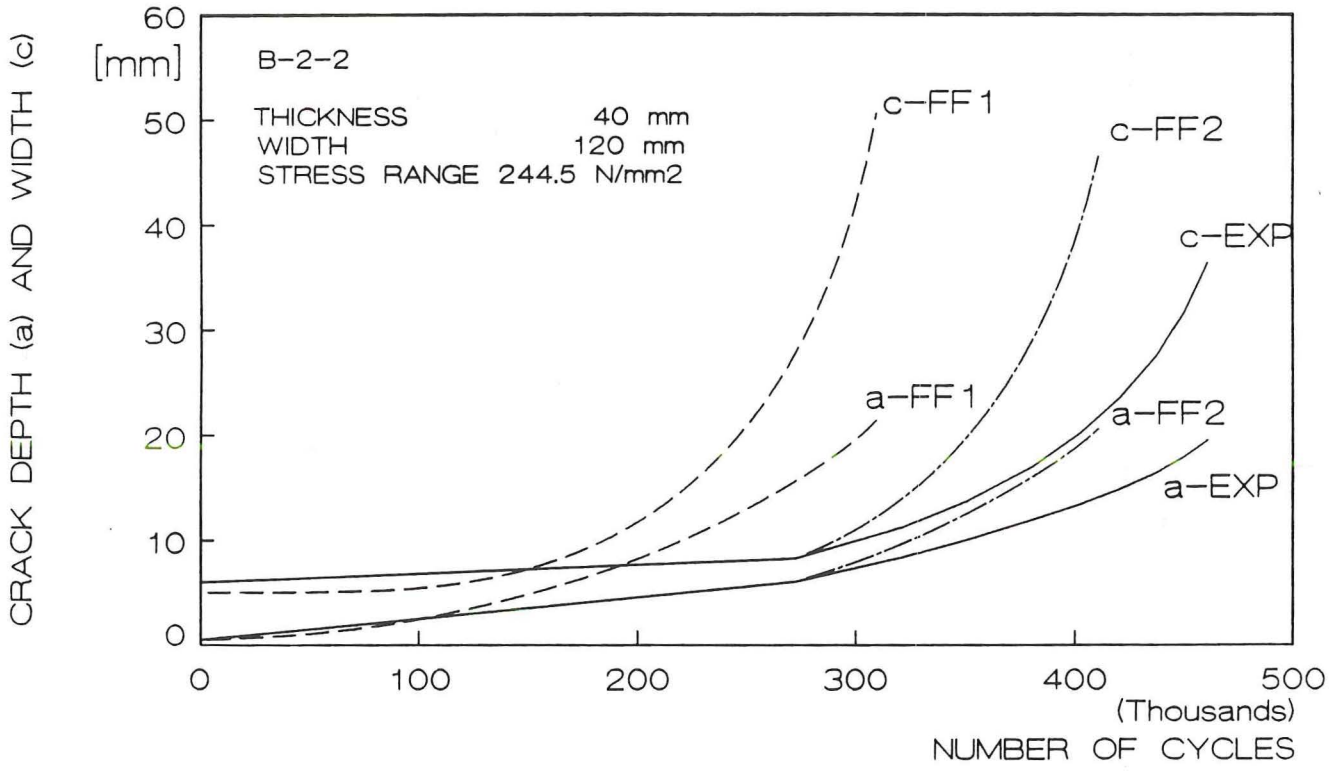

Figure 6-23: Crack growth curves specimen B-2-2

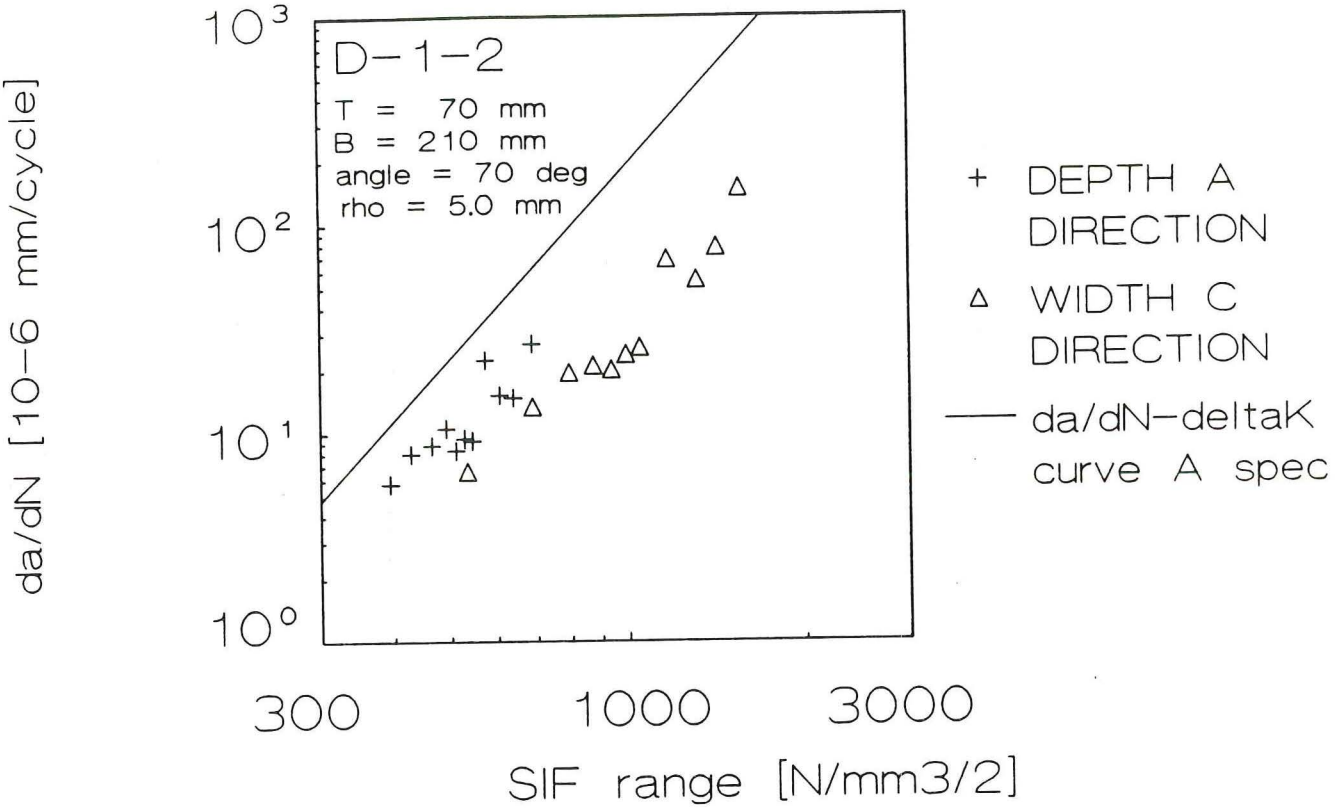

Figure 6-24: Crack growth rate data specimen D-1-2

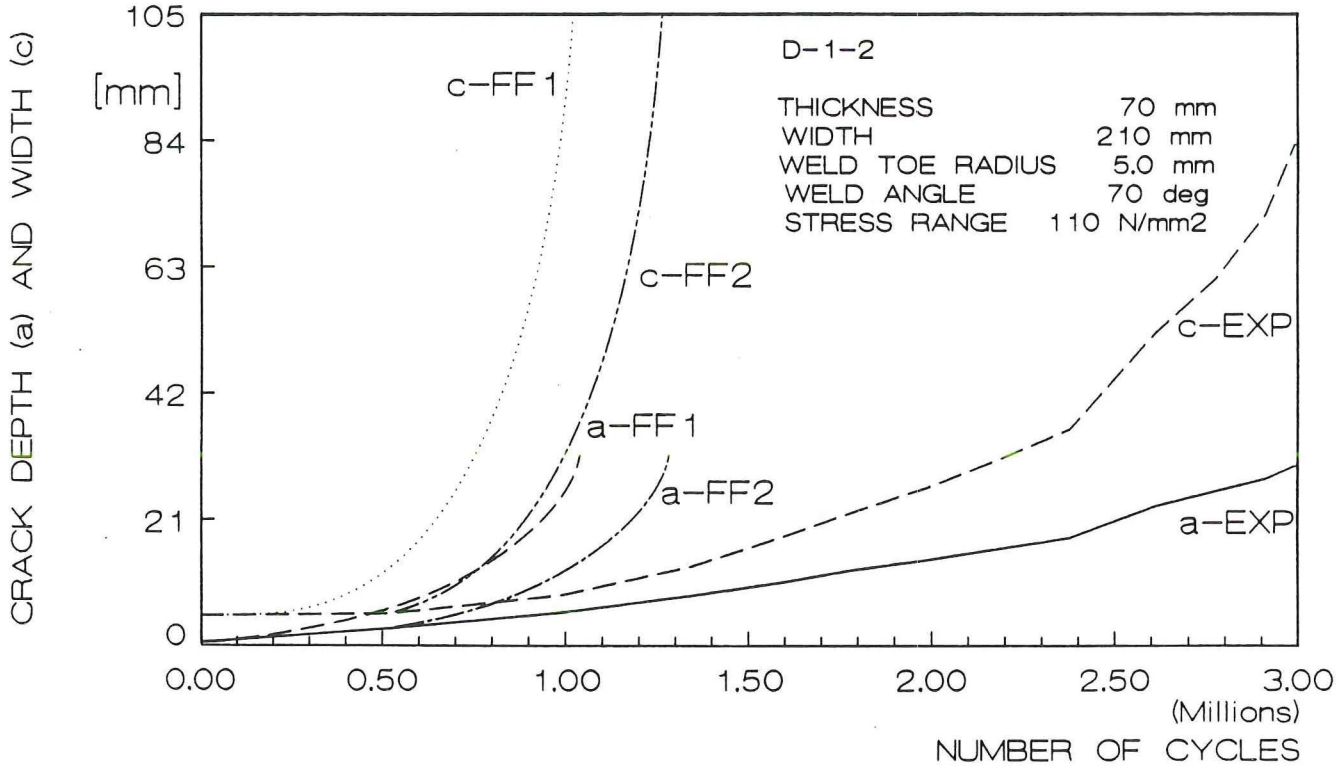

Figure 6-25: Crack growth curves specimen D-1-2

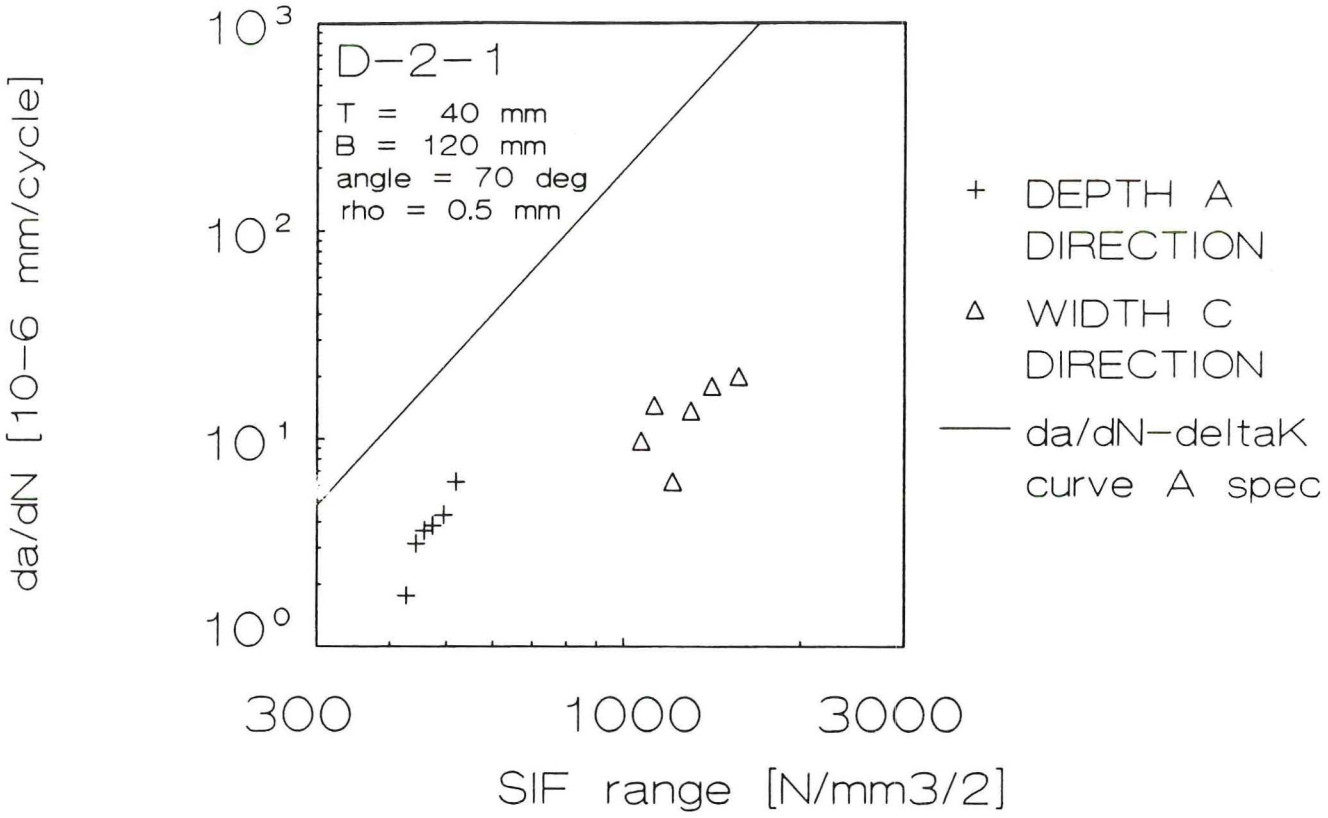

Figure 6-26: Crack growth rate data specimen D-2-1

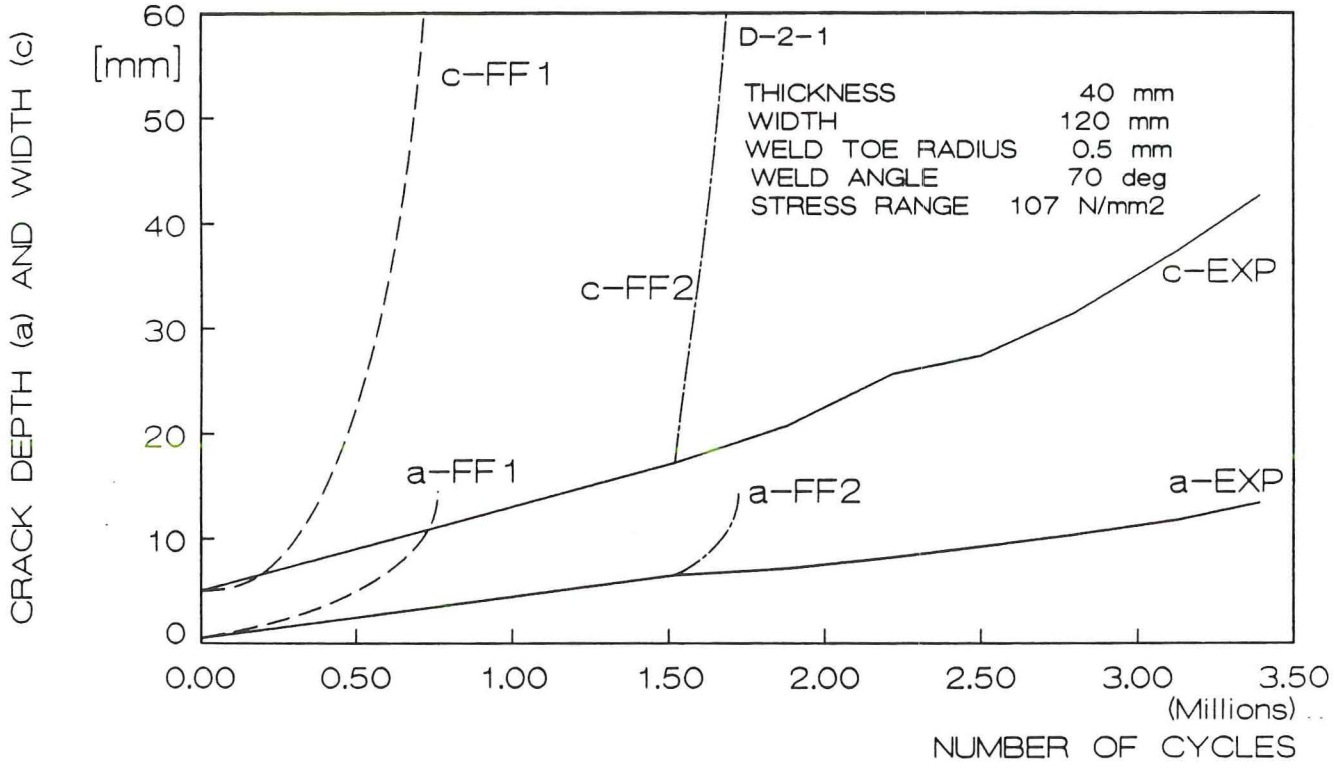

Figure 6-27: Crack growth curves specimen D-2-1

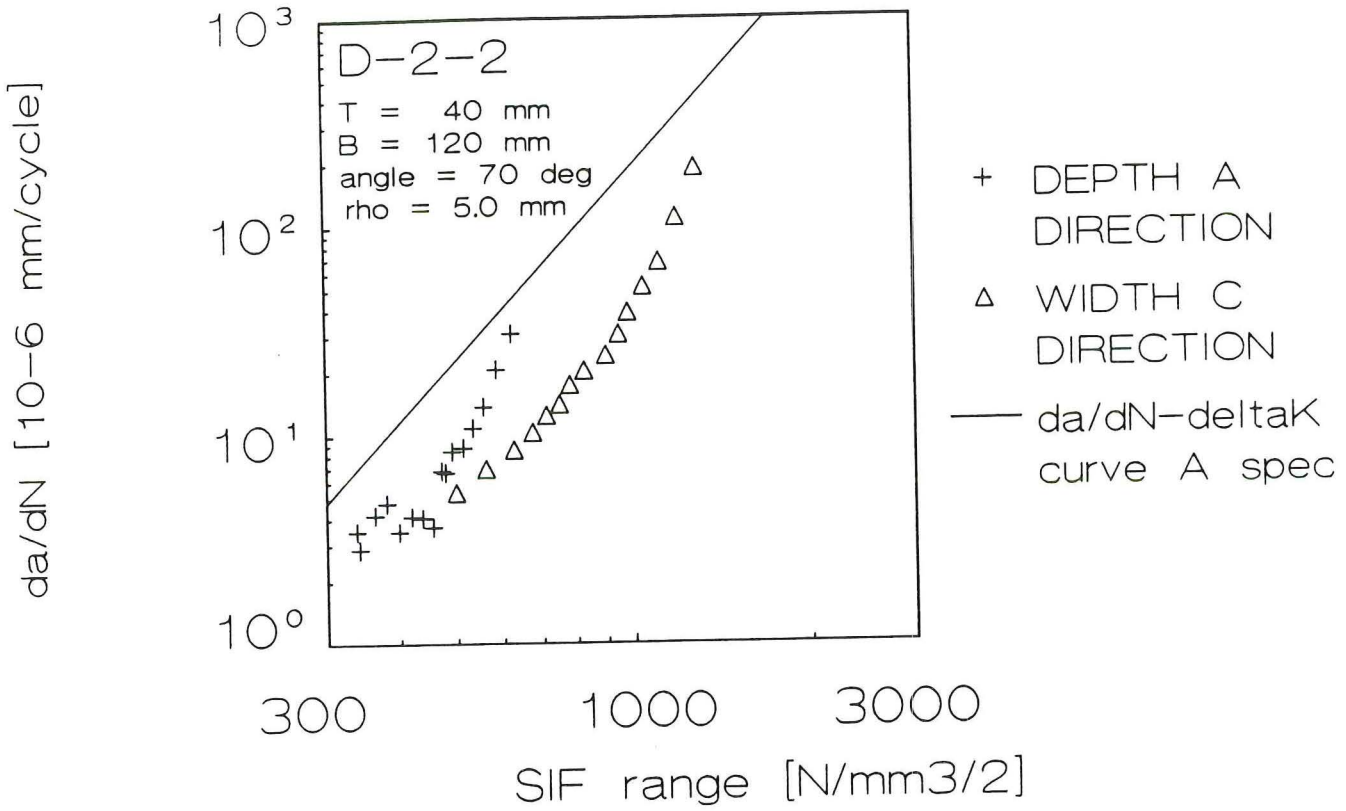

Figure 6-28: Crack growth rate data specimen D-2-2

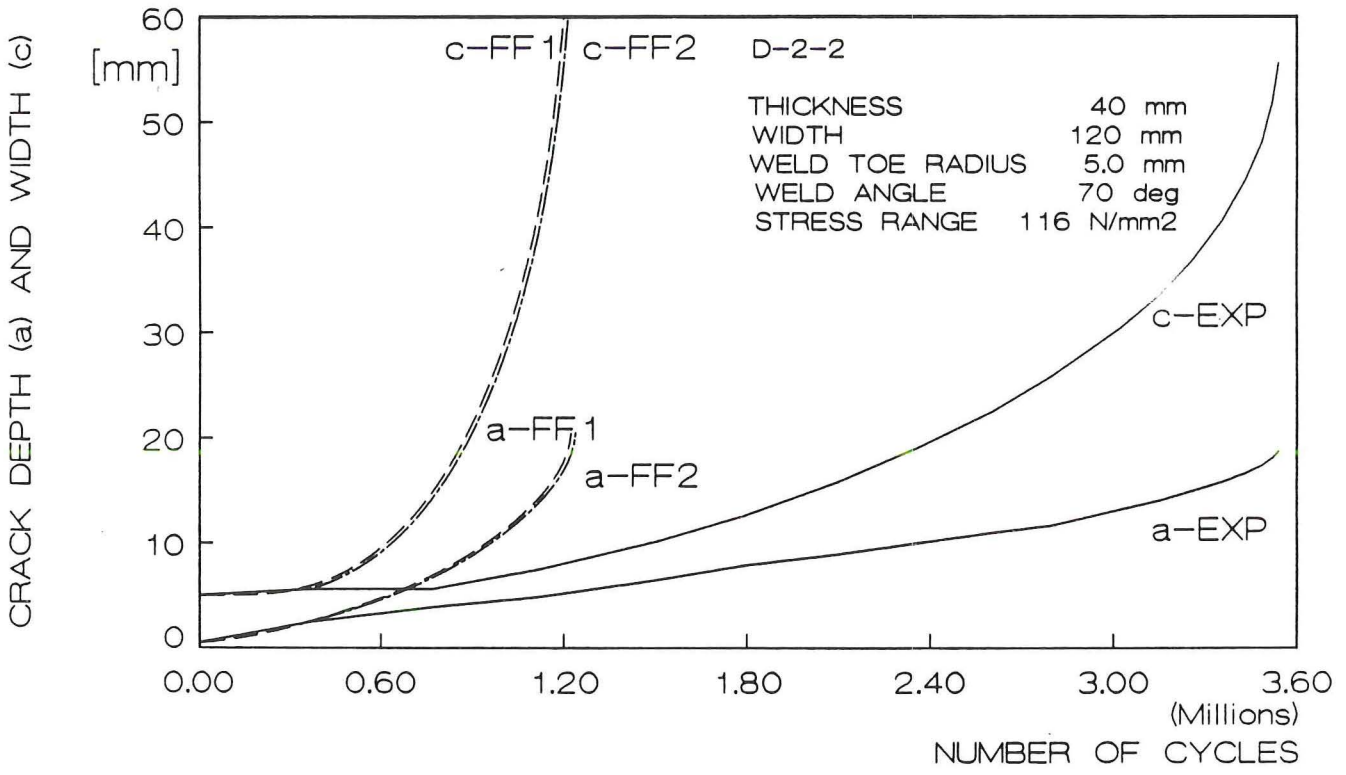

Figure 6-29: Crack growth curves specimen D-2-2

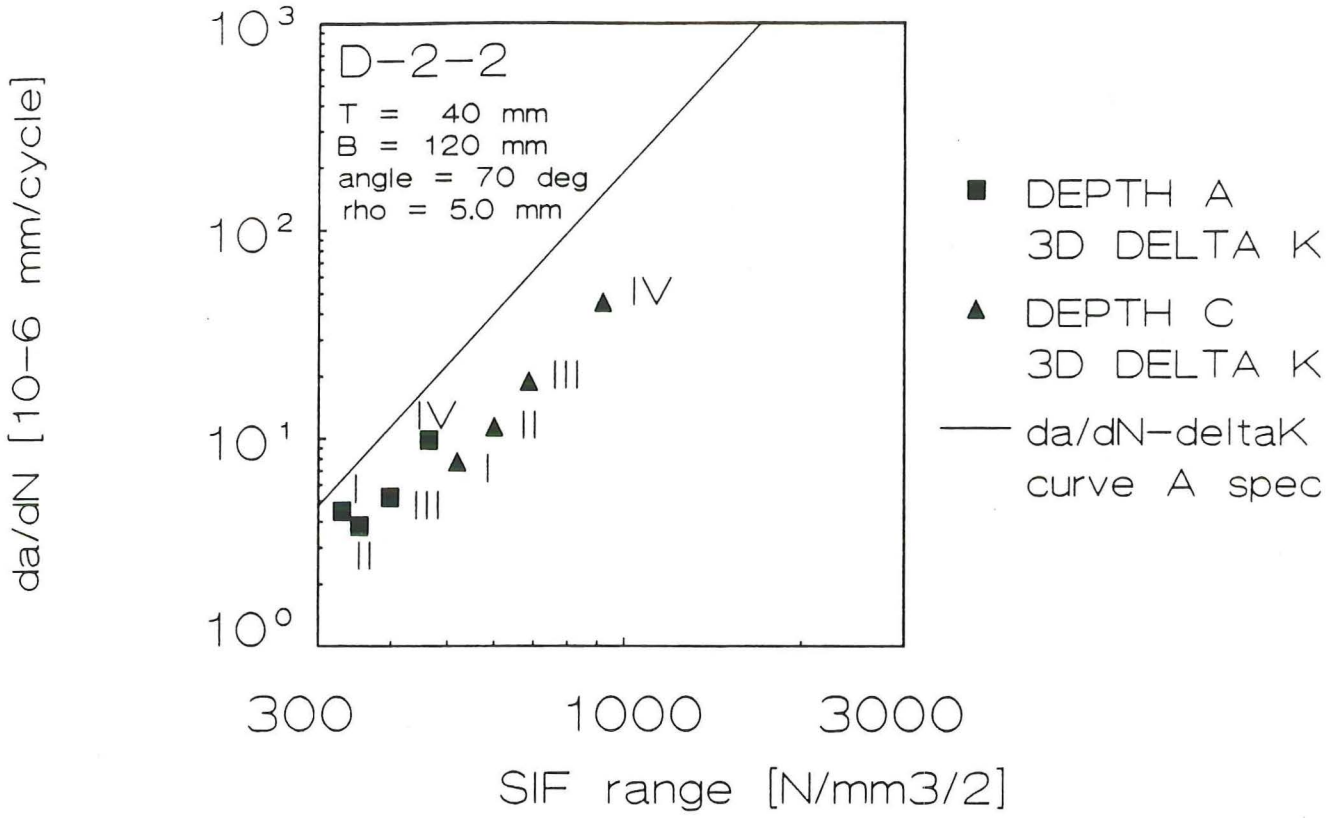

Figure 6-30: Crack growth rate specimen D-2-2 based on 3D FEM ΔK

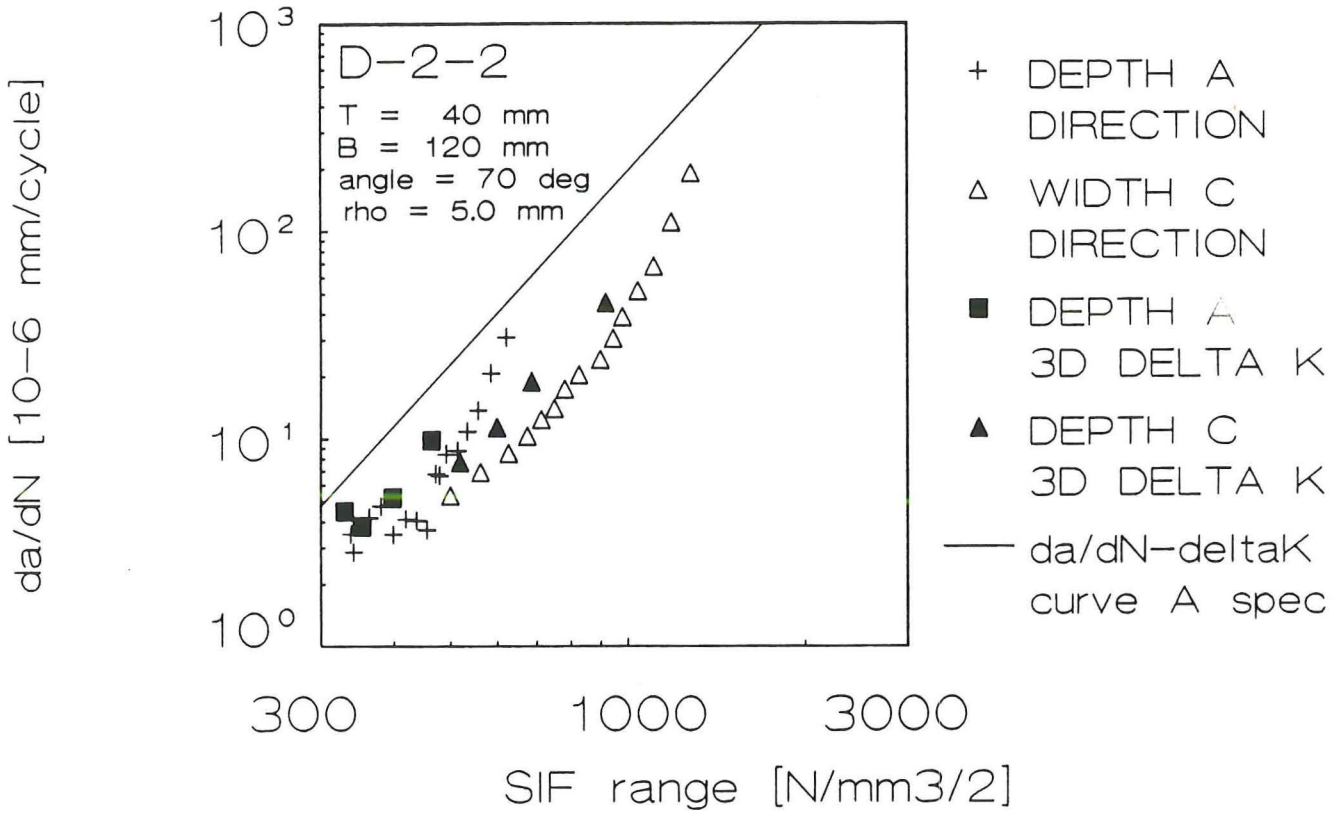

Figure 6-31: Comparison crack growth rate with 2D and 3D SIF

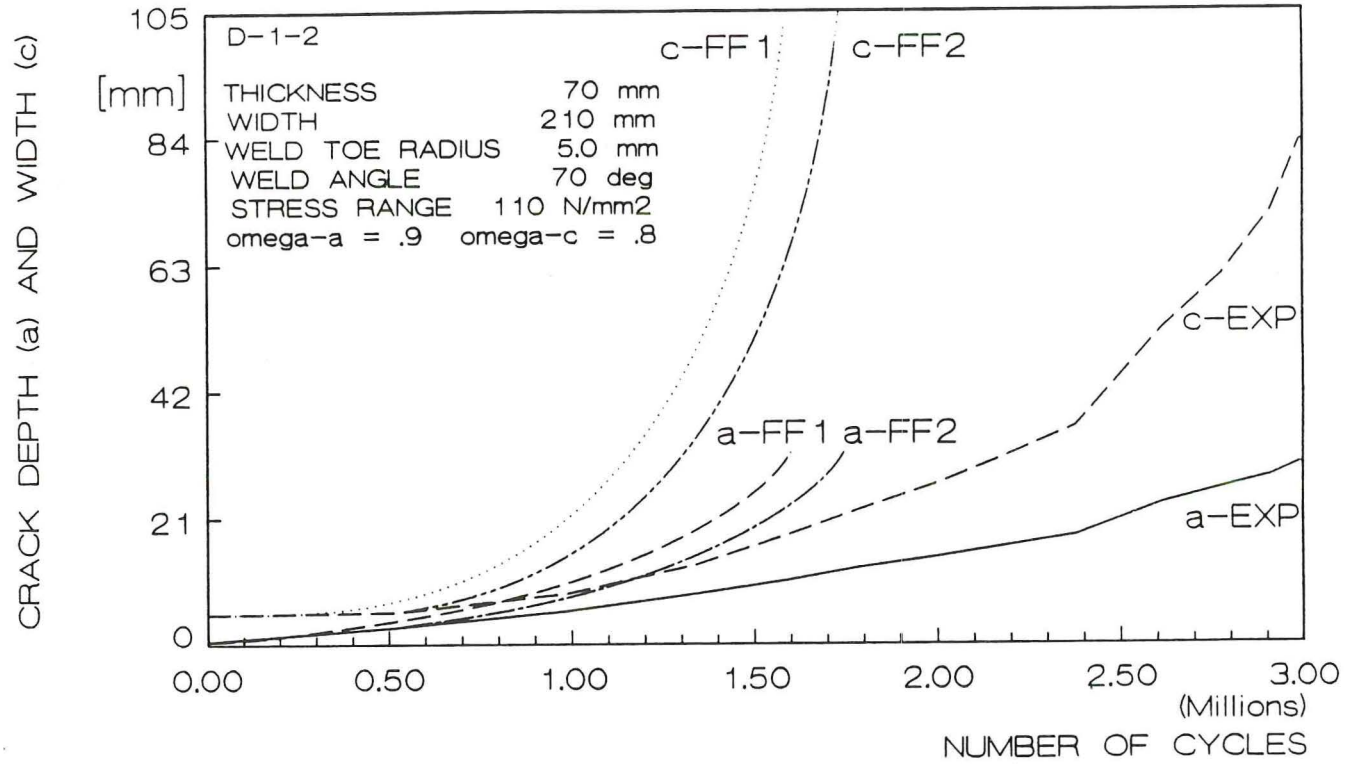

Figure 6-32: Crack growth curves with reduction factor ω for specimen C-1-2

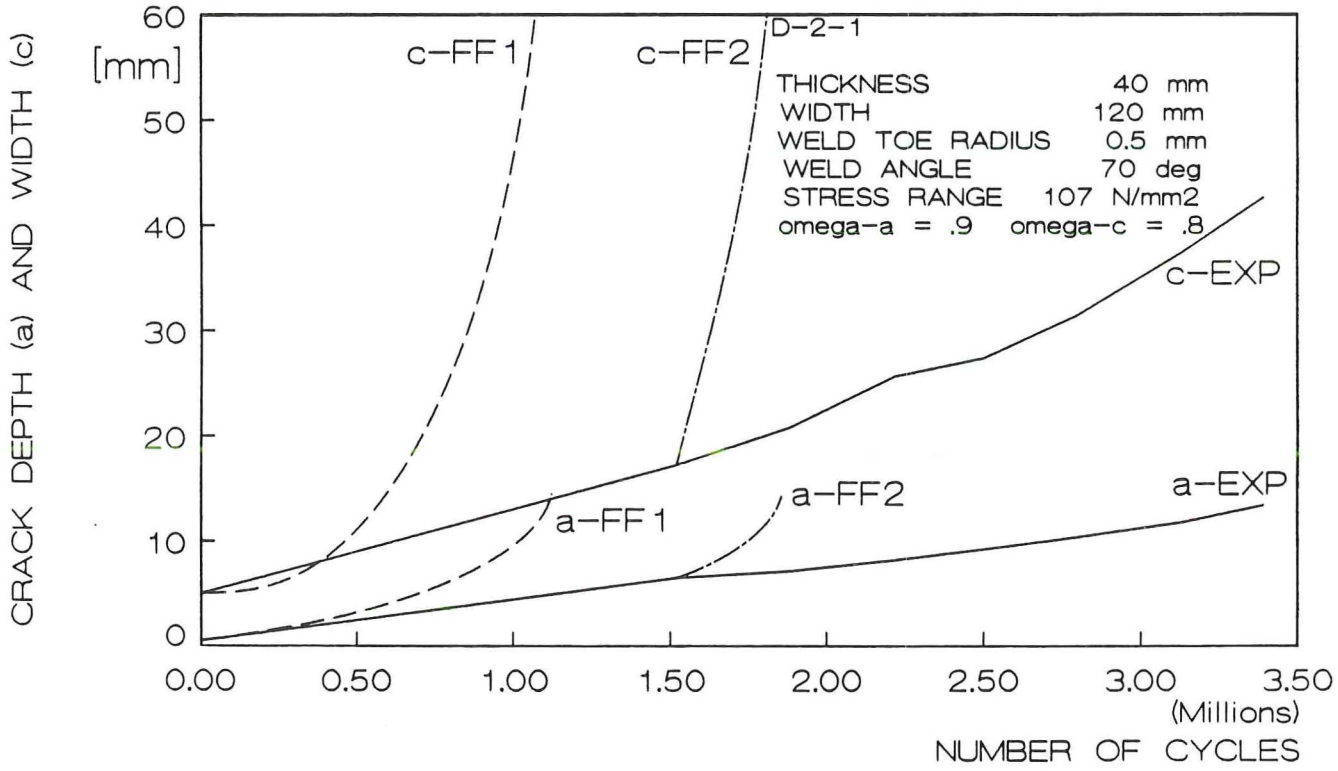

Figure 6-33: Crack growth curves with reduction factor ω for specimen D-2-1

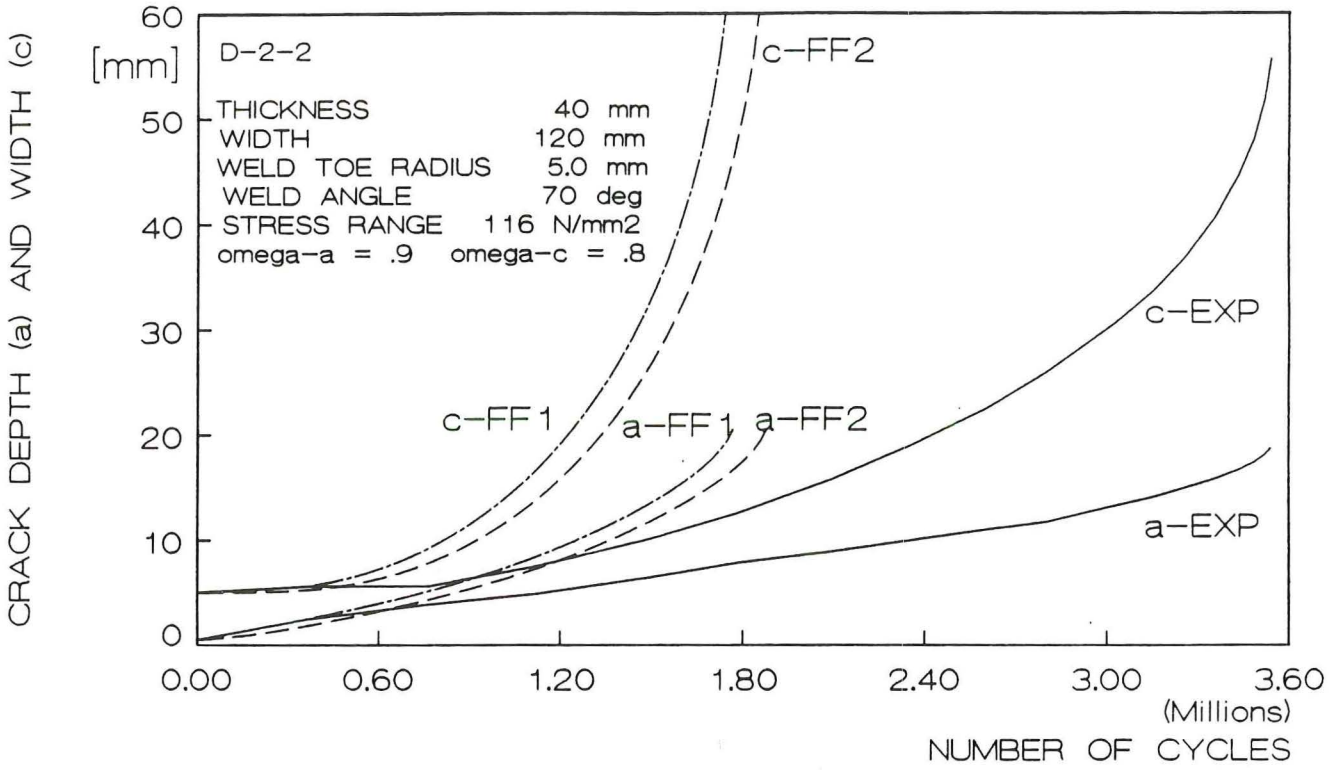

Figure 6-34: Crack growth curves with reduction factor ω for specimen D-2-2

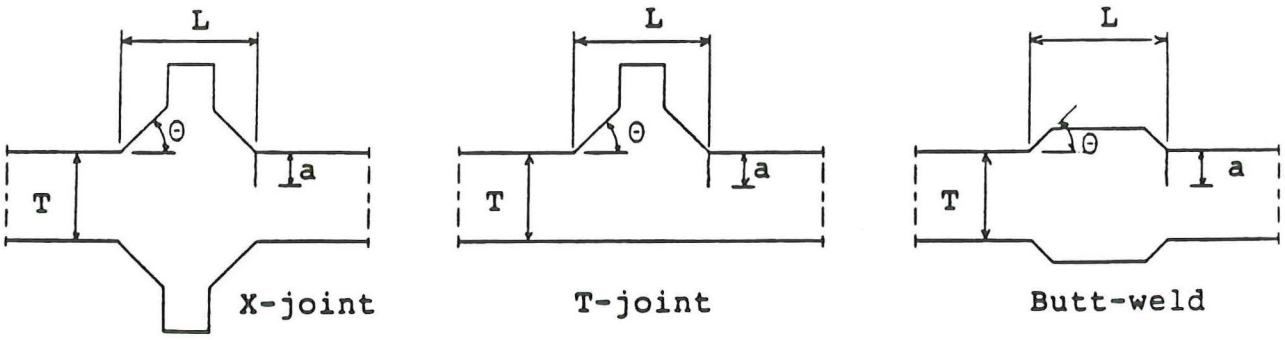

Figure 7-1: Geometries studied by Smith and Hurworth [47] and Maddox et al. [46]

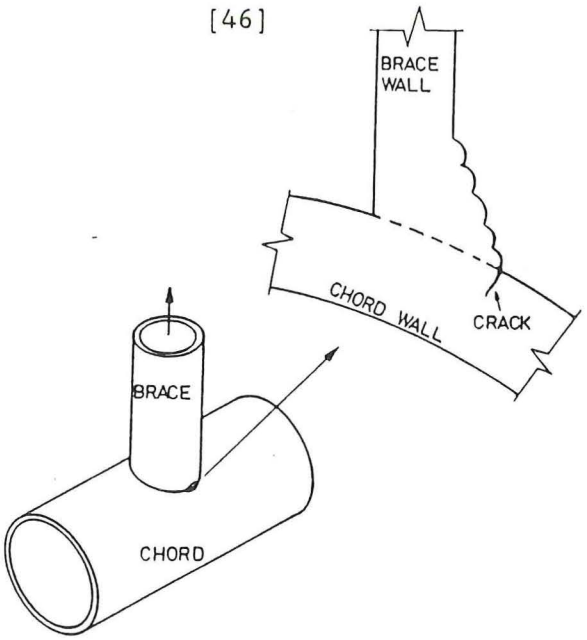

Figure 7-2: Tubular T-joint with fatigue crack at hot spot

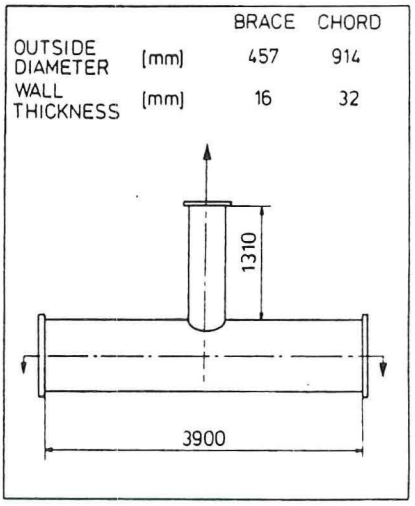

Figure 7-3: Dimensions of tested specimen B3

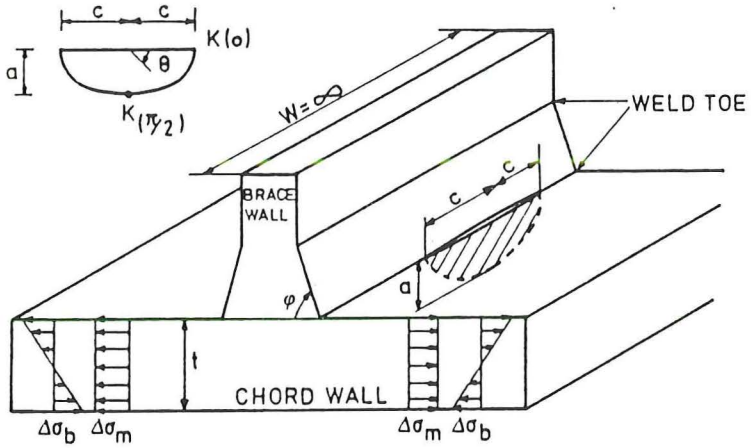

Figure 7-4: Simplified geometry for crack growth model

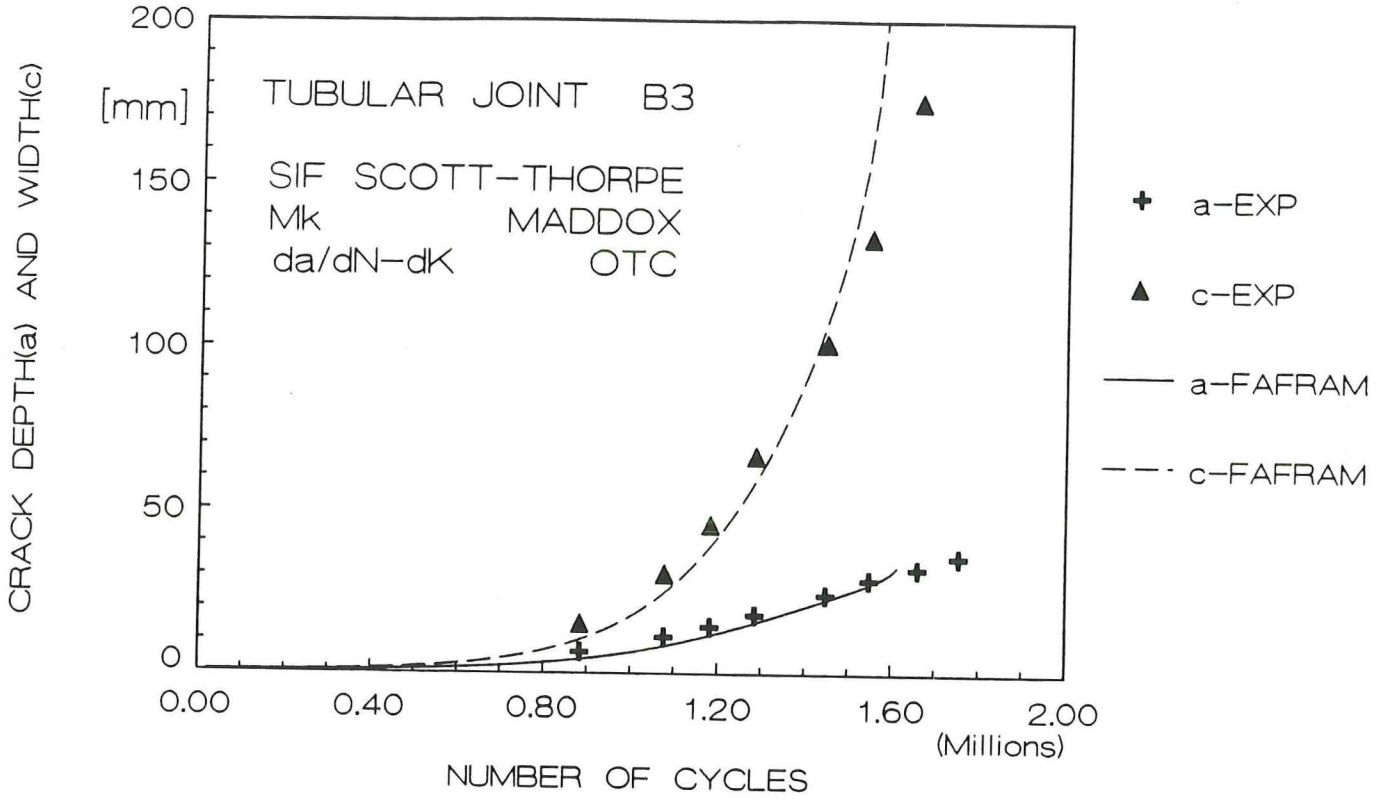

Figure 7-5: Crack growth curve as determined in ref. [29] (calculation A)

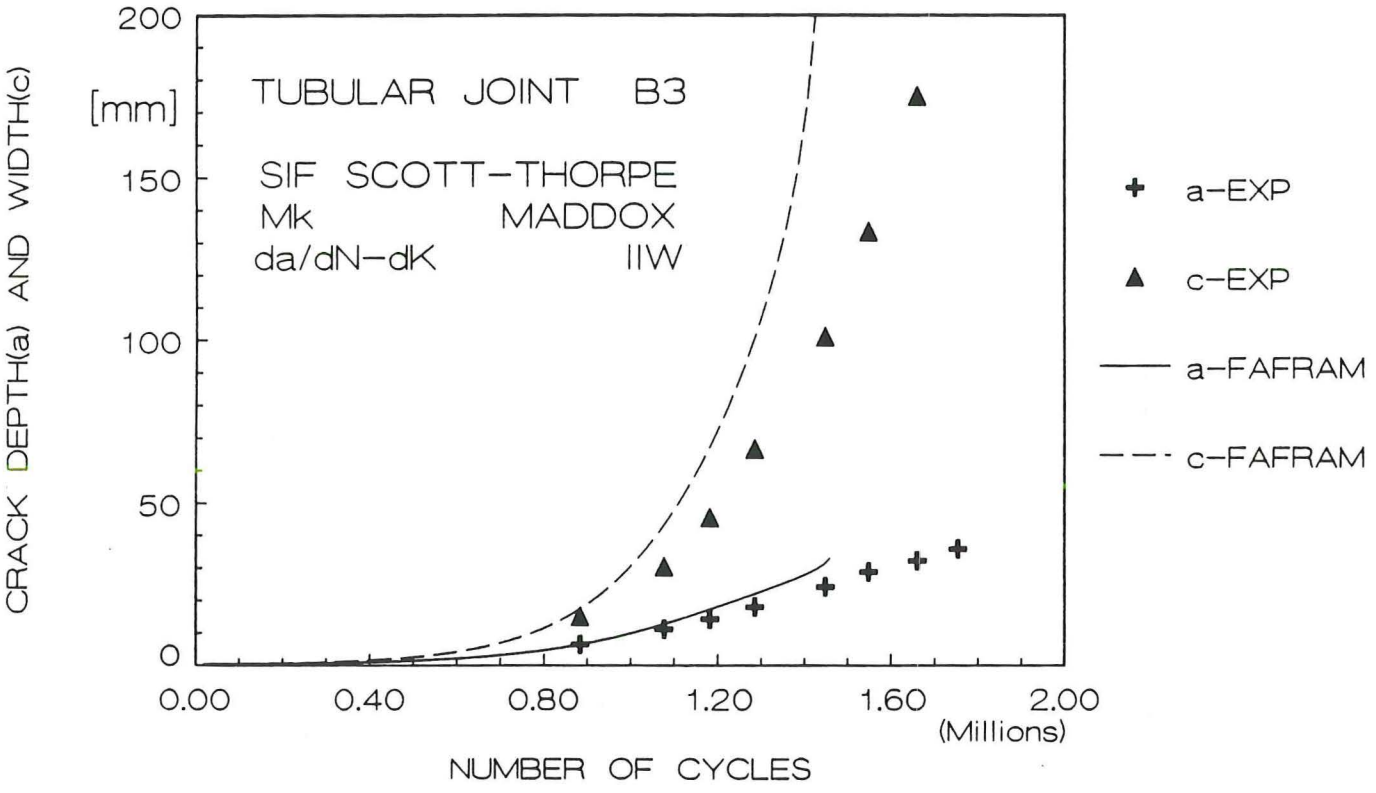

Figure 7-6: Crack growth curve calculation B

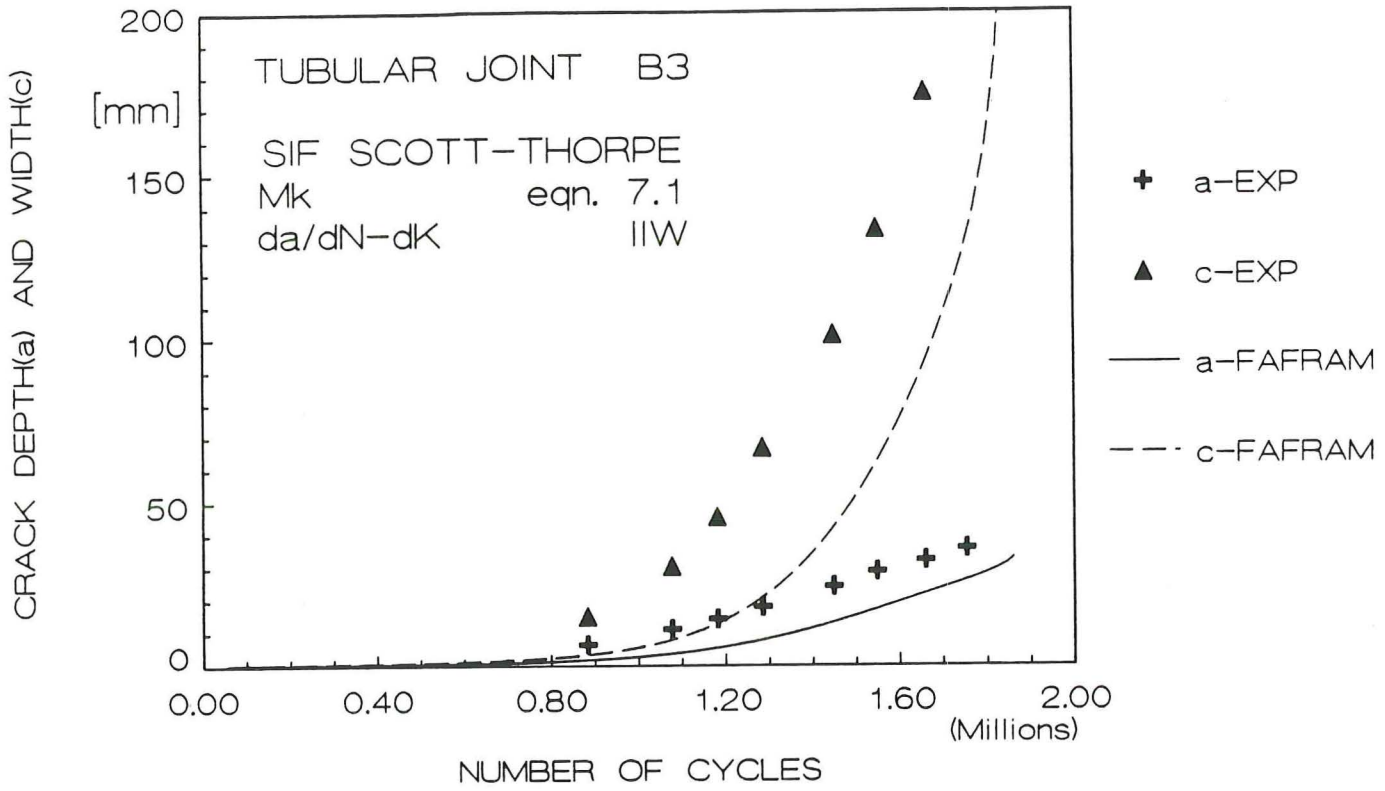

Figure 7-7: Crack growth curve calculation C

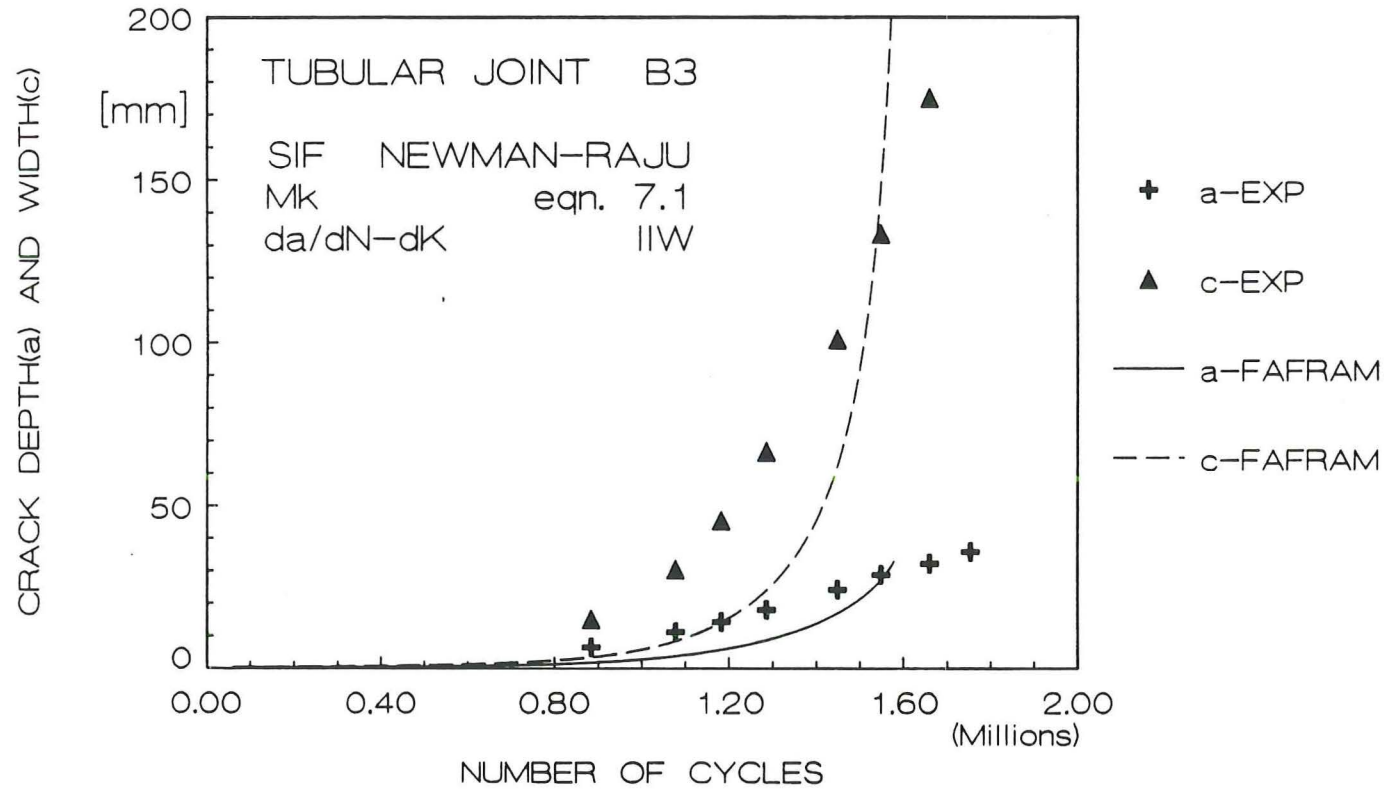

Figure 7-8: Crack growth curve calculation D

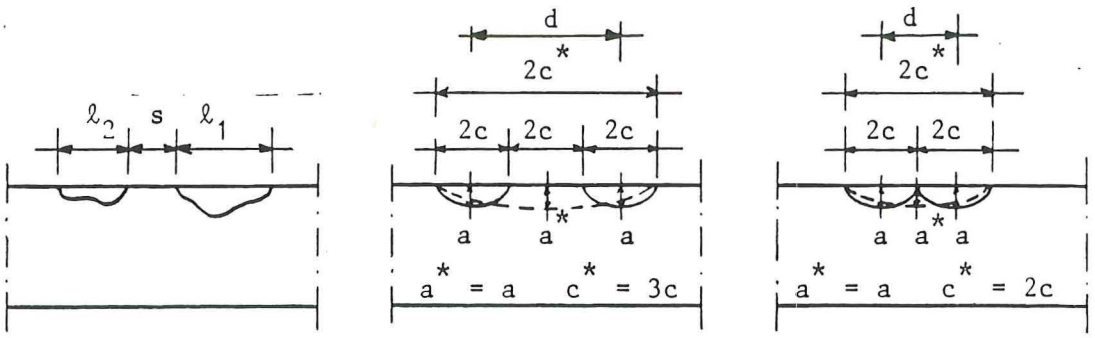

Figure 7-9: Recharacterization rules

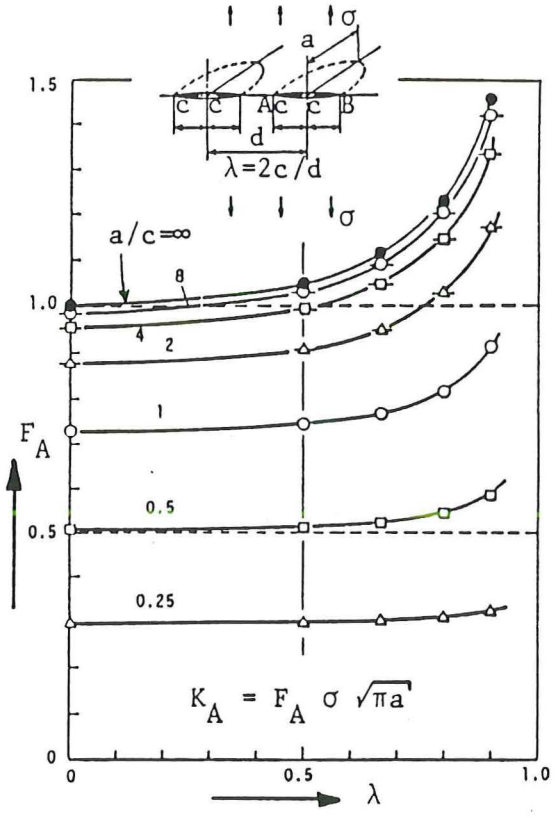

Figure 7-10: Interaction of two cracks [28]

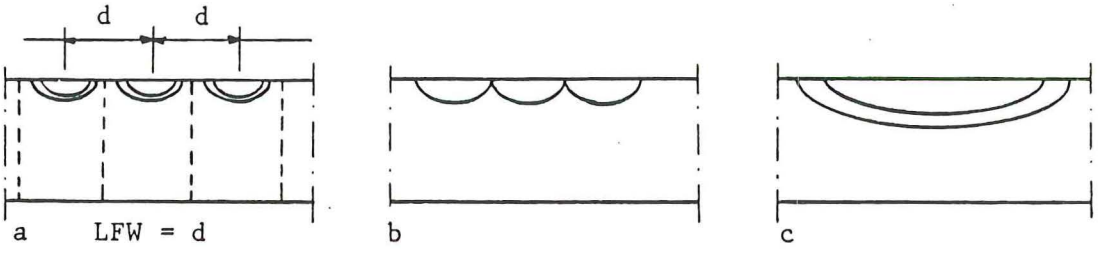

Figure 7-11: Independent growth (a) until coalescence (b) resulting in growth as one single crack (c)

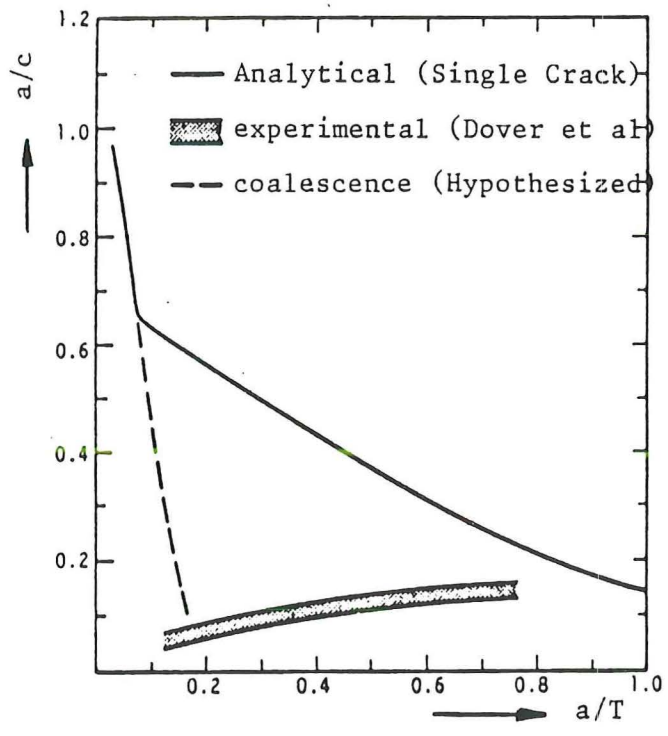

Figure 7-12: Crack shape changes during fatigue crack growth in a T-joint

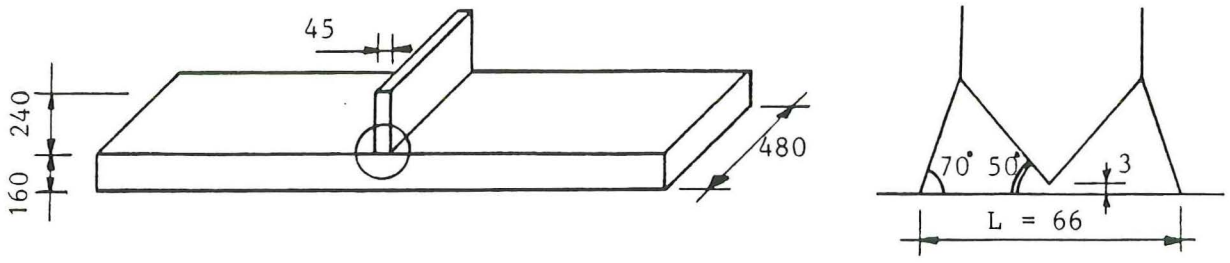

Figure 7-13: Geometry of specimen TBB2

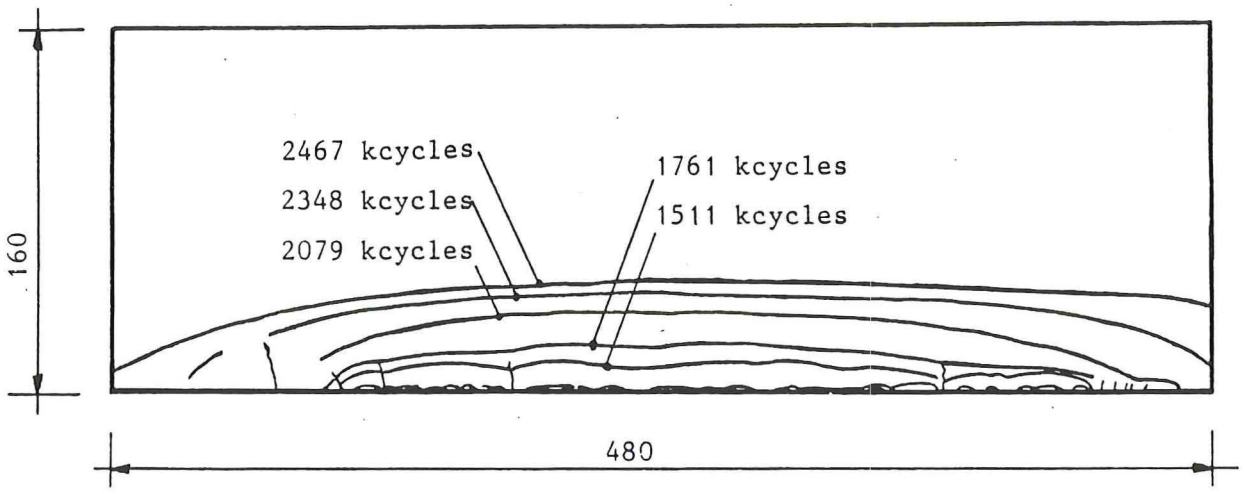

Figure 7-14: Crack growth in specimen TBB2

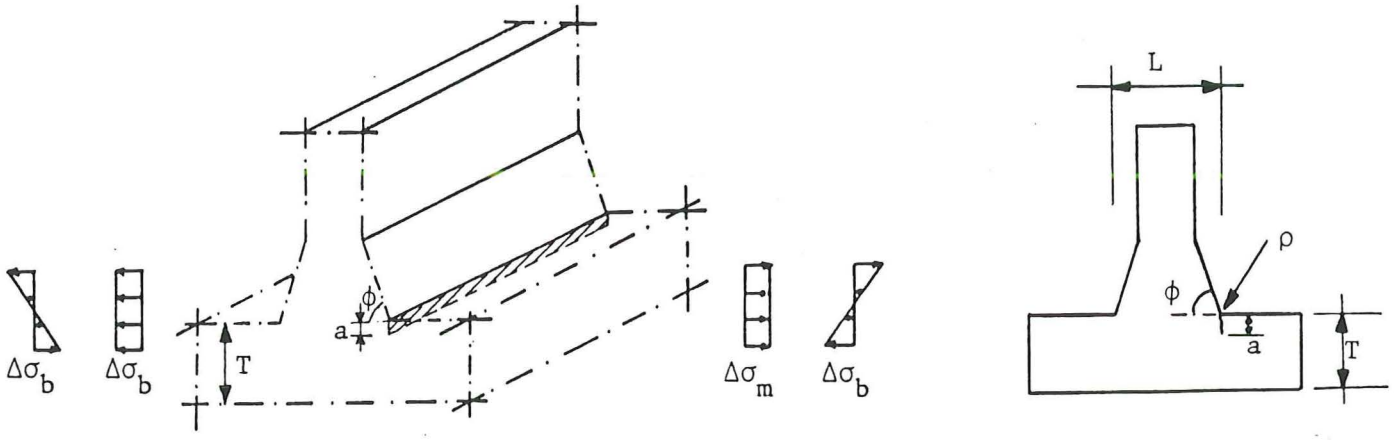

Figure 7-15: Straight fronted crack in T-plate joint

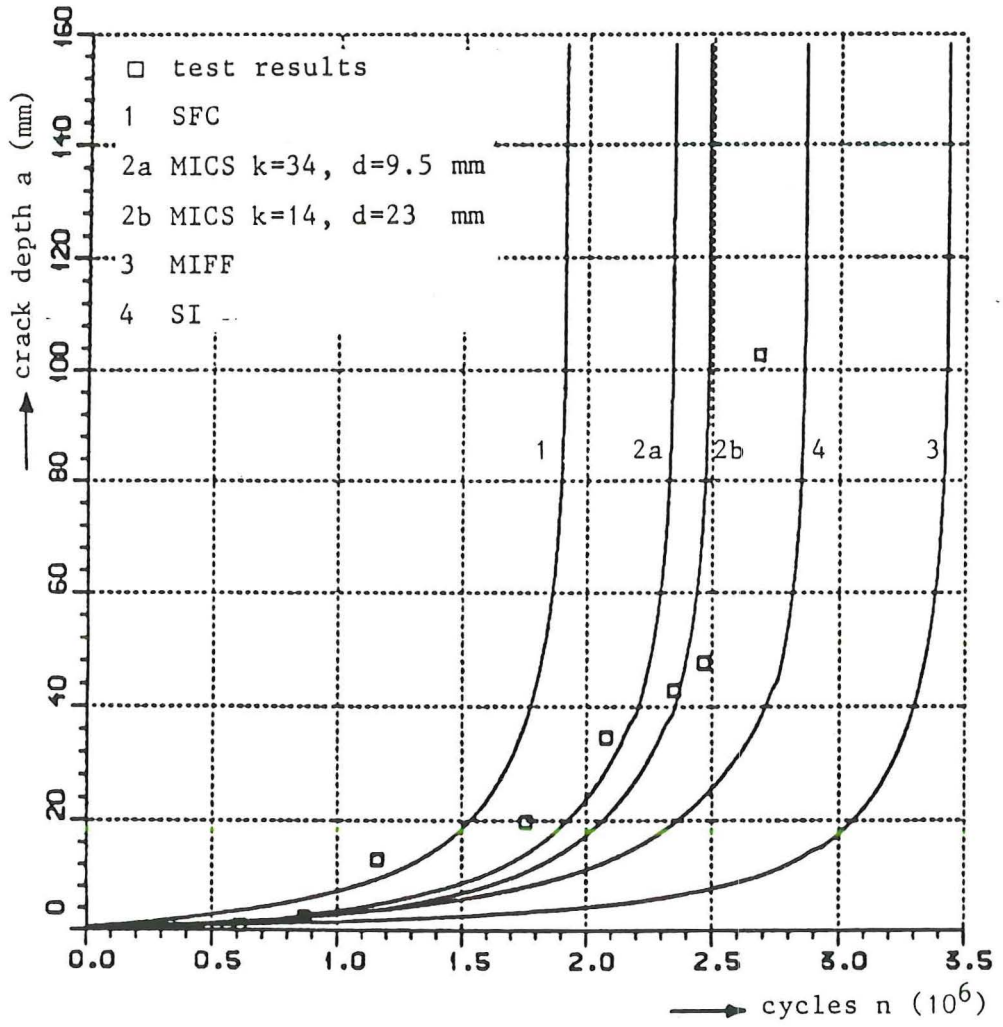

Figure 7-16: Calculation results for specimen TBB2 - crack depth versus load cycles

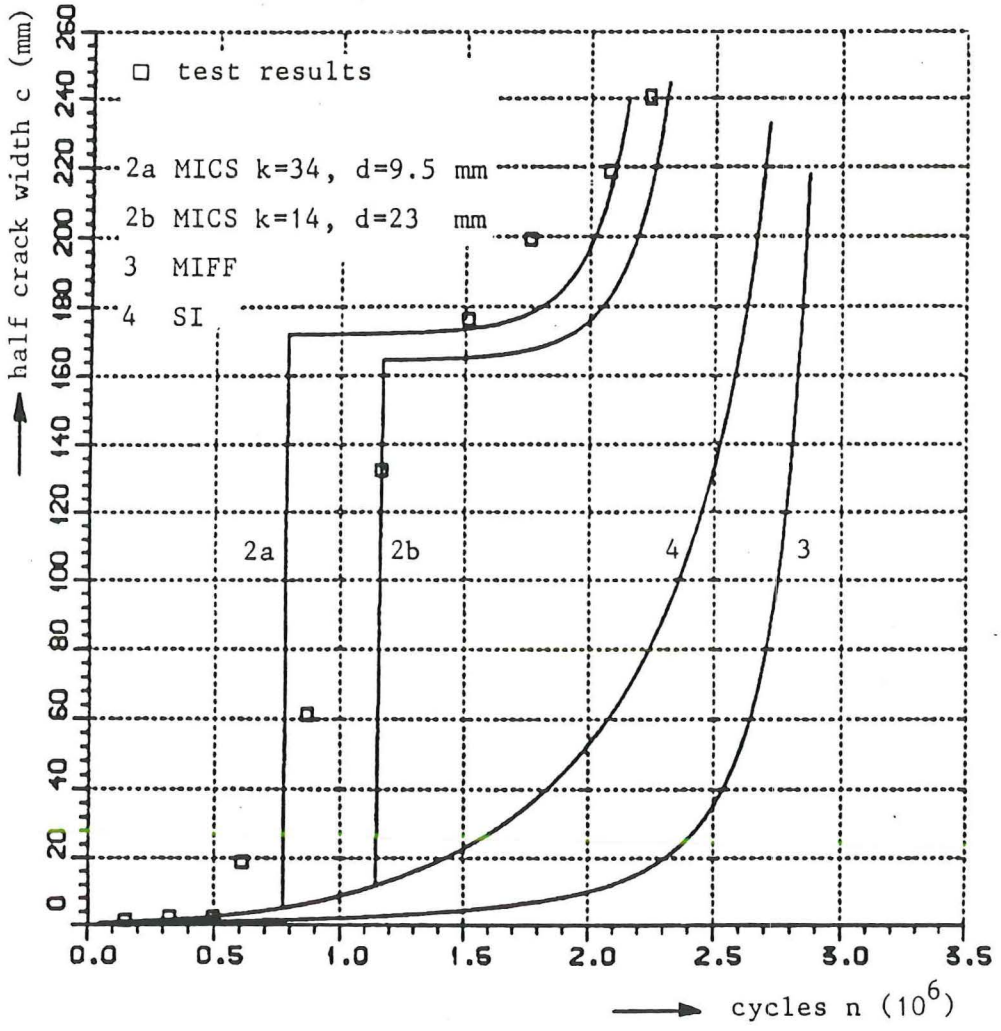

Figure 7-17: Calculation results for specimen TBB2 - half crack width versus load cycles

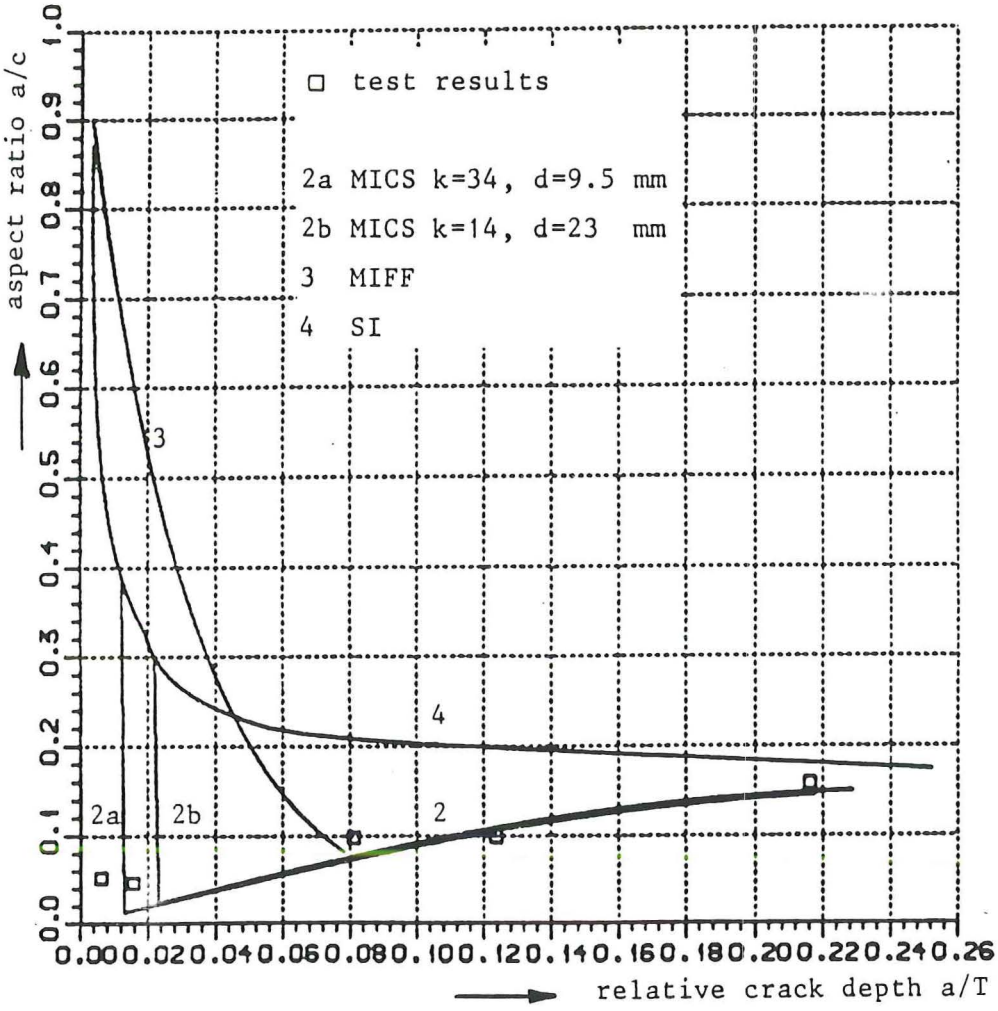

Figure 7-18: Calculation results for specimen TBB2 - aspect ratio versus relative crack depth

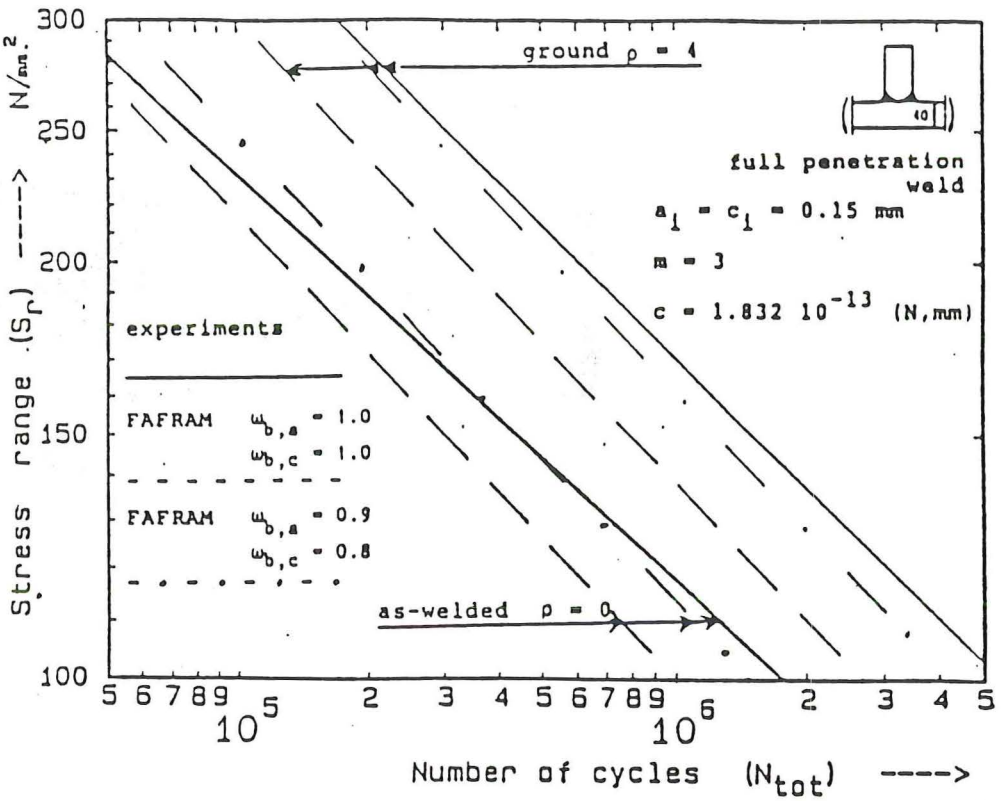

Figure 7-19: Comparison experiments and crack growth calculations for as-welded and ground specimens

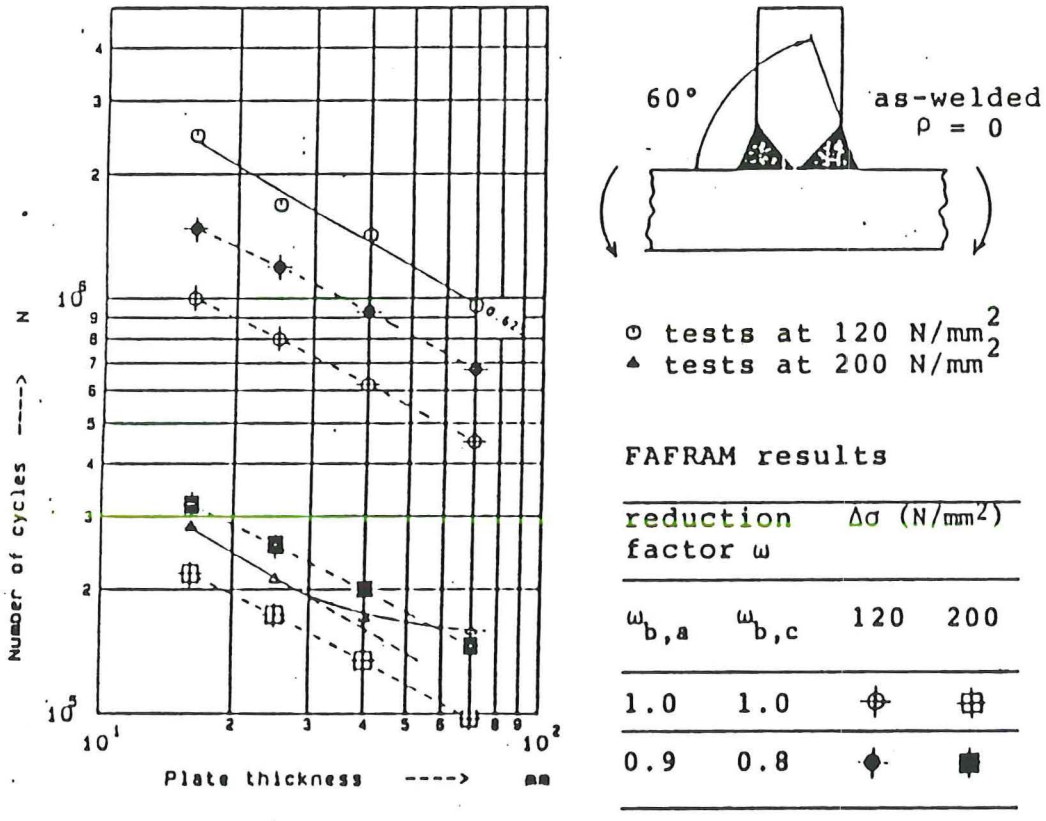

FAFRAM results

reduction factor ω		Δσ (N/mm²)	
$\omega_{b,a}$	$\omega_{b,c}$	120	200
1.0	1.0	⊕	⊞
0.9	0.8	◆	■

Figure 7-20: Experimental and calculated thickness effect

APPENDIX A

CORRECTION PROCEDURE FOR CRACK MARKING CYCLES

Crack length versus number of load cycles.
Elimination of discontinuities originating from crack front markings.

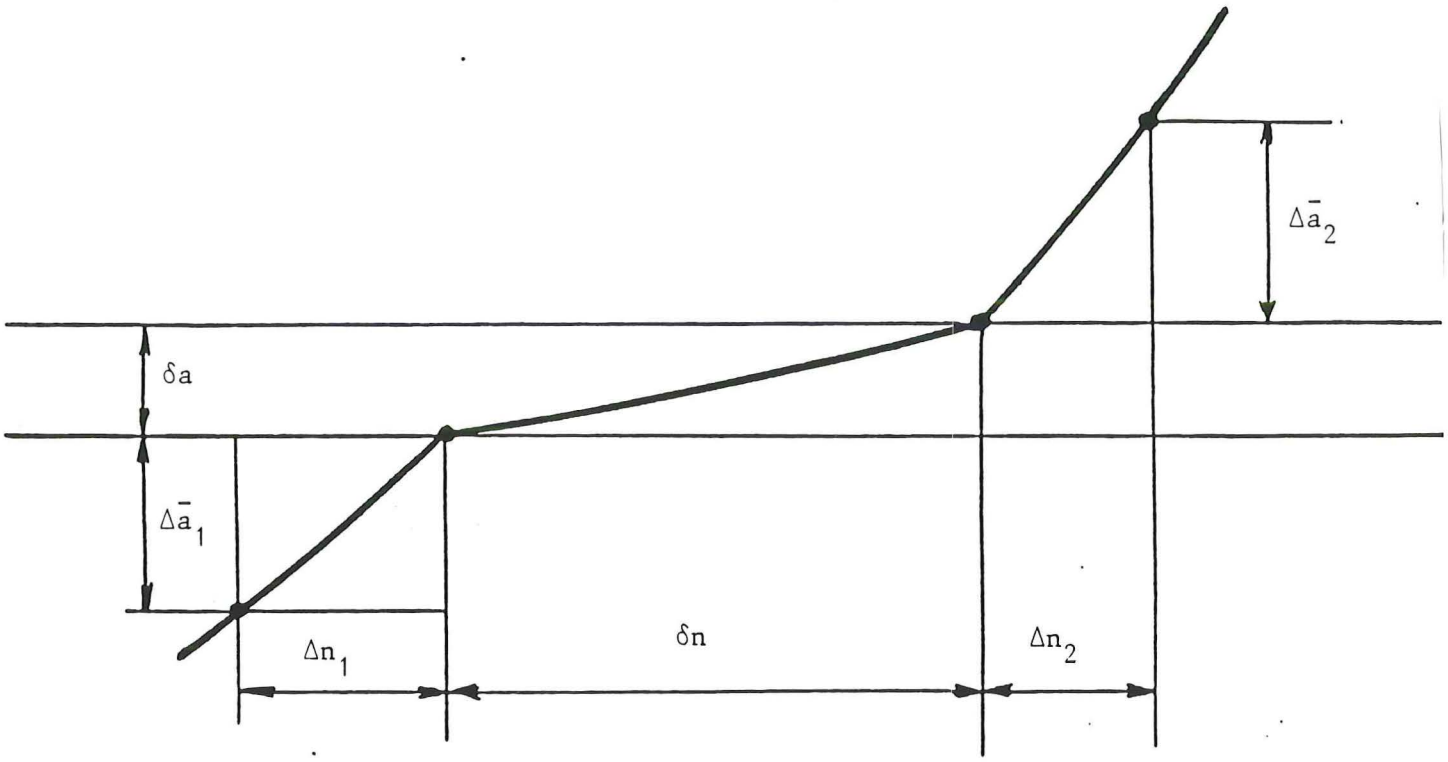

δa = crack extension during crack front marking
δn = number of load cycles during crack front marking

Correction term for number of cycles at a crack front marking

$$\Delta n' = -\delta n + \tfrac{1}{2}\left[\left(\frac{\Delta n}{\Delta \bar{a}}\right)_1 + \left(\frac{\Delta n}{\Delta \bar{a}}\right)_2 \right] \delta a$$

with:

$\left(\frac{\Delta n}{\Delta \bar{a}}\right)_1$ = slope of n versus a curve just before marking

$\left(\frac{\Delta n}{\Delta \bar{a}}\right)_2$ = slope of n versus a curve just after marking

Procedure for smoothening the a versus n curve

APPENDIX B

NUMERICAL BACKGROUND TO THE EVALUATION BASED ON FATIGUE CRACK GROWTH RATE

This appendix gives the numerical background of the evaluation, based on a comparison of the fatigue crack growth rate curve (da/dN-ΔK curve) of the specimen considered with the curve of the A-type specimens (see section 6.2.1 of the main report). The results given in the tables in this appendix can be found in a graphical form in the main report. The corresponding table and figure numbers are given below:

specimen		table		figure	
	C-1-1		B-1		6-2
	C-1-2		B-2		6-4
	C-1-4		B-3		6-6
	C-2-1		B-4		6-8
	C-2-2		B-5		6-10
	C-2-3		B-6		6-12
	C-2-4		B-7		6-14
	B-1-1		B-8		6-16
	B-1-2		B-9		6-18
	B-2-1		B-10		6-20
	B-2-2		B-11		6-22
	D-1-2		B-12		6-24
	D-2-1		B-13		6-26
	D-2-2		B-14		6-28

The tables give the following information:

N = number of cycles in the fatigue test
a = crack depth corresponding with N
c = half crack width corresponding with N
da/dNe = experimental crack growth rate in depth direction
dc/dNe = experimental crack growth rate in width direction
dKa = stress intensity factor range in depth direction
dKc = stress intensity factor range in width direction
dKa– = average value of dKa over the interval considered
dKc– = average value of dKc over the interval considered
da/dNt = theoretical crack growth rate in depth direction
$da/dNt = C\ (dKa-)^m$

dc/dNt = theoretical crack growth rate in width direction
$dc/dNt = C\ (dKc-)^m$

ea = ratio of experimental and theoretical crack growth in depth direction (da/dNe)/(da/dNt)

ec = ratio of experimental and theoretical crack growth in width direction (dc/dNe)/(dc/dNt)

The ratios ea and ec give the relative position of the data points to the lines of the da/dN - ΔK curve of the A-type specimens in the figures.

The stress intensity factors are determined as given in section 6.3 and 6.4 of the main report.

Table B- 1

CRACK GROWTH RATE EVALUATION SPECIMEN C-1-1

THICKNESS T = 70 mm
WELD TOE RADIUS RHO = 0.5 mm
WELD ANGLE THETA = 70 deg
STRESS RANGE SIGMA = 76 N/mm2

CRACK GROWTH CONSTANTS: C = 1.105 E-13 (N,mm)
m = 3.081

EXPERIMENT			EVALUATION			
NUMBER OF CYCLES	CRACK DEPTH	CRACK GROWTH RATE (CGRE)	STRESS INTENSITY FACTOR		CRACK GROWTH RATE (CGRT)	RATIO CGRE / CGRT
N [c]	a [mm]	da/dNe [mm/c]	dKa [N/mm3/2]	dKa-	da/dNt [mm/c]	ea [-]
200000.	.65	.411E-05	269.47	285.08	.405E-05	1.015
351000.	1.27	.583E-05	300.70	313.33	.541E-05	1.077
471000.	1.97	.535E-05	325.96	338.97	.690E-05	.775
658000.	2.97	.783E-05	351.98	361.99	.845E-05	.927
778000.	3.91	.900E-05	372.01	382.35	.100E-04	.900
898000.	4.99	.924E-05	392.70	402.50	.117E-04	.789
1016000.	6.08	.967E-05	412.29	419.86	.133E-04	.725
1106000.	6.95	.131E-04	427.42	436.80	.151E-04	.871
1186000.	8.00	.137E-04	446.18	454.76	.171E-04	.804
1256000.	8.96	.168E-04	463.35	472.45	.192E-04	.877
1316000.	9.97	.207E-04	481.56	487.20	.211E-04	.980

Table B- 1 (continued)

EXPERIMENT			EVALUATION			
NUMBER OF CYCLES	CRACK DEPTH	CRACK GROWTH RATE (CGRE)	STRESS INTENSITY FACTOR		CRACK GROWTH RATE (CGRT)	RATIO CGRE / CGRT
N [c]	a [mm]	da/dNe [mm/c]	dKa [N/mm3/2]	dKa-	da/dNt [mm/c]	ea [-]
1346000.	10.59	.173E-04	492.84	499.99	.228E-04	.759
1391000.	11.37	.175E-04	507.14	513.62	.248E-04	.705
1431000.	12.07	.217E-04	520.11	528.27	.271E-04	.803
1471000.	12.94	.263E-04	536.43	546.45	.300E-04	.874
1511000.	13.99	.290E-04	556.47	564.93	.333E-04	.871
1541000.	14.86	.307E-04	573.39	582.52	.366E-04	.838
1571000.	15.78	.363E-04	591.65	602.73	.406E-04	.894
1601000.	16.87	.455E-04	613.82	623.31	.451E-04	1.010
1621000.	17.78	.423E-04	632.81	646.49	.504E-04	.839
1651000.	19.05	.513E-04	660.17	677.51	.583E-04	.881
1681000.	20.59	.593E-04	694.85	705.29	.659E-04	.900
1696000.	21.48	.660E-04	715.74	723.71	.714E-04	.924
1706000.	22.14	.680E-04	731.68	744.41	.779E-04	.873
1721000.	23.16	.990E-04	757.14	770.02	.864E-04	1.145

Table B- 1 (continued)

EXPERIMENT			EVALUATION			
NUMBER OF CYCLES	CRACK DEPTH	CRACK GROWTH RATE (CGRE)	STRESS INTENSITY FACTOR		CRACK GROWTH RATE (CGRT)	RATIO CGRE / CGRT
N [c]	a [mm]	da/dNe [mm/c]	dKa [N/mm3/2]	dKa-	da/dNt [mm/c]	ea [-]
1731000.	24.15	.960E-04	782.90	795.93	.957E-04	1.003
1741000.	25.11	.133E-03	808.96	828.01	.108E-03	1.230
1751000.	26.44	.132E-03	847.06	856.99	.120E-03	1.098
1756000.	27.10	.151E-03	866.91	889.71	.135E-03	1.119
1766000.	28.61	.227E-03	912.52	936.94	.158E-03	1.433
1772000.	29.97	.187E-03	961.36	971.97	.177E-03	1.054
1775000.	30.53	.240E-03	982.58	1001.59	.194E-03	1.235
1779000.	31.49	.232E-03	1020.59	1040.08	.218E-03	1.065
1783000.	32.42	.293E-03	1059.57	1085.74	.249E-03	1.174
1787000.	33.59	.323E-03	1111.91	1135.15	.286E-03	1.132
1790000.	34.56	.357E-03	1158.38	1184.94	.326E-03	1.094
1793000.	35.63	.390E-03	1211.50	1231.54	.367E-03	1.062
1795000.	36.41		1251.58			

Table B- 2

CRACK GROWTH RATE EVALUATION SPECIMEN C-1-2

THICKNESS T = 70 mm
WELD TOE RADIUS RHO = 0.5 mm
WELD ANGLE THETA = 70 deg
STRESS RANGE SIGMA = 76 N/mm2

CRACK GROWTH CONSTANTS: C = 1.105 E-13 (N,mm)
m = 3.081

EXPERIMENT			EVALUATION			
NUMBER OF CYCLES	CRACK DEPTH	CRACK GROWTH RATE (CGRE)	STRESS INTENSITY FACTOR		CRACK GROWTH RATE (CGRT)	RATIO CGRE / CGRT
N [c]	a [mm]	da/dNe [mm/c]	dKa [N/mm3/2]	dKa-	da/dNt [mm/c]	ea [-]
500000.	1.08	.561E-05	292.58	308.96	.519E-05	1.082
655000.	1.95	.665E-05	325.35	339.23	.692E-05	.961
816000.	3.02	.593E-05	353.12	362.56	.849E-05	.699
966000.	3.91	.773E-05	372.01	383.09	.101E-04	.769
1116000.	5.07	.113E-04	394.18	402.09	.117E-04	.966
1194000.	5.95	.927E-05	410.00	418.88	.132E-04	.700
1304000.	6.97	.123E-04	427.76	436.53	.150E-04	.815
1384000.	7.95	.129E-04	445.29	454.50	.170E-04	.756
1464000.	8.98	.160E-04	463.71	472.36	.192E-04	.834
1524000.	9.94	.157E-04	481.02	490.77	.216E-04	.729
1592000.	11.01	.163E-04	500.52	510.31	.243E-04	.670

Table B- 2 (continued)

EXPERIMENT			EVALUATION			
NUMBER OF CYCLES	CRACK DEPTH	CRACK GROWTH RATE (CGRE)	STRESS INTENSITY FACTOR		CRACK GROWTH RATE (CGRT)	RATIO CGRE / CGRT
N [c]	a [mm]	da/dNe [mm/c]	dKa [N/mm3/2]	dKa-	da/dNt [mm/c]	ea [-]
1657000.	12.07	.196E-04	520.11	528.36	.271E-04	.722
1702000.	12.95	.224E-04	536.62	546.25	.300E-04	.748
1747000.	13.96	.251E-04	555.89	566.91	.336E-04	.746
1792000.	15.09	.290E-04	577.92	586.60	.374E-04	.776
1822000.	15.96	.280E-04	595.27	603.82	.409E-04	.685
1852000.	16.80	.338E-04	612.37	626.53	.458E-04	.737
1892000.	18.15	.345E-04	640.68	648.13	.508E-04	.679
1912000.	18.84	.415E-04	655.57	664.75	.549E-04	.755
1932000.	19.67	.516E-04	673.92	688.69	.613E-04	.842
1957000.	20.96	.545E-04	703.45	716.47	.692E-04	.787
1977000.	22.05	.680E-04	729.48	742.17	.772E-04	.881
1992000.	23.07	.710E-04	754.85	764.00	.844E-04	.842
2002000.	23.78	.930E-04	773.14	785.55	.919E-04	1.012
2012000.	24.71	.100E-03	797.96	811.91	.102E-03	.983

Table B- 2 (continued)

EXPERIMENT			EVALUATION			
NUMBER OF CYCLES	CRACK DEPTH	CRACK GROWTH RATE (CGRE)	STRESS INTENSITY FACTOR		CRACK GROWTH RATE (CGRT)	RATIO CGRE / CGRT
N [c]	a [mm]	da/dNe [mm/c]	dKa [N/mm3/2]	dKa- [N/mm3/2]	da/dNt [mm/c]	ea [-]
2022000.	25.71	.115E-03	825.85	842.73	.114E-03	1.008
2032000.	26.86	.142E-03	859.62	872.74	.127E-03	1.114
2038000.	27.71	.173E-03	885.87	901.62	.141E-03	1.233
2044000.	28.75	.207E-03	917.38	939.74	.160E-03	1.294
2050000.	29.99	.240E-03	962.11	980.53	.182E-03	1.319
2054000.	30.95	.267E-03	998.95	1020.74	.206E-03	1.299
2058000.	32.02	.307E-03	1042.53	1069.42	.238E-03	1.293
2062000.	33.25	.365E-03	1096.30	1113.27	.269E-03	1.356
2064000.	33.98	.347E-03	1130.25	1155.36	.302E-03	1.149
2067000.	35.02	.390E-03	1180.48	1200.33	.339E-03	1.149
2069000.	35.80	.465E-03	1220.18	1244.24	.379E-03	1.227
2071000.	36.73	.520E-03	1268.31	1296.47	.430E-03	1.208
2073000.	37.77	.530E-03	1324.62	1355.59	.494E-03	1.074

Table B- 2 (continued)

EXPERIMENT			EVALUATION			
NUMBER OF CYCLES	CRACK DEPTH	CRACK GROWTH RATE (CGRE)	STRESS INTENSITY FACTOR		CRACK GROWTH RATE (CGRT)	RATIO CGRE / CGRT
N [c]	a [mm]	da/dNe [mm/c]	dKa [N/mm3/2]	dKa-	da/dNt [mm/c]	ea [-]
2075000.	38.83		1386.56			
		.607E-03		1415.73	.564E-03	1.075
2076500.	39.74		1444.91			
		.692E-03		1474.21	.639E-03	1.082
2077700.	40.57		1503.51			

Table B- 3

CRACK GROWTH RATE EVALUATION SPECIMEN C-1-4

THICKNESS T = 70 mm
WELD TOE RADIUS RHO = 5.0 mm
WELD ANGLE THETA = 70 deg
STRESS RANGE SIGMA = 76 N/mm2

CRACK GROWTH CONSTANTS: C = 1.105 E-13 (N,mm)
m = 3.081

EXPERIMENT			EVALUATION			
NUMBER OF CYCLES	CRACK DEPTH	CRACK GROWTH RATE (CGRE)	STRESS INTENSITY FACTOR		CRACK GROWTH RATE (CGRT)	RATIO CGRE / CGRT
N [c]	a [mm]	da/dNe [mm/c]	dKa [N/mm3/2]	dKa- [N/mm3/2]	da/dNt [mm/c]	ea [-]
1000000.	1.54		280.52			
		.338E-05		292.50	.438E-05	.772
1139000.	2.01		304.48			
		.373E-05		322.98	.594E-05	.628
1415000.	3.04		341.47			
		.476E-05		354.85	.794E-05	.599
1625000.	4.04		368.22			
		.687E-05		379.71	.979E-05	.702
1775000.	5.07		391.20			
		.632E-05		401.41	.116E-04	.544
1938000.	6.10		411.63			
		.833E-05		420.92	.134E-04	.620
2058000.	7.10		430.21			
		.978E-05		438.02	.152E-04	.643
2148000.	7.98		445.82			
		.118E-04		455.30	.171E-04	.688
2238000.	9.04		464.78			
		.132E-04		471.91	.191E-04	.689
2298000.	9.83		479.03			
		.140E-04		485.38	.209E-04	.671
2348000.	10.53		491.74			
		.151E-04		502.30	.232E-04	.653

Table B- 3 (continued

EXPERIMENT			EVALUATION			
NUMBER OF CYCLES	CRACK DEPTH	CRACK GROWTH RATE (CGRE)	STRESS INTENSITY FACTOR		CRACK GROWTH RATE (CGRT)	RATIO CGRE / CGRT
N [c]	a [mm]	da/dNe [mm/c]	dKa [N/mm3/2]	dKa-	da/dNt [mm/c]	ea [-]
2424000.	11.68	.168E-04	512.87	520.69	.259E-04	.649
2474000.	12.52	.192E-04	528.52	535.79	.283E-04	.681
2514000.	13.29	.205E-04	543.06	550.92	.308E-04	.665
2554000.	14.11	.216E-04	558.78	568.25	.339E-04	.636
2599000.	15.08	.240E-04	577.72	584.89	.370E-04	.648
2629000.	15.80	.260E-04	592.05	603.97	.409E-04	.636
2674000.	16.97	.265E-04	615.88	627.00	.459E-04	.577
2714000.	18.03	.327E-04	638.12	648.71	.510E-04	.641
2744000.	19.01	.350E-04	659.29	671.00	.566E-04	.619
2774000.	20.06	.470E-04	682.71	693.55	.626E-04	.751
2794000.	21.00	.520E-04	704.39	716.81	.693E-04	.750
2814000.	22.04	.560E-04	729.24	739.64	.764E-04	.733
2829000.	22.88	.667E-04	750.05	762.91	.840E-04	.794
2844000.	23.88	.880E-04	775.76	787.55	.926E-04	.950

Table B- 3 (continued

EXPERIMENT			EVALUATION			
NUMBER OF CYCLES	CRACK DEPTH	CRACK GROWTH RATE (CGRE)	STRESS INTENSITY FACTOR		CRACK GROWTH RATE (CGRT)	RATIO CGRE / CGRT
N [c]	a [mm]	da/dNe [mm/c]	dKa [N/mm3/2]	dKa-	da/dNt [mm/c]	ea [-]
2854000.	24.76	.910E-04	799.33	812.02	.102E-03	.894
2864000.	25.67	.107E-03	824.71	840.35	.113E-03	.946
2874000.	26.74	.124E-03	856.00	875.23	.128E-03	.967
2884000.	27.98	.162E-03	894.45	906.62	.143E-03	1.133
2889000.	28.79	.198E-03	918.78	936.55	.158E-03	1.253
2894000.	29.78	.206E-03	954.32	973.88	.178E-03	1.156
2899000.	30.81	.258E-03	993.44	1014.22	.202E-03	1.275
2903000.	31.84	.290E-03	1035.00	1053.59	.227E-03	1.277
2906000.	32.71	.310E-03	1072.19	1093.21	.254E-03	1.218
2909000.	33.64	.386E-03	1114.24	1161.34	.307E-03	1.259
2914000.	35.57	.445E-03	1208.44	1231.31	.367E-03	1.212
2916000.	36.46	.430E-03	1254.18	1277.00	.411E-03	1.047
2918000.	37.32	.555E-03	1299.83	1331.18	.467E-03	1.189
2920000.	38.43	.580E-03	1362.52	1398.71	.544E-03	1.067

EXPERIMENT			EVALUATION			
NUMBER OF CYCLES	CRACK DEPTH	CRACK GROWTH RATE (CGRE)	STRESS INTENSITY FACTOR		CRACK GROWTH RATE (CGRT)	RATIO CGRE / CGRT
N [c]	a [mm]	da/dNe [mm/c]	dKa [N/mm3/2]	dKa-	da/dNt [mm/c]	ea [-]
2922000.	39.59		1434.90			
		.675E-03		1483.23	.651E-03	1.036
2924000.	40.94		1531.57			

Table B- 4

CRACK GROWTH RATE EVALUATION SPECIMEN C-2-1

THICKNESS T = 40 mm
WELD TOE RADIUS RHO = 0.5 mm
WELD ANGLE THETA = 70 deg
STRESS RANGE SIGMA =102 N/mm2

CRACK GROWTH CONSTANTS: C = 1.105 E-13 (N,mm)
m = 3.081

EXPERIMENT			EVALUATION			
NUMBER OF CYCLES	CRACK DEPTH	CRACK GROWTH RATE (CGRE)	STRESS INTENSITY FACTOR		CRACK GROWTH RATE (CGRT)	RATIO CGRE / CGRT
N [c]	a [mm]	da/dNe [mm/c]	dKa [N/mm3/2]	dKa-	da/dNt [mm/c]	ea [-]
111000.	.56	.291E-05	287.62	306.36	.505E-05	.575
290000.	1.08	.661E-05	325.11	339.63	.694E-05	.953
383750.	1.70	.817E-05	354.15	363.72	.857E-05	.953
443750.	2.19	.100E-04	373.30	384.00	.101E-04	.987
503750.	2.79	.975E-05	394.69	402.61	.117E-04	.832
551970.	3.26	.117E-04	410.52	416.25	.130E-04	.898
581970.	3.61	.157E-04	421.98	429.58	.143E-04	1.095
611970.	4.08	.150E-04	437.18	444.27	.159E-04	.945
641970.	4.53	.187E-04	451.36	460.24	.177E-04	1.054
671970.	5.09	.204E-04	469.13	482.44	.205E-04	.997
712650.	5.92	.185E-04	495.75	501.75	.231E-04	.801

Table B- 4 (continued)

EXPERIMENT			EVALUATION			
NUMBER OF CYCLES	CRACK DEPTH	CRACK GROWTH RATE (CGRE)	STRESS INTENSITY FACTOR		CRACK GROWTH RATE (CGRT)	RATIO CGRE / CGRT
N [c]	a [mm]	da/dNe [mm/c]	dKa [N/mm3/2]	dKa-	da/dNt [mm/c]	ea [-]
732650.	6.29	.247E-04	507.75	519.91	.258E-04	.957
762650.	7.03	.258E-04	532.07	542.63	.294E-04	.876
787110.	7.66	.290E-04	553.18	568.13	.339E-04	.856
817110.	8.53	.325E-04	583.07	594.93	.390E-04	.833
837710.	9.20	.358E-04	606.79	616.41	.435E-04	.822
852510.	9.73	.413E-04	626.04	637.61	.483E-04	.855
867510.	10.35	.513E-04	649.18	664.07	.548E-04	.937
882510.	11.12	.490E-04	678.96	693.89	.627E-04	.781
897610.	11.86	.743E-04	708.83	718.03	.697E-04	1.067
903530.	12.30	.702E-04	727.23	740.00	.765E-04	.919
911930.	12.89	.803E-04	752.76	766.52	.852E-04	.942
919530.	13.50	.925E-04	780.28	797.84	.964E-04	.959
927530.	14.24	.108E-03	815.40	823.06	.106E-03	1.014
930410.	14.55	.122E-03	830.73	856.33	.120E-03	1.022

Table B- 4 (continued)

EXPERIMENT			EVALUATION			
NUMBER OF CYCLES	CRACK DEPTH	CRACK GROWTH RATE (CGRE)	STRESS INTENSITY FACTOR		CRACK GROWTH RATE (CGRT)	RATIO CGRE / CGRT
N [c]	a [mm]	da/dNe [mm/c]	dKa [N/mm3/2]	dKa-	da/dNt [mm/c]	ea [-]
938410.	15.53	.183E-03	881.92	895.70	.138E-03	1.331
941410.	16.08	.197E-03	909.48	927.66	.153E-03	1.282
944410.	16.67	.210E-03	945.83	967.08	.174E-03	1.202
947510.	17.32	.276E-03	988.32	1016.45	.203E-03	1.357
950410.	18.12	.169E-03	1044.58	1050.12	.225E-03	.750
951300.	18.27	.283E-03	1055.66	1088.82	.251E-03	1.127
954300.	19.12	.337E-03	1121.98	1165.16	.310E-03	1.087
957300.	20.13	.393E-03	1208.34	1235.11	.371E-03	1.061
958800.	20.72	.533E-03	1261.89	1299.77	.434E-03	1.230
960300.	21.52	.580E-03	1337.66	1367.41	.507E-03	1.144
961300.	22.10	.490E-03	1397.16	1441.33	.596E-03	.822
962870.	22.87	.730E-03	1485.51	1534.17	.723E-03	1.010
963870.	23.60	.100E-02	1582.82	1613.01	.844E-03	1.186
964270.	24.00		1643.20			

Table B- 5

CRACK GROWTH RATE EVALUATION SPECIMEN C-2-2

THICKNESS T = 40 mm
WELD TOE RADIUS RHO = 0.5 mm
WELD ANGLE THETA = 70 deg
STRESS RANGE SIGMA =102 N/mm2

CRACK GROWTH CONSTANTS: C = 1.105 E-13 (N,mm)
m = 3.081

EXPERIMENT			EVALUATION			
NUMBER OF CYCLES	CRACK DEPTH	CRACK GROWTH RATE (CGRE)	STRESS INTENSITY FACTOR		CRACK GROWTH RATE (CGRT)	RATIO CGRE / CGRT
N [c]	a [mm]	da/dNe [mm/c]	dKa [N/mm3/2]	dKa-	da/dNt [mm/c]	ea [-]
101800.	.56	.385E-05	287.62	300.93	.478E-05	.805
190100.	.90	.523E-05	314.23	327.89	.623E-05	.840
287600.	1.41	.882E-05	341.55	354.21	.790E-05	1.116
356800.	2.02	.932E-05	366.88	375.90	.949E-05	.983
409360.	2.51	.127E-04	384.92	391.52	.108E-04	1.178
439360.	2.89	.967E-05	398.11	402.99	.118E-04	.822
469360.	3.18	.143E-04	407.87	414.92	.129E-04	1.114
499360.	3.61	.147E-04	421.98	429.11	.143E-04	1.028
529360.	4.05	.142E-04	436.24	445.06	.160E-04	.887
568890.	4.61	.170E-04	453.89	459.28	.176E-04	.967
588890.	4.95	.210E-04	464.67	471.37	.191E-04	1.102

Table B- 5 (continued)

EXPERIMENT			EVALUATION			
NUMBER OF CYCLES	CRACK DEPTH	CRACK GROWTH RATE (CGRE)	STRESS INTENSITY FACTOR		CRACK GROWTH RATE (CGRT)	RATIO CGRE / CGRT
N [c]	a [mm]	da/dNe [mm/c]	dKa [N/mm3/2]	dKa-	da/dNt [mm/c]	ea [-]
608890.	5.37	.175E-04	478.07	489.33	.214E-04	.818
648890.	6.07	.201E-04	500.60	512.37	.246E-04	.814
684790.	6.79	.230E-04	524.13	531.76	.276E-04	.833
704790.	7.25	.270E-04	539.40	548.49	.304E-04	.888
724790.	7.79	.250E-04	557.59	566.16	.335E-04	.746
744790.	8.29	.285E-04	574.73	580.83	.363E-04	.786
757070.	8.64	.320E-04	586.92	595.42	.391E-04	.818
772070.	9.12	.340E-04	603.92	613.15	.428E-04	.794
787070.	9.63	.407E-04	622.37	633.70	.474E-04	.858
802070.	10.24	.425E-04	645.02	658.65	.534E-04	.796
818760.	10.95	.530E-04	672.28	682.80	.597E-04	.888
828760.	11.48	.590E-04	693.33	705.44	.660E-04	.894
838760.	12.07	.598E-04	717.55	730.34	.734E-04	.814
848800.	12.67	.110E-03	743.13	755.31	.814E-04	1.351

Table B- 5 (continued)

EXPERIMENT			EVALUATION			
NUMBER OF CYCLES	CRACK DEPTH	CRACK GROWTH RATE (CGRE)	STRESS INTENSITY FACTOR		CRACK GROWTH RATE (CGRT)	RATIO CGRE / CGRT
N [c]	a [mm]	da/dNe [mm/c]	dKa [N/mm3/2]	dKa- [N/mm3/2]	da/dNt [mm/c]	ea [-]
853800.	13.22	.104E-03	767.50	779.48	.897E-04	1.159
858800.	13.74	.120E-03	791.45	805.88	.994E-04	1.207
863800.	14.34	.160E-03	820.30	840.66	.113E-03	1.413
868800.	15.14	.169E-03	861.03	881.17	.131E-03	1.287
873190.	15.88	.183E-03	901.31	916.06	.148E-03	1.242
876190.	16.43	.220E-03	930.80	951.89	.166E-03	1.324
879190.	17.09	.253E-03	972.98	999.02	.193E-03	1.314
882190.	17.85	.235E-03	1025.07	1041.11	.219E-03	1.075
884060.	18.29	.320E-03	1057.15	1069.30	.238E-03	1.346
885060.	18.61	.320E-03	1081.45	1120.58	.275E-03	1.165
888060.	19.57	.420E-03	1159.71	1178.21	.320E-03	1.311
889060.	19.99	.390E-03	1196.72	1213.82	.351E-03	1.110
890060.	20.38	.470E-03	1230.92	1259.83	.394E-03	1.193
891400.	21.01	.470E-03	1288.75	1311.24	.446E-03	1.055

Table B- 5 (continued)

EXPERIMENT			EVALUATION			
NUMBER OF CYCLES	CRACK DEPTH	CRACK GROWTH RATE (CGRE)	STRESS INTENSITY FACTOR		CRACK GROWTH RATE (CGRT)	RATIO CGRE / CGRT
N [c]	a [mm]	da/dNe [mm/c]	dKa [N/mm3/2]	dKa-	da/dNt [mm/c]	ea [-]
892400.	21.48	.530E-03	1333.73	1360.66	.499E-03	1.061
893400.	22.01	.660E-03	1387.59	1424.46	.575E-03	1.148
894400.	22.67	.670E-03	1461.32	1503.86	.680E-03	.986
895400.	23.34	.920E-03	1546.40	1615.97	.848E-03	1.085
896400.	24.26		1685.54			

Table B- 6

CRACK GROWTH RATE EVALUATION SPECIMEN C-2-3

THICKNESS T = 70 mm
WELD TOE RADIUS RHO = 0.5 mm
WELD ANGLE THETA = 45 deg
STRESS RANGE SIGMA = 76 N/mm2

CRACK GROWTH CONSTANTS: C = 1.105 E-13 (N,mm)
m = 3.081

EXPERIMENT			EVALUATION			
NUMBER OF CYCLES	CRACK DEPTH	CRACK GROWTH RATE (CGRE)	STRESS INTENSITY FACTOR		CRACK GROWTH RATE (CGRT)	RATIO CGRE / CGRT
N [c]	a [mm]	da/dNe [mm/c]	dKa [N/mm3/2]	dKa- [N/mm3/2]	da/dNt [mm/c]	ea [-]
300000.	.68		253.06			
		.587E-05		266.60	.329E-05	1.782
375000.	1.12		280.13			
		.247E-05		300.33	.475E-05	.520
731000.	2.00		320.54			
		.667E-05		336.87	.677E-05	.985
881000.	3.00		353.19			
		.683E-05		366.70	.879E-05	.777
1042000.	4.10		380.20			
		.792E-05		390.13	.106E-04	.744
1162000.	5.05		400.06			
		.956E-05		408.31	.122E-04	.781
1252000.	5.91		416.56			
		.108E-04		427.13	.141E-04	.770
1360000.	7.08		437.71			
		.125E-04		443.78	.158E-04	.790
1420000.	7.83		449.85			
		.145E-04		457.10	.173E-04	.837
1480000.	8.70		464.35			
		.152E-04		472.11	.191E-04	.792
1540000.	9.61		479.87			
		.174E-04		490.53	.215E-04	.809

Table B- 6 (continued)

EXPERIMENT			EVALUATION			
NUMBER OF CYCLES	CRACK DEPTH	CRACK GROWTH RATE (CGRE)	STRESS INTENSITY FACTOR		CRACK GROWTH RATE (CGRT)	RATIO CGRE / CGRT
N [c]	a [mm]	da/dNe [mm/c]	dKa [N/mm3/2]	dKa-	da/dNt [mm/c]	ea [-]
1610000.	10.83	.162E-04	501.18	511.75	.245E-04	.659
1683000.	12.01	.202E-04	522.31	529.72	.273E-04	.742
1723000.	12.82	.243E-04	537.12	546.16	.300E-04	.808
1763000.	13.79	.263E-04	555.21	563.97	.331E-04	.794
1798000.	14.71	.282E-04	572.74	585.16	.371E-04	.761
1843000.	15.98	.340E-04	597.59	607.88	.417E-04	.815
1873000.	17.00	.323E-04	618.17	628.23	.462E-04	.700
1903000.	17.97	.395E-04	638.30	646.71	.505E-04	.782
1923000.	18.76	.420E-04	655.13	664.31	.548E-04	.766
1943000.	19.60	.485E-04	673.49	684.43	.601E-04	.807
1963000.	20.57	.585E-04	695.36	709.06	.670E-04	.873
1983000.	21.74	.673E-04	722.76	735.09	.749E-04	.899
1998000.	22.75	.787E-04	747.41	762.48	.839E-04	.938
2013000.	23.93	.930E-04	777.54	789.97	.935E-04	.994

Table B- 6 (continued)

EXPERIMENT			EVALUATION			
NUMBER OF CYCLES	CRACK DEPTH	CRACK GROWTH RATE (CGRE)	STRESS INTENSITY FACTOR		CRACK GROWTH RATE (CGRT)	RATIO CGRE / CGRT
N [c]	a [mm]	da/dNe [mm/c]	dKa [N/mm3/2]	dKa-	da/dNt [mm/c]	ea [-]
12023000.	24.86		802.41			
		.122E-03		819.55	.105E-03	1.165
2033000.	26.08		836.69			
		.135E-03		848.64	.117E-03	1.158
2039000.	26.89		860.60			
		.158E-03		875.28	.128E-03	1.234
2045000.	27.84		889.95			
		.173E-03		905.94	.143E-03	1.215
2051000.	28.88		921.93			
		.205E-03		936.65	.158E-03	1.297
2055000.	29.70		951.37			
		.227E-03		968.52	.175E-03	1.298
2059000.	30.61		985.66			
		.237E-03		1004.56	.196E-03	1.211
2063000.	31.56		1023.45			
		.270E-03		1046.29	.222E-03	1.215
2067000.	32.64		1069.12			
		.307E-03		1097.07	.257E-03	1.195
2071000.	33.87		1125.03			
		.337E-03		1149.70	.297E-03	1.133
2074000.	34.88		1174.37			
		.370E-03		1202.14	.341E-03	1.085
2077000.	35.99		1229.90			
		.425E-03		1252.01	.386E-03	1.100
2079000.	36.84		1274.11			

Table B- 7

CRACK GROWTH RATE EVALUATION SPECIMEN C-2-4

THICKNESS T = 70 mm
WELD TOE RADIUS RHO = 0.5 mm
WELD ANGLE THETA = 45 deg
STRESS RANGE SIGMA = 76 N/mm2

CRACK GROWTH CONSTANTS: C = 1.105 E-13 (N,mm)
m = 3.081

EXPERIMENT			EVALUATION			
NUMBER OF CYCLES	CRACK DEPTH	CRACK GROWTH RATE (CGRE)	STRESS INTENSITY FACTOR		CRACK GROWTH RATE (CGRT)	RATIO CGRE / CGRT
N [c]	a [mm]	da/dNe [mm/c]	dKa [N/mm3/2]	dKa-	da/dNt [mm/c]	ea [-]
368000.	1.09	.400E-05	278.53	297.29	.461E-05	.869
568000.	1.89	.530E-05	316.06	331.20	.642E-05	.826
732000.	2.76	.653E-05	346.34	359.16	.825E-05	.792
882000.	3.74	.775E-05	371.98	382.18	.998E-05	.776
1002000.	4.67	.800E-05	392.37	404.09	.119E-04	.675
1152000.	5.87	.922E-05	415.81	423.39	.137E-04	.674
1242000.	6.70	.120E-04	430.96	439.99	.154E-04	.779
1332000.	7.78	.135E-04	449.03	458.04	.174E-04	.774
1412000.	8.86	.155E-04	467.05	475.02	.195E-04	.794
1472000.	9.79	.185E-04	482.98	489.44	.214E-04	.865
1512000.	10.53	.175E-04	495.89	505.67	.237E-04	.738

Table B- 7 (continued)

EXPERIMENT			EVALUATION			
NUMBER OF CYCLES	CRACK DEPTH	CRACK GROWTH RATE (CGRE)	STRESS INTENSITY FACTOR		CRACK GROWTH RATE (CGRT)	RATIO CGRE / CGRT
N [c]	a [mm]	da/dNe [mm/c]	dKa [N/mm3/2]	dKa-	da/dNt [mm/c]	ea [-]
1575000.	11.63	.204E-04	515.45	524.72	.265E-04	.769
1625000.	12.65	.222E-04	533.99	543.28	.295E-04	.753
1670000.	13.65	.267E-04	552.57	564.00	.331E-04	.805
1715000.	14.85	.270E-04	575.44	583.35	.367E-04	.735
1745000.	15.66	.300E-04	591.25	600.24	.401E-04	.748
1775000.	16.56	.327E-04	609.22	619.26	.442E-04	.740
1805000.	17.54	.373E-04	629.31	641.14	.492E-04	.759
1835000.	18.66	.420E-04	652.98	662.13	.543E-04	.774
1855000.	19.50	.460E-04	671.28	681.60	.594E-04	.775
1875000.	20.42	.545E-04	691.93	704.60	.657E-04	.829
1895000.	21.51	.647E-04	717.28	729.00	.730E-04	.886
1910000.	22.48	.760E-04	740.73	755.10	.814E-04	.934
1925000.	23.62	.910E-04	769.48	781.47	.905E-04	1.006
1935000.	24.53	.970E-04	793.46	806.80	.998E-04	.972

Table B- 7 (continued)

EXPERIMENT			EVALUATION			
NUMBER OF CYCLES	CRACK DEPTH	CRACK GROWTH RATE (CGRE)	STRESS INTENSITY FACTOR		CRACK GROWTH RATE (CGRT)	RATIO CGRE / CGRT
N [c]	a [mm]	da/dNe [mm/c]	dKa [N/mm3/2]	dKa-	da/dNt [mm/c]	ea [-]
11945000.	25.50	.118E-03	820.14	837.22	.112E-03	1.055
1955000.	26.68	.137E-03	854.31	866.79	.124E-03	1.098
1961000.	27.50	.143E-03	879.28	891.60	.136E-03	1.056
1967000.	28.36	.173E-03	903.92	922.18	.151E-03	1.151
1973000.	29.40	.187E-03	940.45	961.32	.171E-03	1.090
1979000.	30.52	.222E-03	982.19	999.77	.193E-03	1.152
1983000.	31.41	.240E-03	1017.34	1037.38	.217E-03	1.109
1987000.	32.37	.273E-03	1057.42	1081.66	.246E-03	1.107
1991000.	33.46	.323E-03	1105.90	1128.94	.281E-03	1.151
1994000.	34.43	.350E-03	1151.98	1177.92	.320E-03	1.093
1997000.	35.48	.413E-03	1203.86	1235.82	.371E-03	1.113
2000000.	36.72		1267.78			

Table B- 8

CRACK GROWTH RATE EVALUATION SPECIMEN B-1-1

THICKNESS T = 70 mm
WIDTH B = 210 mm
STRESS RANGE SIGMA = 225 N/mm2

CRACK GROWTH CONSTANTS: C = 1.105 E-13 (N,mm)
m = 3.081

EXPERIMENT			EVALUATION DEPTH a			EVALUATION WIDTH c		
CYCLES N [c]	CRACK DEPTH a [mm]	CRACK WIDTH c [mm]	SIF dKa [N/mm3/2]			SIF dKc [N/mm3/2]		
	CRACK RATE da/dNe [mm/c]	CRACK RATE dc/dNe [mm/c]	SIF dKa- [N/mm3/2]	CRACK RATE da/dNt [mm/c]	RATIO CRe/CRt [-]	SIF dKc- [N/mm3/2	CRACK RATE dc/dNt [mm/c]	RATIO CRe/CRt [-]
407000.	8.10	9.00	680.55			800.14		
	.467E-04	.732E-04	735.46	.750E-04	.623	864.76	.124E-03	.592
471200.	11.10	13.70	790.38			929.38		
	.106E-03	.107E-03	803.42	.985E-04	1.072	989.61	.187E-03	.572
503400.	14.50	17.15	816.46			1049.85		
	.134E-03	.187E-03	834.43	.111E-03	1.207	1107.12	.265E-03	.707
529600.	18.00	22.05	852.39			1164.39		
	.155E-03	.293E-03	871.93	.127E-03	1.226	1213.39	.351E-03	.834
548900.	21.00	27.70	891.46			1262.39		
	.171E-03	.316E-03	898.98	.139E-03	1.227	1306.07	.440E-03	.719
564700.	23.70	32.70	906.50			1349.75		
	.176E-03	.379E-03	913.23	.146E-03	1.207	1391.00	.535E-03	.708
578300.	26.10	37.85	919.97			1432.25		
	.154E-03	.357E-03	924.16	.152E-03	1.018	1471.03	.635E-03	.562
591900.	28.20	42.70	928.35			1509.82		
	.191E-03	.500E-03	933.74	.157E-03	1.220	1553.22	.751E-03	.666
602900.	30.30	48.20	939.13			1596.62		
	.170E-03	.505E-03	945.42	.163E-03	1.045	1636.90	.883E-03	.572
612900.	32.00	53.25	951.71			1677.17		
	.213E-03	.606E-03	954.48	.168E-03	1.269	1721.16	.103E-02	.588

Table B- 8 (continued)

EXPERIMENT			EVALUATION DEPTH a			EVALUATION WIDTH c		
CYCLES N [c]	CRACK DEPTH a [mm]	CRACK WIDTH c [mm]	SIF dKa [N/mm3/2]			SIF dKc [N/mm3/2]		
	CRACK RATE da/dNe [mm/c]	CRACK RATE dc/dNe [mm/c]	SIF dKa- [N/mm3/2]	CRACK RATE da/dNt [mm/c]	RATIO CRe/CRt [-]	SIF dKc- [N/mm3/2	CRACK RATE dc/dNt [mm/c]	RATIO CRe/CRt [-]
620900.	33.70	58.10	957.26			1765.15		
	.148E-03	.409E-03	957.19	.169E-03	.875	1813.79	.121E-02	.338
632400.	35.40	62.80	957.12			1862.42		
	.200E-03	.812E-03	973.04	.178E-03	1.125	1929.69	.147E-02	.554
640900.	37.10	69.70	988.97			1996.96		
	.436E-03	.106E-02	978.82	.181E-03	2.411	2087.09	.187E-02	.570
646400.	39.50	75.55	968.67			2177.23		
	.273E-03	.169E-02	1013.93	.202E-03	1.352	2299.40	.251E-02	.672
651900.	41.00	84.85	1059.20			2421.56		

Table B- 9

CRACK GROWTH RATE EVALUATION SPECIMEN B-1-2

THICKNESS T = 70 mm
WIDTH B = 210 mm
STRESS RANGE SIGMA = 225 N/mm2

CRACK GROWTH CONSTANTS: C = 1.105 E-13 (N,mm)
m = 3.081

EXPERIMENT			EVALUATION DEPTH a			EVALUATION WIDTH c		
CYCLES N [c]	CRACK DEPTH a [mm]	CRACK WIDTH c [mm]	SIF dKa [N/mm3/2]			SIF dKc [N/mm3/2]		
	CRACK RATE da/dNe [mm/c]	CRACK RATE dc/dNe [mm/c]	SIF dKa- [N/mm3/2]	CRACK RATE da/dNt [mm/c]	RATIO CRe/CRt [-]	SIF dKc- [N/mm3/2	CRACK RATE dc/dNt [mm/c]	RATIO CRe/CRt [-]
0.	.40	5.50	280.10			83.51		
	.688E-05	.123E-05	436.76	.151E-04	.457	290.48	.429E-05	.287
407000.	3.20	6.00	593.42			497.45		
	.427E-04	.360E-04	668.68	.560E-04	.762	682.75	.597E-04	.603
557000.	9.60	11.40	743.94			868.05		
	.812E-04	.102E-03	779.95	.899E-04	.904	942.42	.161E-03	.634
605000.	13.50	16.30	815.97			1016.80		
	.109E-03	.164E-03	841.66	.114E-03	.960	1077.76	.244E-03	.672
638000.	17.10	21.70	867.35			1138.71		
	.114E-03	.181E-03	882.03	.131E-03	.864	1205.61	.344E-03	.526
675000.	21.30	28.40	896.71			1272.52		
	.133E-03	.257E-03	905.27	.142E-03	.937	1318.32	.453E-03	.568
696000.	24.10	33.80	913.82			1364.13		
	.150E-03	.312E-03	918.22	.149E-03	1.009	1405.45	.552E-03	.566
712000.	26.50	38.80	922.63			1446.77		

Table B-10

CRACK GROWTH RATE EVALUATION SPECIMEN B-2-1

THICKNESS T = 40 mm
WIDTH B = 120 mm
STRESS RANGE SIGMA = 203.8 N/mm2

CRACK GROWTH CONSTANTS: C = 1.105 E-13 (N,mm)
m = 3.081

EXPERIMENT			EVALUATION DEPTH a			EVALUATION WIDTH c		
CYCLES N [c]	CRACK DEPTH a [mm]	CRACK WIDTH c [mm]	SIF dKa [N/mm3/2]			SIF dKc [N/mm3/2]		
	CRACK RATE da/dNe [mm/c]	CRACK RATE dc/dNe [mm/c]	SIF dKa- [N/mm3/2]	CRACK RATE da/dNt [mm/c]	RATIO CRe/CRt [-]	SIF dKc- [N/mm3/2]	CRACK RATE dc/dNt [mm/c]	RATIO CRe/CRt [-]
359750.	2.53	5.89	498.39			381.44		
	.143E-04	.427E-05	511.02	.244E-04	.584	476.65	.197E-04	.216
535550.	5.04	6.64	523.65			571.87		
	.208E-04	.231E-04	545.66	.299E-04	.694	632.49	.471E-04	.490
659850.	7.62	9.51	567.66			693.12		
	.249E-04	.373E-04	583.81	.368E-04	.675	731.38	.738E-04	.506
735100.	9.49	12.32	599.96			769.63		
	.333E-04	.574E-04	613.28	.429E-04	.776	810.31	.101E-03	.568
797950.	11.58	15.93	626.60			850.99		
	.322E-04	.751E-04	639.27	.487E-04	.662	880.36	.131E-03	.575
843250.	13.04	19.33	651.93			909.74		
	.376E-04	.963E-04	661.59	.541E-04	.694	936.91	.158E-03	.609
877300.	14.32	22.61	671.25			964.07		
	.580E-04	.163E-03	680.81	.591E-04	.981	995.73	.191E-03	.854
900750.	15.68	26.43	690.37			1027.39		
	.519E-04	.163E-03	707.13	.665E-04	.780	1048.48	.224E-03	.729
922150.	16.79	29.92	723.89			1069.57		
	.606E-04	.201E-03	723.66	.714E-04	.849	1107.31	.265E-03	.760
938150.	17.76	33.14	723.42			1145.05		
	.696E-04	.232E-03	730.57	.735E-04	.947	1178.83	.321E-03	.721

Table B-10 (continued)

EXPERIMENT			EVALUATION DEPTH a			EVALUATION WIDTH c		
CYCLES N [c]	CRACK DEPTH a [mm]	CRACK WIDTH c [mm]	SIF dKa [N/mm3/2]			SIF dKc [N/mm3/2]		
	CRACK RATE da/dNe [mm/c]	CRACK RATE dc/dNe [mm/c]	SIF dKa- [N/mm3/2]	CRACK RATE da/dNt [mm/c]	RATIO CRe/CRt [-]	SIF dKc- [N/mm3/2	CRACK RATE dc/dNt [mm/c]	RATIO CRe/CRt [-]
952230.	18.74	36.40	737.71			1212.62		
	.887E-04	.293E-03	744.62	.779E-04	1.138	1254.11	.388E-03	.753
963950.	19.78	39.83	751.53			1295.60		
	.106E-03	.345E-03	759.04	.827E-04	1.284	1352.79	.491E-03	.704
975250.	20.98	43.73	766.54			1409.98		
	.161E-03	.545E-03	777.19	.889E-04	1.808	1485.19	.654E-03	.833
982900.	22.21	47.90	787.84			1560.40		

Table B-11

CRACK GROWTH RATE EVALUATION SPECIMEN B-2-2

THICKNESS T = 40 mm
WIDTH B = 120 mm
STRESS RANGE SIGMA = 244.5 N/mm2

CRACK GROWTH CONSTANTS: C = 1.105 E-13 (N,mm)
m = 3.081

EXPERIMENT			EVALUATION DEPTH a			EVALUATION WIDTH c		
CYCLES N [c]	CRACK DEPTH a [mm]	CRACK WIDTH c [mm]	SIF dKa [N/mm3/2]			SIF dKc [N/mm3/2]		
	CRACK RATE da/dNe [mm/c]	CRACK RATE dc/dNe [mm/c]	SIF dKa- [N/mm3/2]	CRACK RATE da/dNt [mm/c]	RATIO CRe/CRt [-]	SIF dKc- [N/mm3/2	CRACK RATE dc/dNt [mm/c]	RATIO CRe/CRt [-]
0.	.50	6.00	336.49			108.05		
	.205E-04	.836E-05	505.57	.236E-04	.865	428.35	.142E-04	.589
272750.	6.08	8.28	674.65			748.64		
	.471E-04	.602E-04	697.32	.637E-04	.739	810.22	.101E-03	.596
322050.	8.40	11.25	719.98			871.81		
	.557E-04	.845E-04	732.47	.741E-04	.751	910.67	.145E-03	.583
351150.	10.02	13.71	744.97			949.54		
	.646E-04	.111E-03	755.86	.816E-04	.792	994.20	.190E-03	.583
380850.	11.94	17.00	766.76			1038.87		
	.680E-04	.147E-03	777.20	.889E-04	.765	1074.97	.242E-03	.608
402900.	13.44	20.24	787.63			1111.06		
	.802E-04	.186E-03	795.02	.954E-04	.841	1147.32	.295E-03	.631
420600.	14.86	23.54	802.40			1183.58		
	.928E-04	.235E-03	809.16	.101E-03	.921	1228.94	.365E-03	.643
437850.	16.46	27.59	815.91			1274.30		
	.121E-03	.331E-03	821.20	.105E-03	1.151	1323.94	.459E-03	.721
450300.	17.97	31.71	826.50			1373.57		
	.147E-03	.445E-03	833.47	.110E-03	1.334	1435.13	.588E-03	.756
460700.	19.50	36.34	840.45			1496.68		

Table B-12

CRACK GROWTH RATE EVALUATION SPECIMEN D-1-2

THICKNESS T = 70 mm
WIDTH B = 210 mm
WELD TOE RADIUS RHO = 5.0 mm
WELD ANGLE THETA = 70 deg
STRESS RANGE SIGMA = 110 N/mm2

CRACK GROWTH CONSTANTS: C = 1.105 E-13 (N,mm)
m = 3.081

EXPERIMENT			EVALUATION DEPTH a			EVALUATION WIDTH c		
CYCLES N [c]	CRACK DEPTH a [mm]	CRACK WIDTH c [mm]	SIF dKa [N/mm3/2]			SIF dKc [N/mm3/2]		
	CRACK RATE da/dNe [mm/c]	CRACK RATE dc/dNe [mm/c]	SIF dKa- [N/mm3/2]	CRACK RATE da/dNt [mm/c]	RATIO CRe/CRt [-]	SIF dKc- [N/mm3/2	CRACK RATE dc/dNt [mm/c]	RATIO CRe/CRt [-]
520000.	2.90	5.40	380.12			443.32		
	.574E-05	.660E-05	394.45	.110E-04	.522	534.06	.280E-04	.236
990000.	5.60	8.50	408.78			624.80		
	.800E-05	.134E-04	428.24	.142E-04	.564	690.05	.617E-04	.218
1340000.	8.40	13.20	447.70			755.30		
	.880E-05	.196E-04	465.04	.183E-04	.482	796.27	.958E-04	.205
1590000.	10.60	18.10	482.37			837.23		
	.106E-04	.212E-04	492.18	.218E-04	.487	874.38	.128E-03	.166
1788000.	12.70	22.30	502.00			911.53		
	.829E-05	.202E-04	511.14	.245E-04	.339	938.82	.159E-03	.127
1993000.	14.40	26.45	520.29			966.11		
	.947E-05	.239E-04	528.51	.271E-04	.349	994.46	.190E-03	.126
2183000.	16.20	31.00	536.73			1022.82		
	.923E-05	.259E-04	544.95	.298E-04	.310	1050.82	.225E-03	.115
2378000.	18.00	36.05	553.17			1078.83		
	.226E-04	.685E-04	574.04	.350E-04	.645	1169.84	.314E-03	.219
2613000.	23.30	52.15	594.90			1260.86		
	.152E-04	.546E-04	606.99	.415E-04	.367	1313.40	.448E-03	.122

Table B-12 (continued)

EXPERIMENT			EVALUATION DEPTH a			EVALUATION WIDTH c		
CYCLES N [c]	CRACK DEPTH a [mm]	CRACK WIDTH c [mm]	SIF dKa [N/mm3/2]			SIF dKc [N/mm3/2]		
	CRACK RATE da/dNe [mm/c]	CRACK RATE dc/dNe [mm/c]	SIF dKa- [N/mm3/2]	CRACK RATE da/dNt [mm/c]	RATIO CRe/CRt [-]	SIF dKc- [N/mm3/2]	CRACK RATE dc/dNt [mm/c]	RATIO CRe/CRt [-]
777000.	25.80	61.10	619.08			1365.93		
	.148E-04	.781E-04	640.09	.489E-04	.303	1420.45	.570E-03	.137
2912000.	27.80	71.65	661.09			1474.96		
	.269E-04	.149E-03	688.91	.613E-04	.439	1552.89	.750E-03	.199
2990000.	29.90	83.30	716.72			1630.81		

Table B-13

CRACK GROWTH RATE EVALUATION SPECIMEN D-2-1

THICKNESS T = 40 mm
WIDTH B = 120 mm
WELD TOE RADIUS RHO = 0.5 mm
WELD ANGLE THETA = 70 deg
STRESS RANGE SIGMA = 107 N/mm2

CRACK GROWTH CONSTANTS: C = 1.105 E-13 (N,mm)
m = 3.081

EXPERIMENT			EVALUATION DEPTH a			EVALUATION WIDTH c		
CYCLES N [c]	CRACK DEPTH a [mm]	CRACK WIDTH c [mm]	SIF dKa [N/mm3/2]			SIF dKc [N/mm3/2]		
	CRACK RATE da/dNe [mm/c]	CRACK RATE dc/dNe [mm/c]	SIF dKa- [N/mm3/2]	CRACK RATE da/dNt [mm/c]	RATIO CRe/CRt [-]	SIF dKc- [N/mm3/2	CRACK RATE dc/dNt [mm/c]	RATIO CRe/CRt [-]
1519000.	6.52	17.23	417.51			1057.00		
	.176E-05	.975E-05	427.12	.141E-04	.125	1071.83	.239E-03	.041
1882150.	7.16	20.77	436.73			1086.67		
	.314E-05	.145E-04	443.84	.158E-04	.198	1128.69	.281E-03	.052
2219550.	8.22	25.66	450.94			1170.71		
	.363E-05	.622E-05	458.04	.174E-04	.208	1212.73	.350E-03	.018
2500850.	9.24	27.41	465.15			1254.75		
	.383E-05	.136E-04	473.41	.193E-04	.198	1302.31	.436E-03	.031
2798300.	10.38	31.46	481.67			1349.88		
	.431E-05	.179E-04	494.65	.221E-04	.195	1414.42	.563E-03	.032
3128000.	11.80	37.36	507.63			1478.96		
	.621E-05	.200E-04	519.05	.256E-04	.242	1570.06	.776E-03	.026
3390600.	13.43	42.60	530.46			1661.16		

Table B-14

CRACK GROWTH RATE EVALUATION SPECIMEN D-2-2

THICKNESS T = 40 mm
WIDTH B = 120 mm
WELD TOE RADIUS RHO = 5.0 mm
WELD ANGLE THETA = 70 deg
STRESS RANGE SIGMA = 116 N/mm2

CRACK GROWTH CONSTANTS: C = 1.105 E-13 (N,mm)
m = 3.081

EXPERIMENT			EVALUATION DEPTH a			EVALUATION WIDTH c		
CYCLES N [c]	CRACK DEPTH a [mm]	CRACK WIDTH c [mm]	SIF dKa [N/mm3/2]			SIF dKc [N/mm3/2]		
	CRACK RATE da/dNe [mm/c]	CRACK RATE dc/dNe [mm/c]	SIF dKa- [N/mm3/2]	CRACK RATE da/dNt [mm/c]	RATIO CRe/CRt [-]	SIF dKc- [N/mm3/2	CRACK RATE dc/dNt [mm/c]	RATIO CRe/CRt [-]
369200.	2.51	5.63	346.54			359.02		
	.349E-05	.000E+00	338.40	.686E-05	.509	416.08	.130E-04	.000
767400.	3.90	5.63	330.25			473.15		
	.285E-05	.534E-05	342.00	.709E-05	.403	499.57	.228E-04	.235
1124750.	4.92	7.54	353.75			525.99		
	.418E-05	.693E-05	363.65	.857E-05	.488	562.57	.329E-04	.211
1500100.	6.49	10.14	373.56			599.15		
	.477E-05	.853E-05	380.71	.987E-05	.483	627.85	.461E-04	.185
1789500.	7.87	12.61	387.86			656.55		
	.347E-05	.103E-04	399.38	.114E-04	.303	675.71	.578E-04	.179
2097950.	8.94	15.80	410.89			694.87		
	.411E-05	.125E-04	419.77	.133E-04	.309	713.70	.684E-04	.182
2353250.	9.99	18.98	428.64			732.52		
	.404E-05	.141E-04	437.73	.152E-04	.267	751.12	.801E-04	.176
2607900.	11.02	22.56	446.81			769.72		
	.365E-05	.174E-04	455.99	.172E-04	.212	782.19	.907E-04	.192
2799750.	11.72	25.90	465.17			794.66		
	.679E-05	.204E-04	472.30	.192E-04	.354	827.35	.108E-03	.189
3017850.	13.20	30.35	479.43			860.05		
	.665E-05	.242E-04	479.40	.201E-04	.331	899.79	.140E-03	.173

Table B-14 (continued)

EXPERIMENT			EVALUATION DEPTH a			EVALUATION WIDTH c		
CYCLES N [c]	CRACK DEPTH a [mm]	CRACK WIDTH c [mm]	SIF dKa [N/mm3/2]			SIF dKc [N/mm3/2]		
	CRACK RATE da/dNe [mm/c]	CRACK RATE dc/dNe [mm/c]	SIF dKa- [N/mm3/2]	CRACK RATE da/dNt [mm/c]	RATIO CRe/CRt [-]	SIF dKc- [N/mm3/2	CRACK RATE dc/dNt [mm/c]	RATIO CRe/CRt [-]
3150200.	14.08	33.55	479.37			939.52		
	.842E-05	.305E-04	491.93	.217E-04	.387	946.35	.163E-03	.187
3257100.	14.98	36.81	504.49			953.18		
	.876E-05	.387E-04	514.17	.249E-04	.352	982.02	.183E-03	.212
3357600.	15.86	40.70	523.86			1010.85		
	.109E-04	.516E-04	534.50	.281E-04	.388	1042.94	.220E-03	.234
3432050.	16.67	44.54	545.14			1075.03		
	.137E-04	.676E-04	557.66	.320E-04	.430	1109.60	.266E-03	.254
3484450.	17.39	48.08	570.17			1144.17		
	.208E-04	.110E-03	586.76	.374E-04	.555	1188.17	.329E-03	.335
3519600.	18.12	51.95	603.35			1232.17		
	.309E-04	.190E-03	622.67	.449E-04	.688	1281.82	.416E-03	.457
3538700.	18.71	55.58	642.00			1331.48		

APPENDIX C

NUMERICAL BACKGROUND TO THE EVALUATION BASED ON FATIGUE CRACK GROWTH CURVE

This appendix gives the fatigue crack growth calculation procedure on which the computer program FAFRAM is based. The fatigue crack growth curves given in section 6 and 7 of the main report are determined with FAFRAM.

FAFRAM (FAtigue FRActure Mechanics) is based on the numerical integration of a crack growth relation. In this report the Paris relation (C.1) is used as the crack growth law.

$$da/dN = C(\Delta K)^m \qquad (C.1)$$

As the governing parameter for the calculation a crack extension (Δa) has been chosen. In order to get acceptable accuracy relatively small values should be taken for Δa (Crack extensions Δa of 5% of the present crack size give in general acceptable results).
The numerical procedure will be illustrated for the semi-elliptical crack. Assuming only bending stresses ($\Delta\sigma$) the expressions for ΔK_a and ΔK_c can be simplified to:

$$\Delta K_a = f_a \cdot \Delta\sigma \sqrt{\pi a} \qquad (C.2)$$

$$\Delta K_c = f_c \cdot \Delta\sigma \sqrt{\pi a} \qquad (C.3)$$

where:

$$f_a = \frac{Mk_{b,a} \cdot M_{b,a}}{E_k} \qquad (C.4)$$

$$f_c = \frac{Mk_{b,c} \cdot M_{b,c}}{E_k} \qquad (C.5)$$

The procedure is as follows:

1. With the actual crack depth (a_i) and half crack width (c_i) and the other geometrical parameters the values for f_a and f_c can be calculated.

2. Using the stress range ($\Delta\sigma$) the SIFs for crack depth (ΔK_a) and crack width (ΔK_c) can be calculated with equations (C.2) and (C.3).

3. Assuming a crack extension Δa the corresponding number of cycles can be calculated with equation (C.6)

$$\frac{\Delta a}{\Delta N} = C\ (\Delta K_a)^m \qquad \text{(C.6a)}$$

or:

$$\Delta N = \frac{\Delta a}{C\ (\Delta K_a)^m} \qquad \text{(C.6b)}$$

4. The crack extension in the width direction can also be calculated with equation (C.7)

$$\frac{\Delta c}{\Delta N} = C\ (\Delta K_c)^m \qquad \text{(C.7a)}$$

or:

$$\Delta c = \Delta N\ C\ (\Delta K_c)^m = \Delta a\ \left(\frac{\Delta K_c}{\Delta K_a}\right)^m \qquad \text{(C.7b)}$$

5. The number of cycles has to be increased with ΔN

$$N_{i+1} = N_i + \Delta N \qquad \text{(C.8)}$$

6. The crack dimensions have to be increased with the crack extensions:

$$a_{i+1} = a_i + \Delta a \qquad \text{(C.9)}$$

$$c_{i+1} = c_i + \Delta c \qquad \text{(C.10)}$$

7. With the new crack dimensions (a_{i+1}, c_{i+1}) the next step can be calculated, starting with point 1 above.

8. The calculation has to be continued until the allowable crack depth (a_f) or until the required number of cycles.

For 2D geometries the calculation has to be carried out in the a-direction only.

Table C-1 through C-5 give the results of 5 crack growth calculations as exemples.
The results of these calculations are also given in the figures of the main report. The corresponding numbers are:

specimen	C-1-2	table	C-1	figure	6-5
	C-1-2*		C-2		6-5
	B-1-1		C-3		6-17
	B-1-1*		C-4		6-17
	D-1-2		C-5		6-25

The stress intensity factors are determined as given in section 6.3 and 6.4 of the main report.

Table C-1

COMPUTERPROGRAM FAFRAM

FATIGUE CRACK GROWTH CALCULATION BASED ON FRACTURE MECHANICS

SPECIMEN C-1-2

CRACK GROWTH COEFFICIENT C (N,mm)	.11050000E-12
CRACK GROWTH COEFFICIENT M	3.081
PLATE THICKNESS T (mm)	70.000
WELD ANGLE PHI (degree)	70.000
WELD TOE RADIUS RHO (mm)	.500
INITIAL DEFECT Ai (mm)	.500
CRITICAL CRACK DEPTH Af (mm)	40.570
INITIAL NUMBER OF LOAD CYCLES Ni	0
CRACK GROWTH FACTOR ALPHA	.050
MEMBRANE STRESS RANGE SIGM (N/mm2)	.000
BENDING STRESS RANGE SIGB (N/mm2)	76.000

GEOMETRY		A-DIRECTION								
A mm	A/T	Mkm	Mm	Mkb	Mb	DK Nmm-1.5	DA mm	Ni	DN	Ni+1
.50	.007	2.12	1.12	2.44	1.11	264.07	.025	0.	7821.	7821.
.52	.007	2.09	1.12	2.40	1.11	266.35	.026	7821.	7998.	15818.
.55	.008	2.06	1.12	2.36	1.11	268.60	.028	15818.	8182.	24001.
.58	.008	2.03	1.12	2.33	1.11	270.84	.029	24001.	8374.	32375.
.61	.009	2.00	1.12	2.29	1.11	273.07	.030	32375.	8574.	40949.
.64	.009	1.97	1.12	2.25	1.11	275.29	.032	40949.	8781.	49730.
.67	.010	1.94	1.12	2.22	1.11	277.50	.034	49730.	8995.	58726.
.70	.010	1.91	1.12	2.18	1.11	279.71	.035	58726.	9217.	67942.
.74	.011	1.88	1.12	2.15	1.11	281.93	.037	67942.	9445.	77388.
.78	.011	1.85	1.12	2.12	1.10	284.15	.039	77388.	9680.	87068.
.81	.012	1.82	1.12	2.08	1.10	286.39	.041	87068.	9922.	96989.
.86	.012	1.79	1.12	2.05	1.10	288.64	.043	96989.	10169.	107159.
.90	.013	1.77	1.12	2.02	1.10	290.92	.045	107159.	10423.	117581.
.94	.013	1.74	1.12	1.99	1.10	293.22	.047	117581.	10681.	128263.
.99	.014	1.71	1.12	1.96	1.10	295.55	.049	128263.	10945.	139207.
1.04	.015	1.69	1.12	1.92	1.10	297.92	.052	139207.	11213.	150420.
1.09	.016	1.66	1.12	1.90	1.10	300.33	.055	150420.	11485.	161905.
1.15	.016	1.64	1.12	1.87	1.10	302.78	.057	161905.	11761.	173666.
1.20	.017	1.62	1.12	1.84	1.10	305.29	.060	173666.	12039.	185705.
1.26	.018	1.59	1.12	1.81	1.10	307.85	.063	185705.	12319.	198024.
1.33	.019	1.57	1.12	1.78	1.09	310.48	.066	198024.	12602.	210626.
1.39	.020	1.55	1.12	1.76	1.09	313.16	.070	210626.	12885.	223511.
1.46	.021	1.53	1.12	1.73	1.09	315.93	.073	223511.	13168.	236679.
1.54	.022	1.51	1.12	1.71	1.09	318.76	.077	236679.	13451.	250130.
1.61	.023	1.49	1.12	1.68	1.09	321.68	.081	250130.	13733.	263862.
1.69	.024	1.47	1.12	1.66	1.09	324.68	.085	263862.	14012.	277875.
1.78	.025	1.45	1.12	1.64	1.09	327.73	.089	277875.	14295.	292170.
1.87	.027	1.43	1.12	1.61	1.09	330.71	.093	292170.	14598.	306768.
1.96	.028	1.41	1.12	1.59	1.08	333.70	.098	306768.	14908.	321676.

Table C-1 (continued)

GEOMETRY		A-DIRECTION								
A mm	A/T	Mkm	Mm	Mkb	Mb	DK Nmm-1.5	DA mm	Ni	DN	Ni+1
2.06	.029	1.39	1.12	1.57	1.08	336.71	.103	321676.	15226.	336901.
2.16	.031	1.37	1.12	1.55	1.08	339.76	.108	336901.	15550.	352451.
2.27	.032	1.36	1.12	1.53	1.08	342.84	.113	352451.	15880.	368331.
2.38	.034	1.34	1.12	1.51	1.08	345.95	.119	368331.	16216.	384547.
2.50	.036	1.32	1.12	1.49	1.08	349.11	.125	384547.	16556.	401103.
2.63	.038	1.31	1.12	1.47	1.08	352.32	.131	401103.	16900.	418003.
2.76	.039	1.29	1.13	1.45	1.07	355.59	.138	418003.	17248.	435251.
2.90	.041	1.28	1.13	1.43	1.07	358.92	.145	435251.	17598.	452848.
3.04	.043	1.26	1.13	1.41	1.07	362.32	.152	452848.	17949.	470797.
3.19	.046	1.25	1.13	1.39	1.07	365.79	.160	470797.	18300.	489097.
3.35	.048	1.24	1.13	1.37	1.07	369.35	.168	489097.	18650.	507747.
3.52	.050	1.22	1.13	1.35	1.06	373.00	.176	507747.	18999.	526746.
3.70	.053	1.21	1.13	1.34	1.06	376.74	.185	526746.	19344.	546090.
3.88	.055	1.20	1.13	1.32	1.06	380.59	.194	546090.	19685.	565776.
4.07	.058	1.19	1.14	1.30	1.06	384.55	.204	565776.	20020.	585796.
4.28	.061	1.18	1.14	1.29	1.06	388.64	.214	585796.	20348.	606144.
4.49	.064	1.17	1.14	1.27	1.05	392.85	.225	606144.	20668.	626811.
4.72	.067	1.16	1.14	1.26	1.05	397.20	.236	626811.	20977.	647788.
4.95	.071	1.15	1.15	1.25	1.05	401.70	.248	647788.	21274.	669062.
5.20	.074	1.14	1.15	1.23	1.05	406.36	.260	669062.	21558.	690620.
5.46	.078	1.13	1.15	1.22	1.05	411.19	.273	690620.	21827.	712448.
5.73	.082	1.12	1.16	1.21	1.04	416.20	.287	712448.	22079.	734527.
6.02	.086	1.11	1.16	1.19	1.04	421.40	.301	734527.	22312.	756839.
6.32	.090	1.11	1.17	1.18	1.04	426.81	.316	756839.	22525.	779364.
6.64	.095	1.10	1.17	1.17	1.04	432.44	.332	779364.	22715.	802079.
6.97	.100	1.09	1.18	1.16	1.04	438.31	.348	802079.	22880.	824960.
7.32	.105	1.08	1.18	1.15	1.04	444.78	.366	824960.	22964.	847924.
7.68	.110	1.08	1.19	1.14	1.04	451.43	.384	847924.	23034.	870959.
8.07	.115	1.07	1.20	1.13	1.03	458.44	.403	870959.	23065.	894024.
8.47	.121	1.07	1.21	1.12	1.03	465.82	.424	894024.	23056.	917080.
8.89	.127	1.06	1.22	1.11	1.03	473.59	.445	917080.	23005.	940085.
9.34	.133	1.06	1.23	1.11	1.03	481.78	.467	940085.	22912.	962997.
9.81	.140	1.05	1.24	1.10	1.03	490.42	.490	962997.	22776.	985773.
10.30	.147	1.05	1.25	1.09	1.03	499.54	.515	985773.	22596.	1008369.
10.81	.154	1.04	1.26	1.08	1.03	509.16	.541	1008369.	22371.	1030741.
11.35	.162	1.04	1.28	1.08	1.04	519.33	.568	1030741.	22101.	1052842.
11.92	.170	1.04	1.29	1.07	1.04	530.09	.596	1052842.	21785.	1074626.
12.52	.179	1.03	1.31	1.07	1.04	541.49	.626	1074626.	21422.	1096049.
13.14	.188	1.03	1.33	1.06	1.04	553.59	.657	1096049.	21013.	1117062.
13.80	.197	1.03	1.35	1.06	1.05	566.44	.690	1117062.	20558.	1137620.
14.49	.207	1.02	1.37	1.05	1.05	580.11	.724	1137620.	20057.	1157677.
15.21	.217	1.02	1.40	1.05	1.06	594.69	.761	1157677.	19509.	1177186.
15.97	.228	1.02	1.43	1.04	1.06	610.26	.799	1177186.	18917.	1196103.
16.77	.240	1.02	1.46	1.04	1.07	626.92	.839	1196103.	18281.	1214384.
17.61	.252	1.01	1.49	1.03	1.08	644.79	.881	1214384.	17602.	1231987.
18.49	.264	1.01	1.53	1.03	1.09	664.02	.925	1231987.	16883.	1248869.
19.42	.277	1.01	1.57	1.03	1.10	684.76	.971	1248869.	16124.	1264993.

Table C-1 (continued)

GEOMETRY		A-DIRECTION								
A mm	A/T	Mkm	Mm	Mkb	Mb	DK Nmm-1.5	DA mm	Ni	DN	Ni+1
20.39	.291	1.01	1.62	1.02	1.11	707.22	1.019	1264993.	15328.	1280321.
21.41	.306	1.01	1.67	1.02	1.12	731.62	1.070	1280321.	14497.	1294819.
22.48	.321	1.00	1.73	1.02	1.14	758.25	1.124	1294819.	13635.	1308453.
23.60	.337	1.00	1.80	1.01	1.16	787.45	1.180	1308453.	12743.	1321196.
24.78	.354	1.00	1.87	1.01	1.18	819.65	1.239	1321196.	11826.	1333022.
26.02	.372	1.00	1.95	1.01	1.21	855.37	1.301	1333022.	10888.	1343910.
27.32	.390	1.00	2.05	1.00	1.23	895.28	1.366	1343910.	9934.	1353844.
28.69	.410	1.00	2.16	1.00	1.27	937.78	1.434	1353844.	9042.	1362885.
30.12	.430	1.00	2.28	1.00	1.31	990.90	1.506	1362885.	8011.	1370897.
31.63	.452	1.00	2.43	1.00	1.35	1051.55	1.581	1370897.	7005.	1377902.
33.21	.474	1.00	2.60	1.00	1.41	1121.45	1.660	1377902.	6032.	1383934.
34.87	.498	1.00	2.80	1.00	1.48	1202.81	1.743	1383934.	5105.	1389039.
36.61	.523	1.00	3.02	1.00	1.57	1309.30	1.831	1389039.	4127.	1393166.
38.44	.549	1.00	3.26	1.00	1.65	1415.03	1.922	1393166.	3411.	1396577.
40.37	.577	1.00	3.57	1.00	1.76	1545.68	2.018	1396577.	2729.	1399306.
42.38	.605	1.00	3.99	1.00	1.91	1718.58	2.119	1399306.	2067.	1401372.

Table C-2

COMPUTERPROGRAM FAFRAM

FATIGUE CRACK GROWTH CALCULATION BASED ON FRACTURE MECHANICS

SPECIMEN C-1-2

CRACK GROWTH COEFFICIENT C (N,mm)	.11050000E-12
CRACK GROWTH COEFFICIENT M	3.081
PLATE THICKNESS T (mm)	70.000
WELD ANGLE PHI (degree)	70.000
WELD TOE RADIUS RHO (mm)	.500
INITIAL DEFECT Ai (mm)	1.080
CRITICAL CRACK DEPTH Af (mm)	40.570
INITIAL NUMBER OF LOAD CYCLES Ni	500000
CRACK GROWTH FACTOR ALPHA	.050
MEMBRANE STRESS RANGE SIGM (N/mm2)	.000
BENDING STRESS RANGE SIGB (N/mm2)	76.000

GEOMETRY		A-DIRECTION								
A mm	A/T	Mkm	Mm	Mkb	Mb	DK Nmm-1.5	DA mm	Ni	DN	Ni+1
1.08	.015	1.67	1.12	1.90	1.10	299.80	.054	500000.	11426.	511426.
1.13	.016	1.64	1.12	1.87	1.10	302.25	.057	511426.	11701.	523127.
1.19	.017	1.62	1.12	1.84	1.10	304.74	.060	523127.	11979.	535105.
1.25	.018	1.60	1.12	1.82	1.10	307.29	.063	535105.	12259.	547364.
1.31	.019	1.58	1.12	1.79	1.10	309.90	.066	547364.	12541.	559905.
1.38	.020	1.55	1.12	1.76	1.09	312.58	.069	559905.	12824.	572728.
1.45	.021	1.53	1.12	1.74	1.09	315.32	.072	572728.	13107.	585835.
1.52	.022	1.51	1.12	1.71	1.09	318.14	.076	585835.	13390.	599225.
1.60	.023	1.49	1.12	1.69	1.09	321.04	.080	599225.	13672.	612897.
1.68	.024	1.47	1.12	1.67	1.09	324.03	.084	612897.	13952.	626849.
1.76	.025	1.45	1.12	1.64	1.09	327.09	.088	626849.	14231.	641080.
1.85	.026	1.43	1.12	1.62	1.09	330.06	.092	641080.	14532.	655612.
1.94	.028	1.41	1.12	1.60	1.08	333.05	.097	655612.	14840.	670453.
2.04	.029	1.40	1.12	1.57	1.08	336.06	.102	670453.	15156.	685609.
2.14	.031	1.38	1.12	1.55	1.08	339.10	.107	685609.	15479.	701088.
2.25	.032	1.36	1.12	1.53	1.08	342.17	.112	701088.	15808.	716896.
2.36	.034	1.34	1.12	1.51	1.08	345.27	.118	716896.	16143.	733039.
2.48	.035	1.33	1.12	1.49	1.08	348.42	.124	733039.	16482.	749521.
2.60	.037	1.31	1.12	1.47	1.08	351.62	.130	749521.	16826.	766347.
2.73	.039	1.30	1.12	1.45	1.07	354.88	.136	766347.	17173.	783519.
2.87	.041	1.28	1.13	1.43	1.07	358.19	.143	783519.	17522.	801041.
3.01	.043	1.27	1.13	1.41	1.07	361.58	.150	801041.	17873.	818914.
3.16	.045	1.25	1.13	1.39	1.07	365.03	.158	818914.	18224.	837138.
3.32	.047	1.24	1.13	1.37	1.07	368.57	.166	837138.	18575.	855713.
3.48	.050	1.23	1.13	1.36	1.06	372.20	.174	855713.	18924.	874637.
3.66	.052	1.22	1.13	1.34	1.06	375.92	.183	874637.	19270.	893907.
3.84	.055	1.20	1.13	1.32	1.06	379.75	.192	893907.	19612.	913519.
4.03	.058	1.19	1.14	1.31	1.06	383.69	.202	913519.	19948.	933467.

Table C-2 (continued)

GEOMETRY		A-DIRECTION								
A mm	A/T	Mkm	Mm	Mkb	Mb	DK Nmm-1.5	DA mm	Ni	DN	Ni+1
4.23	.060	1.18	1.14	1.29	1.06	387.74	.212	933467.	20278.	953745.
4.45	.064	1.17	1.14	1.28	1.05	391.93	.222	953745.	20599.	974345.
4.67	.067	1.16	1.14	1.26	1.05	396.25	.233	974345.	20911.	995256.
4.90	.070	1.15	1.15	1.25	1.05	400.72	.245	995256.	21211.	1016467.
5.15	.074	1.14	1.15	1.23	1.05	405.34	.257	1016467.	21498.	1037965.
5.40	.077	1.13	1.15	1.22	1.05	410.13	.270	1037965.	21770.	1059735.
5.67	.081	1.12	1.16	1.21	1.04	415.10	.284	1059735.	22026.	1081761.
5.96	.085	1.12	1.16	1.20	1.04	420.26	.298	1081761.	22264.	1104025.
6.26	.089	1.11	1.16	1.18	1.04	425.62	.313	1104025.	22481.	1126506.
6.57	.094	1.10	1.17	1.17	1.04	431.21	.328	1126506.	22676.	1149182.
6.90	.099	1.09	1.18	1.16	1.04	437.02	.345	1149182.	22847.	1172029.
7.24	.103	1.08	1.18	1.15	1.04	443.39	.362	1172029.	22944.	1194973.
7.60	.109	1.08	1.19	1.14	1.04	449.97	.380	1194973.	23023.	1217996.
7.98	.114	1.07	1.20	1.13	1.03	456.89	.399	1217996.	23062.	1241058.
8.38	.120	1.07	1.20	1.12	1.03	464.19	.419	1241058.	23061.	1264119.
8.80	.126	1.06	1.21	1.11	1.03	471.88	.440	1264119.	23020.	1287139.
9.24	.132	1.06	1.22	1.11	1.03	479.98	.462	1287139.	22936.	1310075.
9.70	.139	1.05	1.23	1.10	1.03	488.52	.485	1310075.	22809.	1332884.
10.19	.146	1.05	1.25	1.09	1.03	497.53	.509	1332884.	22639.	1355523.
10.70	.153	1.05	1.26	1.09	1.03	507.04	.535	1355523.	22424.	1377946.
11.23	.160	1.04	1.27	1.08	1.04	517.09	.562	1377946.	22163.	1400109.
11.80	.169	1.04	1.29	1.07	1.04	527.72	.590	1400109.	21857.	1421966.
12.38	.177	1.03	1.31	1.07	1.04	538.98	.619	1421966.	21505.	1443471.
13.00	.186	1.03	1.33	1.06	1.04	550.92	.650	1443471.	21106.	1464577.
13.65	.195	1.03	1.35	1.06	1.05	563.60	.683	1464577.	20660.	1485237.
14.34	.205	1.03	1.37	1.05	1.05	577.09	.717	1485237.	20169.	1505405.
15.05	.215	1.02	1.39	1.05	1.05	591.46	.753	1505405.	19631.	1525037.
15.81	.226	1.02	1.42	1.04	1.06	606.81	.790	1525037.	19049.	1544085.
16.60	.237	1.02	1.45	1.04	1.07	623.22	.830	1544085.	18422.	1562508.
17.43	.249	1.02	1.49	1.03	1.08	640.82	.871	1562508.	17753.	1580260.
18.30	.261	1.01	1.52	1.03	1.08	659.75	.915	1580260.	17042.	1597302.
19.21	.274	1.01	1.56	1.03	1.10	680.15	.961	1597302.	16291.	1613593.
20.17	.288	1.01	1.61	1.02	1.11	702.22	1.009	1613593.	15503.	1629096.
21.18	.303	1.01	1.66	1.02	1.12	726.17	1.059	1629096.	14679.	1643775.
22.24	.318	1.00	1.72	1.02	1.14	752.30	1.112	1643775.	13823.	1657598.
23.35	.334	1.00	1.78	1.01	1.15	780.91	1.168	1657598.	12938.	1670536.
24.52	.350	1.00	1.85	1.01	1.18	812.42	1.226	1670536.	12026.	1682562.
25.75	.368	1.00	1.93	1.01	1.20	847.33	1.287	1682562.	11092.	1693654.
27.03	.386	1.00	2.03	1.01	1.23	886.27	1.352	1693654.	10141.	1703795.
28.39	.406	1.00	2.13	1.00	1.26	927.16	1.419	1703795.	9266.	1713061.
29.81	.426	1.00	2.26	1.00	1.30	978.85	1.490	1713061.	8232.	1721293.
31.30	.447	1.00	2.40	1.00	1.34	1037.74	1.565	1721293.	7220.	1728513.
32.86	.469	1.00	2.56	1.00	1.40	1105.47	1.643	1728513.	6239.	1734752.
34.50	.493	1.00	2.75	1.00	1.46	1184.14	1.725	1734752.	5301.	1740053.
36.23	.518	1.00	2.97	1.00	1.55	1288.45	1.811	1740053.	4291.	1744344.
38.04	.543	1.00	3.20	1.00	1.63	1390.59	1.902	1744344.	3562.	1747905.
39.94	.571	1.00	3.49	1.00	1.74	1514.57	1.997	1747905.	2875.	1750780.
41.94	.599	1.00	3.88	1.00	1.88	1676.60	2.097	1750780.	2207.	1752987.

COMPUTERPROGRAM FAFRAM

FATIGUE CRACK GROWTH CALCULATION BASED ON FRACTURE MECHANICS

SPECIMEN B-1-1

CRACK GROWTH COEFFICIENT C (N,mm) : .11050000E-12
CRACK GROWTH COEFFICIENT M : 3.081

PLATE THICKNESS T (mm) : 70.000
PLATE WIDTH W (mm) : 210.000
INITIAL DEFECT Ai (mm) : .500
INITIAL DEFECT Ci (mm) : 5.000
CRITICAL CRACK DEPTH Af (mm) : 39.500
INITIAL NUMBER OF LOAD CYCLES Ni : 0
CRACK GROWTH FACTOR ALPHA : .050
MEMBRANE STRESS RANGE SIGM (N/mm2) : .000
BENDING STRESS RANGE SIGB (N/mm2) : 225.000

GEOMETRY			A-DIRECTION					C-DIRECTION									
A mm	C mm	Ek	Mkm	Mm	Mkb	Mb	DK Nmm-1.5	Mkm	Mm	Mkb	Mb	DK Nmm-1.5	DA mm	DC mm	Ni	DN	Ni+1
.50	5.00	1.016	1.00	1.12	1.00	1.11	315.98	1.00	.39	1.00	.39	110.61	.025	.001	0.	4499.	4499.
.52	5.00	1.018	1.00	1.12	1.00	1.11	323.09	1.00	.40	1.00	.40	115.92	.026	.001	4499.	4411.	8910.
.55	5.00	1.019	1.00	1.12	1.00	1.11	330.30	1.00	.41	1.00	.41	121.46	.028	.001	8910.	4327.	13237.
.58	5.00	1.021	1.00	1.12	1.00	1.11	337.62	1.00	.42	1.00	.42	127.25	.029	.001	13237.	4247.	17484.
.61	5.00	1.022	1.00	1.12	1.00	1.11	345.05	1.00	.43	1.00	.43	133.29	.030	.002	17484.	4170.	21654.
.64	5.01	1.024	1.00	1.12	1.00	1.11	352.58	1.00	.44	1.00	.44	139.59	.032	.002	21654.	4097.	25750.
.67	5.01	1.026	1.00	1.12	1.00	1.10	360.20	1.00	.45	1.00	.45	146.16	.034	.002	25750.	4027.	29777.
.70	5.01	1.028	1.00	1.12	1.00	1.10	367.91	1.00	.46	1.00	.46	153.01	.035	.002	29777.	3961.	33739.
.74	5.01	1.031	1.00	1.12	1.00	1.10	375.71	1.00	.47	1.00	.47	160.15	.037	.003	33739.	3899.	37638.
.78	5.02	1.033	1.00	1.12	1.00	1.10	383.58	1.00	.48	1.00	.48	167.58	.039	.003	37638.	3841.	41479.
.81	5.02	1.036	1.00	1.12	1.00	1.10	391.52	1.00	.49	1.00	.49	175.31	.041	.003	41479.	3786.	45265.
.86	5.02	1.039	1.00	1.11	1.00	1.10	399.52	1.00	.51	1.00	.50	183.34	.043	.004	45265.	3735.	49000.
.90	5.03	1.042	1.00	1.11	1.00	1.10	407.57	1.00	.52	1.00	.52	191.68	.045	.004	49000.	3688.	52688.
.94	5.03	1.045	1.00	1.11	1.00	1.09	415.67	1.00	.53	1.00	.53	200.35	.047	.005	52688.	3645.	56333.
.99	5.04	1.049	1.00	1.11	1.00	1.09	423.79	1.00	.54	1.00	.54	209.33	.049	.006	56333.	3606.	59938.
1.04	5.04	1.053	1.00	1.11	1.00	1.09	431.93	1.00	.56	1.00	.55	218.64	.052	.006	59938.	3570.	63509.
1.09	5.05	1.057	1.00	1.11	1.00	1.09	440.07	1.00	.57	1.00	.57	228.27	.055	.007	63509.	3539.	67048.

Table C-3

Table C-3 (continued)

GEOMETRY			A-DIRECTION					C-DIRECTION									
A mm	C mm	Ek	Mkm	Mm	Mkb	Mb	DK Nmm-1.5	Mkm	Mm	Mkb	Mb	DK Nmm-1.5	DA mm	DC mm	Ni	DN	Ni+1
1.15	5.05	1.061	1.00	1.11	1.00	1.09	448.21	1.00	.58	1.00	.58	238.23	.057	.008	67048.	3512.	70560.
1.20	5.06	1.066	1.00	1.11	1.00	1.09	456.33	1.00	.59	1.00	.59	248.52	.060	.009	70560.	3489.	74049.
1.26	5.07	1.071	1.00	1.11	1.00	1.08	464.41	1.00	.61	1.00	.60	259.14	.063	.010	74049.	3471.	77520.
1.33	5.08	1.077	1.00	1.11	1.00	1.08	472.44	1.00	.62	1.00	.62	270.07	.066	.012	77520.	3457.	80977.
1.39	5.09	1.083	1.00	1.11	1.00	1.08	480.41	1.00	.64	1.00	.63	281.33	.070	.013	80977.	3448.	84425.
1.46	5.11	1.089	1.00	1.10	1.00	1.08	488.29	1.00	.65	1.00	.65	292.89	.073	.015	84425.	3443.	87868.
1.54	5.12	1.096	1.00	1.10	1.00	1.07	496.08	1.00	.66	1.00	.66	304.76	.077	.017	87868.	3443.	91311.
1.61	5.14	1.103	1.00	1.10	1.00	1.07	503.77	1.00	.68	1.00	.67	316.92	.081	.019	91311.	3448.	94759.
1.69	5.16	1.110	1.00	1.10	1.00	1.07	511.34	1.00	.69	1.00	.69	329.36	.085	.022	94759.	3458.	98216.
1.78	5.18	1.118	1.00	1.10	1.00	1.06	518.77	1.00	.71	1.00	.70	342.06	.089	.025	98216.	3473.	101689.
1.87	5.21	1.127	1.00	1.10	1.00	1.06	526.07	1.00	.72	1.00	.72	355.02	.093	.028	101689.	3493.	105181.
1.96	5.23	1.136	1.00	1.10	1.00	1.06	533.22	1.00	.74	1.00	.73	368.22	.098	.031	105181.	3518.	108699.
2.06	5.26	1.145	1.00	1.10	1.00	1.05	540.23	1.00	.75	1.00	.75	381.63	.103	.035	108699.	3548.	112247.
2.16	5.30	1.155	1.00	1.09	1.00	1.05	547.08	1.00	.77	1.00	.76	395.25	.108	.040	112247.	3584.	115831.
2.27	5.34	1.165	1.00	1.09	1.00	1.05	553.78	1.00	.78	1.00	.77	409.05	.113	.045	115831.	3624.	119455.
2.38	5.38	1.175	1.00	1.09	1.00	1.04	560.34	1.00	.80	1.00	.79	423.01	.119	.050	119455.	3670.	123125.
2.50	5.43	1.186	1.00	1.09	1.00	1.04	566.77	1.00	.81	1.00	.80	437.12	.125	.056	123125.	3720.	126845.
2.63	5.49	1.197	1.00	1.09	1.00	1.04	573.09	1.00	.83	1.00	.82	451.37	.131	.063	126845.	3775.	130621.
2.76	5.55	1.209	1.00	1.09	1.00	1.03	579.31	1.00	.84	1.00	.83	465.73	.138	.070	130621.	3834.	134455.
2.90	5.62	1.221	1.00	1.08	1.00	1.03	585.47	1.00	.86	1.00	.84	480.20	.145	.079	134455.	3897.	138352.
3.04	5.70	1.232	1.00	1.08	1.00	1.02	591.58	1.00	.87	1.00	.86	494.76	.152	.088	138352.	3963.	142314.
3.19	5.79	1.244	1.00	1.08	1.00	1.02	597.69	1.00	.88	1.00	.87	509.41	.160	.098	142314.	4031.	146346.
3.35	5.89	1.256	1.00	1.08	1.00	1.01	603.82	1.00	.90	1.00	.88	524.15	.168	.108	146346.	4102.	150448.
3.52	6.00	1.268	1.00	1.08	1.00	1.01	610.02	1.00	.91	1.00	.89	538.98	.176	.120	150448.	4174.	154621.
3.70	6.12	1.280	1.00	1.08	1.00	1.00	616.33	1.00	.92	1.00	.90	553.89	.185	.133	154621.	4245.	158867.
3.88	6.25	1.291	1.00	1.08	1.00	1.00	622.78	1.00	.93	1.00	.91	568.90	.194	.147	158867.	4317.	163184.
4.07	6.40	1.302	1.00	1.07	1.00	.99	629.43	1.00	.94	1.00	.92	584.02	.204	.162	163184.	4387.	167571.
4.28	6.56	1.313	1.00	1.07	1.00	.99	636.29	1.00	.95	1.00	.93	599.26	.214	.178	167571.	4455.	172025.
4.49	6.74	1.323	1.00	1.07	1.00	.98	643.43	1.00	.96	1.00	.94	614.63	.225	.195	172025.	4520.	176545.
4.72	6.93	1.333	1.00	1.07	1.00	.98	650.85	1.00	.97	1.00	.95	630.16	.236	.214	176545.	4581.	181126.
4.95	7.14	1.342	1.00	1.07	1.00	.97	658.60	1.00	.98	1.00	.95	645.86	.248	.233	181126.	4638.	185764.
5.20	7.38	1.350	1.00	1.07	1.00	.97	666.70	1.00	.99	1.00	.96	661.76	.260	.254	185764.	4690.	190453.
5.46	7.63	1.357	1.00	1.07	1.00	.96	675.16	1.00	1.00	1.00	.96	677.87	.273	.276	190453.	4736.	195190.
5.73	7.91	1.364	1.00	1.07	1.00	.95	684.00	1.00	1.00	1.00	.97	694.21	.287	.300	195190.	4778.	199968.
6.02	8.21	1.370	1.00	1.07	1.00	.95	693.21	1.00	1.01	1.00	.97	710.81	.301	.325	199968.	4814.	204782.
6.32	8.53	1.376	1.00	1.07	1.00	.94	702.82	1.00	1.01	1.00	.97	727.68	.316	.352	204782.	4845.	209627.
6.64	8.89	1.380	1.00	1.07	1.00	.93	712.79	1.00	1.02	1.00	.98	744.85	.332	.380	209627.	4871.	214498.

GEOMETRY			A-DIRECTION					C-DIRECTION									
A	C	Ek	Mkm	Mm	Mkb	Mb	DK	Mkm	Mm	Mkb	Mb	DK	DA	DC	Ni	DN	Ni+1
mm	mm						Nmm-1.5					Nmm-1.5	mm	mm			
6.97	9.27	1.384	1.00	1.07	1.00	.93	723.14	1.00	1.02	1.00	.98	762.33	.348	.410	214498.	4893.	219391.
7.32	9.68	1.387	1.00	1.07	1.00	.92	733.84	1.00	1.02	1.00	.98	780.14	.366	.442	219391.	4910.	224300.
7.68	10.12	1.389	1.00	1.07	1.00	.91	744.87	1.00	1.03	1.00	.98	798.30	.384	.476	224300.	4924.	229224.
8.07	10.59	1.391	1.00	1.07	1.00	.91	756.21	1.00	1.03	1.00	.98	816.82	.403	.512	229224.	4935.	234159.
8.47	11.10	1.392	1.00	1.07	1.00	.90	767.84	1.00	1.03	1.00	.98	835.72	.424	.550	234159.	4943.	239102.
8.89	11.65	1.392	1.00	1.07	1.00	.89	779.73	1.00	1.03	1.00	.98	855.02	.445	.591	239102.	4951.	244053.
9.34	12.24	1.392	1.00	1.07	1.00	.88	791.85	1.00	1.03	1.00	.97	874.74	.467	.635	244053.	4957.	249010.
9.81	12.88	1.391	1.00	1.07	1.00	.87	804.17	1.00	1.03	1.00	.97	894.89	.490	.682	249010.	4963.	253973.
10.30	13.56	1.389	1.00	1.07	1.00	.86	816.65	1.00	1.03	1.00	.97	915.50	.515	.732	253973.	4970.	258943.
10.81	14.29	1.387	1.00	1.07	1.00	.85	829.26	1.00	1.03	1.00	.97	936.58	.541	.787	258943.	4978.	263920.
11.35	15.08	1.384	1.00	1.07	1.00	.84	841.97	1.00	1.03	1.00	.96	958.16	.568	.845	263920.	4987.	268907.
11.92	15.92	1.381	1.00	1.07	1.00	.83	854.74	1.00	1.03	1.00	.96	980.28	.596	.909	268907.	4999.	273907.
12.52	16.83	1.378	1.00	1.08	1.00	.82	867.53	1.00	1.03	1.00	.95	1002.97	.626	.978	273907.	5014.	278921.
13.14	17.81	1.373	1.00	1.08	1.00	.81	880.31	1.00	1.03	1.00	.95	1026.26	.657	1.054	278921.	5033.	283954.
13.80	18.87	1.369	1.00	1.08	1.00	.80	893.05	1.00	1.03	1.00	.94	1050.20	.690	1.137	283954.	5056.	289010.
14.49	20.00	1.364	1.00	1.08	1.00	.79	905.71	1.00	1.03	1.00	.94	1074.86	.724	1.228	289010.	5083.	294094.
15.21	21.23	1.358	1.00	1.09	1.00	.78	918.27	1.00	1.03	1.00	.93	1100.29	.761	1.328	294094.	5116.	299209.
15.97	22.56	1.352	1.00	1.09	1.00	.77	930.70	1.00	1.02	1.00	.93	1126.59	.799	1.439	299209.	5154.	304363.
16.77	24.00	1.346	1.00	1.09	1.00	.75	942.98	1.00	1.02	1.00	.92	1153.84	.839	1.562	304363.	5197.	309560.
17.61	25.56	1.339	1.00	1.10	1.00	.74	955.09	1.00	1.02	1.00	.91	1182.18	.881	1.699	309560.	5247.	314807.
18.49	27.26	1.331	1.00	1.10	1.00	.72	967.05	1.00	1.02	1.00	.91	1211.76	.925	1.853	314807.	5302.	320108.
19.42	29.11	1.323	1.00	1.11	1.00	.71	978.86	1.00	1.02	1.00	.90	1242.77	.971	2.026	320108.	5362.	325471.
20.39	31.14	1.315	1.00	1.11	1.00	.69	990.56	1.00	1.02	1.00	.89	1275.45	1.019	2.221	325471.	5428.	330899.
21.41	33.36	1.305	1.00	1.12	1.00	.68	1002.21	1.00	1.01	1.00	.89	1310.11	1.070	2.443	330899.	5498.	336397.
22.48	35.80	1.296	1.00	1.13	1.00	.66	1013.92	1.00	1.01	1.00	.88	1347.15	1.124	2.697	336397.	5570.	341967.
23.60	38.50	1.286	1.00	1.13	1.00	.65	1025.86	1.00	1.01	1.00	.87	1387.08	1.180	2.989	341967.	5641.	347608.
24.78	41.49	1.275	1.00	1.14	1.00	.63	1038.27	1.00	1.01	1.00	.87	1430.61	1.239	3.327	347608.	5708.	353316.
26.02	44.81	1.264	1.00	1.15	1.00	.61	1051.51	1.00	1.01	1.00	.86	1478.66	1.301	3.719	353316.	5764.	359080.
27.32	48.53	1.252	1.00	1.17	1.00	.59	1066.14	1.00	1.01	1.00	.85	1532.54	1.366	4.178	359080.	5800.	364879.
28.69	52.71	1.240	1.00	1.18	1.00	.57	1082.98	1.00	1.01	1.00	.84	1594.08	1.434	4.720	364879.	5803.	370682.
30.12	57.43	1.227	1.00	1.20	1.00	.55	1103.27	1.00	1.01	1.00	.84	1666.02	1.506	5.362	370682.	5754.	376436.
31.63	62.79	1.213	1.00	1.22	1.00	.54	1128.97	1.00	1.01	1.00	.83	1752.50	1.581	6.129	376436.	5628.	382064.
33.21	68.92	1.200	1.00	1.24	1.00	.52	1163.31	1.00	1.01	1.00	.83	1860.20	1.660	7.052	382064.	5388.	387452.
34.87	75.98	1.185	1.00	1.27	1.00	.50	1211.84	1.00	1.02	1.00	.82	2000.60	1.743	8.169	387452.	4988.	392441.
36.61	84.14	1.171	1.00	1.29	1.00	.48	1285.12	1.00	1.02	1.00	.81	2195.30	1.831	9.530	392441.	4371.	396812.
38.44	93.67	1.156	1.00	1.33	1.00	.46	1405.92	1.00	1.03	1.00	.81	2490.80	1.922	11.195	396812.	3480.	400291.
40.37	104.87	1.141	1.00	1.37	1.00	.44	1635.81	1.00	1.03	1.00	.81	3012.40	2.018	13.243	400291.	2291.	402583.

Table C-3 (continued)

COMPUTERPROGRAM FAFRAM

FATIGUE CRACK GROWTH CALCULATION BASED ON FRACTURE MECHANICS

SPECIMEN B-1-1

CRACK GROWTH COEFFICIENT C (N,mm) : .11050000E-12
CRACK GROWTH COEFFICIENT M : 3.081

PLATE THICKNESS T (mm) : 70.000
PLATE WIDTH W (mm) : 210.000
INITIAL DEFECT Ai (mm) : 8.100
INITIAL DEFECT Ci (mm) : 9.000
CRITICAL CRACK DEPTH Af (mm) : 39.500
INITIAL NUMBER OF LOAD CYCLES Ni : 407000
CRACK GROWTH FACTOR ALPHA : .050
MEMBRANE STRESS RANGE SIGM (N/mm2) : .000
BENDING STRESS RANGE SIGB (N/mm2) : 225.000

GEOMETRY			A-DIRECTION					C-DIRECTION									
A mm	C mm	Ek	Mkm	Mm	Mkb	Mb	DK Nmm-1.5	Mkm	Mm	Mkb	Mb	DK Nmm-1.5	DA mm	DC mm	Ni	DN	Ni+1
8.10	9.00	1.493	1.00	1.05	1.00	.89	693.90	1.00	1.10	1.00	1.05	815.84	.405	.667	407000.	6457.	413457.
8.51	9.67	1.478	1.00	1.05	1.00	.88	713.80	1.00	1.09	1.00	1.04	835.42	.425	.691	413457.	6215.	419672.
8.93	10.36	1.465	1.00	1.06	1.00	.88	732.83	1.00	1.09	1.00	1.03	855.24	.447	.719	419672.	6017.	425689.
9.38	11.08	1.453	1.00	1.06	1.00	.87	751.14	1.00	1.08	1.00	1.02	875.34	.469	.751	425689.	5856.	431545.
9.85	11.83	1.443	1.00	1.06	1.00	.86	768.84	1.00	1.07	1.00	1.01	895.79	.492	.788	431545.	5722.	437267.
10.34	12.62	1.433	1.00	1.06	1.00	.86	786.02	1.00	1.07	1.00	1.00	916.64	.517	.830	437267.	5613.	442880.
10.85	13.45	1.424	1.00	1.07	1.00	.85	802.75	1.00	1.06	1.00	.99	937.91	.543	.877	442880.	5524.	448404.
11.40	14.32	1.416	1.00	1.07	1.00	.84	819.05	1.00	1.06	1.00	.98	959.65	.570	.928	448404.	5451.	453855.
11.97	15.25	1.408	1.00	1.07	1.00	.83	834.96	1.00	1.05	1.00	.98	981.89	.598	.986	453855.	5394.	459250.
12.57	16.24	1.400	1.00	1.07	1.00	.82	850.51	1.00	1.05	1.00	.97	1004.68	.628	1.050	459250.	5351.	464601.
13.19	17.29	1.392	1.00	1.07	1.00	.81	865.70	1.00	1.04	1.00	.96	1028.06	.660	1.120	464601.	5320.	469922.
13.85	18.41	1.384	1.00	1.08	1.00	.80	880.55	1.00	1.04	1.00	.95	1052.09	.693	1.199	469922.	5301.	475223.
14.55	19.61	1.376	1.00	1.08	1.00	.79	895.06	1.00	1.04	1.00	.95	1076.81	.727	1.286	475223.	5293.	480516.
15.27	20.89	1.369	1.00	1.08	1.00	.78	909.22	1.00	1.03	1.00	.94	1102.32	.764	1.382	480516.	5295.	485811.
16.04	22.27	1.361	1.00	1.09	1.00	.76	923.05	1.00	1.03	1.00	.93	1128.68	.802	1.490	485811.	5307.	491119.
16.84	23.76	1.353	1.00	1.09	1.00	.75	936.55	1.00	1.03	1.00	.93	1156.01	.842	1.611	491119.	5329.	496448.

Table C-4

Table C-4 (continued)

GEOMETRY			A-DIRECTION					C-DIRECTION									
A	C	Ek	Mkm	Mm	Mkb	Mb	DK	Mkm	Mm	Mkb	Mb	DK	DA	DC	Ni	DN	Ni+1
mm	mm						Nmm-1.5					Nmm-1.5	mm	mm			
17.68	25.37	1.344	1.00	1.10	1.00	.74	949.72	1.00	1.03	1.00	.92	1184.44	.884	1.746	496448.	5360.	501808.
18.57	27.12	1.335	1.00	1.10	1.00	.72	962.59	1.00	1.02	1.00	.91	1214.11	.928	1.898	501808.	5399.	507207.
19.49	29.02	1.326	1.00	1.11	1.00	.71	975.20	1.00	1.02	1.00	.90	1245.23	.975	2.070	507207.	5446.	512653.
20.47	31.09	1.317	1.00	1.11	1.00	.69	987.59	1.00	1.02	1.00	.90	1278.04	1.023	2.265	512653.	5501.	518154.
21.49	33.35	1.307	1.00	1.12	1.00	.68	999.84	1.00	1.02	1.00	.89	1312.86	1.075	2.487	518154.	5560.	523714.
22.57	35.84	1.297	1.00	1.13	1.00	.66	1012.08	1.00	1.02	1.00	.88	1350.09	1.128	2.742	523714.	5623.	529337.
23.69	38.58	1.286	1.00	1.13	1.00	.64	1024.48	1.00	1.01	1.00	.87	1390.28	1.185	3.035	529337.	5687.	535025.
24.88	41.62	1.275	1.00	1.14	1.00	.63	1037.32	1.00	1.01	1.00	.87	1434.11	1.244	3.375	535025.	5747.	540771.
26.12	44.99	1.264	1.00	1.16	1.00	.61	1050.98	1.00	1.01	1.00	.86	1482.56	1.306	3.770	540771.	5796.	546567.
27.43	48.76	1.252	1.00	1.17	1.00	.59	1066.02	1.00	1.01	1.00	.85	1536.97	1.371	4.234	546567.	5825.	552392.
28.80	52.99	1.239	1.00	1.18	1.00	.57	1083.31	1.00	1.01	1.00	.84	1599.23	1.440	4.781	552392.	5820.	558212.
30.24	57.78	1.226	1.00	1.20	1.00	.55	1104.15	1.00	1.01	1.00	.84	1672.15	1.512	5.431	558212.	5763.	563975.
31.75	63.21	1.212	1.00	1.22	1.00	.53	1130.57	1.00	1.01	1.00	.83	1760.04	1.588	6.209	563975.	5626.	569600.
33.34	69.42	1.199	1.00	1.24	1.00	.51	1165.94	1.00	1.01	1.00	.82	1869.87	1.667	7.144	569600.	5372.	574973.
35.01	76.56	1.184	1.00	1.27	1.00	.49	1216.09	1.00	1.02	1.00	.82	2013.65	1.750	8.278	574973.	4954.	579927.
36.76	84.84	1.170	1.00	1.30	1.00	.47	1292.20	1.00	1.02	1.00	.81	2214.25	1.838	9.660	579927.	4315.	584242.
38.60	94.50	1.155	1.00	1.33	1.00	.46	1418.70	1.00	1.03	1.00	.81	2521.55	1.930	11.352	584242.	3398.	587639.
40.53	105.85	1.140	1.00	1.37	1.00	.44	1663.32	1.00	1.03	1.00	.81	3073.36	2.026	13.434	587639.	2185.	589825.

Table C-5

COMPUTERPROGRAM FAFRAM

FATIGUE CRACK GROWTH CALCULATION BASED ON FRACTURE MECHANICS

SPECIMEN D-1-2

CRACK GROWTH COEFFICIENT C (N,mm)	:	.11050000E-12
CRACK GROWTH COEFFICIENT M	:	3.081
PLATE THICKNESS T (mm)	:	70.000
PLATE WIDTH W (mm)	:	210.000
WELD ANGLE PHI (degree)	:	70.000
WELD TOE RADIUS RHO (mm)	:	5.000
INITIAL DEFECT Ai (mm)	:	.500
INITIAL DEFECT Ci (mm)	:	5.000
CRITICAL CRACK DEPTH Af (mm)	:	29.900
INITIAL NUMBER OF LOAD CYCLES Ni	:	0
CRACK GROWTH FACTOR ALPHA	:	.050
MEMBRANE STRESS RANGE SIGM (N/mm2)	:	.000
BENDING STRESS RANGE SIGB (N/mm2)	:	110.000

GEOMETRY			A-DIRECTION					C-DIRECTION								
A mm	C mm	Ek	Mkm	Mm	Mkb	Mb	DK Nmm-1.5	Mkm	Mm	Mkb	Mb	DK Nmm-1.5	DA mm	DC mm	Ni	DN	Ni+1
.50	5.00	1.016	1.62	1.12	1.75	1.11	269.87	1.79	.39	1.91	.39	103.29	.025	.001	0.	7315.	7315.
.52	5.00	1.018	1.61	1.12	1.74	1.11	274.87	1.79	.40	1.91	.40	108.24	.026	.001	7315.	7258.	14573.
.55	5.00	1.019	1.61	1.12	1.73	1.11	279.89	1.79	.41	1.91	.41	113.41	.028	.002	14573.	7207.	21780.
.58	5.00	1.021	1.60	1.12	1.73	1.11	284.92	1.79	.42	1.91	.42	118.81	.029	.002	21780.	7164.	28944.
.61	5.01	1.022	1.59	1.12	1.72	1.11	289.94	1.79	.43	1.91	.43	124.44	.030	.002	28944.	7128.	36072.
.64	5.01	1.024	1.58	1.12	1.71	1.11	294.95	1.79	.44	1.91	.44	130.32	.032	.003	36072.	7099.	43171.
.67	5.01	1.026	1.58	1.12	1.70	1.10	299.96	1.79	.45	1.91	.45	136.45	.034	.003	43171.	7078.	50249.
.70	5.01	1.028	1.57	1.12	1.70	1.10	304.93	1.79	.46	1.91	.46	142.83	.035	.003	50249.	7064.	57314.
.74	5.02	1.031	1.56	1.12	1.69	1.10	309.88	1.79	.47	1.91	.47	149.48	.037	.004	57314.	7059.	64372.
.78	5.02	1.033	1.55	1.12	1.68	1.10	314.79	1.79	.48	1.91	.48	156.40	.039	.004	64372.	7061.	71434.
.81	5.03	1.036	1.54	1.12	1.67	1.10	319.64	1.79	.49	1.91	.49	163.59	.041	.005	71434.	7073.	78507.
.86	5.03	1.039	1.53	1.11	1.66	1.10	324.44	1.79	.51	1.91	.50	171.06	.043	.006	78507.	7093.	85600.
.90	5.04	1.042	1.53	1.11	1.65	1.10	329.17	1.79	.52	1.91	.52	178.82	.045	.007	85600.	7123.	92723.
.94	5.04	1.045	1.52	1.11	1.64	1.09	333.82	1.79	.53	1.91	.53	186.86	.047	.008	92723.	7163.	99886.

GEOMETRY			A-DIRECTION					C-DIRECTION									
A	C	Ek	Mkm	Mm	Mkb	Mb	DK	Mkm	Mm	Mkb	Mb	DK	DA	DC	Ni	DN	Ni+1
mm	mm						Nmm-1.5					Nmm-1.5	mm	mm			
.99	5.05	1.049	1.51	1.11	1.63	1.09	338.39	1.79	.54	1.91	.54	195.20	.049	.009	99886.	7213.	107099.
1.04	5.06	1.052	1.50	1.11	1.62	1.09	342.85	1.79	.55	1.91	.55	203.83	.052	.010	107099.	7274.	114372.
1.09	5.07	1.056	1.49	1.11	1.61	1.09	347.21	1.79	.57	1.91	.56	212.75	.055	.012	114372.	7346.	121718.
1.15	5.08	1.061	1.48	1.11	1.60	1.09	351.46	1.79	.58	1.91	.58	221.96	.057	.014	121718.	7430.	129147.
1.20	5.10	1.065	1.47	1.11	1.59	1.09	355.58	1.79	.59	1.91	.59	231.46	.060	.016	129147.	7526.	136673.
1.26	5.11	1.070	1.46	1.11	1.58	1.08	359.56	1.79	.61	1.91	.60	241.24	.063	.018	136673.	7635.	144309.
1.33	5.13	1.076	1.45	1.11	1.57	1.08	363.41	1.79	.62	1.91	.62	251.29	.066	.021	144309.	7759.	152067.
1.39	5.15	1.081	1.44	1.11	1.56	1.08	367.11	1.79	.63	1.91	.63	261.62	.070	.025	152067.	7896.	159963.
1.46	5.18	1.087	1.43	1.11	1.55	1.08	370.67	1.79	.65	1.91	.64	272.20	.073	.028	159963.	8048.	168011.
1.54	5.21	1.093	1.42	1.10	1.54	1.07	374.08	1.79	.66	1.91	.65	283.03	.077	.033	168011.	8215.	176227.
1.61	5.24	1.100	1.41	1.10	1.53	1.07	377.34	1.79	.67	1.91	.67	294.08	.081	.037	176227.	8398.	184625.
1.69	5.28	1.107	1.39	1.10	1.52	1.07	380.46	1.79	.69	1.91	.68	305.36	.085	.043	184625.	8597.	193222.
1.78	5.32	1.114	1.38	1.10	1.50	1.07	383.33	1.79	.70	1.91	.69	316.83	.089	.049	193222.	8821.	202043.
1.87	5.37	1.121	1.37	1.10	1.49	1.06	385.83	1.79	.71	1.91	.71	328.49	.093	.057	202043.	9079.	211122.
1.96	5.43	1.128	1.36	1.10	1.48	1.06	388.20	1.79	.73	1.91	.72	340.30	.098	.065	211122.	9354.	220475.
2.06	5.49	1.136	1.35	1.10	1.46	1.06	390.49	1.79	.74	1.91	.73	352.25	.103	.075	220475.	9646.	230121.
2.16	5.57	1.143	1.33	1.10	1.45	1.05	392.70	1.79	.75	1.91	.74	364.32	.108	.086	230121.	9953.	240074.
2.27	5.65	1.151	1.32	1.09	1.44	1.05	394.87	1.79	.76	1.91	.75	376.50	.113	.098	240074.	10275.	250349.
2.38	5.75	1.159	1.31	1.09	1.43	1.05	397.02	1.79	.77	1.91	.76	388.75	.119	.112	250349.	10609.	260958.
2.50	5.86	1.166	1.30	1.09	1.41	1.04	399.20	1.79	.79	1.91	.77	401.08	.125	.127	260958.	10953.	271911.
2.63	5.99	1.173	1.29	1.09	1.40	1.04	401.44	1.79	.80	1.91	.78	413.46	.131	.144	271911.	11304.	283215.
2.76	6.13	1.180	1.28	1.09	1.39	1.04	403.78	1.79	.81	1.91	.79	425.89	.138	.163	283215.	11659.	294875.
2.90	6.29	1.186	1.26	1.09	1.37	1.03	406.25	1.79	.81	1.91	.80	438.36	.145	.183	294875.	12014.	306889.
3.04	6.48	1.192	1.25	1.09	1.36	1.03	408.89	1.79	.82	1.91	.81	450.86	.152	.205	306889.	12366.	319255.
3.19	6.68	1.197	1.24	1.09	1.35	1.03	411.72	1.79	.83	1.91	.81	463.40	.160	.230	319255.	12711.	331966.
3.35	6.91	1.202	1.23	1.09	1.33	1.02	414.78	1.79	.83	1.91	.82	475.97	.168	.256	331966.	13045.	345011.
3.52	7.17	1.205	1.22	1.09	1.32	1.02	418.09	1.79	.84	1.91	.82	488.59	.176	.284	345011.	13367.	358378.
3.70	7.45	1.208	1.21	1.09	1.31	1.01	421.66	1.79	.84	1.91	.83	501.26	.185	.315	358378.	13672.	372050.
3.88	7.77	1.211	1.20	1.09	1.30	1.01	425.50	1.79	.85	1.91	.83	513.98	.194	.347	372050.	13960.	386010.
4.07	8.11	1.212	1.19	1.09	1.28	1.01	429.62	1.79	.85	1.91	.83	526.76	.204	.382	386010.	14229.	400239.
4.28	8.50	1.213	1.18	1.09	1.27	1.00	434.01	1.79	.85	1.91	.83	539.62	.214	.418	400239.	14480.	414719.
4.49	8.92	1.213	1.17	1.09	1.26	1.00	438.68	1.79	.85	1.91	.83	552.57	.225	.457	414719.	14711.	429430.
4.72	9.37	1.213	1.16	1.09	1.25	.99	443.60	1.79	.85	1.91	.83	565.60	.236	.499	429430.	14925.	444354.
4.95	9.87	1.212	1.15	1.09	1.23	.99	448.77	1.79	.85	1.91	.83	578.75	.248	.542	444354.	15121.	459476.
5.20	10.41	1.211	1.14	1.09	1.22	.99	454.17	1.79	.85	1.91	.82	592.00	.260	.588	459476.	15303.	474779.
5.46	11.00	1.209	1.13	1.09	1.21	.98	459.78	1.79	.85	1.91	.82	605.39	.273	.637	474779.	15471.	490250.

Table C-5 (continued)

GEOMETRY			A-DIRECTION					C-DIRECTION									
A	C	Ek	Mkm	Mm	Mkb	Mb	DK	Mkm	Mm	Mkb	Mb	DK	DA	DC	Ni	DN	Ni+1
mm	mm						Nmm-1.5					Nmm-1.5	mm	mm			
5.73	11.64	1.206	1.12	1.09	1.20	.98	465.60	1.79	.84	1.91	.82	618.91	.287	.689	490250.	15628.	505878.
6.02	12.33	1.204	1.12	1.09	1.19	.97	471.59	1.79	.84	1.91	.81	632.58	.301	.744	505878.	15776.	521653.
6.32	13.07	1.201	1.11	1.09	1.18	.97	477.74	1.79	.84	1.91	.81	646.41	.316	.802	521653.	15915.	537569.
6.64	13.87	1.197	1.10	1.09	1.17	.96	484.05	1.79	.83	1.91	.80	660.42	.332	.864	537569.	16050.	553618.
6.97	14.74	1.194	1.09	1.10	1.16	.96	490.49	1.79	.83	1.91	.80	674.61	.348	.930	553618.	16180.	569798.
7.32	15.67	1.190	1.08	1.10	1.15	.95	497.15	1.79	.83	1.91	.79	689.01	.366	1.000	569798.	16297.	586095.
7.68	16.67	1.187	1.08	1.10	1.14	.95	503.84	1.79	.82	1.91	.79	703.64	.384	1.075	586095.	16422.	602517.
8.07	17.74	1.183	1.07	1.10	1.13	.94	510.74	1.79	.82	1.91	.78	718.51	.403	1.155	602517.	16535.	619052.
8.47	18.90	1.179	1.07	1.10	1.12	.93	517.84	1.79	.82	1.91	.78	733.65	.424	1.239	619052.	16639.	635691.
8.89	20.14	1.175	1.06	1.10	1.11	.93	525.11	1.79	.81	1.91	.77	749.09	.445	1.329	635691.	16736.	652427.
9.34	21.47	1.171	1.06	1.11	1.11	.92	532.56	1.79	.81	1.91	.77	764.87	.467	1.425	652427.	16826.	669254.
9.81	22.89	1.167	1.05	1.11	1.10	.91	540.17	1.79	.80	1.91	.76	781.03	.490	1.527	669254.	16912.	686166.
10.30	24.42	1.163	1.05	1.11	1.09	.91	547.93	1.79	.80	1.91	.75	797.61	.515	1.637	686166.	16994.	703160.
10.81	26.06	1.159	1.04	1.11	1.08	.90	555.85	1.79	.80	1.91	.75	814.66	.541	1.755	703160.	17073.	720233.
11.35	27.81	1.155	1.04	1.12	1.08	.89	563.92	1.79	.79	1.91	.74	832.25	.568	1.883	720233.	17147.	737380.
11.92	29.69	1.151	1.04	1.12	1.07	.88	572.17	1.79	.79	1.91	.74	850.45	.596	2.021	737380.	17216.	754596.
12.52	31.71	1.147	1.03	1.12	1.07	.87	580.61	1.79	.79	1.91	.73	869.34	.626	2.170	754596.	17280.	771876.
13.14	33.89	1.143	1.03	1.13	1.06	.87	589.27	1.79	.78	1.91	.73	889.03	.657	2.333	771876.	17335.	789210.
13.80	36.22	1.139	1.03	1.13	1.06	.86	598.19	1.79	.78	1.91	.72	909.65	.690	2.510	789210.	17378.	806589.
14.49	38.73	1.135	1.02	1.14	1.05	.85	607.42	1.79	.78	1.91	.72	931.35	.724	2.703	806589.	17407.	823995.
15.21	41.43	1.131	1.02	1.14	1.05	.84	617.03	1.79	.77	1.91	.71	954.32	.761	2.915	823995.	17414.	841409.
15.97	44.35	1.128	1.02	1.15	1.04	.83	627.12	1.79	.77	1.91	.71	978.81	.799	3.148	841409.	17394.	858803.
16.77	47.50	1.124	1.02	1.16	1.04	.82	637.81	1.79	.77	1.91	.70	1005.13	.839	3.405	858803.	17336.	876139.
17.61	50.90	1.120	1.01	1.17	1.03	.81	649.27	1.79	.77	1.91	.70	1033.66	.881	3.690	876139.	17231.	893371.
18.49	54.59	1.116	1.01	1.17	1.03	.80	661.73	1.79	.77	1.91	.69	1064.93	.925	4.005	893371.	17063.	910434.
19.42	58.60	1.112	1.01	1.18	1.03	.79	675.49	1.79	.77	1.91	.69	1099.60	.971	4.356	910434.	16816.	927250.
20.39	62.95	1.108	1.01	1.20	1.02	.78	690.98	1.79	.77	1.91	.68	1138.59	1.019	4.749	927250.	16466.	943715.
21.41	67.70	1.104	1.01	1.21	1.02	.76	708.76	1.79	.77	1.91	.68	1183.13	1.070	5.190	943715.	15987.	959702.
22.48	72.89	1.100	1.00	1.22	1.02	.75	729.67	1.79	.77	1.91	.68	1234.99	1.124	5.686	959702.	15348.	975051.
23.60	78.58	1.096	1.00	1.24	1.01	.74	754.92	1.79	.77	1.91	.68	1296.72	1.180	6.248	975051.	14511.	989562.
24.78	84.83	1.092	1.00	1.25	1.01	.73	786.39	1.79	.78	1.91	.67	1372.21	1.239	6.887	989562.	13436.	1002998.
26.02	91.71	1.088	1.00	1.27	1.01	.72	827.05	1.79	.78	1.91	.67	1467.63	1.301	7.616	1002998.	12078.	1015076.
27.32	99.33	1.084	1.00	1.30	1.00	.70	882.05	1.79	.78	1.91	.67	1593.61	1.366	8.452	1015076.	10400.	1025476.
28.69	107.78	1.079	1.00	1.32	1.00	.69	958.65	1.79	.79	1.91	.67	1770.13	1.434	9.490	1025476.	8449.	1033925.
30.12	117.27	1.075	1.00	1.35	1.00	.68	1086.46	1.79	.80	1.91	.67	2042.23	1.506	10.527	1033925.	6033.	1039958.

Table C-5 (continued)